Characterisation of the multi-isomeric protein nesprin-1 in p-body and mRNA dynamics

Rajgor, Dipen

Awarding institution:
King's College London

Title: Characterisation of the multi-isomeric protein nesprin-1 in p-body and mRNA dynamics

Author: Dipen Rajgor

CHARACTERISATION OF THE MULTI-ISOMERIC PROTEIN NESPRIN-1 IN P-BODY AND mRNA DYNAMICS

PhD Thesis

Dipen Rajgor

September 2012

Submitted for the Degree of Doctor of Philosophy from
King's College London

King's College London,
Cardiovascular Division,
School of Medicine

Supervisor: Professor Catherine M. Shanahan

Table of Contents

Declaration

I declare that the work undertaken in this thesis was conducted by myself, except where indicated.

Dipen Rajgor

King's College London

Acknowledgments

It takes a lot of reading and referencing to write a PhD thesis, therefore I would like to first and foremost thank my Endnote library (Endnote X3, Macintosh edition) for not creating major havoc when compiling this thesis. More significantly, I would like to extend my heartfelt gratitude to my supervisor Professor Cathy Shanahan for her support, guidance and craziness throughout my Project. Without her dedication and enthusiasm towards my work this project could well have been a shambolic disaster.

I have been very fortunate in joining a lab full of diverse, weird, crazy and intelligent individuals who have made the last four years an unforgettable experience. I would like to thank former lab member Jason Mellad for his continued support throughout my PhD and for showing me how to send needy/desperate e-mails to other laboratories asking for plasmids which were used throughout this thesis. Equally, I would like to thank Derek Warren and Qiuping Zhang for showing me how to do basic biochemical and cell biology techniques at the beginning of my PhD and for their constant input throughout my project. I would like to thank Flavia Autore for helping me design the new nesprin schematics that were used helping me achieve my first publication, even though it resulted in extra cloning and repeating multiple experiments towards the end of my PhD.

I would also like to thank Andrew Cobb and Yiwen Liu for making my time in the lab and office an enjoyable experience, especially the mini scientific debates we had in which Cobby was often wrong, causing him to glow like a tomato. I would like to thank Alexs Kapustin for providing constant laughter over the four years and keeping his OCD in check when I kept throwing bacterial waste from maxi-preps into his bin for the first two years. I will never forget the diverse range of eccentric PhD students in the lab which contributed to many happy times during my PhD. I would like to thank Gosia Furmanik for playing her classical music in tissue culture which seemed to keep my cells healthy and provided much needed results in the final year. I would also like to acknowledge Anne Jacob and Lauren Porter for being good friends throughout the time I have known then. I would like to thank Daniel Brayson, who was sadly separated from his identical twin Michael Fassbender

at birth, for playing his depressing music through headphones rather than out loud which contributed to me maintaining my sanity. I would like to thank Leilani Beltran for being a loud mouth American who kept the lab in order and provided great support before she was abducted by the lab next door, and Robert Hayward for doing a great job when taking over as lab technician. Although I have only known Roshni Molls for about a year her guidance throughout the final and hardest part of my PhD and constant support both in and out of the lab will never be forgotten.

Last but not least, I would like to convey my gratitude to my parents, brother, cousins and friends for their great support not only throughout my PhD but also for supporting my desire to become a scientist from as far back as I can remember.

Abstract

Nuclear envelope spectrin repeat proteins, or Nesprins, are a novel family of nuclear and cytoskeletal proteins with rapidly expanding roles as intracellular scaffolds and linkers. Nesprins are characterized by a central spectrin repeat (SR) rod domain and a C-terminal KASH domain, which acts as a nuclear envelope (NE) targeting motif. At the NE, via interactions with the Sun domain family of proteins and the nuclear lamina, nesprins on both the inner and outer nuclear membranes form the linker of the nucleoskeleton and cytoskeleton (LINC) complex. This complex requires the giant nesprin-1 and nesprin-2 isoforms, which possess a pair of N-terminal calponin homology domains that bind directly to Filamentous-actin. However, via alternative promoter usage and alternative 3' end processing, the nesprins are able to generate multiple mRNA transcripts, leading to the production of diverse tissue specific isoforms with potential roles beyond the NE.

To explore further the capacity of nesprin-1 to generate alternative transcripts, 5' and 3' RACE was performed to identify cDNA ends which represent novel 5' and 3' untranslated regions (UTRs) respectively. By alternatively combining the differential 5' and 3' UTRs, multiple tissue specific nesprin-1 variants could be generated. Transfection of tagged constructs showed localizations to multiple sub-cellular compartments such as the nucleolus, focal adhesions, actin stress fibres and cytoplasmic particles, supporting the notion that nesprins are more than NE-cytoskeletal couplers.

One of these novel nesprin-1 variants, $p50^{Nesp1}$, was found to localize to cytoplasmic RNA granules called mRNA processing bodies (P-bodies). Using GST pull-downs and co-immunoprecipitations (co-IPs), $p50^{Nesp1}$ was found to complex with mRNA decapping factors and translational repressors. Furthermore, $p50^{Nesp1}$ was required for the efficient silencing function of miRNAs, shown using luciferase reporter constructs. More importantly, $p50^{Nesp1}$ associated strongly with microtubules, both *in vitro* and *in vivo,* and was required for scaffolding P-body complexes to microtubules. By disrupting P-body-microtubule association with a dominant negative $p50^{Nesp1}$ construct, time-lapse microscopy demonstrated impairment of fluorescently-labelled P-body proteins. Furthermore, this disruption resulted in P-bodies failing to

associate with RNA stress granules and transferring β-globin mRNA reporter transcripts between compartments during the stress response.

Further co-IP experiments identified a host of mRNA processing proteins that also associated with nesprin-1, including Matrin-3; an abundant nuclear matrix protein involved in a number of key nuclear processes. A novel isoform of matrin-3 localized to P-bodies and was required for miRNA-mediated translational repression. By identifying and tethering matrin-3 P-body localizing domains to a luciferase reporter construct, it was also found that matrin-3 could induce translational repression, which was significantly hampered when a single point mutation (S85C), previously described in a form of autosomal dominant distal myopathy, was introduced.

List of Figures

List of Tables

List of Abbreviations

AChR	Acetylcholine Receptors
Ago	Argonaute
AP-1	Activating Protein-1
ARA	Autosomal Recessive Arthrogryposis
ARCA1	Autosomal Recessive Spinocerebellar Ataxia 1
AMD	ARE Mediated Decay
AMV	Avian Myeloblastosis Virus
ARE	AU-rich-element
ARVD2	Arrythmogenic Right Ventricular Dysplasia Type 2
BAF	Barrier to Auto-Integration Factor
BD	Bipolar Disorder
BPAG1	Bullous Pemphigoid Antigen 1
BRF	Butyrate Response Factor
BSA	Bovine Serum Albumin
CHD	Calponin Homology Domain
β-COP	β-coatomer
C. elegans	Caenorhabditis elegans
Co-IP	Co-Immunoprecipitation
CPG2	Candidate Plasticity Gene 2
CPVT	Catecholaminergic Polymorphic Ventricular Tachychardia
DAPI	4',6'-Diamidino-2-Pheylindoledihydrochloride
DEPC	Diethylpyrocarbonate
DGAP	Developmental Genome Anatomy Project
DGC	Dystrophin-Glycoprotein Complex
D. melanogaster	Drosophila melanogaster
DMEM	Dulbecco's Modified Eagle's Medium
dnKASH	Dominant Negative KASH
DS	Down's Syndrome
ECM	Extra-Cellular Matrix
EDMD	Emery Dreifuss muscular dystrophy
ER	Endoplasmic Reticulum
ES	Embryonic Stem

ESEs	Exon Splicing Enhancers
ESS	Exon Splicing Silencers
F-actin	Filamentous-actin
FBS	Foetal Bovine Serum
GAS2	Growth Arrest Specific-2
GAR	GAS2-Related
GSRP-56	Golgi-Localized Spectrin-Repeat containing Protein-56
GST	Glutathione-S-Transefrase
HDFs	Human Dermal Fibroblasts
Hedls	Human Enhancer of Decapping Large Subunit
hnRNP	Heterogeneous Nuclear Ribonucleoprotein
HP1	Heterochromatin Protein-1
HRP	Horseradish Peroxidase
Htt	Huntington Protein
IF	Intermediate Filament
INM	Inner Nuclear Membrane
IPTG	Isopropyl β-D-1-thiogalactopyranoside
KASH	Klarsicht, ANC-1 and Syne homology
Lamin A precursor	Pre-lamin A
LB	Luria Broth
LCS	Let-7 Complementary Sites
LINC	Linkers of Nucleoskeleton to Cytoskeleton
MACF1	Microtubule-Actin Cross-Linking Factor 1
mAKAP	Muscle A-Kinase Anchor Protein
MAN1	LEM Domain Containing Protein 3
MAP	Microtubule Associated Protein
Matr3-469	Matrin-3-469
Matrin-3C	C-terminal Matrin-3 antibody
Matrin-3N	N-terminal Matrin-3 antibody
MEFs	Mouse Embryonic Fibroblasts
MACF-1	Microtubule-Actin Crosslinking Factor-1
miRISC	miRNA-Induced Silencing Complex
MKS	Meckel-Gruber Syndrome
mRNPs	mRNA-Protein Complexes

MTT	(3-[1]-2,5-Diphenyl Tetrazolium Bromide
MuSK	Muscle Receptor Tyrosine Kinase
NE	Nuclear Envelope
Nesprin	Nuclear Envelope Spectrin Repeat Protein
NMD	Nonsense Mediated Decay
NMJ	Neuromuscular Junction
ONM	Outer Nuclear Membrane
ORF	Open Reading Frame
P-bodies	RNA Processing Bodies
PABP	PolyA Binding Protein
PBS	Phosphate Buffer Saline
PCR	Polymerase Chain Reaction
PD	Plakin Domain
PDE4D3	Phosphodiesterase 4D3
PDI	Protein Disulfide ISomerase
PFA	Paraformaldehyde
PHD	Pleckstrin Homology Domain
PKA	Protein Kinase A
PML	Promyelocytic Leukaemia
pRB	Phospho- Retinoblastoma
PRC1	Protein Regulator of Cytokinesis 1
PSF	PTB-associated Splicing Factor
PTB	Polypyrimidine Tract Binding Protein
PTC	Premature Termination Codons
qPCR	Quatitative PCR
RACE	Rapid Amplification of cDNA Ends
Rb	Retinoblastoma
RBD	RNA Binding Domains
RISC	RNA-Induced Silencing Complex
RT	Room Temperature
RT	Reverse Transcription
RyR	Ryanodine Receptor
SCA2	Spinocerebellar Ataxia Type 2

SDS-PAGE	Sodium Dodecyl Sulfate Polyacrylamide Gel Electrophoresis
SGs	Stress Granules
SH3	src Homology-3
Smg	Suppressor with a Morphogenetic effect on Genitalia
S. pombe	Schizosaccharomyces pombe
SR	Spectrin Repeat
SREBP1	Sterol Response Element Binding Protein-1
SUN	Sad1p-UNC84
TPM2	Tropomyosin-2
TRPV2	Vanilloid Family Type 2
TTP	Tristetraprolin
U2OS	Osteosarcoma
Upf	Up-Frameshift
VCPDM	Autosomal-Dominant Distal Myopathy with Vocal Cord and Pharyngeal Weakness
VSMCs	Vascular Smooth Muscle Cells
ZnF	Zinc Finger

Chapter 1: Introduction

The eukaryotic cytoplasm contains three major types of cytoskeletal filaments: Filamentous-actin (F-actin), microtubules and intermediate filaments. These components provide cells with internal scaffolds which regulate cell shape, cell polarity, cell adhesion and migration, cytokinesis, inter- and intracellular communication, and intracellular trafficking of cellular organelles, vesicles, proteins and RNA [2,3].

Spectrin repeat (SR) containing proteins have been identified as key cytoskeletal scaffolds and linkers [4]. SR proteins not only cross link different components of the cytoskeleton but also scaffold protein complexes and organelles, allowing cells to undergo dynamic re-modelling in response to altered mechanical cues.

Nuclear envelope spectrin repeat proteins, or Nesprins, are the latest family of SR proteins associated with nuclear and cytoplasmic signalling and scaffolding events [5,6]. In this chapter, I will comprehensively review the structural properties that distinguish nesprins from other SR proteins, their rapidly expanding roles in cellular signalling and scaffolding processes, and diseases associated with nesprin mutations.

1.1 Spectrin Repeat super family

The SR super family is composed of a number of SR proteins including α-actinins, α/β spectrins, dystrophins, spectraplakins and the nesprins. All the family members are typically characterized by an N-terminal calponin homology domain (CHD) which binds F-actin, and a rod domain composed of multiple SRs. The SR superfamily are generally distinguished by their C-terminal domains which give the individual proteins a specialized function (Figure 1.1) [4]. Mutations in SR proteins lead to a wide range of diseases, emphasizing their functional importance in multiple tissues (Table 1.1).

1.1.1 α-Actinin

In humans, α-actinin-1, α-actinin-2, α-actinin-3 and α-actinin-4 are encoded by four separate genes [7,8,9]. α-actinins consist of an N-terminal CHD, a central rod composed of four SRs and two C-terminal EF- hands, a 12

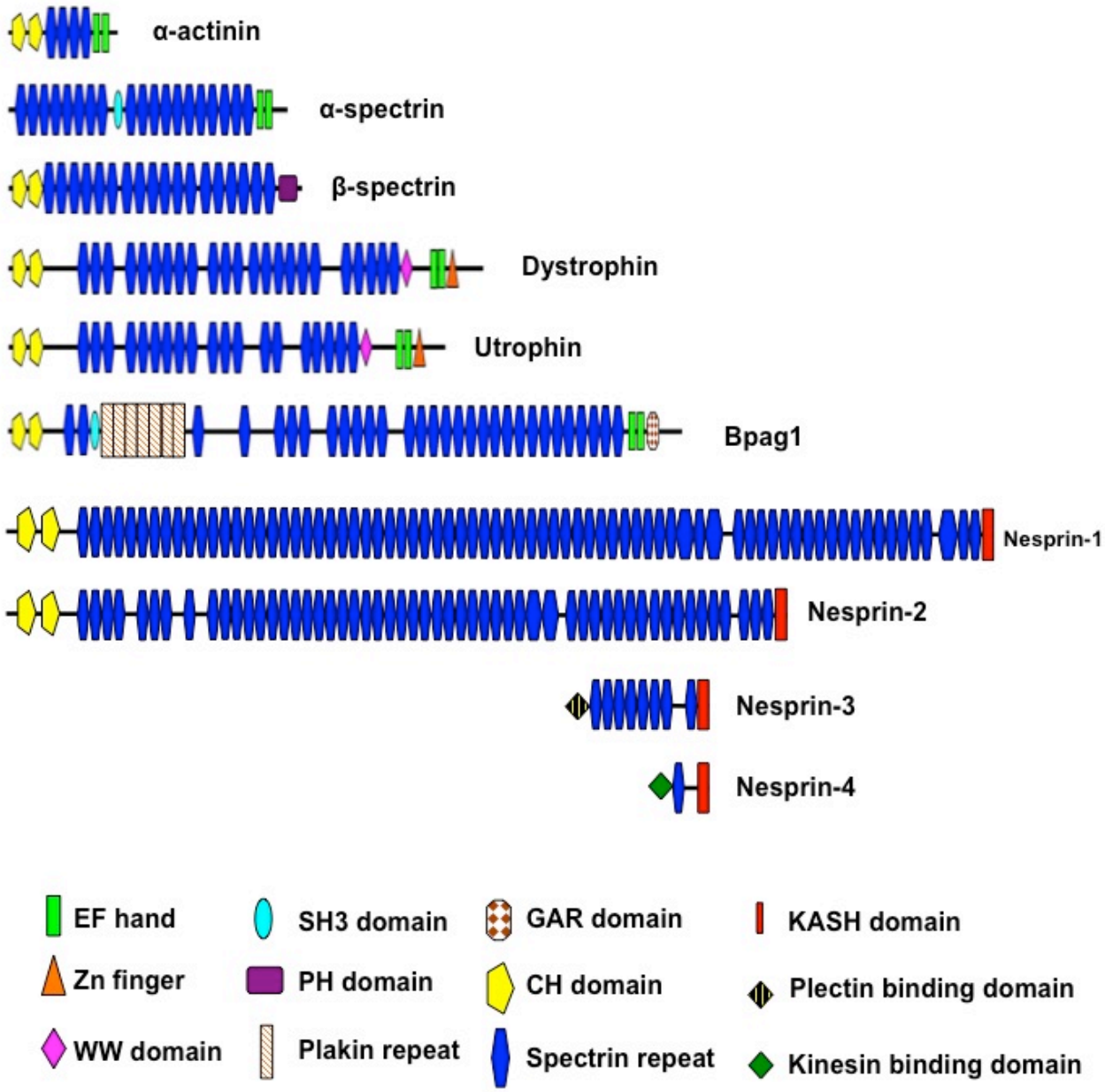

Figure 1.1. The spectrin repeat superfamily. The family of proteins consists of five main subfamilies, the α-actinins, α/β-spectrins, dystrophins, spectraplakins and nesprins. The depicted family members are illustrated to scale to represent their relative sizes.

Table 1.1 Spectrin repeat proteins and human diseases

Disease	Gene	Protein	Phenotype	Ref
Focal Segmental Glomerulosclerosis	*ACTN4*	α-Actinin-4	Renal dysfunction	[10]
Dilated Cardiomyopathy	*ACTN4* *Syne-1*	α-Actinin-4 Nesprin-1	Cardiac dysfunction	[11, 12]
Autosomal Recessive Cerebellar Ataxia	*Syne-1*	Nesprin-1	Impaired limb coordination	[13]
Emery Dreifuss Muscular Dystrophy	*Syne-1* *Syne-2*	Nesprin-1 Nesprin-2	Muscle degeneration, Cardiac dysfunction	[14]
Spinocerebellar Ataxia Type V	*SPTBN2*	βIII Spectrin	Impaired limb coordination	[15]
Hereditary Elliptocytosis	*SPTA1* *SPTB*	αI Spectrin βI Spectrin	Anaemia	[16, 17]
Hereditary Spherocytosis	*SPTA1* *SPTB*	αI Spectrin βI Spectrin	Anaemia	[18, 19]
Hereditary Pyropoikilocytosis	*SPTA1* *SPTB*	αI Spectrin βI Spectrin	Anaemia	[20, 21]
Duchenne Muscular Dystrophy	*DMD*	Dystrophin	Muscle degeneration, Paralysis	[22]

residue helix-loop-helix Ca^{2+} binding domain (Figure 1.1) [23,24]. The α-actinin SRs facilitate their anti-parallel homodimerization, bringing the CHD in close proximity to the EF hands, which may convey calcium-sensitivity to CHD-mediated interactions. α-actinins cross-link actin fibres to the plasma membrane, facilitate cellular migration and are also key structural components of contractile apparatuses in striated muscle sarcomere and smooth muscle dense bodies [25,26,27,28]. Of the SR super family, α-actinins are one of the simplest SR proteins and are believed to be the early evolutionary precursors [29,30,31].

1.1.2 α- and β-Spectrins

As signalling pathways and cellular architecture became increasingly complex, SR proteins evolved into larger, more diverse scaffolds. αI-spectrin and βI-spectrin are the primary components of the human erythrocyte cytoskeleton [32,33,34]. Mutations in these proteins distort red blood cell morphology, leading to a wide range of haematologic disorders. Non-erythrocytic family members αII-spectrin, βII-spectrin, βIII-spectrin, βIV-spectrin, and βV-spectrin provide structural support for the plasma membrane as well as intracellular membranous organelles, such as the Golgi and trafficking vesicles [35,36,37,38]. Both α- and β-spectrins contain a central SR rod, however α-spectrins usually possess two C-terminal EF hands while β-spectrins are characterized by an N–terminal CHD and a C-terminal pleckstrin homology domain (PHD) which facilitates membrane association [39,40]. The α-spectrins are also characterized by a src homology-3 (SH3) motif which serves as a cytoskeletal and signalling protein docking site (Figure 1.1). [41,42]. Similar to the α-actinins, α- and β-spectrins can form anti-parallel heterodimers, which then couple end-to-end to form an actin cross-linking heterotetramer [43,44].

1.1.3 Dystrophins and Utrophins

Dystrophin, and the closely related homologue utrophin are larger SR scaffolds which link the cytoskeleton to the extra-cellular matrix (ECM). The ~430 kDa dystrophin connects the skeletal muscle sarcolemma to the actin

cytoskeleton, sarcomere and basement membrane via interactions with β-dystroglycan, a plasma transmembrane glycoprotein which forms a complex with extracellular laminin-binding α-dystroglycan [45,46]. Utrophin is a ubiquitously expressed dystrophin which can partially compensate for the loss of dystrophin expression [47,48,49]. The two proteins have similar overall structures, with dystrophin containing a greater number of SRs [50] (Figure 1.1).

Unlike the α-actinins and α/β spectrins, the divergent SRs of the dystrophin family do not facilitate dimerization *in vitro* and therefore the dystrophins are not believed to promote actin cross-linking. Instead, the dystrophins anchor the dystrophin-glycoprotein complex (DGC) to actin via their N-terminal CHDs and unique C-terminal WW and Zn-finger motifs. The WW domain consists of two Tryptophan residues separated by 21 amino acids that binds to a conserved *PPPY* sequence in the cytoplasmic C-terminal portion of β-dystroglycan. The Zn-finger and EF hands, both located within a cysteine-rich domain, stabilize the WW interaction with β-dystroglycan (Figure 1.1). The SR rod of dystrophin, but not utrophin, can also directly interact with actin and provides an alternative CHD-independent connection to the cytoskeleton [51,52,53].

1.1.4 Spectraplakins

Spectraplakins were named based on their shared features of both the SR and plakin super families. Members of the plakin super family were originally identified as proteins of the epithelium, which secured keratin based intermediate filaments to desmosomes and hemidesmosomes. The two major spectraplakins in humans are the bullous pemphigoid antigen 1 (BPAG1) and microtubule-actin cross-linking factor 1 (MACF1) [54].

Spectraplakins contain several distinct motifs in addition to the SR rod, CHD and EF hands. A plakin domain (PD) proximal to the N-terminus, contains of four divergent SRs interrupted by an SH3 domain and is necessary for targeting to the hemidesmosome [55,56,57]. Because the majority of plakin superfamily members, such as desmoplakin, envoplakin, plectin, and peri-plakin also contain PDs, they can be considered close

relatives of the SR protein superfamily [57,58]. Plakin repeats, 38 aa motifs organized into a β-hairpin and two anti-parallel α-helices, convey intermediate filament binding to spectraplakins and are also capable of binding to other cytoskeletal proteins such as peri-phillin [59,60,61,62]. Finally, a C-terminal growth arrest specific-2 (GAS2)-related (GAR) domain, which is absent from other plakins and SR proteins, facilitates microtubule bundling (Figure 1.1). [63,64,65]. These domains make spectraplakins master cytoskeletal cross-linkers of microtubules, actin and intermediate filaments.

The dystrophins and spectraplakins were once the largest scaffolding protein family encoded by the human genome, but have now been replaced by the relatively newly identified Nesprins.

1.2 Nesprins

To date, four nesprin genes have been identified in vertebrates; nesprin-1 on chromosome 6q25, nesprin-2 on chromosome 14q23, nesprin-3 on chromosome 14q32.13 and nesprin-4 on chromosome 19q13.12. Full length nesprin-1 and nesprin-2 are giant proteins with molecular weights of ~1000 kDa and ~800 kDa respectively, making them the two largest SR proteins. Nesprin-3 and nesprin-4 are of a more modest size, with molecular weights of ~110 kDa and ~42 kDa respectively [66,67,68,69].

Nesprins differ from other SR proteins as they localize to the nuclear envelope (NE) via their unique C-terminal Klarsicht, ANC-1 and Syne homology (KASH) domains. The N-terminal domains of the nesprins interact with various components of the cytoskeleton and molecular motors, suggesting the primary function of nesprins is to act as a cytoskeletal-NE scaffold [6]. As with the other SR family members, nesprin-1 and nesprin-2 associate with F-actin through a pair of N-terminal CHDs [67]. Nesprin-3 and nesprin-4 differ in their N-terminal domains with nesprin-3 possessing a plectin binding domain which links the NE to the intermediate filament network, while nesprin-4 has a kinesin-1 binding domain which links the NE to the microtubule network [68,69] (Figure 1.1).

Nesprins have been described as multi-isomeric proteins that can generate truncated KASH variants that have the ability to localize on both the inner and outer NE membranes. Furthermore, KASH-less nesprin variants

have been described which localize to sub-cellular compartments beyond the NE, suggesting nesprins are SR proteins with global cellular localizations and functions. The multi-isomeric nature of nesprins will be described throughout the latter sections of this thesis chapter.

1.2.1 Nesprin cytoskeletal binding domains

1.2.1.1 Calponin homology domain

A pair of N-terminal CHDs are present in multiple SR proteins, including those described so far. The CHD is composed of ~100 amino acids that form four α-helices connected by interspersed loops [70,71]. Nesprins and other SR proteins possess two CHDs, designated CHD1 for the most N-terminal motif and CHD2 for the adjacent motif. The tandem arrangements of the two motifs bind F-actin with high affinity, with CHD2 acting as an enhancer binding motif [71,72]. The affinity of F-actin for the CHDs was previously shown to be regulated by alternative splicing, post-translational modifications and through signalling modules like calmodulin in other SR proteins, suggesting that the strength of F-actin binding is variable and tightly regulated [73,74,75,76,77].

The two CHDs of nesprin-1 and nesprin-2 are separated by a 45-50 amino acid Proline and Serine rich region, whilst the CHDs in dystrophin are separated by a 15 amino acid a-helical linker. This suggests the nesprin CHDs may have a higher degree of flexibility in enhancing the spatial versatility of actin binding [78].

1.2.1.2 Plectin binding domain

The N-terminus of nesprin-3 interacts with plectin, a member of the plakin family of cytoskeletal linker proteins. Interestingly, nesprin-3 was initially identified as a binding partner of the plectin CHD in a yeast two-hybrid screen. The nesprin-3 gene encodes for two nesprin-3 variants, nesprin-3α and nesprin-3β. Both variants retain the C-terminal KASH domain, however only the larger nesprin-3α is able to interact with plectin [68]. Plectin is a highly versatile molecule that is able to cross-link the actin cytoskeleton and microtubules with intermediate filaments via its N-terminal CHDs and C-

terminal plakin repeats [79]. The overlapping binding sites for F-actin and nesprin-3 within plectin means that plectin can either associate with F-actin or nesprin-3. As a consequence, plectin can only interact with intermediate filaments when bound to nesprin-3α [80].

The CHD of plectin has high homology to the CHD of MACF-1 and specific neuronal and muscle BPAG1 variants. Therefore, it has been proposed that nesprin-3 may also be able to interact with the CHD of MACF-1 and BPAG1, allowing nesprin-3 to also associate with microtubules in a MACF-1 or BPAG1 mediated manner. The ability of nesprin-3 to act as a cytoskeletal switchboard could allow cells to rapidly change cytoskeletal-nuclear dynamics in response to both intra-nuclear and/or extra-nuclear signals [68,81].

1.2.1.3 Kinesin Binding domains

Over recent years, multiple kinesins have been identified to interact with the SRs of nesprins-1, -2 and -4. The heavy chain subunit of kinesin-1, kif5b was identified as a binding partner for nesprin-4, an epithelial specific nesprin protein [69]. When nesprin-4 was overexpressed in HeLa cells, it induced cell polarization and there was a significant increase in the distance of the centrosome from the nucleus, indicating a possible role in microtubule-dependent nuclear positioning. Kif3b, a subunit of kinesin-2, was identified as a nesprin-1 binding partner when a portion of the central SR rod region of nesprin-1 was used as bait in a yeast-two-hybrid screen. Overexpression of the SRs which associate with kif3b, promoted accumulation of binucleated cells, suggesting a role for nesprin-1 in cytokinesis [82]. More recently, nesprin-1 and nesprin-2 were found to interact with dynein and kinesin-1 motor proteins in the developing mouse brain. Loss of these interactions in double nesprin-1/2- KASH knockout mice uncoupled the centrosome from the neuronal nucleus resulting in severe nucleokinesis and inter-kinetic nuclear migration defects [83]. These findings suggest that other kinesin binding sites may exist throughout the nesprin family, allowing different kinesins to be recruited to the NE using different nesprins variants.

1.2.2 Spectrin repeat rod domain

SRs are composed of triple α-helical bundles with a left-handed twist [84,85,86,87]. These α-helices are characterized by 7 amino acid heptad repeats also found in the less ordered coiled-coil motifs of structural and signalling proteins [88,89]. Multiple SRs combine to form a flexible rod which separates the specialized N- and C-terminal domains of SR proteins. In addition to its functions as a domain spacer, the SR rod scaffolds signalling complexes and can directly interact with cytoskeletal proteins [51,90,91,92,93].

The SR rod domain of nesprins is made up entirely of SRs, forming an almost complete run of unbroken repeats from the N-terminus to the C-terminal KASH domains. Nesprin-1 is composed of 72 SRs, neprin-2 contains 56 and nesprin-3 is made up of 8 SRs, making rod domains which are ~400nm, 300nm and 40nm long respectively. All 8 SRs of nesprin-3 appear to be highly conserved with those of nesprin-1, whereas the majority of SRs in nesprin-2 are highly conserved with those in nesprin-1 [78]. As lower organisms only have one nesprin orthrologue, nesprin-2 and nesprin-3 may have developed during evolution through gene duplication and mutations in nesprin-1.

1.2.3 KASH domain

The KASH domain is the minimal sequence required for targeting nesprins to the NE. The domain is a typical type II transmembrane sequence followed by a C-terminal tail that extends into the NE lumen [94,95]. The KASH domain tail terminates in a conserved *PPPX* motif which binds to the lumenal Sad1p-UNC84 (SUN) domain of the inner nuclear membrane type II transmembrane Sun proteins, and is required for anchoring nesprins to the NE [95,96,97].

1.3 Nuclear Envelope

1.3.1 Structure and function

The nucleus is surrounded by a system of two concentric membranes, referred to as the inner nuclear membrane (INM) and outer nuclear membrane (ONM). Together, these two membranes make up the NE and separate the cells nuclear contents from the cytosol. The highly organized double membrane structures are separated by a ~50nm lumen, perforated by nuclear pore complexes (NPCs) that control protein and RNA trafficking across the NE. Although the ONM and INM are continuous membranes, the macromolecular compositions of the two sides vary. The ONM is continuous with the peripheral endoplasmic reticulum (ER), the primary home of ribosomes and site of protein synthesis. The continuity between the two structures makes it difficult to distinguish whether proteins are ER-associated or NE-associated, however there appears to be a high degree of heterogeneity [98]. Although the giant/full-length nesprins are primarily ONM associated, they are able to localize within the ER boundary when its functional NE spanning complexes are abrogated [99]. However, the INM seems to host a wider range of NE transmembrane proteins, which play roles in linking ONM nesprins and the INM to the underlying nuclear lamina. The nuclear lamina is composed of polymerized lamins which form type-V intermediate filament proteins, or a nucleoskeleton, which provides structural support to the nucleus and a scaffold for nuclear signalling complexes [100,101,102,103]. Conventional cell biological techniques initially only identified ~15 NE transmembrane proteins, including the well characterized Emerin, Sun-domain proteins, Lamin Associated Polypeptides (LAPs), LEM domain containing protein 3 (MAN1), Lamin B Receptor (LBR) and smaller nesprin isoforms, concentrated around the NE [98,104,105] (The individual transmembrane proteins are further described throughout this thesis). However, proteomics analysis of the NE has identified an additional 67 potential transmembrane proteins [106]. Although many of these proteins have yet to be characterized, when 8 of the detected NE proteins were transfected into cultured cells, they all displayed NE localization suggesting

that the other proteins identified through this screen will also prove to be NE proteins [106]. As well as identifying nesprin-1 and -2, multiple proteins contained the conserved LEM-domains, named for its occurrence in the NE proteins LAP2, Emerin, and MAN1 [103]. Twelve of the 67 proteins contained additional functional domains such as phosphatases, acetyltransferases, and glycosyltransferases, suggesting transmembrane proteins with enzymatic activity are located within the INM. Furthermore, extensive proteomic analysis of the INM has shown the NE transmembrane proteome to exhibit some variations amongst different tissues [107]. Tissue specific NE transmembrane proteins suggest the nucleus may scaffold cell-type specific NE-associated protein complexes, which may regulate specific intra-nuclear organization and signalling cascades, consequently explaining the tissue specificity exhibited by many NE-linked disorders.

1.3.2 Nuclear lamina

The type-V intermediate filament proteins which make up the nuclear lamina are composed of polymerized lamin proteins. Lamins can be divided into two classes, 1) A-type lamins; lamin A, lamin AΔ10, lamin C, and lamin C2 are tissue specific lamins generated by alternative splicing of the *LMNA* gene [108,109,110,111]. 2) B-type lamins; lamin B1 and lamin B2 are encoded by the *LMNB1* and *LMNB2* genes respectively, and are ubiquitously expressed [112]. Other components of the lamina include lamin associated polypeptides LAP1 and LAP2, MAN1, Emerin and DNA-binding protein barrier to auto-integration factor (BAF) [113,114,115,116].

1.3.2.1 Lamins and development

The composition of the nuclear lamina is highly dynamic and undergoes extensive re-modelling throughout development in a tissue specific manner. Most cells express at least one B-type lamin at all stages of development [117,118,119]. A-type lamins are absent in early embryonic development, embryonic stem cells and certain stem cell populations in adults and seem to appear at the onset of tissue differentiation [120,121].

Although A-type lamins are not essential for viability, *LMNA* knockout mice exhibit growth retardation 2-3 weeks post-birth, muscular dystrophy at 3-

4 weeks, dilated cardiomyopathy at 4-6 weeks and die at approximately 8 weeks of age [122,123].

The lamin A protein undergoes extensive post-translational modification to become mature lamin A which resides at the NE. The expression levels of one of the processing enzymes, Zmpste24/Face-1, decreases throughout ageing, resulting in the accumulation of a lamin A precursor (pre-lamin A) [124,125]. Pre-lamin A within the nuclear lamina results in cellular senescence associated with changes in gene expression, heterochromatin organization, and failure to effect DNA repair [126,127,128,129].

1.3.2.2 Lamin binding proteins

Lamin A and INM proteins interact with chromatin-associated proteins, including H2A-H2B histone dimers and the non-histone proteins Ha95, Baf and the heterochromatin protein-1 (HP1), which can affect chromatin re-modelling and modulate gene silencing through heterochromatin organization [130,131,132,133]. The multi-molecular complexes associated with the nuclear lamina represent functional platforms at which factors involved in DNA replication, cell survival, and tissue-specific transcription factors can interact to modulate gene expression [131,134].

Specific transcription factors have been shown to interact with nuclear lamina proteins, modulating their activities [135]. Lamin A-LAP2a complexes in the nuclear interior bind the tumour suppressor retinoblastoma (Rb) protein, impairing the expression of E2F-target genes upon cell cycle exit and differentiation. [136,137]. Functional interactions among lamin A/C, phosphorylated-Rb (pRb) and cyclin D3 occur in muscle cell differentiation [138]. In many cases, the nuclear lamina appears to be able to temporarily sequester transcription factors, preventing their binding to target genes [139]. Lamin A/C has been demonstrated to bind c-Fos, which in serum-starved quiescent cells, is retained at the nuclear periphery; upon serum addition c-Fos is released to the nucleoplasm, thus forming together with c-Jun the transcription factor activating protein-1 (AP-1) [140]. Interaction of lamin A with the sterol response element binding protein-1 (SREBP1) appears particularly intriguing, as the transcription factor is involved in multiple

differentiation pathways. Pre-lamin A is able to bind SREBP1 *in vivo* and to negatively regulate SREBP1 nuclear translocation in adipocytes. Therefore, it is thought that pre-lamin A limits the access of SREBP1 to the nuclear interior [141]. The tethering of transcription factors to the NE might aid in fine-tuning pathways that are prone to fluctuations, such as growth factor signalling. In particular, the nuclear lamina might bind and inactivate transcription factors to ensure that no transcription occurs when activating signals are absent [139].

1.3.2.3 The nuclear lamina in cellular signalling

The ability of the nuclear lamina to interact with various transcription factors suggest that lamins can be viewed as signalling modules of the nucleus, which are able to receive signals from the extra-nuclear environment and transduce them within the nucleus.

Lamin A/C has been reported to bind TGF-β induced smads 2/3 and repress TGF-β/smad dependent gene expression [142]. Furthermore, altered signalling via smads occurs in cells bearing mutations in lamin A/C binding partner MAN1. Wild-type MAN1 is able to bind smads and antagonize TGF-β signalling by retaining active smads within the cytosol [115]. Mutant MAN1 leads to enhanced smad signalling, promoting osteoblast differentiation and increased bone density [143].

Rb is an important regulator of cell cycle exit through modulation of the E2F transcription factor. In *LMNA* knockout mice, the Rb pathway is affected and targets of Rb signalling such as MyoD, Desmin and M-cadherin are down regulated [144].

Zmpste24/Face-1 knockout mice accumulate pre-lamin A within the nuclear lamina, making them an ideal model for mimicking an aged phenotype. Hyper activation of the p53 pathway occurs in Zmpste24 knockout mice and is directly linked to premature ageing, since double knockout of p53 and Zmpste24 partially rescues the ageing phenotype [145]. The Zmpste24 knockout mice and the p53 pathway provide a good example of how nuclear signalling pathways change in response to alterations in the nuclear lamina.

1.3.2.4 Nuclear envelopathies and Laminopathies

Nuclear envelopathies or laminopathies are genetic diseases arising from mutations or altered post-translational processing of NE/lamina proteins. The majority of laminopathies are caused by mutations in the *LMNA* gene, with ~410 different mutations identified to date. These mutations manifest in a diverse range of tissue specific pathologies including cardiomyopathies, muscular dystrophy, lipodystrophy, neuropathy, and progeroid syndromes (Table 1.2) [146].

The underlying mechanisms of how mutations in lamina proteins cause laminopathies remain elusive. Defects in the ability of lamins to associate with their binding partners or impairments in the lamin associated signalling pathways described so far may be accountable for the tissue specific nature of laminopathic diseases [146,147,148]. Another plausible explanation surrounding laminopathies is based on the 'structural hypothesis', which involves maintaining the mechanical integrity of the cell through the LINC (linker of nucleoskeleton and cytoskeleton) complex; a transmembrane complex bridging the nuclear lamina to the cytoskeleton (see below) [97]. A 'weakened' lamina, contributing to the overall loss of the cells ability to withstand stress-induced damage would have a significant impact in contracting tissues, such as those which make up skeletal and cardiac muscle [149,150,151]. Furthermore, both lamin A/C-null and emerin-null mouse fibroblasts show impaired mechano-sensitive transduction pathways involving NF-κB–regulated transcription in response to mechanical or cytokine stimulation [150,152,153].

1.4 Nesprins link the nucleoskeleton to the cytoskeleton

1.4.1 The LINC complex

Nesprins associated with components of the cytoskeleton are recruited to the ONM of the NE via their KASH domains. At the NE, the *PPPX* C-terminal peptide sequence of the KASH domain binds to the lumenal domain of the inner nuclear transmembrane Sun proteins to form a double membrane spanning complex [94,95,96,97,154,155]. The Sun proteins in turn interact with components of the nuclear lamina underlying the nuclear interior to form

Table 1.2 Nuclear envelopathies display a range of phenotypes

Disease	Gene	Protein	Phenotype	Ref
Atypical Werner Syndrome	*LMNA*	Lamin A/C	Premature ageing	[156]
Charcot-Marie Tooth Disease	*LMNA*	Lamin A/C	Neurological defects, Muscle wasting	[157]
Dilated Cardiomyopathy	*LMNA* *Syne-1*	Lamin A/C Nesprin-1	Cardiac dysfunction	[158, 159]
Emery Dreifuss Muscular Dystrophy	*STA* *LMNA* *Syne-1* *Syne-2*	Emerin Lamin A/C Nesprin-1 Nesprin-2	Skeletal muscle wasting, Cardiac dysfunction	[14, 160, 161]
Hutchinson-Gilford Progeria	*LMNA*	Lamin A/C	Premature ageing	[162]
Dunnigan-type Familial Partial Lipodystrophy	*LMNA*	Lamin A/C	Lipodystrophy	[163]
Limb-Girdle Muscular Dystrophy	*LMNA*	Lamin A/C	Skeletal muscle weakness, Cardiomyopathy	[164]
Restrictive Dermopathy	*LMNA* *ZMPSTE24*	Lamin A/C Face-1	Growth Retardation, Neonatal death	[165]
Pelizaeus-Merzbacher Disease	*LMNB1*	Lamin B1	Leukodystrophy	[166]
Barraquer-Simons Syndrome	*LMNB2*	Lamin B2	Lipodystrophy	[167]
Greenberg Dysplasia	*LBR*	Lamin B receptor	Skeletal deformities	[168]

a NE membrane spanning complex which joins the cytoskeleton to the nucleoskeleton, referred to as the 'linkers of nucleoskeleton to cytoskeleton' (LINC) complex [154]. Nesprin-1α and nesprin-2β are small nesprin KASH variants that have previously been identified to be embedded within the INM. At the INM, their SRs project towards the nuclear lamina where they are able to strongly interact with lamin A/C and emerin, suggesting they may be integral in proving scaffolds at the INM for transmembrane proteins and the nuclear lamina (Figure 1.2) [14,169]. Specific mutations in lamin A/C and emerin which result in Emery Dreifuss Muscular Dystrophy (EDMD), disrupt interactions with nesprin-1α and nesprin-2β, highlighting the importance of this interaction in muscle diseases [170].

The LINC complex has mainly been characterized to serve three major functions; 1) To anchor the nucleus to the cytoskeleton and govern nuclear positioning, 2) facilitate the transfer of mechanotransductive signals to the nucleus, 3) regulate the organization of cytoskeletal filaments at the NE.

LINCs are evolutionarily conserved, with KASH-SUN partnerships identified in *Schizosaccharomyces pombe (S. pombe), Caenorhabditis elegans (C. elegans), Drosophila melanogaster (D. melanogaster),* as well as vertebrates [154,171,172,173,174,175].

1.4.1.1 Actin LINCs

The most characterized nesprin LINCs are those associated with F-actin, through nesprin-1 and nesprin-2. The actin LINCs mediate the mechanical properties of the entire cell by propagating mechanotransductive signals between the cytoplasm and the nucleus [176]. Uncoupling actin-LINCs by overexpressing a dominant negative nesprin KASH domain (dnKASH) construct or using cells from nesprin-1 KASH domain knockout mice, results in nuclear morphology defects, abnormal localization of skeletal muscle nuclei and defects in strain transmission between the cell and nucleus. Furthermore, uncoupling of the nucleus from the actin cytoskeleton triggers a loss of cellular tension. This loss of tension impacts on maturation of focal adhesions, important macromolecular cell–matrix adhesions that transmit mechanical force and other signals, as well as on cell motility

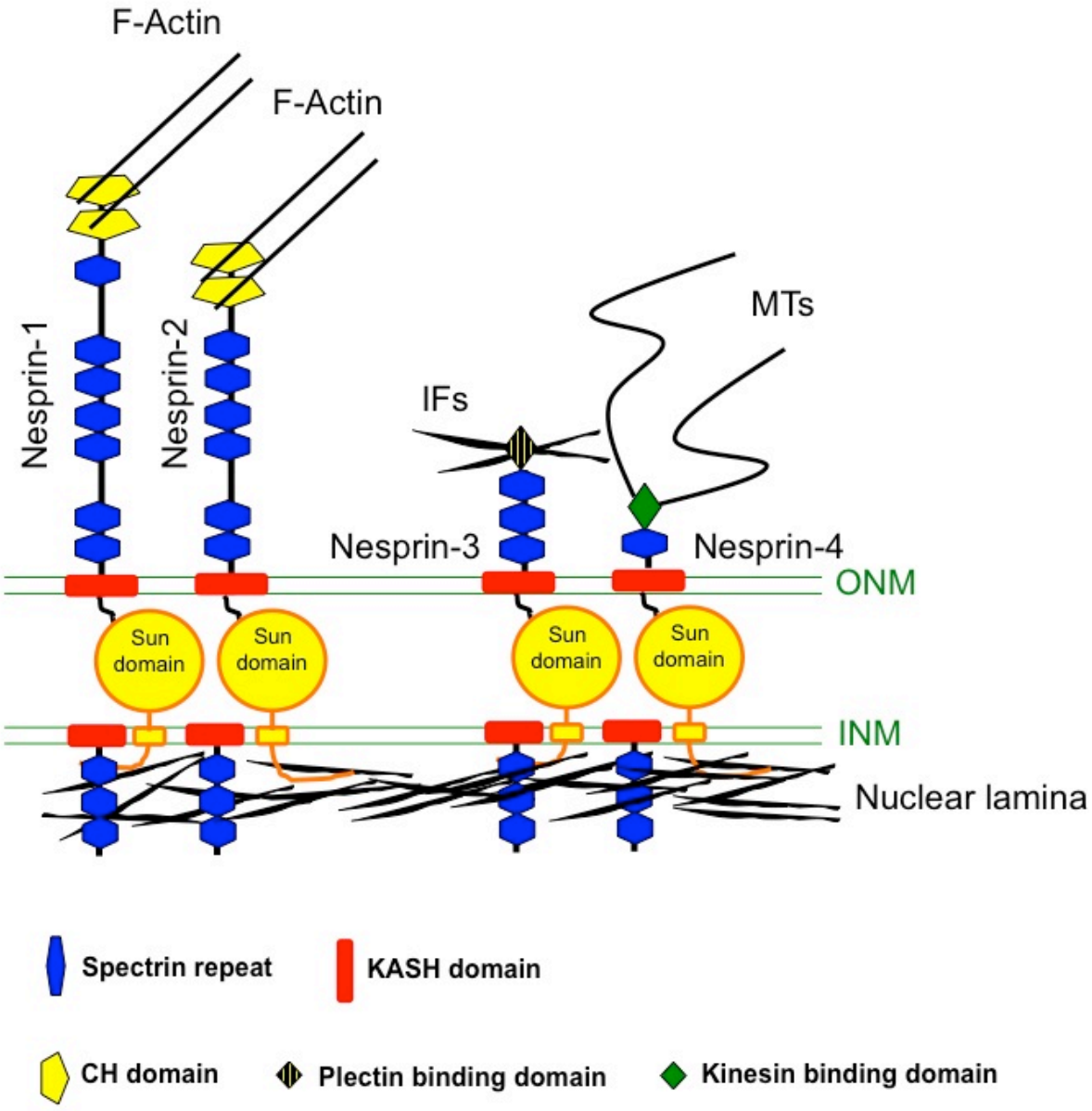

Figure 1.2. Nesprins link the nucleoskeleton to components of the cytoskeleton. The LINC complex couples the nuclear lamina to cytoskeletal networks via the nesprins. The Sun domain containing proteins (Sun1 and 2) on the inner nuclear membrane (INM) bind to the nuclear lamina, via interactions with the lamin proteins, smaller nesprin-1/2 isoforms and other INM transmembrane proteins. The KASH domains of full length nesprins-1, -2, -3 and -4 on the outer nuclear membrane (ONM), associate with the Sun domain within the luminal space and tether the nuclear envelope to cytoplasmic F-actin, intermediate filaments (IFs) or microtubules (MTs).

[159,177,178]. This suggests that nuclear tethering to the actin cytoskeleton may be crucial for F-actin organization throughout the cell.

Recently, the N-terminal SRs of nesprin-3 have been shown to interact with the N-terminal SRs of nesprin-1 and also directly with F-actin [179]. Although the significance of these findings still remain unclear, emerging evidence suggests that nesprin-3 may be a master organizer of the way cytoskeletal networks form around the NE, given its capabilities to interact with all three major cytoskeletal filaments [68,80,180,181].

1.4.1.2 Intermediate filament LINCs

By associating with plectin, nesprin-3 is the only known nesprin which links the nucleus to the intermediate filament (IF) network and forms a connection between the NE and hemidesmosomes [68,182]. Nesprin-3 appears to be central to IF LINC complex function as both plectin and keratins are drawn to the nuclear periphery of keratinocytes overexpressing nesprin-3α [68]. It has been proposed that when F-actin is naturally or experimentally depolymerised, the nesprin-3-dependent re-localization of endogenous plectin to the nuclear periphery may facilitate rapid reorganization of the cytoskeletal structures [68]. In endothelial cells, siRNA-mediated nesprin-3 knockdown resulted in a reduction of plectin and loss of vimentin around the nucleus; promoting increased separation between the centrosome and the nucleus. As a result, nesprin-3 depleted endothelial cells adopted an elongated phenotype and were inhibited to flow induced polarization in a shear stress flow assay [183]. Furthermore, nesprin-3 knockout zebrafish had reduced concentrations of IFs around the nuclear periphery, which did not hamper embryonic development, viability or fertility of the fish [80]. Studies have demonstrated that IF localization around the nucleus is partially dependent on nesprin-2, therefore compensatory mechanisms may arise in nesprin-3 deficient zebrafish and provide an explanation as to why no phenotype is observed [184].

1.4.1.3 Microtubule LINCs

By connecting the nucleus to the microtubule network, nesprins form

microtubule motor LINCs with the centrosome that help govern cell polarity and cytokinesis. As described before, kinesin binding domains have been identified in nesprins-1 and -4 [69,83]. With nesprin-3 also having the potential to interact with microtubules via associating with MACF1 or BPAG1, multiple microtubule LINCs could potentially be established [180].

With the four nesprin genes displaying cell/tissue specificity to a certain degree, it is likely that different specialized microtubule LINCs are established to meet the cells needs. For example, nesprin-4 is only expressed in specialized secretory epithelial cells where it is thought to be essential for establishing centrosome positioning and cell polarity [69]. On the other hand, nesprin-3 is more ubiquitously expressed and the LINCs it establishes may be dependent on the availability of plectin, MACF1 and BPAG1 [68]. The larger nesprin-1 and nesprin-2 proteins are enriched in muscle and could play a role in cross-linking CHD bound F-actin to SR bound microtubule motors [185].

1.4.2 Functions of LINC complex

To date, the functional and structural purposes of the LINC complex have been studied in depth using dominant negative over expression constructs and nesprin, Sun-domain and lamin animal models to uncouple cytoskeletal-nuclear lamina interactions.

1.4.2.1 Nuclear anchorage and positioning

The dynamic nature of cytoskeletal filament associations and scaffolding functions which other SR proteins provide with respect to the cytoskeleton, suggest that nesprins may play a role in nuclear anchorage. The early insights into the cytoskeletal-nuclear coupling came from studying the LINC complex in lower organisms such as *C. elegans* and *D. melanogaster*. In C. elegans, the nesprin-1/2 orthologue, ANC-1, is critical for actin-dependent nuclear positioning in muscle cells during development [186]. Mutations in the Sun1 orthologue, UNC-84, similarly resulted in defective nuclear migration and anchoring [187]. In nesprin-1 KASH domain knockout mice, but not nesprin-2 KASH domain knockout mice, nuclear anchorage of

synaptic nuclei at the neuromuscular junction in skeletal muscle is severly disrupted [177,188].

Recent studies in mouse and human fibroblasts expressing dominant-negative LINC complex components or lacking specific nesprin, lamin A/C, emerin or SUN proteins have reported defects in centrosome attachment to the nucleus. In scratch-wound assays, the initial cell polarization towards the wound fails to occur, and the subsequent migration of cells into the wound is impaired [83,189,190,191,192]. Nesprin-1 knockdown, prevents the reorientation of endothelial cells in response to cyclic strain and causes a decrease in endothelial cell migration in a scratch-wound assay [193].

1.4.2.2 Mechanical stiffness

The nucleus is responsible for the majority of the mechanical stiffness of a cell, therefore defects in nuclear anchorage to the cytoskeleton impact nuclear strength [194,195]. *LMNA*$^{-/-}$ mouse embryonic fibroblasts (MEFs) put under mechanical stretch and unconfined compression showed a significant reduction in mechanical stiffness, with their nuclei spontaneously bursting post-compression [150,152]. Furthermore, C2C12 myoblasts expressing dnKASH constructs had similar mechanical instability to the *LMNA*$^{-/-}$ null MEFs, and endothelial cells depleted of nesprin-1 were more susceptible to nuclear deformations upon cyclic stretching [96,196].

1.4.2.3 Mechanotransduction

Mechanotransduction is the ability of cells to respond to mechanical stimulation by activating mechano-sensitive genes through specific signalling pathways. Originally, altered nuclear mechanics and impaired expression of the mechano-sensitive genes, *Lex-1* and *Egr-1* in response to cyclic strain [109] were identified in *LMNA*$^{-/-}$ and *STA*$^{-/-}$ (gene encoding emerin) MEFs [148,152,153]. However, since lamins A/C can also regulate signalling pathways by directly interacting with transcription factors, it remains unclear whether the observed mechanotransduction defects result from impaired nucleo-cytoskeletal coupling, or simply a loss of biochemical interactions between transcription factors and the nuclear lamina. Recent experiments in which the LINC complex was disrupted with dnKASH constructs without

affecting lamin A/C or emerin levels suggest the latter, as the mechanically induced expression of *Lex-1* and *Egr-1* was not significantly different from control cells, in spite of dramatically reduced nuclear deformations in the LINC complex-disrupted cells [197].

Using a C2C12 inducible *in vitro* model of muscle differentiation, the mechanotransductive properties of the LINC complex have been studied in muscle cell differentiation. C2C12 myoblasts normally differentiate into multi-nucleated myotubes within 5 days of culturing in muscle cell differentiation media, a process which can be inhibited by cyclic strain. However when cyclic strain was applied to C2C12 myoblasts expressing dnKASH, myotube formation was induced. Levels of MyoD and myogenin, two major transcription factors that drive myogenesis, were substantially elevated in dnKASH mechanically stressed cells compared to control stressed cells one day after cyclic strain application in muscle cell differentiation media [198,199,200]. This data suggests that the LINC complex mediates mechanotransduction of myogenic transcription factors during myogenesis and plays an important role in muscle physiology.

1.4.2.4 Intracellular force transmission

Micro-needle biophysical assays have recently been used to identify the LINC complex as the major force-transmitting element between the cytoskeleton and nucleus. Disruption of the LINC complex using a dnKASH construct resulted in defective organization of F-actin and IFs around the nucleus, promoting impaired intracellular force transmission, measured by the length of cytoskeletal and nuclear displacements through passing a micro-needle along the cell [197]. As a result, cells expressing dnKASH had severe functional defects in cell polarization and migration, which may explain why nesprins are critical in nuclear positioning.

1.5 Nesprins and disease

Over recent years the importance of the LINC complex in cytoskeletal organization, mechanical stiffness and signalling pathways has become apparent. Importantly it has been implicated in a wide range of disease

phenotypes, many resulting from mutations in the nesprin genes. These diseases include cardiac and skeletal muscle defects in Emery Dreifuss muscular dystrophy, dilated cardiomyopathy, cerebellar defects in autosomal recessive spinocerebellar ataxia 1, tendon contractures in autosomal recessive arthrogryposis and bipolar disorder (Table 1.3) [13,14,159,201,202].

1.5.1 Emery Dreifuss Muscular Dystrophy

Emery Dreifuss muscular dystrophy (EDMD) is a heterogeneous late-onset disease involving skeletal muscle wasting and heart defects. Initially, mutations in the *STA* and *LMNA* genes were identified as the underlying cause for EDMD. Multiple mutations have been identified in *STA* and *LMNA* that result in EDMD phenotypes, with the severity of the disease varying between mutations [160]. More recently, four heterozygous missense mutations were identified in nesprin-1 and nesprin-2 when performing DNA screens on patients with EDMD or EDMD-like phenotypes (Table 1.4). Fibroblasts from these patients exhibited nuclear morphology defects, mislocalized emerin and Sun-2, and impaired nesprin/emerin/lamin binding interactions, suggesting that defects in the LINC complex in these patients may be an underlying cause of EDMD. siRNA-mediated knockdown of nesprin-1 or nesprin-2 in normal fibroblasts reproduced the nuclear morphological changes and mislocalization of emerin and Sun-2 observed in patient fibroblasts [14]. Later studies demonstrated that one of the nesprin-1 mutant-derived EDMD primary fibroblast cells were less adhesive, migrated slower in a wound healing assay and were more susceptible to senescence [203].

Nesprin-1 KASH domain or C-terminal SR knockout mice generally have reduced survival rates, growth retardation, muscle pathologies and cardiac conduction defects, mimicking an EDMD phenotype [159,177]. Nesprin-2 KASH knockout mice have no obvious phenotype, however nesprin-1 and nesprin-2 KASH double knockout mice develop motor neuron innervation defects and die shortly after birth due to respiratory failure [188]. The cause of the respiration failure and lethality associated with the double knockout mice remains unclear but may be due to an unknown cellular

Table 1.3 Nesprin mutations resulting in disease

Disease	Gene(s)	Phenotype	Ref
Emery Dreifuss Muscular Dystrophy (EDMD)	*Syne-1* *Syne-2*	Muscle degeneration, Cardiac dysfunction	[14]
Autosomal Recessive Spinocerebellar Ataxia 1 (ARCA1)	*Syne-1*	Impaired limb coordination	[13]
Autosomal Recessive Arthrogryposis (ARA)	*Syne-1*	Bilateral clubfoot, Joint contractures, Motor neuron defects	[201]
Bipolar Disease	*Syne-1*	Manic depression, Mood swings	[202]

Table 1.4 Nesprin-1 and Nesprin-2 EDMD mutations

Nesprin Variant	DNA variation	Amino Acid Exchange
Nesprin-1α_1	966G>A	R257H
Nesprin-1α_1	1910G>T	V572L
Nesprin-1α_1	2132G>A	E646K
Nesprin-1α_2	466C>T	T89M
Nesprin-1β_1	29A>G	5UTR
Nesprin-2α_2	525G>A	5'UTR

function associated with the two nesprin proteins, such as defects during the development of the central nervous system.

1.5.2 Cardiomyopathies

Mutations in *LMNA* and nesprin-1 have been identified in severe cardiac conduction diseases called cardiomyopathies. A patient with a missense mutation near the KASH domain of nesprin-1 developed severe dilated cardiomyopathy (DCM) requiring cardiac transplantation. Fibroblasts from this individual had increased expression of nesprin-1α and lamins A and C, indicating changes in the nuclear membrane complex [12]. These findings mirror what has been described from lamin A/C mutations, suggesting the importance of an intact nuclear lamina and LINC complex for a normal functioning heart.

1.5.3 Autosomal Recessive Cerebellar Ataxia 1

Five nesprin-1 mutations have been identified in patients suffering from autosomal recessive cerebellar ataxia (ARCA1), providing the first link between nesprins and neurological diseases (Table 1.5) [13]. ARCA1 is characterized by neurological abnormalities such as irregular gait and lack of limb coordination, without the nuclear morphology defects characteristic of laminopathies. Interestingly, 3 out of the 5 mutations result in premature termination codons, suggesting that these patients have impaired nuclear anchorage to the actin cytoskeleton. In supports of this theory, neurological defects were observed in nesprin-1 and nesprin-2 double knockout mice which developed motor neuron innervation and died shortly after birth, as described above [188].

1.5.4 Autosomal Recessive Arthrogryposis

A myogenic form of autosomal recessive arthrogryposis (ARA) has been identified in a family spanning two generations. Clinical symptoms of ARA include bilateral clubfoot, multiple joint contractures, delay in motor milestones followed by progressive motor decline after the first decade. A genome wide screen in the ARA family line has indicated an A to G mutation in a splice acceptor site, resulting in retention of intron 136 of nesprin-1 [201].

Table 1.5 Nesprin-1 ARCA1 mutations

Syne-1 gene mutation	Exon or Intron	Protein change in nesprin-1 giant
247012 A>T	Exon 56	R2906X
306434 A>G	Intron 81	Premature stop at 5244
310067 A>G	Intron 84	Premature stop at 5402
334338-334342 Deletion ATTTG	Exon 93	Premature stop at 5880
426494 C>T	Exon 126	Q7640X

As with some of the ARCA1 mutations, this mutation produces a premature termination codon, resulting in nesprin-1 variants that lack the KASH domain. Thus, the production of truncated nesprin-1 KASH variants appear to result in two distinct human disease phenotypes, myopathic or neurological, a feature similar to that found in laminopathies [204,205].

1.5.5 Bipolar disorder

The Psychiatric Genome-Wide Association Study Consortium Bipolar Disorder group, performed a genome wide screen from 7481 bipolar individuals and 9250 control individuals. The screen identified a conserved single nucleotide polymorphisms within intron 16 of the nesprin-1 gene [202]. Although this mutation should have no significant effect on the functionality of nesprin-1 LINCs due to the position of the mutation within an upstream intron, it may effect the production of nesprin-1 isoforms generated through alternative transcription (See 1.6).

1.6 Nesprin Isoforms

The majority of nesprin research so far has primarily focused on how disruption of NE nesprins alter LINC complex functionality. However, immunofluorescence microscopy studies using antibodies targeting the different domains of the nesprin-1 and nesprin-2 giants suggest that nesprins localize to multiple sub-cellular compartments in a tissue specific manner [66,188,206,207,208]. Furthermore, multiple nesprin mRNA transcripts have been identified which transcribe a wide collection of tissue specific nesprin isoforms (Figure 1.3). Of these isoforms, many terminate to produce KASH-less nesprins that localize and have probable functions beyond the NE.

1.6.1 Nesprin isoforms and muscle

Immunofluorescence microscopy has localized nesprin-1 and nesprin-2 isoforms to the cardiac and skeletal muscle sarcomere Z-lines, suggesting they may be important in muscle cell function [66,67,206,209]. Interestingly, nesprin-1 has been described as both increasing and decreasing at the NE of differentiated myotubes *in vitro*, with accompanying re-localizations to the

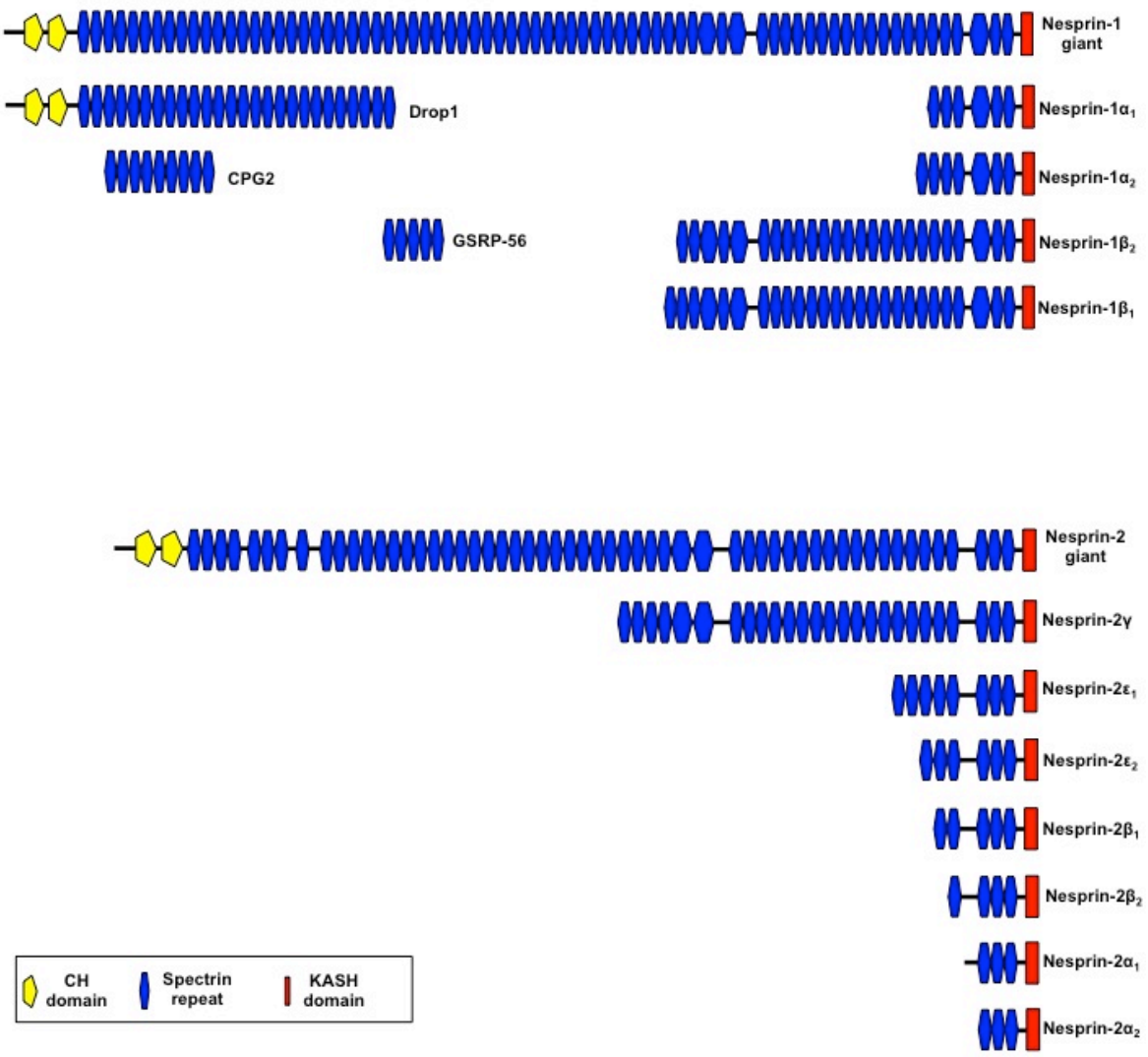

Figure 1.3. Nesprin variants generated through alternative transcription. A) Published nesprin-1 variants generated by alternative initiation and termination. B) Published nesprin-2 variants generated by alternative initiation and termination.

nuclear matrix, when compared to undifferentiated mouse C2C12 myoblasts [66,209]. In hindsight, nesprin-2 re-localizes from the NE and intranuclear speckles to the sarcomere of differentiated myotubes [206]. Despite slight variances in staining, which may be due to isoform variation between the cell lines examined in each study and the epitopes chosen for antibody production, the results support the idea that nesprins are important muscle regulatory proteins and that different isoforms may serve different functions during muscle development.

1.6.1.1 Nesprins and calcium signalling in striated muscle

To date, two muscle-specific nesprin isoforms have been identified; nesprin-2α_1 and nesprin-1α_2 [206] (Unpublished data Professor Shanahan laboratory, King's College London). SRs within nesprin-1α_2 binds to muscle A-kinase anchor protein (mAKAP), a striated muscle Ca^{2+} and cAMP signalling regulator. Overexpression of dominant negative nesprin-1α_2 displaces mAKAP from cardiomyocyte nuclei *in vitro*, demonstrating that nesprin is essential for mAKAP localization to the NE [210]. mAKAP forms a cAMP signalling complex with several co-factors, including Ca^{2+} ion-channel ryanodine receptor (RyR), protein kinase A (PKA), and phosphodiesterase 4D3 (PDE4D3) [91,211,212,213]. Similarly, a region within the nesprin-2α_1 SR rod binds cardiac RyR, indicating that both nesprin-1 and nesprin-2 could stabilize the mAKAP complex at the NE (Unpublished data-Professor Shanahan laboratory, King's College London).

Although no diseases have been directly attributed to mAKAP dysfunction, mutations in human cardiac RyR give rise to catecholaminergic polymorphic ventricular tachychardia (CPVT) and arrythmogenic right ventricular dysplasia type 2 (ARVD2), often responsible for sudden cardiac-related mortality [214]. Similarly, targeted disruption of mAKAP by mutation or siRNA-mediated knockdown promotes cardiac hypertrophy, a stress-inducible remodelling of the heart which can lead to severe complications and death [211,212]. These results indicate that cardiac-enriched nesprin isoforms, such as nesprin-1α_2 and nesprin-2α_1, may play a key role in the progression of these diseases.

1.6.1.2 Nesprins and the neuromuscular junction

Evidence for the importance of nesprins in skeletal muscle function comes from its enrichment in the postsynaptic myonuclear envelopes of the neuromuscular junction (NMJ), the synapse between motor neurons and skeletal muscle fibres [215,216,217]. Endogenous nesprin-1 is displaced from the NMJ myonuclei of transgenic mice over-expressing a dominant-negative nesprin-1 KASH domain, impeding nuclear migration to the NMJ [218]. Comparable results were seen in nesprin-1 KASH knockout mice, which exhibit abnormal skeletal myonuclear clustering, loss of synaptic nuclear aggregation and motor neuron branching defects. As nesprin-2 KASH knockout mice did not display these defects and were grossly normal, it appears that nesprin-1 and nesprin-2 have distinct functions in muscle and other tissues [188]. Nesprin-1α binding partner, skeletal muscle receptor tyrosine kinase (MuSK), is necessary for the clustering of acetylcholine receptors (AChR) at the NMJ, and therefore plays a key role in synaptic function [215,216,217]. Similar to MuSK knockout mice, double nesprin-1 and nesprin-2 knockout mice suffocate and die peri-natally due to neuromuscular defects that have not yet been characterized, indicating that disruption of the MuSK-nesprin-1 interaction as well as nuclear migration could negatively affect NMJ formation [188,219].

1.6.2 Nesprin-1 isoform CPG2

Given their roles in the regulation of the post-synaptic NMJs, it is not surprising that nesprins also play an important part in neuronal functions. Novel nesprin-1 isoform, candidate plasticity gene 2 (cpg2), was first identified as a gene which contributed to long term plasticity, the ability of neurons to stably alter their phenotype in response to various stimuli such as glutamate receptor activation and exposure to light [220,221]. ICC and electron microscopy using monoclonal anti-cpg2 (nesprin-1 giant amino acids 1315 to 1334), localized the brain-specific isoform to the cytosol, ER and postsynaptic endocytic zone surrounding dendritic spines *in vitro*, suggesting that cpg2 could play a role in the clathrin-mediated uptake and recycling of chemokine receptors [222]. In agreement with this function, knockdown of cpg2 led to an

increase in the number of post-synaptic glutamate receptors with a concomitant increase of clathrin coated vesicles within dendritic arms, indicating that cpg2 is necessary for receptor internalization and vesicle clearance [222]. Interestingly, knockdown of cpg2 decreased spine size, suggesting that nesprin-1 also regulates dendritic spine structure and morphology.

1.6.3 Nesprin-1 and Golgi

1.6.3.1 Novel Golgi-localized region GSRP-56

A 56 kDa Golgi-localized spectrin-repeat containing protein (GSRP-56) nesprin-1 isoform, was originally identified in a yeast-2-hybrid screen as a novel binding partner for transient receptor potential cation channel, vanilloid family type 2 (TRPV2) [208]. Endogenous GSRP-56 was detected and labelled the Golgi apparatus in myoblasts, myotubes, and primary cardiomyocytes. When ectopically expressed in HEK293 cells, GSRP-56 formed large aggregates that surrounded the Golgi apparatus and induced Golgi area expansion, suggesting GSRP-56 may regulate Golgi structure [208]. Although GSRP-56 function has been investigated, its association and function with TRPV2 still remains elusive.

1.6.3.2 Nesprin-1 contains multiple golgi binding regions

In addition to GSRP-56, multiple Golgi localizing domains have been identified in nesprin-1. Nesprin-1 was initially localized to the Golgi by Immunofluorescence microscopy using a cross-reacting erythrocyte spectrin β1 antibody [223]. Two Golgi-binding regions, one with low affinity (nesprin-1 giant amino acids 4606 to 4945) and one with high affinity (nesprin-1 giant amino acids 5015 to 5410) were later mapped. Expression of the high-affinity region disrupted cytoskeletal links to the Golgi, causing the Golgi to collapse. Nesprin-1 Golgi localization was later confirmed by immunofluorescence microscopy using three distinct nesprin-1 specific polyclonal antibodies. Interestingly, antibody SN357-2 (nesprin-1 giant amino acids 1675 to 1688) labelled only the Golgi, while the remaining two antibodies, SN119/120 (nesprin-1 giant amino acids 5862 to 5875) and anti-nesprin-1 (nesprin-1 giant

amino acids 4606 to 4945), additionally labelled the nuclear matrix, indicating that other nesprin-1 isoforms exist which include the Golgi localizing SRs [223]. An additional Golgi-affecting nesprin-1 fragment, GSSF1 was identified upstream of the Golgi-binding sites [224]. Although GSSF1 does not localize to the Golgi, ectopic expression caused the Golgi to collapse and sequester endogenous nesprin-1 into multiple β-coatomer I (β-COP I) positive vesicles, suggesting GSSF1 acts in a dominant negative manner [224]. The COP I and COP II protein complexes promote the formation of non-clathrin coated vesicles which regulate retrograde and anterograde transport respectively within the Golgi, and also between the Golgi and ER [225]. In line with these functions, GSSF1 and the high-affinity Golgi binding sequence both inhibited retrograde transport of protein disulfide isomerase (PDI) from the Golgi to the ER [224]. The retrograde transport defects observed in cells expressing dominant negative nesprin-1 fragments suggested that these sequences may interact with the microtubule network. A yeast-2-hybrid screen for GSSF1 binding partners identified Kif3b, a subunit of the heterotrimer kinesin II microtubule motor complex [82]. Kinesin II is a ubiquitously expressed motor, involved in anterograde transport of vesicles and protein cargo toward the plus-end of microtubules and is also essential for mitotic spindle formation and chromosome segregation [226,227]. In accordance with these functions, GSSF1 transfected cells both had a significantly higher incidence of binucleated cells, a sign of blocked cytokinesis. Overexpressed Kif3b localized to the Golgi but re-distributed to GSSF1 induced vesicles in co-transfected cells, further indicating that nesprin-1 interacts with the kinesin II complex. Immunofluorescence microscopy using Golgi-staining antibody SN120 co-localized endogenous nesprin-1 and kinesin II to the mitotic spindle midbody, the accumulation of membranes which must be cleaved during telophase to release two daughter-cells [82]. Cells expressing the dominant-negative tail of Kif3b lost SN120 staining from the midbody and also had a higher number of binucleated cells. Finally, both constructs blocked the accumulation of syntaxin-positive membrane vesicles at the midbody, suggesting an essential role for nesprin-1 in microtubule dynamics, vesicle transport and the progression of mitosis [82].

1.6.4 Nesprins and cancer

To date, four separate studies have linked nesprins to a collection of epithelial cancers [228,229,230,231]. The nesprin-1 promoter is hypermethylated and consequently transcriptionally silenced in 95% of colorectal cancer cell lines examined [229]. A separate candidate cancer gene study also identified nesprin-1 as a gene mutated in colorectal cancer cell lines, and nesprin-2 as a gene mutated in breast cancers [230]. Finally, hypermethylation of the nesprin-1 promoter occurred in ~50% of lung cancer cell lines examined in a third study, leading to significant down-regulation of at least four nesprin-1 transcripts [231]. This data suggests that nesprins may be a hallmark of cancer and potential targets for cancer therapy.

1.6.4.1 Novel Nesprin-1 isoform Drop1

A cDNA expression array designed to detect genes which were differentially expressed in epithelial ovarian cancer, identified a novel nesprin-1 isoform, Drop1, as a significantly down-regulated gene, further linking nesprins to cancer [232]. Additional analysis determined that Drop1 expression was substantially reduced in 79% of carcinomas examined, including breast, uterus, cervix, vulva, kidney, thyroid, lung and pancreas. The cause of this decrease in expression is unknown but may be induced by nesprin-1 promoter methylation. Full-length Drop1 is predicted to be ~350 kDa and would contain the nesprin-1 CHDs and a stretch of SRs. However, Drop1 would lack the KASH domain and is therefore not expected to contribute to NE function. Although ectopically expressed Drop1 constructs localized to the cytosol, the specific sub-cellular localization of full-length Drop1 cannot be determined until the entire protein is expressed, or attempts are made to detect the endogenous form using immunofluorescence microscopy with Drop1 specific antibodies [232].

1.6.4.2 Nesprin-2 in Meckel-Gruber syndrome

Meckel-Gruber syndrome (MKS) is a severe recessively inherited developmental disorder that is characterized by dysplasia and developmental defects of the central nervous system [233]. MKS is caused by mutations in

genes that encode components of the primary cilium and basal body, such as MKS1 and Meckelin [234]. The N-terminal SRs of nesprin-2 were identified as Meckelin binding partners [191]. Nesprin-2 antibody, K20-478, designed to target the CHDs of nesprin-2, co-localized nesprin-2 CHD isoforms with mecklein at filopodia prior to the establishment of cell polarity and ciliogenesis. Loss of nesprin-2 CHD isoforms impaired centrosome migration, cell polarization and ciliogenesis in a IMCD3 ciliated-cell model. siRNA-mediated Meckelin knockdown caused a dramatic remodelling of the actin cytoskeleton and mislocalization of nesprin-2 to actin stress-fibres and activation of RhoA signalling [191]. These findings further highlight the important roles of the nesprins during cellular and developmental processes, particularly in centrosome positioning and cell polarity. Furthermore, it stipulates that the actin cytoskeleton and KASH-less nesprin-2 variants that retain the CHDs are required for the early stages of ciliogenesis.

1.6.5 Nesprin-2 scaffolds and regulates ERK 1/2 at nuclear PML bodies

ERK1/2 were identified as novel nesprin-2 binding partners in a yeast-2-hybrid screen when using the N-terminus of nesprin-2β as bait [207]. ERK1/2 signalling is activated in response to extracellular stimuli and has essential roles in proliferation, differentiation, and apoptosis [235]. Using co-immunoprecipitations and various nesprin-2 constructs, a KASH-less nesprin-2β variant was shown to interact with ERK1/2 at nuclear promyelocytic leukaemia (PML) bodies, intra-nuclear foci proposed to anchor and regulate many nuclear functions including DNA replication, transcription, or epigenetic silencing [207,236]. siRNA-mediated depletion of nesprin-2 abolished ERK 1/2 localization from PML bodies and increased ERK1/2 activity, resulting in enhanced proliferation of vascular smooth muscle cells (VSMCs) [207]. This data suggests that KASH-less nuclear nesprin-2β variants negatively regulate ERK 1/2, which could be a novel disruption during atherosclerosis.

1.6.6 Nesprin isoform expressions are highly adaptable

The ability of nesprins to generate a wide range of different variants, many with over lapping domains suggest that nesprin expression patterns

may be highly flexible, with cells being able to change their isoform expression patterns in response to different cellular cues or stimuli to adapt to their needs. For example, nesprin-2 CHD knockout mice display an altered expression pattern for specific nesprin-2 C-terminal isoforms in certain tissues to compensate for the loss of nesprin-2 giant or other nesprin-2 CHD variants [237].

Furthermore, the ability of the nesprin-2 giant to switch expression has become evident in S143F lamin A/C progeria dermal fibroblasts. S143F progeria cells have dysmorphic nuclei containing numerous blebs and lobulations, which progressively accumulate as cells age in culture. Immunofluorescence microscopy showed that the nesprin-2 giant localized in the cytoplasm, whereas emerin was unevenly localized along the NE. However, a subpopulation of mutant cells expressing the nesprin-2 giant isoform failed to show any obvious nuclear morphologies, suggesting that not only is nesprin-2 vital for maintaining nuclear architecture, but more importantly its expression is adaptable in disease and mechanisms exist to signal compensatory expression of certain isoforms [99].

1.6.6.1 Nesprin-1 mediated NE changes during embryonic stem cell differentiation

The luminal space between the INM and ONM of embryonic stem (ES) cells appears to be distinctive and wider than their differentiated counterparts under electron microscopy. ES cells also appear to lack heterochromatin around the nuclear periphery, which is present in differentiated cells. When screening a panel of NE proteins, nesprin-1 KASH variants were the only significantly increased species upon differentiation. Although knockdown of nesprin-1 KASH variants using siRNA did not effect ES cell differentiation, the differentiated cells retained a NE phenotype of that found in undifferentiated ES cells [238]. Therefore, it appears that nesprin-1 KASH variants govern NE luminal size in ES cells and may participate in regulating chromatin organization and gene regulation of differentiated cells.

1.6.6.2 Nesprin expression changes during myogenesis

The ability of the nesprins to not only switch isoform expression of the same gene, but to change nesprin gene expression altogether is particularly evident in muscle. Analysis of nesprins during human muscle development revealed an increase in nesprin-1 giant during early myogenesis *in vitro*. During the transition from immature to mature muscle fibres *in vivo*, nesprin-2 partially replaced nesprin-1 at the NE, with the short nesprin KASH isoforms becoming the primarily dominant variants [185]. Nesprin animals models suggest that nuclear positioning nesprins at the ONM appear to be primarily a function of nesprin-1 in muscle; consistent with nesprin-1 dominating the myonuclear envelope at early stages of myogenesis [159,188]. The dominance of nesprin-2 and shorter nesprin KASH isoforms in mature fibres remains unclear. The general acceptance that small KASH isoforms may be present at the INM where they interact with emerin and lamin A/C suggests they may be required for generating a sturdier LINC complex or be required for scaffolding additional sets of nuclear regulatory proteins to the nuclear lamina for muscle function [169,206,209].

1.7 Thesis aims

In summary, nesprins play a variety of roles within cells as intra-cellular scaffolds and linkers. The scaffolding roles of giant nesprins in LINC complexes have been well studied relative to their KASH-less counterparts. To identify new novel nesprin-1 scaffolding roles and/or nesprin regulated signalling pathways, I set out to:

1. Identify new 5' and 3'UTRs which could generate nesprin-1 variants by alternative transcription.
2. Characterize newly identified nesprin variants using tagged-constructs and antibodies to detect and monitor endogenous expression and localizations.

Chapter 2: Materials and Methods

2.1 Cell work

2.1.1 Cell culture

All cell lines were cultured in a 4% CO_2 incubator at 37°C. Osteosarcoma cells (U2OS) and Human Dermal Fibroblasts (HDFs) were cultured in Dulbecco's modified eagle's medium (DMEM) supplemented with 10% Foetal Bovine Serum (FBS), 1% penicillin/streptomycin and 200 μM L-Glutamine. Human vascular smooth muscle cells (VSMC) were cultured in M199 media complemented with 20% FBS, 1% penicillin/streptomycin and 200 μM L-Glutamine, and passaged at 60-80% confluency.

2.1.2 Cell passaging

Once cells had reached 60-80% confluency, the culture media was aspirated and the cells were washed thoroughly in tissue culture grade phosphate buffered saline (PBS) solution. Cells were then incubated in a small volume of trypsin for 3-5 minutes in the culture incubator at 37°C until they detached from surface. U2OS cells were split 1:10, HDFs 1:3 and VSMCs 1:2 in fresh culture media and allowed to adhere in the culture incubator.

2.1.3 Cell treatments

Cells were counted using a haemocytometer and plated out at medium density the day prior to treatment. The following day, cells were treated with sodium arsenite (0.5 mM), nocodazole (10 μg/ml), cycloheximide (10 μg/ml) or hydrogen peroxide (2 μM) in fresh culture media for one hour. Cells were then fixed in 4% paraformaldehyde (PFA) for staining.

2.1.4 DNA plasmid transfection

Cell were counted and plated out at medium density the day prior to transfection. One well of a 96 well plate, 24 well plate or one well of a 6 well

plate was transfected with 0.5 µg, 1 µg or 2 µg of plasmid respectively, using a 1:2 ratio of plasmid to Superfect transfection reagent as described by the manufacturer (Quiagen). The transfection mix was mixed thoroughly and allowed to stand for 10 minutes at room temperature (RT) while transfection complexes assembled. The transfection mix was then applied to cultured cells for rapid uptake of superfect-plasmid complexes. Two hours post-transfection, cells were washed twice with PBS and replaced with fresh culture media. Transfected cells were cultured for 16-24 hours before fixation or harvesting.

2.1.5 siRNA transfection

Cell were counted and plated out at medium dentistry the day prior to transfection. For 6 wells of a 24 well plate or 2 wells of a 6 well plate, 1.5 µl of siRNA oligo (20 µM stock) was incubated in 500 µl of serum free Optimem with 36 µl of Hiperfect transfection reagent (Quiagen). The transfection mix was mixed thoroughly and allowed to stand for 10 minutes at RT while transfection complexes assembled. During this time cells were washed twice with PBS and supplied with fresh media. The transfection mix was split equally between 6 wells of a 24 well plate or 2 wells of a 6 well plate. The cells were incubated with the oligos for 72 hours followed by fixation or harvesting.

2.1.6 MTT assay

In vitro toxicity was measured using a (3-[4,5- dimethylthiazol-2-yl]-2,5-diphenyl tetrazolium bromide (MTT) based assay. Transfected cells were cultured in media supplemented with 10% MTT reagent for 3 hours. Next, the culture was aspirated off and the resulting formazan crystals were dissolved in MTT solubilization solution, equal to the original culture medium volume. The 96 well plate was then placed on a shaker for 10 minutes to enhance the dissolution of the crystals and spectrophotometrically measure were taken at 570 nm and 690 nm absorbances on a plate reader. 690 nm readings were subtracted from 570 nm readings to eliminate background. Statistical analysis for this and other assays were performed using GraphPad Prism software.

2.1.7 Luciferase

2.1.7.1 CXCR4 miRISC assay

50,000 U2OS cells were plated into each well of a 24-well plate and cultured under standard growth conditions overnight. The following day, 3 wells per experimental condition were transfected with Hiperfect siRNA-plasmid complexes containing 1 µg pRL-TK CXCR4 6x *Renilla* luciferase plasmids, 50 ng pGL3.4 *firefly* luciferase plasmid as an internal loading control, 1 µl CXCR4 siRNA oligo (20 µM stock), and 1 µl of siRNA oligo (20 µM stock) targeting proteins to be knocked down. The transfected cells were incubated under standard growth conditions for 48 hours. Each well was washed with PBS and cells lysed in 100 µl 1x passive lysis buffer. Luciferase readings were analysed according to the Promega Dual-Luciferase Reporter assay manufacturer's instructions. Briefly, *Firefly* activity was measured on a Berthold Mithras LB 940 Luminometer by mixing 20 µl of each lysate with 100 µl of Luciferase Assay Substrate. Next *Renilla* readings were measured in the same manner by adding 100 µl of Stop & Glo reagent to each lysate. Luciferase activity was normalized by dividing *Renilla* readings by *firefly* readings.

2.1.7.2 Endogenous Let-7 miRISC assay

50,000 U2OS cells were plated into each well of a 24-well plate and cultured under standard growth conditions overnight. The following day, 3 wells per experimental condition were transfected with Hiperfect siRNA-plasmid complexes containing 1 µg of either FF4LCS (Let-7 WT) or FFr4mLCS (Let-7 mutant), 50 ng pRenilla, and 1 µl of siRNA oligo (20 µM stock) targeting proteins to be knocked down. The transfected cells were incubated under standard growth conditions for 48 hours and dual luciferase readings were taken as described above.

2.1.7.3 Tethering assay

50,000 U2OS cells were plated into each well of a 24-well plate and cultured under standard growth conditions overnight. The following day, 3 wells per experimental condition were transfected with 1 µg of pRL-TK-globin-boxB, 1 µg pc1-λN-V5 and 50ng pGL3.4 using Superfect transfection reagent.

The transfected cells were incubated under standard growth conditions for 24 hours and dual luciferase readings were taken as described above.

2.2 Microscopy work

2.2.1 Immunofluorescence microscopy

Cells grown on 13 mm glass coverslips in 24-well plates were washed twice with PBS and then fixed with either 4% paraformaldehyde (PFA) for 5 minutes at RT or 1:1 Methanol/Acetone (pre-chilled at -80°C) for 2 minutes at RT. Cells were then washed with PBS and PFA fixed cells were permeabilized with 0.5% NP-40 for 2 minutes at RT, followed by two subsequent washes with PBS. PFA and Mehanol/Acetone fixed cells were then blocked in 1% bovine serum albumin (BSA) solution for one hour at RT. Blocked cells were incubated with primary antibody diluted in 1%BSA for 1 hour at RT in humidifying chambers. Excess primary antibody was washed off with PBS and incubated with suitable secondary antibodies diluted in 1% BSA for 1 hour at RT. Cells were next stained with 4',6'-Diamidino-2-Pheylindoledihydrochloride (DAPI), followed by multiple washes with PBS before being mounted onto slides with Mowiol/Dabco mounting media.

Light microscopy images were captured using an Olympus IX81 microscope with a 20x air, 40x air or x 63 oil objective lenses attached to a Hamamatsu Orca-R2 cooled CCD camera. Volocity software (Perkin Elmer, USA) was used to control exposure times and store acquired images. Confocal images were taken using a filter-free Leica SP5 laser scanning confocal microscope. All confocal images were taken with the 63x oil immersion objective lens. All lasers were used at maximum intensity levels with gain and offset being maintained to prevent image saturation. Z-stacks of 0.37μ were taken throughout the height of the cell and restored using Leica confocal software.

2.2.2 Peptide blocking

Blocking peptides were designed to the antibody epitope of interest and synthesized by Peptide Protein Research Ltd, UK. 10 µg of peptide was incubated with every 1 µg of primary antibody diluted in 1% BSA blocking buffer. The mixture was incubated with constant rotation for 1 hour at RT and then incubated with fixed cells on coverslips for 1 hour at RT. The ability of the peptide to block staining was was determined by immunofluorescence microscopy.

2.2.3 Time-lapse

2.2.3.1 P-body tracking

U2OS cells were transfected into 35 mm Matech dishes using Superfect transfection reagent and imaged on an Olympus IX81 microscope with a 40x LCUPlanFLN 0.6NA objective with additional intermediate magnification of 1.6x, giving a total magnification of 64x. Volocity was used to control timelapse acquisition and images were acquired every 200 ms for 2 minutes using a Hamamatsu Orca-R2 cooled CCD camera set to 2x2 binning (effective pixel size of 0.21 um/pixel) and with an exposure of 30 ms. Image stacks were deconvolved in Volocity using 'fast' (non-iterative) method. P-bodies were detected using a threshold of at least 3 standard deviations from the mean of whole image intensity and with a minimum area of 0.5µm^2 and using a 4um local contrast adjustment. Resultant objects were dilated by 1 pixel and subject to a 3x3 pixel Gaussian filter to remove noise. Touching objects were separated by giving a Volocity a size guide of 5µm^2. Dcp1a-YFP bodies were tracked using a 'shortest path' algorithm with a maximum distance of 1µm between frames. The area centroid of each tracked object was exported as a list of coodrinates and converted to .CEL format in a custom-written Mathematica (Wolfram Research, USA) notebook and .cel files were imported into the Chemotaxis Analysis notebook V1.6 (Professor Graham Dunn laboratory, King's College London) for analysis and statistical comparison. P-body single particle tracking was performed by Daniel Soong, (Light microscope officer for Cardiovascular and Randal division, King's College London).

2.2.3.2 Phase-contrast filming

U2OS cells were transfected in 6 well plates and imaged on an Olympus IX81 microscope with a 10x objective. 3 separate points were identified for filming per well of the 6 well plate with each point being acquired every 2 minutes over a 16 hour time-frame with an exposure of 15 ms. Images were compiled by Volocity to form a movie which was analyzed to measure cell death.

2.3 Nucleotide techniques

2.3.1 RNA extraction and Reverse Transcription

Cells grown in 6 well plates were lysed in 200 µl of Triazole RNA STAT- 60. Total RNA was extracted by incubating lysed cells with chloroform for 5 minutes at RT followed by centrifugation at 10350 g for 15 minutes in a 4°C centrifuge. The aqueous phase was transferred into a fresh RNAase free micro-centrifuge tube and incubated with 100 µl of isopropanol for 5 minutes before pelleting total RNA by a subsequent round of centrifugation at 10350 g for 15 minutes. The RNA pellet was washed with 500 µl of 70% ethanol solution made up with diethylpyrocarbonate (DEPC) treated water and centrifugated at 5280 g for 5 minutes to re-pellet washed RNA. The RNA pellet was finally re-suspended in 20 µl of DEPC treated water and 2 µg was used for reverse transcription using random primers, dNTP mix and Promega Avian Myeloblastosis Virus–RT (AMV-RT). The random primers and RNA were denatured by heating at 95°C for 5 minutes before the reverse transcription was carried out at 42°C for 1 hour. Total cDNA was finally diluted to the required concentration using nuclease free water.

2.3.2 Polymerase Chain Reaction (PCR)

PCR amplifications were performed using 5 µmol of each primer and 500 ng of cDNA obtained from RT or a panel of human tissue cDNA (Origene) with *Taq* PCR master mix kit that contains *Taq*, dNTPs and buffer at 2x concentration. The total content of the PCR reaction was mixed by pipetting

in a thin-walled PCR tube and carried out in a thermo-cycler using the following conditions: Initial denaturation 95°C 1 min, denaturation 95°C 30 seconds*, annealing 55°C 40 seconds*, extension 72°C 1 min per kb*, Final extension 72°C 2 min. (*Repeated for 30 cycles).

PCR reactions to be performed with *Pfu* polymerase contained 1U *Pfu*, 3ul 10x *Pfu* buffer, 1ul dNTP mix (100 mM stock), 1 ug DNA and a final volume of water up to 30 ul. The total content of the PCR reaction was mixed by pipetting in a thin-walled PCR tube and carried out in a thermo cycler using the following conditions: Initial denaturation 95°C 1 min, denaturation 95°C 30 seconds*, annealing 55°C 40 seconds*, extension 72°C 2 min per kb*, Final extension 72°C 10 min. (*Repeated for 30 cycles).

PCR reactions were mixed with 6x DNA loading buffer and separated by agarose gel electrophoresis. PCR products were visualized using UV detection before being purified, cloned into pGEM-T sequencing vector and submitted for sequencing. DNA Sequencing was carried out by Geneservice using primers targeting the T7 and SP6 promoters flanking the multiple cloning site of pGEM-T easy. Returned sequences were blasted against the NCBI human genome and human nucleotide database to identify new novel sequences or screened for mutations.

2.3.3 Rapid Amplification of cDNA Ends (RACE)

Whole brain and HeLa cell Marathon-ready cDNA libraries for RACE were purchased from Clontech. All PCR reactions were carried out using Advantage 2 polymerase in a 50 μl reaction using 250 ng of cDNA and 10 μM of adapter and gene specific primers. Initial round of PCR reactions were performed using the following conditions: Denaturation 94°C 1 min, denaturation 94°C 30 seconds*, anneal/extension 68°C 4 minutes*, Final extension 70°C 10 minutes (*Repeated for 30 cycles). The primary PCR reaction was diluted 1 in 50 and 5ul was taken for secondary PCR reactions with nested adapter primer and nested gene specific primers. Nested PCR was performed in a thermo cycler using the following conditions: Denaturation

94°C 1 min, denaturation 94°C 30 seconds**, anneal/extension 68°C 4 minutes*, final extension 70°C for 10 minutes. (**Repeated for 20 cycles).

Nested PCR reaction products were separated by agarose gel electrophoresis and cloned into pGEM-T for sequencing. Returned sequences were blasted against the NCBI human genome to identify new novel cDNA ends.

2.3.4 Quantitative PCR (qPCR)

Prior to qPCR, primers sets were examined using *Taq* based PCR. Purified products were diluted to create a 0.5 pmol stock which was serially diluted 1 in 10 to create 0.05, 0.005, 0.0005, 0.00005 and 0.000005 pmol standards.

cDNA created from RT was diluted to 100 ng/µl and 900 ng was used for each qPCR reaction. qPCR was performed in a 20 µl reaction containing 1x Sybr green PCR master mix and 5 µmol of each primer. Cycling parameters were 94°C for 15 seconds followed by a single step annealing and extension at 60°C for 60 seconds. Reactions were performed on RotorGene-3000 by Corbett. The cycle threshold (Ct) for each sample was automatically determined to be the first cycle at which a significant increase in optical signal above an arbitrary base line was detected. mRNA expression was quantified using standard curves for each primer set and fold changes were calculated using the delta-delta CT method.

2.3.5 Agarose Gel Electrophoresis

PCR products and restriction enzyme digested plasmid DNA were resolved on 1% to 3% TAE agarose gels. Gels were electrophoresed at 150V until adequate separation of bands was seen. Sample loading buffer, 1 kb and 100 bp DNA ladders were obtained from Promega. To facilitate the visualization of bands by UV transillumination, 50µg of ethidium bromide was supplemented to each gel before electrophoresis.

2.3.6 Cloning

DNA sequences of interest were either directly isolated from plasmids by restriction enzyme digest or amplified from plasmid or cDNA templates by PCR. Bands were extracted from agarose gels using the QIAquick Gel gxtraction kit (Qiagen) according to manufacturer's instructions. Briefly, extracted gel pieces were dissolved by heating gel pieces in 800 µl of buffer QG for 10 minutes at 50°C. The dissolved DNA was captured onto QIAquick spin columns by centrifugation and washed 2 times with Buffer PE. Finally the DNA was eluted by incubating the spin column with 20 µl of elution buffer for 1 minute at RT before collecting DNA through centrifugation.

For sequencing and cloning purposes, *Taq* amplified DNA was ligated directly into the Promega pGEM-T Easy vector. For blunt-ended *Pfu* amplified products, an A-tailing procedure was first performed by incubating purified cDNA with 2x *Taq* PCR master mix at 72°C for 30 minutes.

2.3.6.1 Restriction enzyme digest of plasmid DNA

1 µg of plasmid DNA was digested with 1 unit of each restriction enzyme, 2.5 µl of 10x relevant restriction enzyme buffer and 0.25 µl of 100x BSA made up to 25 µl with water. Digests were performed for 3 hours at 37°C and heat-inactivated by a 20 minute, 65°C incubation when appropriate. Digested products were purified by agarose gel electrophoresis. Extracted destination vectors were treated with 1 unit of Antarctic phosphatase for 30 minutes 37°C and heat-inactivated by a 20 minute, 65°C incubation before T4 DNA ligation reactions with extracted inserts were carried out.

2.3.6.2 Ligation of digested DNA

Ligations were carried out in a final 10 µl volume: 1U T4 ligase, 1 µl 10x ligase buffer, 1-5 µl insert, 1 µl vector and an appropriate volume of water up to 10 µl. Reactions were incubated overnight at 4°C and transformed into chemically competent DH5a or BL21 *E. coli* bacteria. 5 µl of ligation reactions were transformed into *E.coli* bacteria and plated onto LB plates containing suitable antibiotics for selection.

2.3.6.3 Transformation

Competent cells were slowly thawed on ice and incubated with up to 5 μl of plasmid DNA for 20 minutes on ice. Bacteria were then submerged into a 42°C water bath for 40 seconds and then rapidly cooled on ice for 2 minutes. 700 μl of antibiotic-free LB added to each transformation reaction and left to shake in a 37°C incubator for 1 hour for expression of antibiotic resistant genes. 200 μl of the transformation was plated out onto appropriate antibiotic treated LB agar plates and allowed to culture at 37°C overnight for colony formation.

2.3.6.4 LB agar plates

LB (Luria Broth) agar plates were created by mixing 35 g of LB-Agar powder with 1L of double distilled water. The mixture was then autoclaved for purification. Upon cooling, the mixture was supplemented with relevant antibiotics (2 ml of 10 mg/ml Kanamycin or 3 ml of 50 mg/ml Ampicillin) and poured into petri dishes. LB agar plates were stored for up to one month before being discarded.

2.3.6.5 LB media

LB media was created by mixing 20 g of LB powder with 1L of double distilled water. The mixture was then autoclaved for purification. Upon cooling, the mixture was supplemented with relevant antibiotics (2 ml of 10 mg/ml Kanamycin or 3 ml of 50 mg/ml Ampicillin) and stored at 4°C n the dark for up to one month.

2.3.6.6 Plasmid isolation

Single colonies were picked and cultured in 5 ml of antibiotic supplemented LB overnight in a 37°C shaking incubator to obtain small yields of purified plasmid. 3 ml of the culture was used for plasmid isolation using Promega PureYield Plasmid Miniprep System according to the manufacturer's instructions and the resulting 2 ml was used stored as a 15% glycerol stock at -80°C for future use. Briefly, the bacteria were pelted by centrifugation at

maximum speed for 2 minutes. The bacteria were lysed in 100 µl of lysis buffer which was then neutralized by the addition of 350 µl of neutralization solution. The mixture was then centrifuged at maximum speed for 5 minutes at RT to pellet cell debris and the supernatant was poured in a minicoloumn. The plasmid was captured onto a minicoloumn by centrifugation and washed with endotoxin removal solution and a coloumn wash solution. Finally the plasmid was eluted by incubating the minicolumn with 30 µl of elution buffer for 1 minute at RT before collecting the plasmid in a clean eppendorf tube by centrifugation at maximum speed for 1 minute.

For isolation of larger amounts of plasmid, bacteria was cultured in 200 ml of LB overnight in a 37°C shaking incubator and isolated using the Qiagen Endofree Plasmid Maxiprep kit according to the manufacturer's instructions. Briefly, bacteria were pelted by centrifugation at maximum speed for 10 minutes. The bacteria were lysed in 10 ml of lysis buffer, which was then neutralized by the addition of 10 ml of neutralization solution. Plasmid was then separated from cell debris passing the mixture through a filtered syringe. The plasmid containing liquid was next incubated with 2.5 ml of endotoxin removal buffer for 20 minutes on ice before the plasmid was captured and washed through a Quiagen-tip coloumn. The DNA was next eluted in 15 ml of elution buffer and precipitated using 10.5 ml of isopropanol followed by centrifugation as 4000 g or 1 hour at 4°C. The DNA pellet was washed in an ethanol-based wash buffer and re-pelleted by centrifugation at 4000 g for 1 hour at 4°C. Finally the pellet was air dried and re-suspended in 500 µl of TE buffer.

2.3.7 Generation of competent *E. coli* DH5α and BL21

E. coli strains DH5α and BL21 were cultured overnight in antibiotic-free LB at 37°C in a shaking incubator. The culture was diluted 1 in 200 the following morning and cultured for a further 3 hours at 37°C. Bacteria were next pelleted by centrifugation at 1150 g for 10 minutes and re-suspended into 20 ml of sterile ice cold 100 mM $CaCl_2$. The bacteria were then re-pelleted at 1150 g for 10 minutes and once again suspended into ice cold 100 mM $CaCl_2$.

After an additional round of centrifugation, pellted bacteria were stored in 100 μl aliquots as 15% glycerol stock at -80°C..

Competency of bacteria was determined by transforming 0.5 ng, 1 ng, 5 ng and 10 ng of pEGFP-C1 plasmid into 30 μl of competent cells and plating out onto kanamycin resistant LB agar plates. The number of colonies formed from each transformant was determined by dividing the number of colonies by amount of plasmid in μg. Anything > 10^4cfu/μg was deemed competent.

2.3.8 Site directed mutagenesis

In vitro site directed mutagenesis was carried out using QuikChange Site-Directed Mutagenesis Kit (Stratagene) to create specific mutations in DNA plasmid. The QuikChange site-directed mutagenesis is a PCR based method which uses oligonucleotide primers containing the region to be mutated, flanked by ~20 nucleotides either side. The forward and reverse primers are created to be complementary to opposite strands of the vector. The PCR reaction is carried out using 50 ng of plasmid to be mutated, *PfuTurbo* DNA polymerase, 10x *Pfu Turbo* buffer and dNTP mix as described by the manufacturer. Cycling parameters were: Initial denaturation 95°C 1 min, denaturation 95°C 30 seconds*, annealing 55°C 1 minute*, extension 68°C 1 min per kb*, Final extension 68°C 20 min. (*Repeated for 18 cycles). Incorporation of the oligonucleotide primers generates a mutated plasmid containing staggered nicks. Following PCR, the product is treated with *Dpn* I endonuclease (target sequence: 5′-Gm6ATC-3′) which is specific for methylated and hemimethylated DNA and is used to digest the parental DNA template and to select for mutation-containing synthesized DNA. DNA isolated from most *E. coli* strains is dam methylated and therefore susceptible to *Dpn* I digestion. The nicked vector DNA containing the desired mutations is then transformed into XL1-Blue super-competent cells. Colonies containing the mutated plasmid is determined by plasmid isolation and DNA sequencing.

2.4 Protein techniques

2.4.1 Cell lysis

2.4.1.1 Whole Cell lysate

Plated cells were washed twice with PBS and harvested by scrapping cells in RIPA buffer. Suspended cells were vortexed for 10 seconds and left on ice for 10 minutes to lyse. Cell debris was pelleted by centrifugation at 13050 g for 12 minutes in a 4°C centrifuge. The supernatant was transferred to a fresh eppendorf tube and its protein concentration was determined by DCA protein assay. Lysates were diluted and boiled at 95ºC in 4x loading buffer with β-mercaptoethanol for 5 minutes and centrifuged at 4°C at max speed for 30 seconds. Protein lysates were separated by 10% sodium dodecyl sulfate-polyacrylamide gel electrophoresis (SDS-PAGE) and analysed by Western blotting.

2.4.1.2 Nuclear and cytosolic fractionation

Plated cells were washed twice with PBS and harvested by scrapping cells in in an appropriate volume of nuclear fractionation buffer. The cells were collected and incubated on ice for 10 minutes followed by a centrifugation at 845 g for 10 minutes in a 4°C centrifuge to pellet nuclei. The supernatant containing the cytoplasmic fraction was transferred to a fresh eppendorf. The pelleted nuclei were re-suspended in an appropriate volume of RIPA buffer, vortexed, incubated on ice for 10 minutes and centrifuged at 13050 g for 10 minutes in a 4°C centrifuge. The supernatant was collected as the nuclear fraction. The protein concentration for each fraction was determined by DCA protein assay and analysed by Western blotting.

2.4.2 DCA protein assay

Purified BSA at a concentration of 1.48 mg/ml was serially diluted to make standards for the DCA protein assay. 2 µl of lysate or standards were incubated with 25 µl of Bio-rad DC Protein Assay Reagent A for 5 minutes in a 96-well plate. Next each sample was mixed and incubated with 200 µl of

Bio-rad DC Protein Assay Reagent B for 10 minutes in the dark before protein concentrations were determined spectrophotometrically at 710 nm by comparing to BSA standards.

2.4.3 Western blotting

10% resolving gels were created and poured into Biorad gel casting kits for maximum resolution. Once set, 4% stacking gels were poured and 10 or 15 wells were created using appropriate combs. Polymerized gels were sub merged into running buffer and appropriate volumes of denatured proteins were loaded into the wells. Proteins were resolved at 200V until adequate separation was achieved. Resolved proteins were immobilized on PVDF membranes by sandwiching PVDF and SDS-PAGE gel between filter papers soaked in transfer buffer. Transfer was performed via semi-dry transfer apparatus as 25V for 90 minutes. Membranes with immobilized proteins were blocked for 1 hour at RT in 5% milk solution made up with 0.1% Tween in PBS (PBS-T). Blocked membranes were incubated overnight at 4°C with primary antibodies diluted in blocking solution. The following day, membranes were subject to 3x 10 minute washes in PBS-T followed by 1 hour incubation with the appropriate horseradish peroxidase (HRP)-conjugated secondary antibody diluted in 5% milk solution. Excess secondary antibody was washed off membranes with 3X 20 minute washes in PBS-T. Western bands were visualized by ECL chemiluminescent development onto X-ray film or a computer attached to a Fuji LAS4010 developing machine.

2.4.4 Peptide blocking

Blocking peptides were designed to the antibody epitope of interest and synthesized by Peptide Protein Research Ltd, UK. 10 µg of peptide was incubated with every 1 µg of primary antibody diluted in 5% milk blocking buffer. The mixture was incubated with constant rotation for 1 hour at RT and then incubated with the PVDF membrane overnight and blocking was determined by Western blotting.

2.4.5 Protein binding techniques

2.4.5.1 GST pull-downs

E. coli strain BL21 were transformed with pGEX vectors encoding Glutathione-S-Transferase (GST) -fused proteins. Single colonies were cultured in 5 ml of ampicillin LB overnight in a 37°C shaker. The following morning 500 µl of the culture was incubated in 200 ml of fresh ampicillin LB at 37°C for 2 hours in a 37°C shaking incubator. Next, GST-fusion proteins were induced by the addition of 1 mM Isopropyl β-D-1-thiogalactopyranoside (IPTG) to the culture and left to shake at 30°C for 2 hours to induce expression of GST-fused proteins. Bacteria were then pelleted and re-suspended in 5 ml of sterile 1x PBS and 1% triton, followed by a brief sonication. Bacteria were left on ice for 10 minutes to lyse and debris pelleted by spinning bacteria at 13050 g for 15 minutes. The recombinant protein was purified by incubating GST beads with the supernatant for 30 minutes at RT. Expression of recombinant proteins was confirmed by SDS-PAGE and comassie staining or by Western blotting for anti-GST.

Human whole cell lysates were prepared by washing cells in PBS and scrapping cells in an appropriate volume of ice cold co-immunoprecipitation (co-IP) buffer. Cells were left in the buffer for 30 minutes before cell debris was pelleted by centrifugation for 12 minutes at 13050 g in a 4°C centrifuge. GST pull-downs were performed by incubating appropriate volume of GST beads with 200 µg of protein lysate for 4-16 hours at 4°C. The beads were then pelleted by centrifugation for 2 minutes at 100 g in a 4°C centrifuge and washed with 500 µl of IP buffer. The wash step was repeated an additional 3 times before proteins were eluted by boiling beads at 95ºC in 4x loading buffer with β-mercaptoethanol for 5 minutes. Pulled-down proteins were analysed by SDS-PAGE and Western blotting.

2.4.5.2 Co-immunoprecipitation (co-IPs)

Endogenous co-IPs were performed on U2OS cells plated out at medium density. Cells were washed with PBS and extracts were prepared by scraping cells in ice cold co-IP buffer. Cells were left in the buffer for 30 minutes before cell debris was pelleted by centrifugation for 12 minutes at

13050 g in a 4°C centrifuge. The supernatant was pre-cleared with 30 µl of Protein-A or Protein-G sepharose beads for 1 hour at 4°C. Endogenous complexes were obtained by incubating 2 µg of relevant antibody with 200 µg of cell lysate over night at 4°C with gentle mixing. Immuno-complexes were purified by incubating fresh Protein-A or Protein-G sepharose beads with the lysate for 2 hours at 4°C. The beads were then pelleted by centrifugation for 2 minutes at 100 g in a 4°C centrifuge and washed with 500 µl of co-IP buffer. The wash step was repeated an additional 3 times before proteins were eluted by boiling beads at 95ºC in 4x loading buffer with β-mercaptoethanol for 5 minutes. The immune-precipitates were separated by SDS-PAGE and analysed by Western blotting or silver staining using Plus One Silver Staining Kit according to the manufacturers protocol.

2.4.5.3 Proteomics

Bands from silver stained gels were excised and cut into small pieces of about 2 mm using a sterile scalpel. In-gel digestion was performed with trypsin on a robotic digestion system (Investigator ProGest, Genomic Solutions). Peptides were separated by a nanoflow LC system on a reverse phase column (C18 PepMap100, 3 µm, 100 Å, 25 cm; Dionex) and subjected to MS/MS analysis (LTQ-Orbitrap XL, Thermo Fisher Scientific). The spectra were matched against the human database (UniProtKB/Swiss-Prot Release 14.6, 20,333 protein entries). Protein hits with identification probability > 99.0% and at least two unique peptides with identification probability > 95% were selected using Scaffold software (version 2.0, Proteome Software Inc., Portland, OR) and considered for further work. Mass spectrometry was performed by Dr. Xiaoke Yin (Professor Mayr lab, King's College London).

2.4.5.4 Microtubule binding assays

In vitro microtubule binding assays were performed using a Microtubule Binding Protein Spin-Down Assay Kit from Cytoskeleton. GST-purified proteins were prepared as described above and incubated with polymerized microtubules in an eppendorf tube according to the manufacturers instructions. Briefly, microtubules were assembled in eppendorfs by incubating Tubulin

protein with a cushion buffer for 20 minutes at 35°C. After assembly, a general tubulin buffer containing taxol was added to the microtubules to maintain their stability for several hours at RT. Next 5 µg of GST-purified proteins were incubated with microtubules for 30 minutes at RT followed by ultracentrifugation at 100 000 g at RT for 40 minutes. The supernatant containing the unbound fraction was carefully placed into an additional eppendorf and the pelleted microtubules were re-suspended into protein loading buffer with β-mercaptoethanol. The two fractions were analysed by Western blotting using a GST antibody.

2.5 Online bioinformatics tools

The following bioinformatics programs were used to throughout the thesis to analyse the structure and potential functional motifs of nesprin and aid with cloning:

1. NCBI Basic Local Alignment Search Tool (BLAST)
   http://www.ncbi.nlm.nih.gov/BLAST
2. Protein Families Database of Alignments and HMMs (Pfam)
   http://www.sanger.ac.uk/Software/Pfam
3. Eukaryotic Linear Motif analysis (ELM)
   http://elm.eu.org/links.html
4. SMART protein analysis
   http://smart.embl-heidelberg.de
5. Prosite
   http://www.expasy.org/prosite
6. NetPhos 2.0 server
   http://www.cbs.dtu.dk/services/NetPhos
7. PredictNLS
   http://cubic.bioc.columbia.edu/predictNLS
8. fr33 DNA translator
   http://www.fr33.net/translator.php
9. ExPASy Protein Mw calculator
   http://www.fr33.net/translator.php
10. IDT Primer Quest

http://eu.idtdna.com/Scitools/Applications/Primerquest/

11. DNA Sequence Reverse and Compliment
    http://www.cellbiol.com/scripts/complement/reverse_complement_sequence.html
12. NEB cutter V.20
    http://tools.neb.com/NEBcutter2/
13. siDESIGN centre
    http://www.dharmacon.com/designcenter/designcenterpage.aspx
14. UCSC human genome browser 19
    http://genome.ucsc.edu/goldenPath/credits.html#human_credits

2.6 Primer Sequences

All primers were designed between 20-50 nucleotides with a Guanine/Cytosine content of approximately 50% depending on purpose of the PCR. Primers were synthesized by IDT DNA and re-constituted into nuclease free water to create a 100 μM stocks. For each PCR reaction, primers were diluted 1 in 20 to make a 5 μM working concentration. Primer sequences shown throughout this thesis are orientated in a 5' to 3' direction.

2.6.1 RACE primers

For the identification of 5' ends, nested primers were synthesized 1-10 nucleotides downstream of the primer used in the first round of amplifications. For the identification of 3' ends, nested primers were synthesized 1-10 nucleotides upstream of the primer used in the first round of amplifications. Primers used for RACE are recorded in table 2.1.

2.6.2 UTR detection primers

For the identification of 5'UTRs, the forward primer was designed within the 5'UTR and the reverse primer within the second coding exon to control for genomic contamination. For the identification of 3'UTRs, the forward primer was designed within the second to last coding exon and the

reverse primer within the 3'UTR to control for genomic contamination. Primers used for UTR detection are recorded in table 2.2.

2.6.3 Isoform detection primers

The expression of newly identified nesprin-1 isoforms were determined by performing PCR amplifications using a forward primer targeting the 5'UTR and a reverse primer targeting the 3'UTR. Primers used for isoform detection are recorded in table 2.3.

Table 2.1 Primers used for 5'RACE and 3'RACE

	Primer	Nested Primer
N1-3'E14	AGGAAACAGCAAACACGATA	CAACGGAAACTTGAGCAACATAAG
N1-3'E44	AAAACAGACATGGAGAG	ACCGTGGACAAATGGCTGGAT
N1-5'E83	TTCAGCTCTTGCTTCACCAACTTTCCA	TTAGTCTTCACTTTCTCCTGCATGA
N1-3'E90	AGGCCAGCCGGCTGCAGCACAC	CGCCATCCAGCAGTGTAACATCATG
Matrin-3 5'RACE	TGTCTGCGGCAGGAATAGGCC	TCTTGCTGCTGCTACCCAGTCTTT

Table 2.2 Primers used for UTR detection

	Forward Primer	Reverse Primer
N1-3'E14	ACAATCTTGGGATAGAGTGACCTCC	AGTAGGGCTGTTATGCTGCAAGGT
N1-3'E44	TGCCAGCAGTGTGATTGTAACCAG	AGCCTGGGCAACAAGAGTGAAAC
N1-5'E83	GGGTTCCTTTCACTTCACTTCTGT	ACTTCAGCCAACTGAAGGGAGAGT
N1-3'E90	AGTTGGACGTCTCAGTCTCAAGGA	TTTGATGGCTGAGCCCACACAATG

Table 2.3 Primers used for isoform detection

	Forward Primer	Reverse Primer
p56CH^{Nesp1}	GTGCTGCAAAGGCCTGGAATTCAT	AGTAGGGCTGTTATGCTGCAAGGT
p252CH^{Nesp1}	GTGCTGCAAAGGCCTGGAATTCAT	AGCCTGGGCAACAAGAGTGAAAC
p31^{Nesp1}	GGGTTCCTTTCACTTCACTTCTGT	CACAGCCCTCTAAGTGTTGTGTCA
p23^{Nesp1}	TACAGCCTTGCCTATAACAGTCCC	CACAGCCCTCTAAGTGTTGTGTCA
p12^{Nesp1}	TCTGATCTCGGGAAACCTGGAGAA	CACAGCCCTCTAAGTGTTGTGTCA
p50^{Nesp1}	GGGTTCCTTTCACTTCACTTCTGT	TTTGATGGCTGAGCCCACACAATG
p41^{Nesp1}	TACAGCCTTGCCTATAACAGTCCC	TTTGATGGCTGAGCCCACACAATG
p30^{Nesp1}	TCTGATCTCGGGAAACCTGGAGAA	TTTGATGGCTGAGCCCACACAATG

2.6.4 Flag cloning primers

Primers were designed for DNA transcripts to be cloned into pCMV-Tag2 vector which places a Flag sequence at the N-terminus of the translated protein. Primers used for Flag-tag cloning are recorded in table 2.4.

2.6.5 GST cloning primers

Primers were designed for DNA transcripts to be cloned into pGEX4T-3 vector which places a GST tag at the N-terminus of the translated protein. Primers used for GST-tag cloning are recorded in table 2.5.

2.6.6 Primers for qPCR

Forward and reverse primers used in qPCR amplifications were separated by at least 1 exon-intron boundary to control for genomic contamination. Primers used for qPCR are recorded in table 2.6.

2.6.7 Matrin-3 Mutagenesis primers

Site directed mutagenesis primers were designed to be ~40 nucleotides with the sequence to be mutated in the central region of the primer. Primers used for matrin-3 site directed mutagenesis are recorded in table 2.7.

2.6.8 Tethering assay cloning primers

Primers were designed for DNA transcripts to be cloned into pCI-λN-V5 vector which places a V5 sequence at the C-terminus of the translated protein. Primers used pCI-λN-V5 are recorded in table 2.8.

2.7 siRNA oligos

Single siRNA oligos of ~21 nucleotides were designed using siDESIGN centre by Dharmacon with a minimum GC content of 30% and a maximum GC content of 64%. siRNA oligos used are recorded in table 2.9.

Table 2.4 Primers used for Flag-Tag cloning

	Forward Primer	Reverse Primer
p56CH^{Nesp1}	GATATCATGCAGGAGAAAGTGAAGACT	CTCGAGCTACTGGTGTGGGTACCCTGC
p252CH^{Nesp1}	GATATCATGCAGGAGAAAGTGAAGACT	GTCGACTCACATCCTTGAATAACGC
p31^{Nesp1}	GATATCATGCAGGAGAAAGTGAAGACT	GATATCTTACTTTTTAAAGATTATTTT
p23^{Nesp1}	GGATCC ATGGCAGAAGAACAGAAGGAGA	GATATCTTACTTTTTAAAGATTATTTT
p12^{Nesp1}	GGATCC ATGGAATTAGATGCAGCAGTAC	GATATCTTACTTTTTAAAGATTATTTT
p41^{Nesp1}	GGATCC ATGGCAGAAGAACAGAAGGAGA	CTCGAGCTACTGGTGTGGGTACCCTG
p50^{Nesp1}	GATATCATGCAGGAGAAAGTGAAGACT	CTCGAGCTACTGGTGTGGGTACCCTG
p50NT	GATATCATGCAGGAGAAAGTGAAGACT	CTCGAGTCACTGATGCAAAATATATTGT
p50CT	GATATCATGACCCTGCTAGAAGAATCCAAA	CTCGAGCTACTGGTGTGGGTACCCTG
G3	GATATCATGAATGATACAGAAAAGAA	CTCGAGTTACTTGTTGTTAAAGCCCG

Table 2.5 Primers used for GST-Tag cloning

	Forward Primer	Reverse Primer
p50^{Nesp1}	CCCGGGATGCAGGAGA AAGTGAAGACT	CTCGAGTCACAGGGTACCCACACC AGTAGCTCGAG
p50NT	CCCGGGATGCAGGAG AAAGTGAAGACT	CTCGAGTCACTGATGCAAAATATAT TGT
p50CT	CCCGGGGCAGCATCAC ATTTAGAAG	CTCGAGTCACAGGGTACCCACA CCAGTAGCTCGAG
p50SR1	CCCGGGATGCAGGAGA AAGTGAAGACT	CTCGAGTCAGCCTTGCTCTGCT CAACTTCT
p50SR2	CCCGGGACGAGCCAGG AACTCAGCC	CTCGAGTCACTGATGCAAAATATA TTGT
p50SR3	CCCGGGGCAGCATCAC ATTTAGAAG	CTCGAGTCAATCCTTAGCTGCAT CTTGGA
p50SR4	CCCGGGATGAAAAAATTTGA AGCAG	CTCGAGTCACAGGGTACCCACACC AGTAGCTCGAG
Matr3-469	CGCGGATCCATGTCCAAG TCATTCCAGCAGTCATCTCTC	GGGCCCTTAATGAACTCTCACTGG C
Matr3 ZnF1	CGCGGATCCATGTCCAAG TCATTCCAGCAGTCATCTCTC	TCCCCCGGGTTAGTGACTTGCTCC ATTGATATGTTGACTCCA
Matr3 ZnF2	CGCGGATCCCTTGAATCTG AAGATGAGCTACTTGTAGAT	TCCCCCGGGTTAAGTTTCCT TCTTCTGTCTGCGTTCTTC
Matr3 RBD	CGCGGATCCAGTCGTCGATG CCAGCTTCTTCTTGAAATC	TCCCCCGGGTTAAAGCATATTA GGTTCCTGCTCTGTCTGGTC

Table 2.6 Primers used for qPCR

	Forward Primer	Reverse Primer
N1-3'E87	TCTCCAAGCTCAATCAGGCAGCAT	CACAGCCCTCTAAGTGTTGTGTCA
N1-3'E90	AGTTGGACGTCTCAGTCTCAAGGA	TTTGATGGCTGAGCCCACACAATG
N1-KASH	GAGGCAAGTGTAGTCTCTCACAG	AGGGCCATTCGTGTATCTGAGCAT
Lamin A/C	TGAGAACAGGCTGCAGACCATGAA	CAAACTCACGCTGCTTCCCATTGT
Matrin-3	TCGTCGATGCCAGCTTCTTCTTGA	CCTTGCAGGTTTCCATTTCCAGCA
N1-Exon 90	AGTTGGACGTCTCAGTCTCAAGGA	AGAGAGGTAAGCTGGCAACCACAT
GAPDH	CGACCACTTTGTCAAGCTC	CAAGGGTCTACATGGCAAC
MACF-1 GE	CACGAGGTAGAACTAACATTGAACTT	GAAGATGGTTTGGACCTTCG
MACF-1 Inc	GGATGGCCTTGGATGAATTT	GGGAGACTGACTGGAAATCG
MACF-1 Exc	ATGATCCCTGCCGAGCAC	GAAGATGGTTTGGACCTTCG
TPM2 GE	AGCTGAAGGGGACAGAGGAT	GCATCAGTGGCCTTCTTCTC
TPM2 Inc	GGCAAAGTTGGAGAAAACCA	TGGTCCAAGGTCTGGTGAAT
TPM2 Exc	GGCAAAGTTGGAGAAAACCA	GTCCAGTTCCTCGCTAATGG
Importin-β	TCCAGTCTGGCTGAAGCTGCTTAT	AGGTTGTTCTGGTGTCCATCAGGT
DDx5	TCAACAAGAGCGTGACTGGGTTCT	TGGTACTGCGAGCAGTTCTTCCAA
hnRNP A2/B1	ACGGCTACTAAGTTCAGCCAGTCT	TGCTCTACACCCTCAGCTTTCGTT
PCNA	ATCCTCAAGAAGGTGTTGGAGGCA	ACGAGTCCATGCTCTGCAGGTTTA

Table 2.7 Primers used for matrin-3 site directed mutagenesis

	Forward Primer	Reverse Primer
1-833	CAGAAATTAAAGAAATTT TAGAATAAATTGGCAGAAGAACGC	GCGTTCTTCTGCCAATTTATTCTA AAATTTCTTTAATTTCTG
1-798	GACTATGTGATACCTAATAA AGGGTTTTACTGTAAGCTG	CAGCTTACAGTAAAACCCTTTATT AGGTATCACATAGTC
1-567	GAGATGTGTGAAGGTTGACTAGTCT GAGAAATATAAAAAACTG	CAGTTTTTTATATTTCTCAGACTAG TCAACCTTCACACATCTC
1-469	GCCAGTGAGAGTTCATTAATCCC AGAAGTATAAAAGA	TCTTTTATACTTCTGGGATTAATG AACTCTCACTGGC
1-399	GTGGAAACTAGCAGAGTTTAACA CATCATGGATTTTCAACG	CGTTGAAAATCCATGATGTGTTAAA CTCTGCTAGTTTCCAC
1-322	CGTCGATGCCAGCTTCTTTAAG AAATCTACCCAGAATGG	CCATTCTGGGTAGATTTCTTAAAGA AGCTGGCATCGACG
1-288	CATGGACTCTTACCGAAGGGTTAAC CCCATCTGTGCTCTATATG	CATATAGAGCACAGATGGGGTTAA CCCTTCGGTAAGAGTCCATG
S85C	TTCTTCCCATAATTTGCAGTGTA TATTTAACATTGGAAGT	ACTTCCAATGTTAAATATACACTGC AAATTATGGGAAGAA
S85A	TTCTTCCCATAATTTGCAGGG TATATTTAACATTGGAAGT	ACTTCCAATGTTAAATATACCCTGC AAATTATGGGAAGAA

Table 2.8 Primers used for pCI-λN-V5 cloning

	Forward Primer	Reverse Primer
Matr3-469	CGTCTAGAAATGTCCAAG TCATTCCAGCAGTCAT	GCGATCCCGGGTTAAGTT TCCTTCTTCTGTCTGCGT
Rck/p54	CGTCTAGA ATGAGCACGGCCAGAACAGAGAA	GCGATCCCGGGTTAAGGTTTCTCATCT TCTACAGG

Table 2.9 siRNA oligos used for knockdown studies

siRNA	Sequence (5' to 3')
Si-Control	AAACCCUCUGAACAGACGACGUU
Si-83	UGAGUCUCCACCAUUUCUCUU
Si-90	AACACUGCUUGCACCUUCGGCUU
Si-136	UUGGGUUUCGGUACUAUGCA
Si-M3N	GUCAUUCCAGCAGUCAUCUUU
Si-M3C	GCUCCUCCAAGUAGCAAUAUU
Si-CXCR4	GUUUUCACUCCAGCUAACATT
Si-Importin-β	AAUGUCACAAACCCCAACAGC
Si-DDx5	AAGAGGUGGAAACAUACAGAA
Si-hnRNP A2/B1	AACUCUUGACGGCUACUAAGU
Si-PCNA	AAGGGCCGAAGAUAACGCGGA
Si-Matrin-3	Smart pool Dharmacon L-017382-00-0005
Si-Rck/p54	Smart pool Dharmacon L-006371-00-000
Si-GW182	Smart pool Dharmacon L-014107-00-0005
Si-Lamin A/C	siGENOME Lamin A/C Control siRNA D-001050-01-05

2.8 Plasmids

Several plasmids used in this thesis were graciously provided by other researchers and are listed below. Plasmids that were spotted onto blotting paper were soaked in a small volume of nuclease-free water and vortexed vigorously before being transformed into competent bacteria for plasmid isolation. Plasmids kindly provided by other laboratories are recorded in table 2.10.

2.9 Antibodies

2.9.1 Generation of nesprin-1 antibodies

Dr. Qiuping Zhang designed synthetic polypeptides specific to nesprin-1 (table 2.2). Immune Systems Ltd, UK (ILT) conjugated each peptide to keyhole limpet heamocyanin and injected these complexes into rabbits to generate polyclonal antibody sera. The immune sera were affinity purified against a peptide column before use. Unless otherwise mentioned, all antibodies used in this study have been evaluated by epitope-specific peptide block on both western blots and immunofluorescence to test for specificity. Nesprin-1 antibodies, peptide sequences generated against and position of sequence within the nesprin-1 giant are recorded in table 2.11 with peptide sequences present amino acids.

2.9.2 Primary Antibodies

Primary antibodies used throughout the thesis were obtained from different manufacturers. The catalogue numbers and the dilutions used for Western blotting and immunofluorescence staining and summarized in table 2.12.

2.9.3 Secondary antibodies

2.9.3.1 Western blotting secondary antibodies

The HRP-conjugated secondary antibodies used for Western blotting and dilutions are summarized in table 2.13.

Table 2.10 Plasmids obtained from external laboratories

Plasmid	Provider	Reference
pEYFP-C1-Dcp1a	Dr. Kedersha , Division of Rheumatology and immunology, Harvard Medical School, Boston	[239]
pCMV-SPORT6-RFP-Rck/p54	Dr. Wilczynska, Institut André Lwoff, 7 rue Guy Moquet, 94801 Villejuif CEDEX, France	[240]
pDNA3-HA-e4E-T	Dr. Dostie, Dpeartment of Biochemistry and McGill Cancer Centre, McGill University	[241]
pDNA3-HA-eIF4E	Add gene Plasmid 17343	[242]
phrGFP-N1-GW182	Dr. Eystathioy Deprtment of Medicine and Biochemistry and Molecular Biology, University of Calgary	[243]
pEYFP-C1-TTP	Dr. Kedersha	[239]
pFRT-TO-FLAG-GW182-HA	Add gene Plasmid 19883	[244]
pEGFP-C1-MS2	Dr. Kedersha	[239]
pEF-7B-MS2bs	Dr. Kedersha	[239]
pRL-TK- CXCR4 6X	Add gene Plasmid 11308	[245]
pcDNA3.1/NT-GFP--Matrin-3	Dr. Zeitz, Department of Biological Sciences, University at Buffalo, State University of New York	[246]
phRL-GI-5BoxB	Dr. Choe, School of Life Sciences and Biotechnology, Korea University	[247]
pCI-λN-V5	Dr. Choe, School of Life Sciences and Biotechnology, Korea University	[247]
pFF4LCS	Dr. Steitz, Department of Molecular Biophysics and Biochemistry, Yale Medical School	[248]
pFFr4mLCS	Dr. Steitz	[248]

Table 2.11 Nesprin-1 antibodies generated and used in thesis

	Peptide sequence	Nesprin-1 giant amino acids
CH2	LQDKYQSFKHFRVQC	297-310
C2	CALSNNFARSFHPMLR	8774-8789
N4	EQNGQLGKPLAKKIGKL	5488-5504
N5	*QTIRQAENRLSKLNQA*	5510-5525

Table 2.12 Primary antibodies used in thesis

Antibody	Western Blotting	Immunofluorescence
β-actin (Sigma A2228)	1:10 000	1:1000
Argounaute-2 (Abcam ab57113)	1:500	-
Dcp1a (Abcam ab57654)	1:100	-
DDx5 (Abcam ab21696)	1:1000	-
eIF3η (Santa Cruz sc-16377)	-	1:200
Focal Adhesion Kinase (Abcam ab28152)	-	1:200
Fibrillarin (Abcam ab4566)	-	1:500
Flag (Sigma F3165)	1:10 000	1:2000
Flag (Sigma F7425)	1:10 000	1:2000
GFP (Abcam ab1218)	1:2000	-
GST (Abcam ab6613)	1:500	-
HA (Abcam ab16918)	1:1000	1:200
Hedls/p70S6Ka (Santa Cruz sc-8418)	-	1:200
Importin beta (Abcam ab2811)	-	1:1000
Lamin A/C (Santa Cruz sc-6215)	1:1000	1:100
Matrin-3C (Abcam ab84422)	1:1000	1:100
Matrin-3N (Abcam ab51081)	1:2000	1:100
Nesprin-1 C2	1:1000	-
Nesprin-1 CH2	1:1000	-
Nesprin-1 N4	1:1000	1:100
Nesprin-1 N5	1:1000	1:100
Nucleophosmin (Abcam ab10530)	1:5000	1:1000
PABP-1 (Santa Cruz sc-32318)	-	1:200
PCNA (Cell Signalling mAb2586)	1:1000	-
PSF (Santa Cruz sc-101137)	1:1000	-
Rck/p54 (Bethyl laboratories A300-461A)	1:1000	1:200
smD1 (Santa Cruz sc-20822)	-	1:50
SRp55 (Santa Cruz sc-34198)	-	1:20

Tra2b (Abcam ab66901)	-	1:250
α-Tubulin (Sigma T9026)	1:10 000	1:1000
U1-70K (Millipore 06-1297)	-	1:500
U2 snRNPA (Santa Cruz sc-132132)	-	1:50
V5 (Invitrogen R-960-25)	1:1000	-

Table 2.13 Secondary antibodies used for Western blotting in thesis

HRP-conjugated secondary antibodies	Dilution
ECL goat IgG, HRP-conjugate (Sigma A9452)	1:5000
ECL mouse IgG, HRP-conjugate (GE healthcare NA931)	1:5000
ECL Rabbit IgG, HRP-conjugate (GE healthcare NA934)	1:5000

2.9.3.2 Immunofluorescence secondary antibodies

Alexa fluorophore-conjugated secondary antibodies used for immunofluorescence staining and dilutions are summarized in table 2.14.

2.10 Laboratory reagents

2.10.1 Stock Reagents

100mM dATP – Promega U1205

13mm Borosilicate Cover Glass thickness No.1 - VWR™ 631-0149

1kb DNA ladder – Promega G571A

1x Trypsin-EDTA solution – Sigma T3924

dNTPs 100mM stock solution – Promega

2mm Electroporation cuvettes (long electrode) – Flowgen FBR-202

30% Acrylamide/Bis solution – BioRad (161-0158)

4',6'-Diamidino-2-Pheylindoledihydrochloride (DAPI) –Sigma (D-9542)

6x DNA loading buffer –Promega G1881

Acetone ($(CH_3)_2CO$) – Fisher Scientific (A/0600/PC17)

Advantage 2 polymerase - Clontech 639201

Ammonium Persulfate – BioRad 161-0700

Ampicillin sodium salt – Sigma A0166

Antarctic Phosphatase – New England Biolabs M0289S

AMV-RT – Promega M5101

BioSafe™ Coomassie Stain – BioRad 161-0787

Bovine Serum Albumin (Cohn V fraction) – Sigma A4503

Bromophenol Blue – Aldrich (11,439-1)

Calcium Chloride ($CaCl_2 \cdot 2H_2O$) – Sigma C1016

Cycloheximide ready made solution – Sigma C4859

DABCO (1,4-diazabicyclo[2.2.2]octane)–Sigma (D-2522)

DC Protein Assay – BioRad 500-0113, 500-0114

Deionized H_2O (DI-H2O) –Millipore purification system

DEPC-treated water – Invitrogen 750023

D-Glucose – Sigma G7528

Dried Skimmed Milk- Marvel

Table 2.14 Secondary antibodies used for immunofluorescence staining in thesis

Alexa Fluor-conjugated secondary antibodies	Dilution
Alexa Fluor 405 goat anti-mouse IgG (Invitrogen A31553)	1:1000
Alexa Fluor 488 donkey anti-goat IgG (Invitrogen A11055)	1:1000
Alexa Fluor 488 goat anti-mouse (Invitrogen A11001)	1:1000
Alexa Fluor 488 goat anti-rabbit (Invitrogen A11008)	1:1000
Alexa Fluor 488 rabbit anti-mouse IgG (Invitrogen A11059)	1:1000
Alexa Fluor 568 donkey anti-goat IgG (Invitrogen A11057)	1:1000
Alexa Fluor 568 goat anti-mouse (Invitrogen A11004)	1:1000
Alexa Fluor 568 goat anti-rabbit (Invitrogen A11011)	1:1000
Alexa Fluor 568 rabbit anti-mouse IgG (Invitrogen A11061)	1:1000

Dulbecco's Modified Eagle's Medium (DMEM) – Sigma D5671

Earl's Balanced Salt solution (EBSS) – Sigma E6267

Ehtidium Bromide – Sigma (E-1385)

Ethanol (CH_3CH_2OH, EtOH) – Sigma E7023

Ethylenediaminetetra-acetic Acid (EDTA) – Sigma (E-5134)

First Strand cDNA Human Set 1 – Origene (CH1101)

First Strand cDNA Human Set 2 - Origene (CH1102)

Foetal Bovine Serum (FBS) – Sigma (F-7524)

Glacial Acetic Acid (GAA)- Sigma 537020

Glycerol –Fisher Scientific BPE229-1

Glycine – BDH444495D

Hepes – Sigma H4034

Hiperfect transfection reagent – QIAGEN 301707

Hydrochloric Acid-Sigma H1758

Hydrogen Peroxide – Sigma H1009

Immobilon-P^{TM} (PVDF Western Blot Membrane) – Millipore (IPVH00010)

In Vitro Toxicology Assay Kit, MTT based – Sigma TOX1

Isopropanol (C_3H_8O)- Sigma I9516

Isopropyl-β-D- Thiogalactopyranoside (IPTG) ready made solution – Sigma I1284

Kanamycin disulfate salt – Sigma K1876

LB Agar – Sigma L2897

LB Media – Sigma L3022

L-Glutamine – Invitrogen 25030-081

M199 Media - Sigma M4530

Magnesium Chloride ($MgCl_2$) – Sigma M8266

Marathon-Ready Brain cDNA libary for RACE – Clontech 639301

Marathon-Ready HeLa cDNA libary for RACE– Clontech 639339

Methanol (CH_3OH,MeOH) - Sigma 322415

Mowiol – Calbiochem 475904

N,N,N',N'-Tetra-Methyl=Ethylenediamine (TEMED) –BioRad 161-0800

Nocodazole – Sigma M1404

Nonidet P-40 (NP-40) Alternative – Calbiochem 492016

Optimem – Invitrogen 11058-21

Paraformaldehyde powder – Sigma P6148

PCR master mix –Promega M7502

Penicillin-Streptomycin-Glutamine solution liquid – Invitrogen 10378-016

pGL3-Control vector – Promega E1741

Phosphate Buffered Saline (PBS) Tablets – Oxoid BR0014G

PBS tissue culture grade – Sigma D1408

Polyoxyethylenesorbitan Monolaurate (Tween-20) – VWR 437082Q

Potassium Chloride (KCl) – Sigma P9333

Precision Plus Protein™ Dual Color Standars – BioRad 161-0374

Protease Inhibitor Cocktail – sigma P8340

Protein Assay Standard II – BioRad 500-0007

Protein-A Sepharose beads – Sigma P944

Protein-G Sepahrose beads – Sigma P3296

Random Primers – Promega C1181

Restore™ Western Blot Stripping Buffer- Thermo Scientific 21059

siRNA buffer (Dharmacon)

siRNA oligos - Dharmacon, Invitrogen

Sodium Arsenite solution- Sigma 35000

Sodium Chloride (NaCl) – Sigma S7653

Sodium Deoxycholate – Sigma D6750

Sodium Hydroxide (NaOH) - Sigma S8045

Sodium Phosphate, dibasic, anhydrous (Na2HPO4) – Sigma S7907

STAT-60 - IsoTex Diagnostics CS-110

Superfect – QIAGEN 301305

Sybr green PCR master mix - Eurogentec RT-SY2X-03+NRWOUB

Triton-X 100 – Sigma X100

Trizma™ base – Sigma T6066

UltraPure™ Agarose – Invitrogen 15510-019

β-Mercaptoethanol (C_2H_6OS, βME) – Sigma (M-6250)

2.10.2 Purchased Kits

BioRad SDS-PAGE gel pouring kit

Cell growth determination kit, MTT based – Sigma CGD1

Dual Luciferase Reporter Assay- Promega E1910

ECL Chemiluminescent Kit – Pierce 32106

Endofree Maxiprep – QIAGEN 12362

pGEM-T Easy Vector System II – Promega A-1380

Plus One Silver Staining Kit – GE Healthcare 17-1150-01

PureYield Plasmid Miniprep System - Promega A1222

QIAquick Gel Extraction Kit – QIAGEN 28706

Microtubule Binding Protein Spin-Down Assay Kit – Cytoskeleton BK029

QuikChange® Site-Directed Mutagenesis Kit – Stratagene 200518

2.10.3 Laboratory Equipment

Applied Biosystems 2720 Thermal Cycler

Berthold Mithras LB 940 Luminometer

Bio-Rad Trans-Blot® SD semi-dry transfer cell

Branson Sonifier 150

Corbett RotorGene-3000 qPCR machien

Eppendorf Centrifuge 5415R microcentrifuge

GENios Pro spectrophotometer

InforsHT Ecotron bacterial shaker

Leica SP5 Confocal Microscope

NanoDrop® ND-1000

Olympus IX81 wide field inverted microscope

Thermo Scientific HERA cellISO incubator

Thermo Scientific HERA Safe biosafety cabinet

Thermo Scientific Heraeus Multifuge 3SR^{+} centrifuge

UVP Bio Spectrum® AC Imaging System

2.10.4 Enzymes

Antartic Phosphatase – New England Biolabs M0289L

Pfu polymerase and buffer- Promega M7741

T4 DNA ligase and buffer – Promega M1804

Taq polymerase and buffer- Promega M2031

ApaI – Promega R6361

BamHI – Promega R6025

EcoRI – Promega R6017

*EcoR*V– Promega R6351

NotI – Proemga R6431

SalI – Promega R6051

XhoI – Promega R6165

SmaI – Promega R6121

2.10.5 Solutions

2M KCl (500 ml)

74.55 g KCl, 500 ml DI-H_2O

5M EDTA (5 ml)

7.3125 g EDTA, 5 ml DI-H_2O

1M Hepes pH 7.4 (50 ml)

11.915 g Hepes, 50 ml DI-H_2O

100 mM CaCl2 (500 ml)

5.549 g CaCl2, 500 ml DI-H_2O

1M MgCl2 (500 ml)

101.5g MgCl2, 500 ml DI-H_2O

10% SDS (w/v) (100 ml)

10 g SDS, + DI-H_2O to 100 ml total

PBS-T (500 ml)

499 ml 1x PBS, 1 ml Tween-20

10x Tris-Buffered Saline (TBS) pH 7.6 (500 ml)

12.11 g Trizma, 6.5 ml absolute HCl, 40 g NaCl, + DI-H_2O to 500 ml

1x TBS-T (500 ml)

499 ml 1x TBS, 1 ml Tween-20

50x Tris-acetate-EDTA (TAE) Buffer (1000 ml)

242 g Trizma, 57.1 ml GAA ,18.6 g EDTA, DI-H_2O to 1000 ml

1% Agarose gel (100 m1)

1 g molecular grade agarose, 100 ml 1x TAE

Co-immunoprecipitation (Co-IP) Buffer pH 7.4 (500 mL)

5 ml 1M Hepes pH 7.4, 2.5 ml 2M KCl, 500 µ 5M EDTA, 5 ml Triton-X 100, DI-H_2O to 500 ml

Radio Immunoprecipitation (RIPA) Buffer (100 ml)

100 µl NP-40, 0.5% Sodiium Deoxycholate, 100 µl 10% SDS, 98.4 ml 1x PBS.

Nuclear fractionation buffer (250 ml)

0.59g Hepes, 0.076g MgCl2, 0.187g KCl, 0.019g DTT, 12.5 ul NP-40

4x SDS-PAGE Sample Loading Buffer (10 ml)

1.25 ml 0.5 M Tris-HCl pH 6.8, 2.5 ml Glycerol, 2.0 ml 10% SDS, 0.20 ml 0.5% (w/v) bromophenol blue, 500 µl β-Mercaptoethanol

10x Transfer Buffer (500 ml)

72.2g Glycine, 15.15g Trizma, DI-H_2O to 500 mL

1x Transfer Buffer (1000 ml)

100 ml 10x Transfer buffer, 200 ml MeOH, 700 ml DI-H_2O.

10x Running Buffer (500 ml)

72.2 g Glycine, 15.15 g Trizma, 10 g SDS, DI-H_2O to 500 ml

10% APS (w/v) (1 mL)

10 mg Ammonium Persulfate, 1 ml DI-H_2O

4% Stacking PAGE gel (~10 ml)

1.7ml 30% acrylamide mix, 2.5 ml 0.5M Tris pH 6.8, 100µl 10% SDS, 6 ml water, 50 µl 10% ammonium persulfate, 7.5 µl TEMED

10% Resolving PAGE gel (~15 ml)

5ml 30% acrylamide, 3.75ml 1.5M Tris pH 8l8, 150 µl 10% SDS, 6 mL DI-H_2O, 100 µl 10% APS, 7.5 µl TEMED

Western blocking buffer (100 ml)

5 g dried milk, 100 ml 1x PBS-T

4% Paraformaldehyde (PFA) (50ml)

2 g paraformaldehyde, 50 ml 1xPBS

MeOH/Acetone Fixative (100 ml)

50 ml MeOH, 50 ml Acetone, -80ºC

Mowiol Mounting media (10ml)

2.4 g Mowiol 4-88, 6 g Glycerol, 6 ml DI-H_2O, 12 ml 0.200M Tris pH 8.5, 2.5% DABCO,

1% Bovine Serum Albumin (BSA) (w/v) (100 ml)

1 g BSA, 100 ml 1x PBS

0.5% NP-40 (100 ml)

500µl NP-40, 100 ml 1x PBS

Chapter 3: Identification of Novel Nesprin-1 Isoforms

3.1 Introduction

The versatility of SR proteins is largely due to the expression of multiple tissue specific variants generated by alternative mRNA transcripts. These alternative transcripts are produced by alternative splicing, alternative promoter selection and alternative pre-mRNA 3'end processing [249]. The significance of this increased diversity is particularly evident in the dystrophins and spectraplakins, which have more than 15 and 13 potential known tissue specific isoforms respectively [58,250,251,252]. Studies are now showing the existence of alternatively transcribed nesprin variants and their generation may be comparable, if not more extensive, than any other SR protein family member [66,206,207,208,232,249].

Disruption of the LINC complex via mutations in nesprin-1 and -2 or their binding partners, such as emerin and lamin A/C, give rise to Emery Dreifuss Muscular Dystrophy (EDMD) [14]. However, emerging evidence implicates nesprin-1 in several other unrelated diseases, including epithelial cancers and autosomal recessive cerebellar ataxia (ARCA1), which are not characterized by NE defects [13,232]. It is likely that these non-canonical roles for nesprin are mediated by alternative nesprin variants that lack either the CHDs, the KASH domain or both, and localize to a number of sub-cellular compartments. For example, in chapter 1 the roles for KASH-less nesprin variants in Golgi structure and function, chromatin organization, clathrin-mediated uptake and recycling of chemokine receptors, and ERK1/2 scaffolding were described [207,208,222,232]

In order to further assess the extent of alternate nesprin-1 functionality, I set out to identify new novel 5'UTRs and 3'UTRs using rapid amplification of cDNA ends (RACE). By combining these newly identified UTRs with ones previously identified by our laboratory, I show that multiple tissue specific nesprin-1 variants can be generated. Furthermore, I show that these variants are translated and localize to unique sub-cellular compartments, implying that nesprin-1 may have functional and/or structural roles beyond the NE.

3.2 Results

3.2.1 Previously identified nesprin-1 UTRs

Originally, our laboratory had screened available online databases to identify *bone fide* novel nesprin-1 5'UTRs and 3'UTRs which may be used to generate alternative nesprin-1 transcripts. The NCBI expressed sequence tag database (EST), which consists of one-shot sequences of cloned mRNA, was blasted with consecutive 500bp-overlapping 1kb nesprin-1 sequences covering the entirety of the giant isoform cDNAs. Several novel UTRs were detected in the EST database screen, typically presenting as retained sequences created through alternative promoter usage and alternative 3'end processing (Table 3.1). 5'UTRs, generated through the utilization of alternative promoters (Figure 3.1), were considered real if they contained an identifiable and viable Kozak sequence surrounding the first start codon. 3'UTRs, generated though alternative pre-mRNA 3'end processing via selection of alternative polyadenylation sites, were considered if they already included a poly(A) tail or contained at least one poly(A) site downstream of the initial ORF termination codon, as determined by scanning with the polyAdq program or manually for non-canonical poly(A) signals (Figure 3.1).

Nine out of the nineteen nesprin-1 UTRs identified through the database screen were verified by Dr. Jason Mellad (Shanahan laboratory, King's College London), using RT-PCR on a multi-tissue cDNA panel and DNA sequencing. Although many UTRs PCR amplified in a range of tissues, most were transcribed in a tissue specific manner suggesting they lead to the creation of tissue specific nesprin variants (Figure 3.2). The UTRs were named based upon their first or last coding exons for 5'UTRs and 3'UTRs respectively. For example, N1-5'E138 is a novel 5'UTR where the first coding exon utilized is exon 138, and N1-3'E18 is a novel 3'UTR where the last coding exon utilized is exon 18.

Figures 3.3 provides an outline of all the identified 5'UTRs and 3'UTRs spread across the 146 exons which make up the nesprin-1 gene, with figure 3.4 highlighting full length isoforms which are known to be expressed, and proposed variants that could be created by alternative UTR usage *in vivo* for

Table 3.1 Nesprin-1 UTRs identified by out laboratory through online databases. Originally our laboratory had previously screened available online databases to identify *bone fide* novel 5' and 3'UTRs which may be used to generate alternative nesprin-1 variants. The NCBI EST database was blasted with consecutive, 500bp-overlapping 1kb nesprin-1 sequences covering the entirety of the giant isoform cDNAs. Several novel UTRs were detected in the EST database screen, typically presenting as retained introns between two exons

Gene	UTR	5' or 3'	Location	NCBI Accession	Verified by PCR
Nesprin-1	**N1-5'I14/15**	5'	Intron 14-15/	DA151121, CR933676, AK055440, BG197747, DB324328	+
Nesprin-1	**N1-3'E18**	3'	Exon 18	BC028616, DB545136, DB540697, DB538738	+
Nesprin-1	**N1-5'I18/19**	5'	Intron 18-19	DA337073	-
Nesprin-1	**N1-3'E20**	3'	Exon 20	DB540697, DB545136, DB538738	-
Nesprin-1	**N1-5'I21/22**	5'	Intron 21-22	DA337073	+
Nesprin-1	**N1-3'E25**	3'	Exon 25	DA151121, CR933676, AK055440, BG197747, DB324328	+
Nesprin-1	**N1-3'E37**	3'	Exon 37	AL713682	+
Nesprin-1	**N1-5'E44**	5'	Exon 44	DB300122	-
Nesprin-1	**N1-3'E62**	3'	Exon 62	BC039121,CA425673,AW300380, BG203678, BG210617, DB516174, CA441052, BX093712,CA312508, DB319424, AA227537,AI866946	+
Nesprin-1	**N1-5'E84**	5'	Exon 84	BU461222	-
Nesprin-1	**N1-3'E87**	3'	Exon 87	AB033088	-
Nesprin-1	**N1-5'E92**	5'	Exon 92	CJ462692, DA229059, DA227411, DA212433, DA509325, DB059554, DA802484, EE366817, DA241105, DA338782, DB289567, DA116814, DA493491	+
Nesprin-1	**N1-5'E97**	5'	Exon 97	BF740426, BF726175	-
Nesprin-1	**N1-5'I128/129**	5'	Intron 128-129	AK304825	+
Nesprin-1	**N1-5'I132/133**	5'	Intron 132-133	DA632075	-
Nesprin-1	**N1-5'E138**	5'	Exon 138	DA827648	+

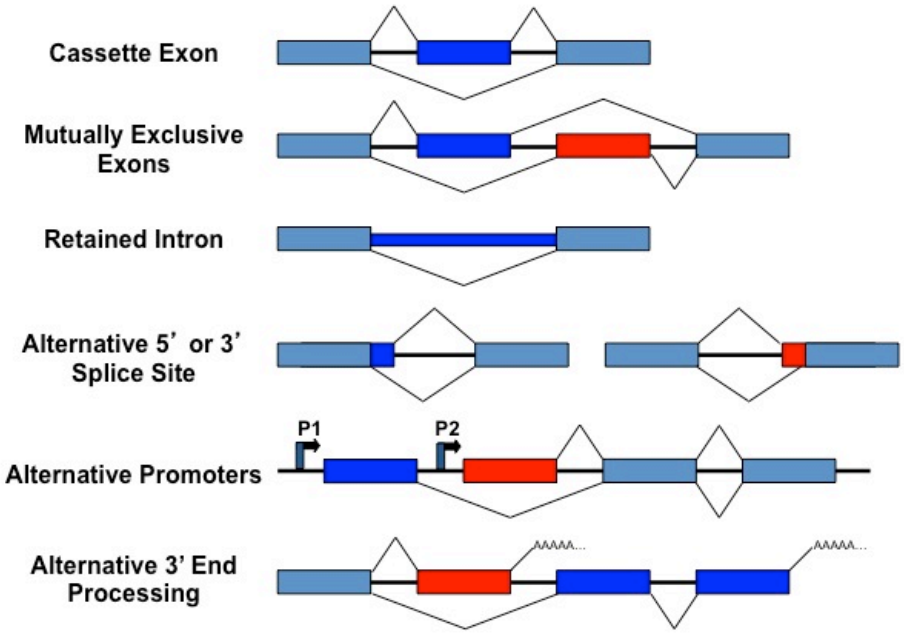

Figure 3.1. Alternative transcript generation. There are several mechanisms of alternative transcript generation which have been observed experimentally. *Cassette exons* can be individually included or excluded from the mature mRNA. For a given pair of *mutually exclusive exons*, only one can be included in any particular mRNA. *Retained introns* often shift the open reading frame (ORF) and also serve as translational regulatory elements. The relative strength of *alternative splice sites* within a given exon or intron determine what sequences are included in the mature transcript. Finally, *alternative promoters* and *alternative 3' end processing* control initiation and termination of nesprin-1 mRNA transcripts respectively, and can affect both the UTRs and ORF.

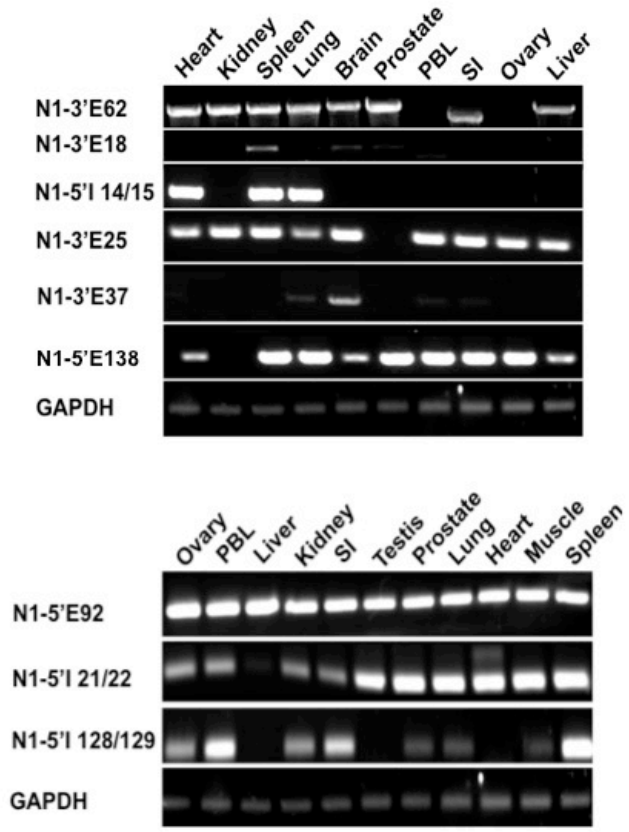

Figure 3.2. Validation of novel UTRs identified through online databases. Validation and tissue specificity of nesprin-1 UTRs identified on online databases were confirmed by RT-PCR amplification from a multiple tissue cDNA panel and DNA sequencing. Nesprin-1 PCRs were carried out on cDNA panels available at the time and are therefore organized into 2 separate sections. The tissue specific nature of nesprin-1 UTRs matches that of other SR proteins including dystrophin and spectraplakins. RT-PCR amplifications were performed by Dr. Jason Mellad (Shanahan lab, King's College London).

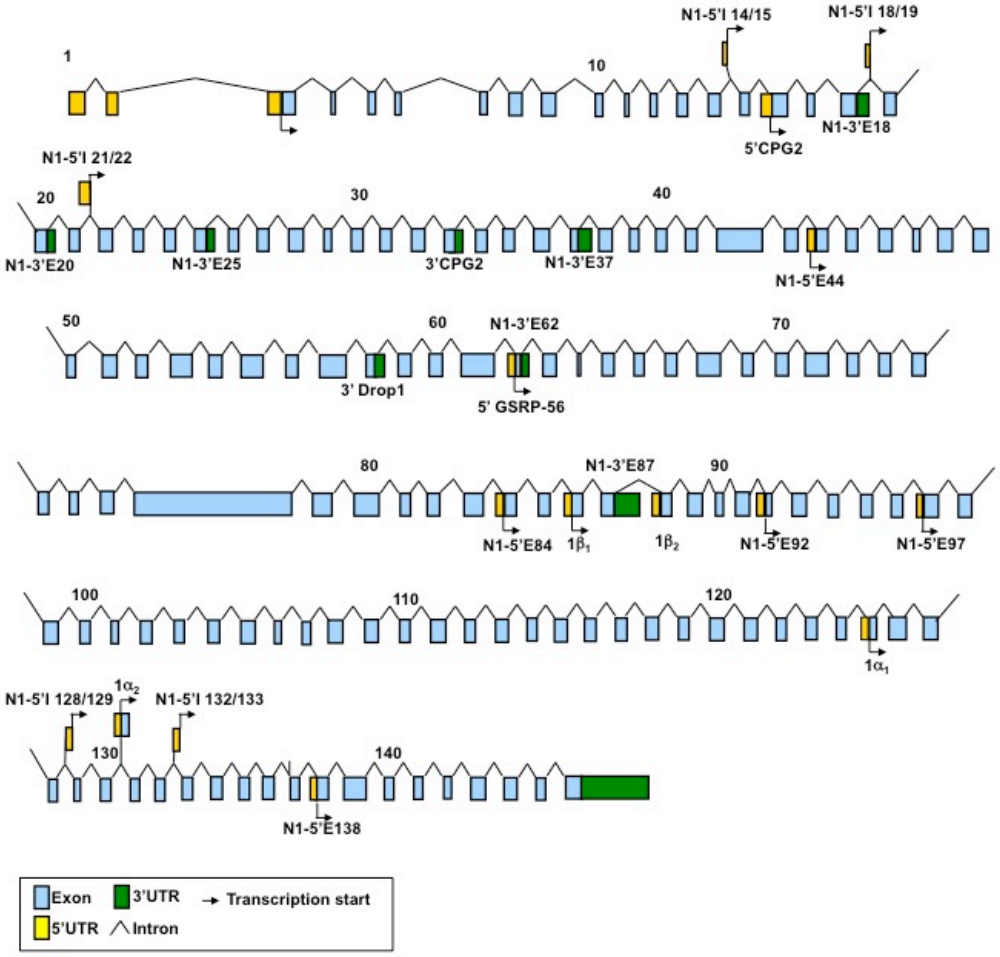

Figure 3.3. Pre-historic Nesprin-1 genomic map. The nesprin-1 gene is composed of 146 exons (light blue boxes) with multiple 5' and 3'UTRs (yellow and green boxes respectively) scattered along its length. The 16 UTRs identified on databases have been added to the pre-existing ones, making a total of 17 5'UTRs and 9 3'UTRs. Using alternative initiation and termination multiple nesprin-1 variants composed of different domains and sizes can be transcribed, as illustrated in Figure 3.3.

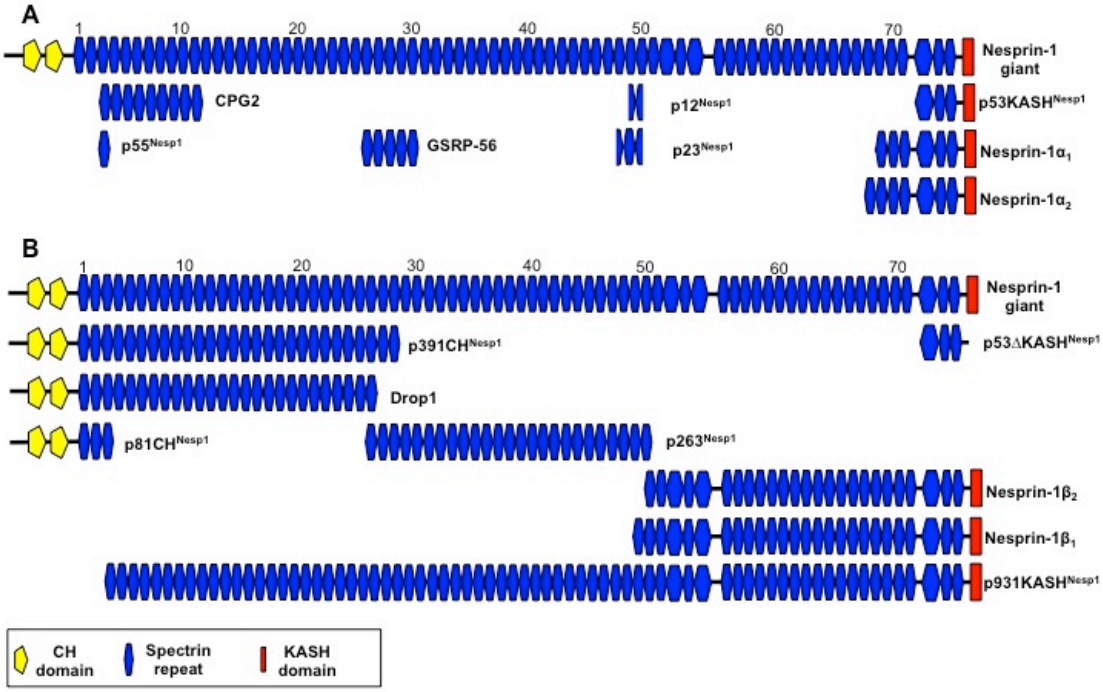

Figure 3.4 Validated and hypothetical nesprin-1 variants. A) Full length nesprin-1 variants known to be expressed that have been identified in publications, within outrlaboratory (unpublished data) or throughout this thesis. B) Potential nesprin-1 variants which could be generated using the UTRs enlisted in table 3.1. The potential combinations of 5' UTRs with 3'UTRs are extensive and would allow generation of many more variants not illustrated. Although many variants could retain the KASH domain, there is a possibility of generating isoforms composed solely of SRs. Therefore, the identified nesprin variants were named according to their predicted molecular weights and the domains they possessed. For example, p81CH^{Nesp1} is a nesprin-1 variant of 81 kDa which has the N-terminal CHDs, p12^{Nesp1} is a 12 kDa nesprin-1 variant which lacks both the CHDs and the KASH domain and is composed of SRs, while p53KASH^{Nesp1} is a 53 kDa KASH containing variant lacking CHDs.

nesprin-1 (Figure 3.4A,B). The potential combinations of the different seventeen 5'UTRs with the nine 3'UTRs are extensive and would allow generation of many variants. The SRs used in the schematics to represent nesprins are based on the predictions of SRs previously described using sequence alignments and evolutionary conservation [78]. Although many variants could retain the KASH domain, there is a possibility of generating isoforms composed solely of SRs and/or CHDs. Therefore, the identified nesprin-1 variants were named according to their predicted molecular weights and the domains they contained. For example, p81CH^{Nesp1} is a nesprin-1 variant of 81 kDa which has the N-terminal CHDs, p12^{Nesp1} is a 12 kDa nesprin-1 variant which lacks both the CHDs and the KASH domain and is composed of SRs, while p53KASH^{Nesp1} is a 53 kDa KASH containing variant lacking both CHDs.

3.2.2 KASH isoforms

So far a number of KASH variants including the nesprin-1α and nesprin-1β isoforms have been identified. In principle, any of the 17 different 5'UTRs could be utilised with the 3'UTR of the nesprin-1 giant to make KASH containing NE localized nesprin-1 variants (Figure 3.5, Table 3.2). The 17 potential nesprin-1 KASH variants which can be translationally expressed, most likely do so in a tissue specific manner due to the specificity of the individual 5'UTRs.

To determine which nesprin-1 KASH variants were translationally expressed, whole-cell lysates from human dermal fibroblasts (HDFs) and human osteosarcoma (U2OS) cells were analysed by Western blotting using the nesprin-1 C2 antibody (Figure 3.6A). The nesprin-1 C2 antibody was created to target the nesprin-1 KASH domain, and therefore recognize all C-terminal KASH domain nesprin-1 variants. As predicted, multiple bands were detected by nesprin-1 C2, including a doublet at ~100 kDa in HDFs which could represent either of the two nesprin-1α and/or p123KASH^{Nesp1} variants. Nesprin-1 C2 only produced a single band at ~100kDa from U2OS cell lysate suggesting only one of the nesprin-1α variants or p123KASH^{Nesp1} are expressed in U2OS cells. An additional band was seen in U2OS cell lysates

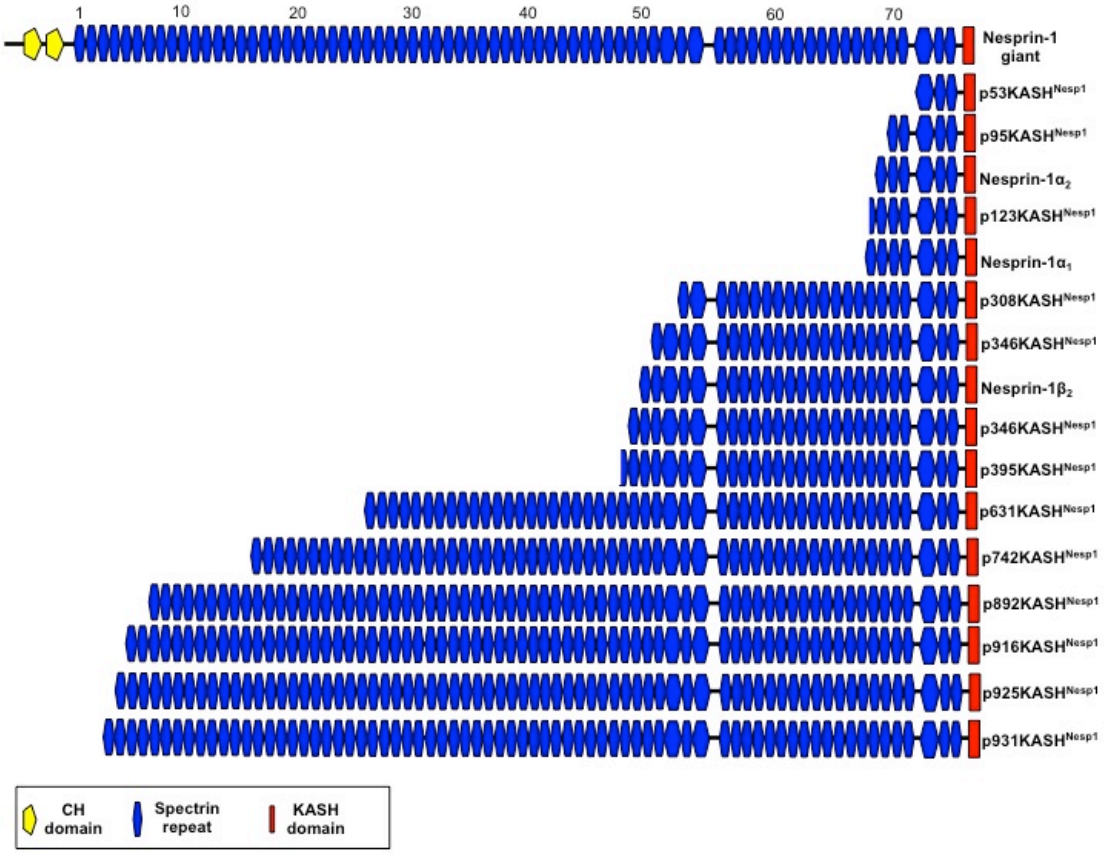

Figure 3.5 Potential nesprin-1 KASH variants. By alternatively initiating transcripts with the 17 different nesprin-1 5'UTRs and terminating with the the nesprin-1 giant 3'UTR, it is possible to create 17 different KASH domain containing nesprin-1 variants that localize to the NE. The tissue specific expression pattern of the individual 5'UTRs suggest that these variants are likely to be expressed in a tissue specific manner.

Table 3.2 Nesprin-1 UTRs utilized to generate the 17 different nesprin-1 KASH variants illustrated in Figure 3.5. By alternatively initiating transcripts with the 17 different nesprin-1 5'UTRs and terminating with the the nesprin-1 giant 3'UTR, it is possible to create 17 different KASH domain containing nesprin-1 variants that localize to the NE. This table enlists the UTR combinations used to generate nesprin-1 KASH variants in Figure 3.5

Isoform	5'UTR	3'UTR	Size (kDa)
p53KASH^{Nesp1}	N1-5'E138	Nesprin-1 Giant	53
p95KASH^{Nesp1}	N1-5'I 132/133	Nesprin-1 Giant	95
Nesprin-1α_2	1α_2	Nesprin-1 Giant	112
p123KASH^{Nesp1}	N1-5'I 128/129	Nesprin-1 Giant	123
Nesprin-1α_1	1α_1	Nesprin-1 Giant	140
p308KASH^{Nesp1}	N1-5'E97	Nesprin-1 Giant	308
p346KASH^{Nesp1}	N1-5'E92	Nesprin-1 Giant	346
Nesprin-1β_2	1β_2	Nesprin-1 Giant	370
Nesprin-1β_1	1β_1	Nesprin-1 Giant	386
p395KASH^{Nesp1}	N1-5'E84	Nesprin-1 Giant	395
p631KASH^{Nesp1}	5' GSRP-56	Nesprin-1 Giant	631
p742KASH^{Nesp1}	N1-5'E44	Nesprin-1 Giant	742
p892KASH^{Nesp1}	N1-5'I 21/22	Nesprin-1 Giant	892
p916KASH^{Nesp1}	N1-5'I 18/19	Nesprin-1 Giant	916
p925KASH^{Nesp1}	5'CPG2	Nesprin-1 Giant	925
p931KASH^{Nesp1}	N1-5'I 14/15	Nesprin-1 Giant	931
Nesprin-1 Giant	Nesprin-1 Giant	Nesprin-1 Giant	~1000

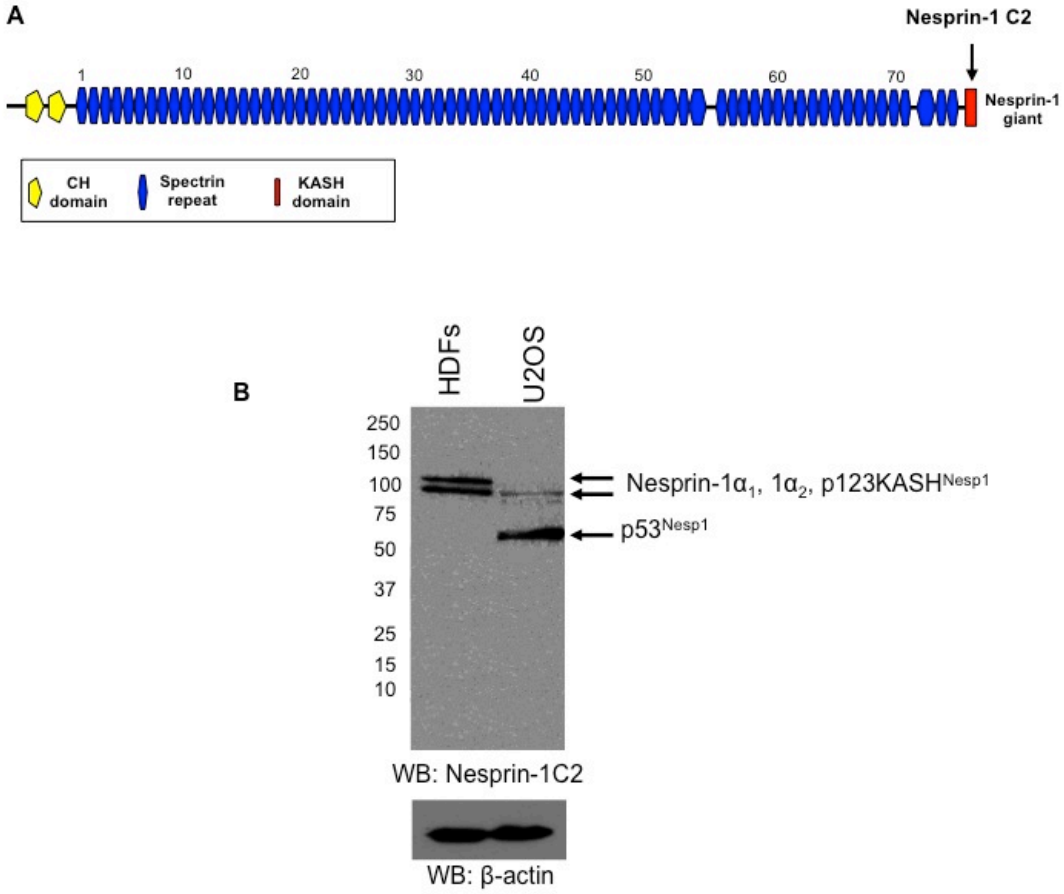

Figure 3.6 Detection of nesprin-1 KASH variants. To determine what sized nesprin-1 KASH variants were translationally expressed, whole-cell lysates from human dermal fibroblasts (HDFs) and human osteosarcoma (U2OS) cells were analysed by Western blotting using the nesprin-1 C2 antibody. A) Anti-Nesprin-1 C2 was generated against a peptide sequence present in the nesprin-1 KASH domain and therefore designed to detect all the nesprin-1 KASH variants. B) Anti-Nesprin-1 C2 detects nesprin-1 variants $p53^{Nesp1}$ and Nesprin-$1\alpha_1$ or $1\alpha_2$ or $p123KASH^{Nesp1}$ from whole cell lysates of human dermal fibroblasts (HDFs) and osteosarcoma (U2OS) cells by Western blotting.

at ~50kDa, which could correspond to p53KASH^{Nesp1} (Figure 3.6B). Although nesprin-1 C2 should detect other nesprin-1 KASH variants such as the nesprin-1 giant and the nesprin-1β isoforms previously described, bands corresponding to these large isoforms were not visualized, possibly due to lack of expression or size-limited migration into the polyacrylamide gels.

3.2.3 CHD isoforms

The only nesprin-1 CHD containing isoforms identified to date are the nesprin-1 giant and Drop1 variants. As with the potential KASH domain isoforms in Figure 3.4, up to 9 CHD isoforms can be generated by combining any of the 9 3'UTRs with the nesprin-1 giant 5'UTR (Figure 3.7, Table 3.3). To determine what CHD variants were expressed in U2OS cells and HDFs, Western blotting on whole cell lysates was performed using the nesprin-1 CH2 antibody, designed to target the second nesprin-1 CHD (Figure 3.8 A,B). Novel nesprin-1 variants p121CH^{Nesp1}, p88CH^{Nesp1} and p81CH^{Nesp1} were detected in both cell lines with an unknown variant detected at ~50 kDa. Furthermore an additional U2OS cell specific nesprin-1 variant was detected at ~250 kDa (Figure 3.8 B), suggesting at least two nesprin-1 CHD variants exist that have yet to be identified.

3.2.4 Rapid Amplification of cDNA Ends (RACE) to identify new cDNA ends.

Online databases did not contain sequences that could encode for nesprin-1 CHD variants of ~50 kDa and ~250 kDa in size, as detected by Western blotting. Therefore to identify potential mRNA species encoding these variants, Rapid Amplification of cDNA Ends (RACE) was performed to identify new 3'UTRs expressed in cells/tissues. RACE is a technique used to obtain the full-length sequence of an mRNA transcript found within a cell. RACE can provide the sequence of an mRNA transcript from a small known sequence within the transcript all the way to the 5' end (5' RACE) or 3' end (3' RACE) of the mRNA. RACE relies on the ligating a known adaptor sequence onto the 5' and 3' ends of a cDNA library. Therefore, by utilizing primers targeting the known adaptor sequence with nesprin-1 gene specific primers, it

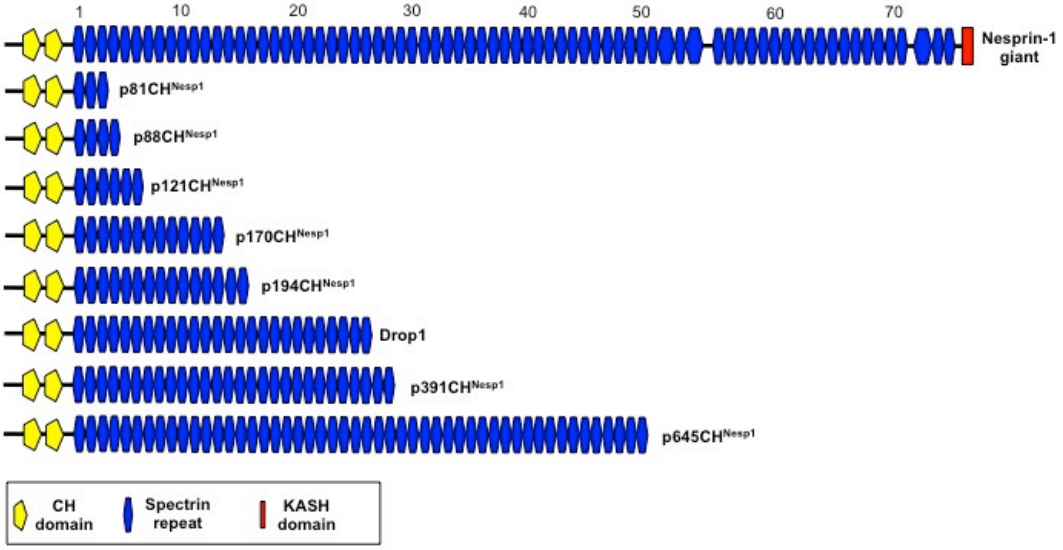

Figure 3.7 Potential nesprin-1 CHD variants. By combining the nesprin-1 giant 5'UTR with the 9 different nesprin-1 3'UTRs, up to 9 different CHD containing nesprin-1 variants, which range in size from 81kDa to 1000 kDa can be generated. The tissue specific expression pattern of the individual 3'UTRs suggest that these variants are likely to be expressed in a tissue specific manner.

Table 3.3 Nesprin-1 UTRs utilized to generate the 9 different nesprin-1 CHD variants illustrated in Figure 3.7. By combining the nesprin-1 giant 5'UTR with the 9 different nesprin-1 3'UTRs, up to 9 different CHD containing nesprin-1 variants, which range in size from 81kDa to 1000 kDa can be generated. This table enlists the UTR combinations used to generate nesprin-1 CH variants in Figure 3.7

Isoform	5'UTR	3'UTR	Size (kDa)
p81CH^{Nesp1}	Nesprin-1 Giant	N1-3'E18	81
p88CH^{Nesp1}	Nesprin-1 Giant	N1-3'E20	88
p121CH^{Nesp1}	Nesprin-1 Giant	N1-3'E25	121
p170CH^{Nesp1}	Nesprin-1 Giant	3'CPG2	170
p194CH^{Nesp1}	Nesprin-1 Giant	N1-3'E37	194
Drop1	Nesprin-1 Giant	3'Drop1	350
p391CH^{Nesp1}	Nesprin-1 Giant	N1-3'E62	391
p645CH^{Nesp1}	Nesprin-1 Giant	N1-3'E87	645

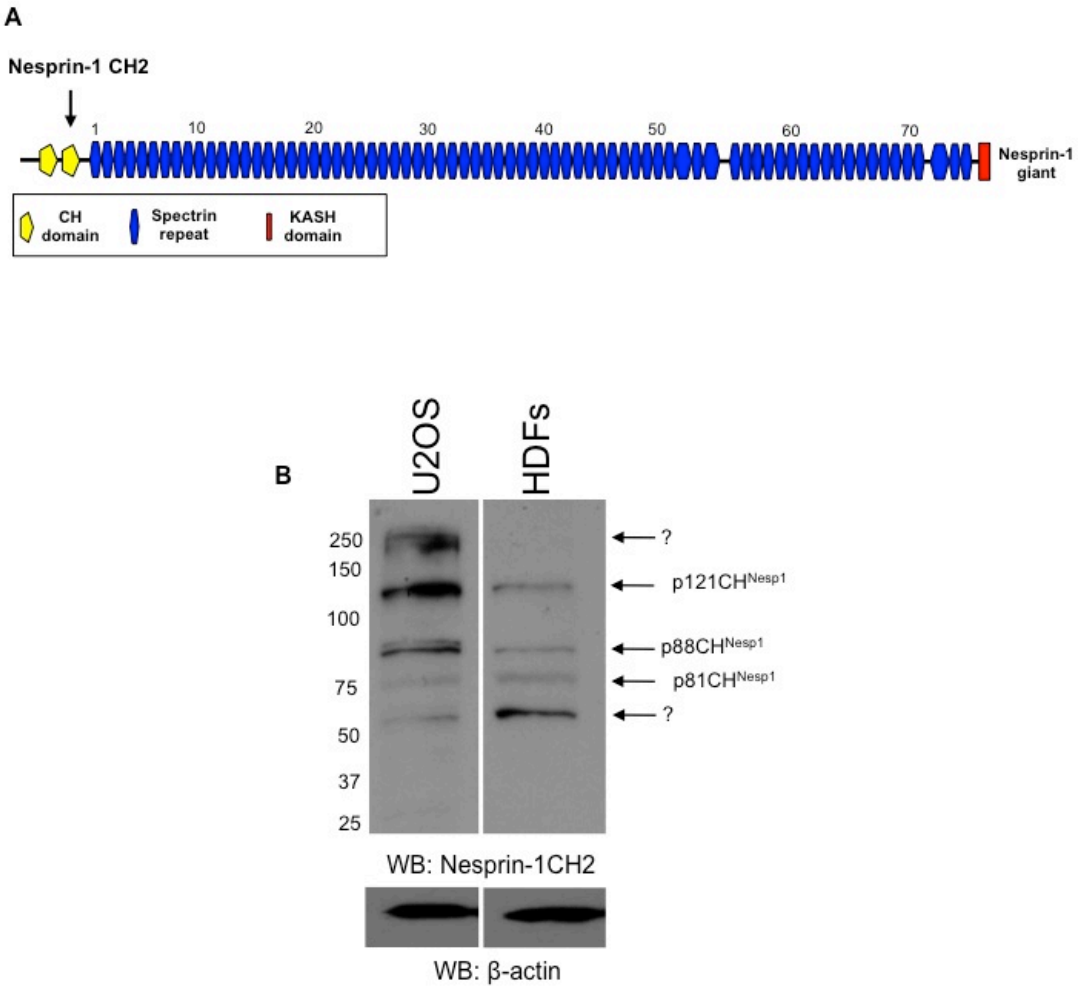

Figure 3.8 Detection of nesprin-1 CHD variants. To determine what nesprin-1 CHD variants were translationally expressed, whole-cell lysates from human dermal fibroblasts (HDFs) and human osteosarcoma (U2OS) cells were analysed by Western blotting using the nesprin-1 CH2 antibody. A) Anti-Nesprin-1 CH2 was generated against a peptide sequence present in the second CHD of nesprin-1 and therefore designed to detect all the nesprin-1 CHD variants. B) Anti-Nesprin-1 CH2 detected nesprin-1 CHD variants p121CH^{Nesp1}, p88CH^{Nesp1}, p81CH^{Nesp1} and additional variants at ~50 kDa from whole cell lysates of HDFs and U2OS cells by western blotting. An additional ~250 kDa band was detected in U2OS who cell lysates.

is possible to PCR amplify novel cDNA ends generated by alternative transcription. Previous studies, and the data shown at the beginning of this chapter, suggest that nesprin isoforms are expressed in a tissue specific manner. Therefore, to increase the probability of identifying novel nesprin-1 cDNA ends, PCRs were performed on RACE-Ready cDNA libraries obtained from HeLa cells, the brain and skeletal muscle.

3.2.5 Characterization of p56CH^{Nesp1}

3.2.5.1 Identification of N1-3'E14

To identify the unknown ~50 kDa nesprin-1 CHD variants detected by the nesprin-1 CH2 antibody in U2OS and HDF cells, 3'RACE analysis was performed using nesprin-1 specific primers in a range of exons that could produce a ~50 kDa CHD containing nesprin-1 product. Forward primers targeting multiple nesprin exons were utilized with RACE, many failing to PCR amplify any fragments. However, by using forward nesprin-1 primers designed within exon 14, PCR products were amplified from all three RACE-ready libraries (Figure 3.9A). DNA sequencing followed by a nucleotide BLAST against the human genome aligned the amplicon to exon 14 and intronic sequences between exons 14 and 15 of the nesprin-1 gene. More in depth analysis of the ampliicon sequence showed the ORF carried on from exon 14 into the retained intron. The stop codon for this cDNA end was found in the retained intron after the unique 37 amino acid coding sequence 'KIEAIRKELPPAPTATSTHLRNCICARIHALHFCYYG'. Downstream of the stop codon was an *AATAAA* polyA signal followed by a polyadenylation site. Using the same nomenclature used to describe the nesprin UTRs identified previously, this UTR was named *N1-3'E14.*

3.2.5.2 N1-3'E14 is ubiquitously expressed

To determine the tissue specificity of N1-3'E14, RT-PCR was performed on a multiple tissue cDNA panel using a primer set to specifically detect N1-3'E14. The PCR primers were designed so that the reverse primer was present within the UTR and the forward primer within exon 13, to control

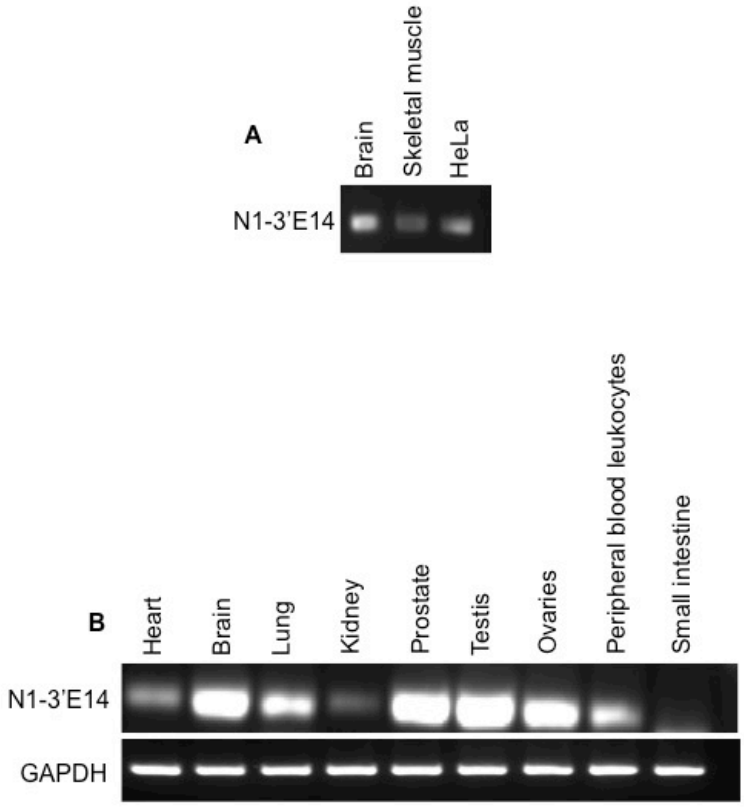

Figure 3.9 Identification of N1-3'E14. To identify the unknown ~50 kDa nesprin-1 CHD variant detected by the nesprin-1 CH2 antibody in U2OS and HDF cells, 3'RACE analysis was performed using nesprin-1 specific primers in a range of exons that could produce a ~50 kDa CHD containing nesprin-1 product. A) 3'RACE using forward primers in exon 14 and reverse primers targeting the 3' adaptor sequence, PCR amplified a product corresponding to N1-3'E14. B) To determine the tissue specificity of N1-3'E14, RT-PCR was performed on a multiple tissue cDNA panel using a primer set whichspecifically detects N1-3'E14. The UTR was undetectable in the small intestine, but present in the heart, brain, lung, kidney, prostate, testis, ovaries and peripheral blood leukocytes.

for genomic DNA contamination. The UTR was undetectable in the small intestine but was present in the heart, brain, lung, kidney, prostate, testis, ovaries and peripheral blood leukocytes by RT-PCR (Figure 3.9B).

3.2.5.3 p56CH^{Nesp1} is a product of N1-3'E14 termination and differentially localizes in U2OS and HDFs

By combining the nesprin-1 giant 5'UTR with N1-3'E14 UTR, a 56kDa nesprin-1 variant containing both CHDs and a single SR could potentially be translated and could account for the ~50kDa band seen in whole cell lysates of U2OS cells and HDFs with the nesprin-1 CH2 antibody (Figures 3.8B, 3.10A). To determine if the mRNA transcript of p56CH^{Nesp1} could be detected, RT-PCR was performed using a forward primer in the 5'UTR of the nesprin-1 giant and a reverse primer in N1-3'E14. The transcript for p56CH^{Nesp1} amplified from all cell lines and tissues examined, suggesting that p56CH^{Nesp1} is ubiquitously expressed (Figure 3.10B).

p56CH^{Nesp1} amplified from brain cDNA was cloned into a vector containing an N-terminal Flag-tag and transfected into U2OS cells to monitor it's sub-cellular localization. Flag staining localized p56CH^{Nesp1} to a sub-nuclear compartments, which co-localized with nucleolar marker nucleophosmin (Figure 3.11). When Flag-p56CH^{Nesp1} was transfected into HDFs, Flag staining surprisingly displayed no nuclear localization. Instead, p56CH^{Nesp1} co-localized with actin stress fibres and focal adhesions, suggesting p56CH^{Nesp1} has unique sub-cellular localizations in unique tissues (Figure 3.12).

3.2.6 Characterization of p252CH^{Nesp1}

3.2.6.1 Identification of N1-3'E44

As with the N1-3'E14, 3'RACE analysis was performed using nesprin-1 specific primers in a range of exons that could produce a ~250 kDa CHD containing nesprin-1 product seen in U2OS cell lysates. By using forward nesprin-1 primers designed within exon 44, a PCR product was amplified from HeLa cell cDNA library (Figure 3.13A). This amplicon contained sequences to exon 44 and intronic sequences between exons 44 and 45 of the nesprin-1

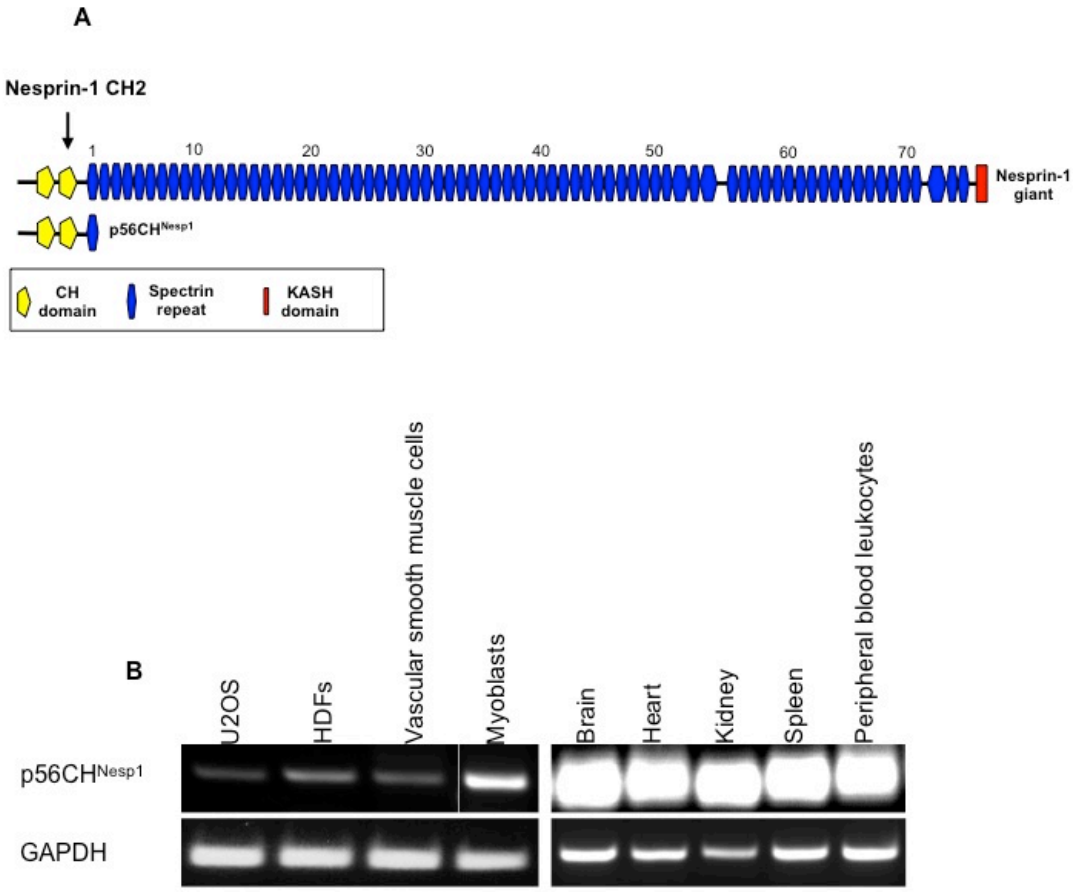

Figure 3.10 p56CH^{Nesp1} is ubiquitously expressed. A) p56CH^{Nesp1} is composed of both the nesprin-1 CHDs and a single SR. p56CH^{Nesp1} is generated using the nesprin-1 giant 5'UTR and N1-3'E14 3'UTR. B) To determine if the mRNA transcript of p56CH^{Nesp1} could be detected, RT-PCR was performed using a forward primer in the 5'UTR of the nesprin-1 giant and a reverse primer in N1-3'E14. The transcript for p56CH^{Nesp1} amplified from all cell lines and tissues examined, suggesting that p56CH^{Nesp1} is ubiquitously expressed.

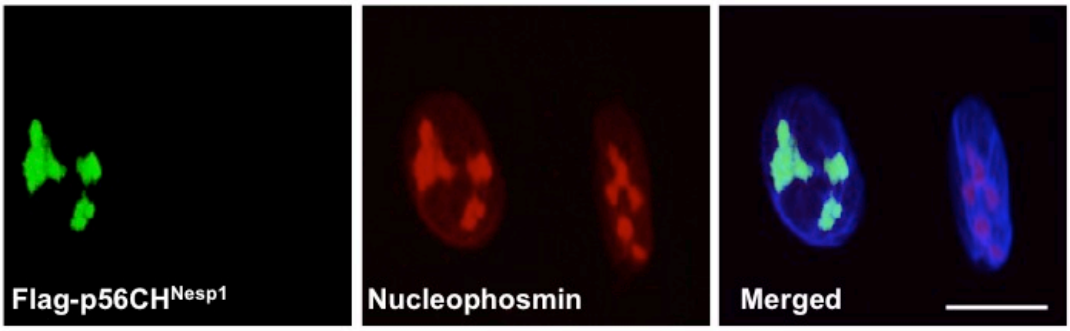

Figure 3.11 p56CH^{Nesp1} localizes to the nucleolus in U2OS cells. p56CH^{Nesp1} amplified from brain cDNA was cloned into a vector containing an N-terminal Flag-tag and transfected into U2OS cells to monitor it's sub-cellular localization. Flag staining localized p56CH^{Nesp1} to a sub-nuclear compartment which co-localized with nucleolar marker nucleophosmin, suggesting p56CH^{Nesp1} localizes to the nucleolus in U2OS cells. Image acquired using confocal microscopy. Scale bar = 10 μM.

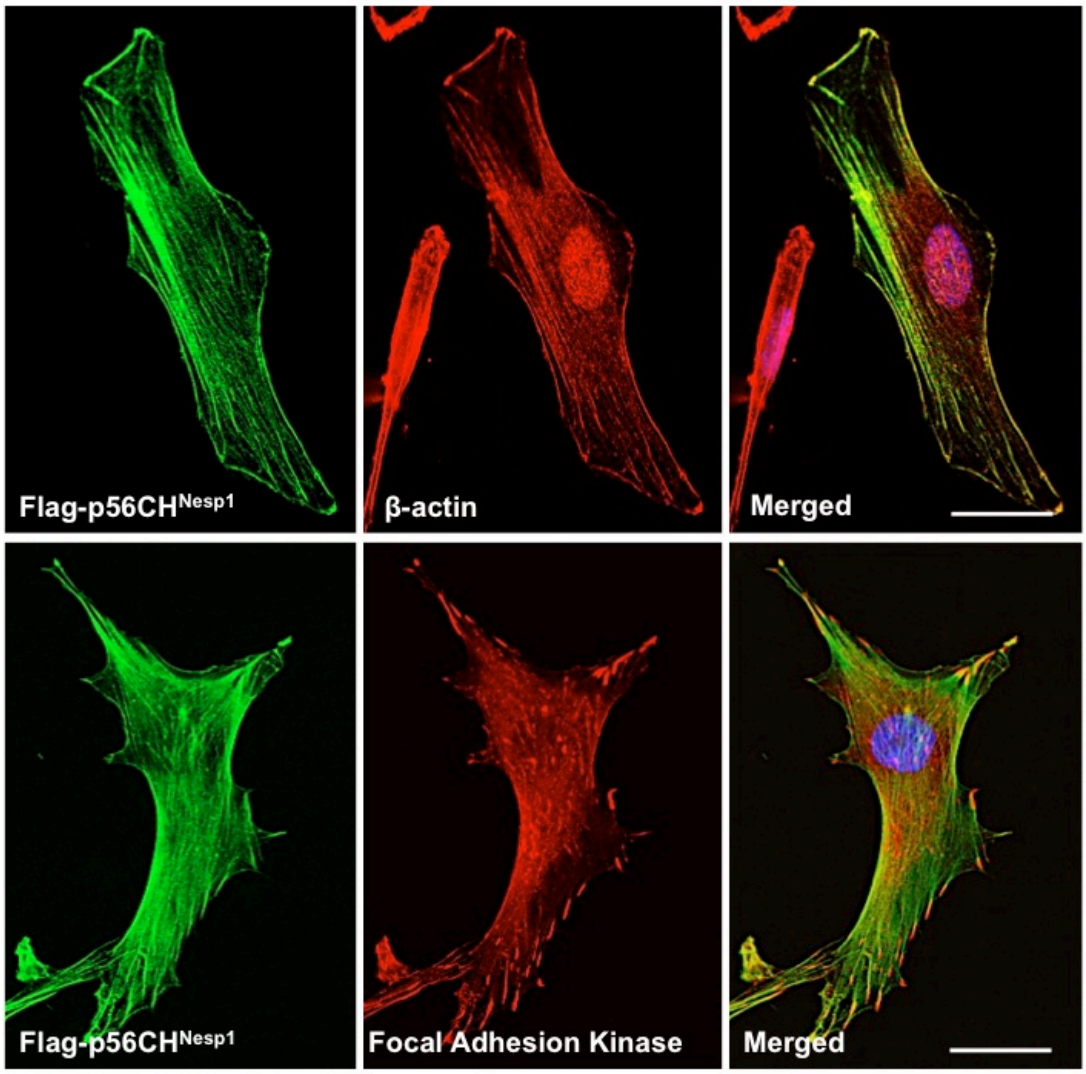

Figure 3.12 p56CH^{Nesp1} localizes to actin stress fibers and focal adhesions in HDF. Flag-p56CH^{Nesp1} displayed no nuclear localization pattern when transfected into HDFs. Instead, p56CH^{Nesp1} co-localized with β-actin and focal adhesion kinase at actin stress fibres and focal adhesions respectively. Images acquired using confocal microscopy. Scale bars = 10 μM.

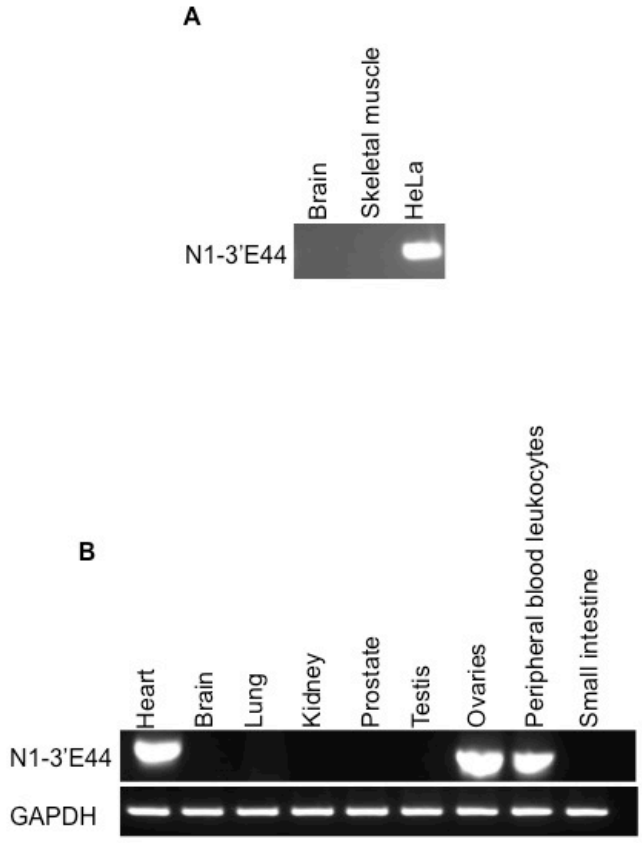

Figure 3.13 Identification of N1-3'E44. To identify the unknown ~250 kDa nesprin-1 CHD variant detected by the nesprin-1 CH2 antibody in U2OS cells, 3'RACE analysis was performed using nesprin-1 specific primers in a range of exons that could produce a ~250 kDa CHD containing nesprin-1 product. A) 3'RACE using forward primers in exon 44 and reverse primers targeting the 3' adaptor sequence, PCR amplified a product corresponding to N1-3'E44. B) To determine the tissue specificity of N1-3'E44, RT-PCR was performed on a multiple tissue cDNA panel using a primer set which specifically detects N1-3'E44. The UTR was undetectable in the majority of tissue examined but was detected in the heart, ovaries and peripheral blood leukocytes, suggesting it is more tissue specific than N1-3'E14.

gene. The ORF carried on from exon 44 into the retained intron. The stop codon for this cDNA end was found in the retained intron after the 30 unique amino acid coding sequence 'VSKIITWDSVNYLNIHIPQSNFWTKRYSRM'. Downstream of the stop codon was an *AATAAA* polyA signal followed by a polyadenylation site.

3.2.6.2 N1-3'E44 is detected in a subset of tissues

Whereas the N1-3E14 UTR was ubiquitously expressed, N1-3'E44 was only detected in a subset of tissues including the heart, ovaries and peripheral blood leukocytes, suggesting it displays a high degree of tissue specificity (Figure 3.13B).

3.2.6.3 p252CH^{Nesp1} is a product of N1-3'E44 termination and localizes to cytoplasmic granular structures

By combining the nesprin-1 giant 5'UTR with N1-3'E44 UTR, a 252kDa nesprin-1 variant containing both CHDs and multiple SR can be translated, which could account for the ~250kDa band seen in whole cell lysates of U2OS cells with the nesprin-1 CH2 antibody (Figures 3.8B, 3.14A). To determine if the mRNA transcript of p252CH^{Nesp1} could be detected, RT-PCR using a forward primer in the 5'UTR of the nesprin-1 giant and a reverse primer in N1-3'E44 was performed. The transcript for p252CH^{Nesp1} amplified specifically from U2OS and heart cDNA, suggesting that p252CH^{Nesp1} is highly cell/tissue specific (Figure 3.14B).

p252CH^{Nesp1} amplified from U2OS cDNA was cloned into a Flag-tag vector and transfected into U2OS cells and HDFs to monitor it's sub-cellular localization. Flag staining localized p252CH^{Nesp1} to granular structures within the cytosol in U2OS cells. However, transfection only appeared in ~1% of plated cells suggesting that expression of the protein may be toxic to the cells. Indeed, HDFs failed to express Flag-p252CH^{Nesp1} altogether (Figure 3.15).

3.2.7 Central rod isoforms

To date, GSRP-56 and CPG2 are the only nesprin-1 variant identified composed entirely of SRs. GSRP-56 has been shown to be an important

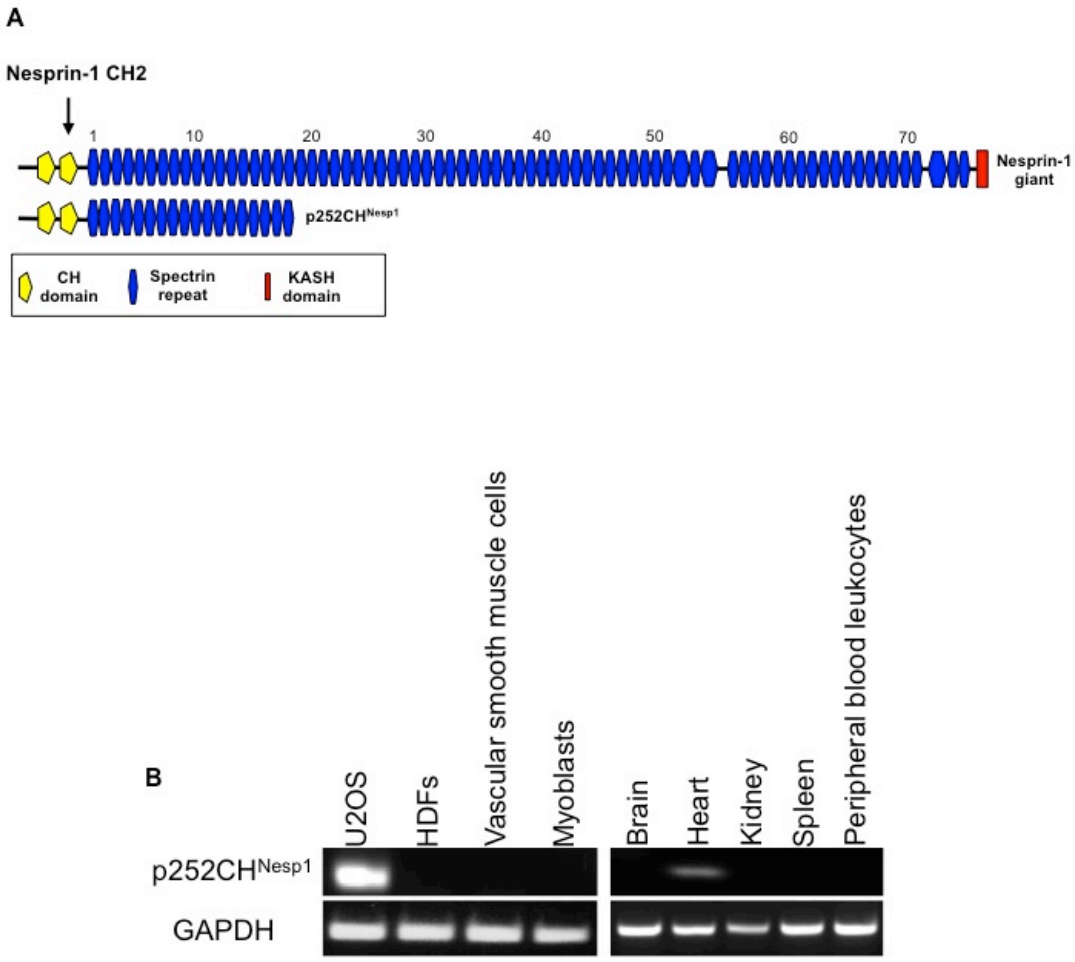

Figure 3.14 p252CH^{Nesp1} is selectively expressed. A) p252CH^{Nesp1} is generated by combining the nesprin-1 giant 5'UTR with the N1-3'E44 3'UTR. The translated protein product of this transcript is composed of both the nesprin-1 CHDs and the first 18 SRs of nesprin-1. B) To determine if the mRNA transcript of p252CH^{Nesp1} could be detected, RT-PCR was performed using a forward primer in the 5'UTR of the nesprin-1 giant and a reverse primer in N1-3'E44. The transcript for p252CH^{Nesp1} amplified only from U2OS cells and heart tissue suggesting it is highly tissue specific.

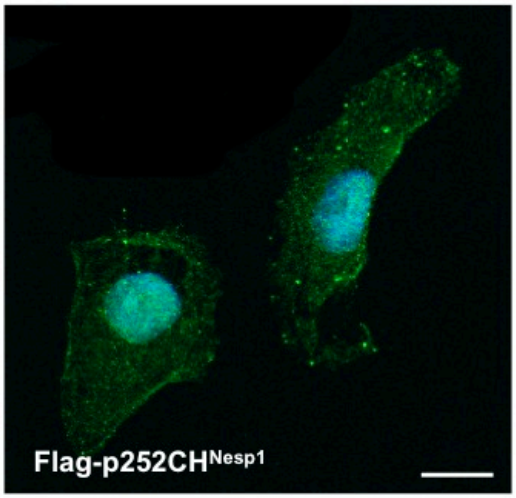

Figure 3.15 p252CH^{Nesp1} localizes to cytoplasmic foci in U2OS cells. p252CH^{Nesp1} amplified from U2OS cDNA, was cloned into a Flag-tag vector and transfected into U2OS cells to monitor it's sub-cellular localization. Flag staining localized p252CH^{Nesp1} to granular structures within the cytosol of U2OS cells. Image acquired using wide-field microscopy. Scale bar = 10 μM.

protein in maintaining Golgi structure and function, while CPG2 is required for clathrin-mediated uptake and recycling of chemokine receptors, suggesting that SRs are not only important in mediating protein-protein interactions but are also crucial as scaffolds and linkers in maintaining cellular architecture. The identification of multiple 5'UTRs and 3'UTRs within the nesprin-1 gene through online databases suggests other SR-only nesprin-1 variants could possibly be generated with structural roles in additional sub-cellular compartments.

3.2.7.1 Nesprin-1 N4 antibody

To identify novel endogenous nesprin-1 isoforms composed only of SRs of the central rod domain, our laboratory created an antibody called nesprin-1 N4. Nesprin-1 N4 antibody was generated to epitope 'EQNGQLGKPLAKKIGKL' encoded by exon 86 and located at amino acids (aa) 5488 to 5504 in SR50 of the nesprin-1 giant (Figure 3.16A). To determine the size of nesprin-1 variants generated by the central rod, Western blotting on whole cell lysates of U2OS cells and HDFs was performed. Multiple bands were seen in both cell lysates ranging from ~10kDa to ~150kDa (Figure 3.16B).

Peptide blocking experiments were performed to determine whether all the bands detected by nesprin-1 N4 were specific for the N4 epitope. U2OS whole cell lysates run out on SDS-PAGE and immobilized on membranes were incubated with the nesprin-1 N4 antibody or the nesprin-1 N4 antibody which had been pre-incubated with its blocking peptide for 1 hour at room temperature. Following Western development, all bands were blocked with the N4 peptide, confirming antibody specificity (Figure 3.17).

3.2.7.2 Potential Nesprin-1 variants

The laboratory had previously identified N1-5'E84 and N1-3'E87 as novel 5'UTRs and 3'UTRs respectively, that could be utilised to generate nesprin-1 variants detected by the nesprin-1 N4 antibody. By combining the N1-3'E87 UTR with N1-5'E84 and the nesprin-1β1 5'UTR it is possible to generate nesprin-1 variants $p23^{Nesp1}$ (23 kDa) and $p12^{Nesp1}$ (12 kDa)

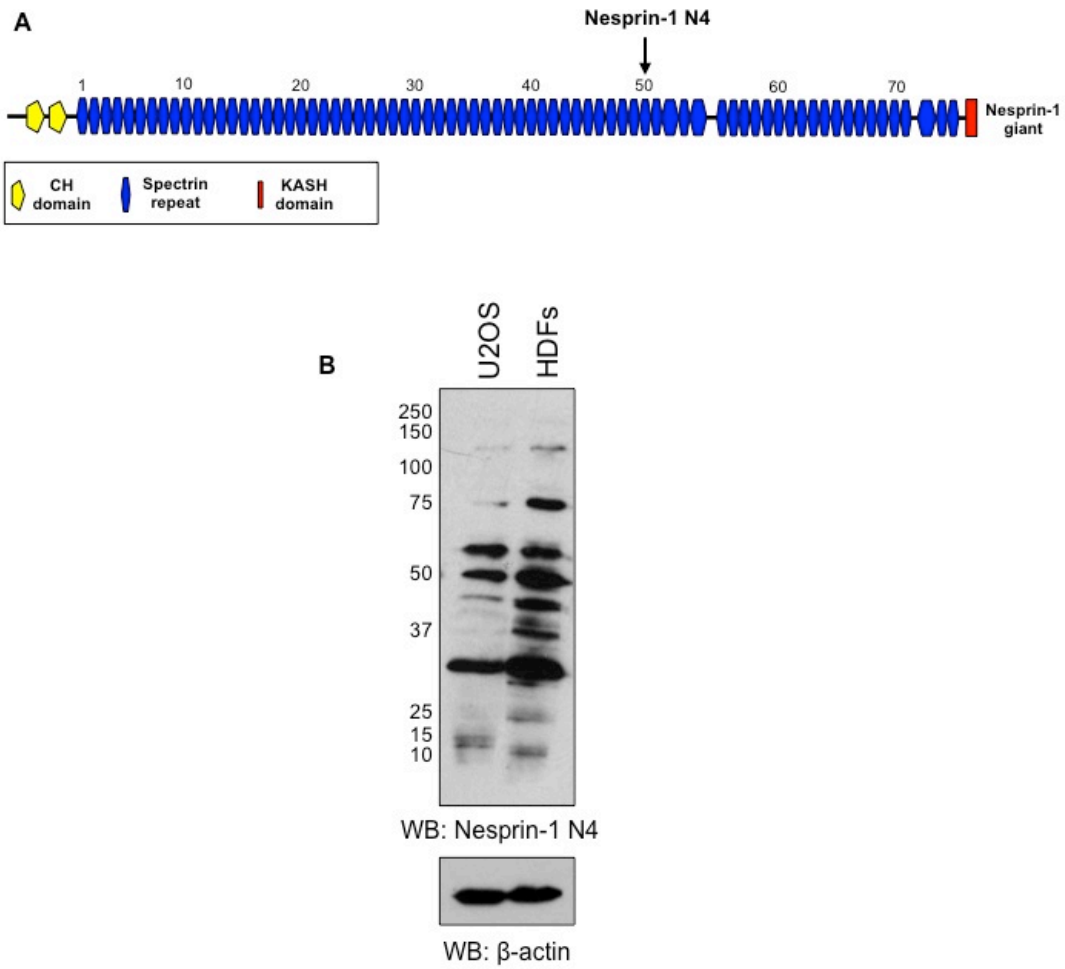

Figure 3.16 Nesprin-1 N4 detects multiple bands. A) To identify if novel nesprin-1 isoforms composed only of SRs of the central rod domain existed, our laboratory created an antibody called nesprin-1 N4 to SR50 of the nesprin-1 giant. B) Nesprin-1 N4 detects multiple bands in whole cell lysates of U2OS cells and HDFs, ranging in size from ~10 kDa to ~150kDa.

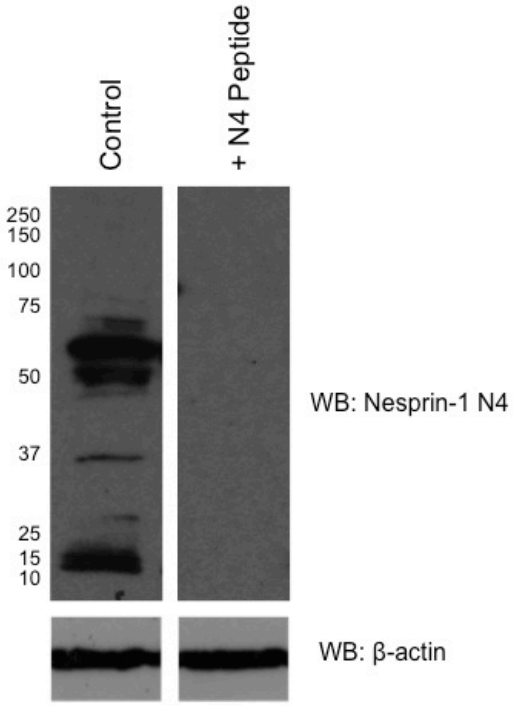

Figure 3.17 Nesprin-1 N4 bands can be blocked with the N4 peptide. Peptide blocking experiments were performed to determine whether all the bands detected by nesprin-1 N4 were specific for the N4 epitope. U2OS whole cell lysates run out on SDS-PAGE and immobilized on membranes were incubated with the N4 antibody (Control) or the N4 antibody which had been pre-incubated with its peptide (+N4 Peptide) for 1 hour at room temperature. Following Western development, all bands were blocked with the N4 peptide, confirming antibody specificity.

respectively (Figure 3.18A,B). Bands of approximately 23 kDa and 12 kDa were seen in both U2OS cells and HDFs suggesting these variants are expressed (Figure 3.16B).

3.2.7.3 Identification of N1-5'E83 and N1-3'E90

The nesprin-1β1 5'UTR, N1-5'E84 and N1-3'E87 alone could not account for the multiple bands seen by the nesprin-1 N4 antibody, therefore both 5' RACE and 3' RACE were performed downstream of exon 84 and upstream of exon 87 respectively, to identify additional UTRs which could account for nesprin-1 isoform diversity.

5'RACE using reverse primers designed in exon 83 amplified a PCR product in brain, skeletal muscle and HeLa cDNA libraries. The amplicon contained a novel 5'UTR with a start codon encoded by exon 83, presumably transcribed by an alternative promoter upstream on exon 83. N1-5'E83 RT-PCR amplified from multiple tissue cDNAs, suggesting it is ubiquitously expressed (Figure 3.19A,B).

3'RACE using forward primers designed in exon 90, amplified a PCR product containing sequences to exon 90 and intronic sequences between exons 90 and 91 of the nesprin-1 gene. The ORF carried on from exon 90 into the retained intron. The stop codon for this cDNA end was found in the retained intron after the unique coding sequence 'AGAGYPHQ'. Downstream of the stop codon was an *AATAAA* polyA signal followed by a polyadenylation site. As with N1-5'E83, N1-3'E90 also RT-PCR amplified from a wide range of tissue cDNA samples (Figure 3.19A,B).

3.2.7.4 Multiple nesprin-1 variants can be generated though alternative UTR combinations

By combining the newly identified N1-5'E83 and N1-3'E90 with each other and the pre-existing nesprin-1β1 5'UTR, N1-5'E84 and N1-3'E87 UTRs, it is possible to create six alternative nesprin-1 variants which may represent some of the bands detected by the nesprin-1 N4 antibody (Table 3.4, Figures 3.20 A,B 3.16B).

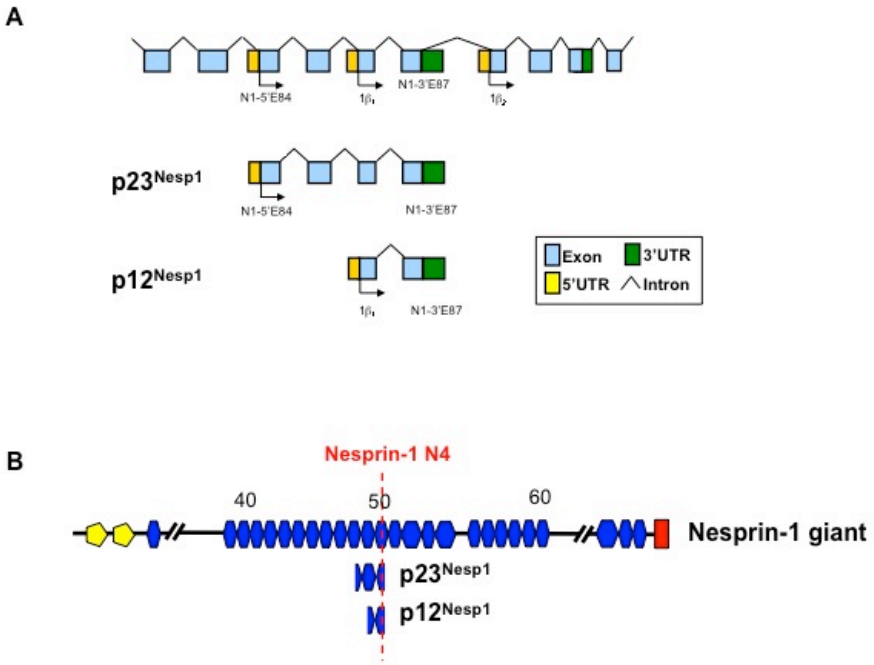

Figure 3.18 Potential Nesprin-1 N4 variants p23^{Nesp1} and p12^{Nesp1}. The laboratory had previously identified N1-5'E84 and N1-3'E87 as novel 5'UTRs and 3'UTRs that could be utilised to generate nesprin-1 variants detected by the nesprin-1 N4 antibody. By combining the N1-3'E87 3'UTR with N1-5'E84 and the nesprin-1β1 5'UTRs, it is possible to create nesprin-1 variants p23^{Nesp1} (23 kDa) and p12^{Nesp1} (12 kDa) respectively (Figure 3.17A,B). A) Nesprin-1 genomic map highlighting the 5'UTR and 3'UTRs for p23^{Nesp1} and p12^{Nesp1} . Both transcripts include exon 86 which encodes for the N4 epitope. B) SR schematics and the position of the N4 epitope within p23^{Nesp1} and p12^{Nesp1}.

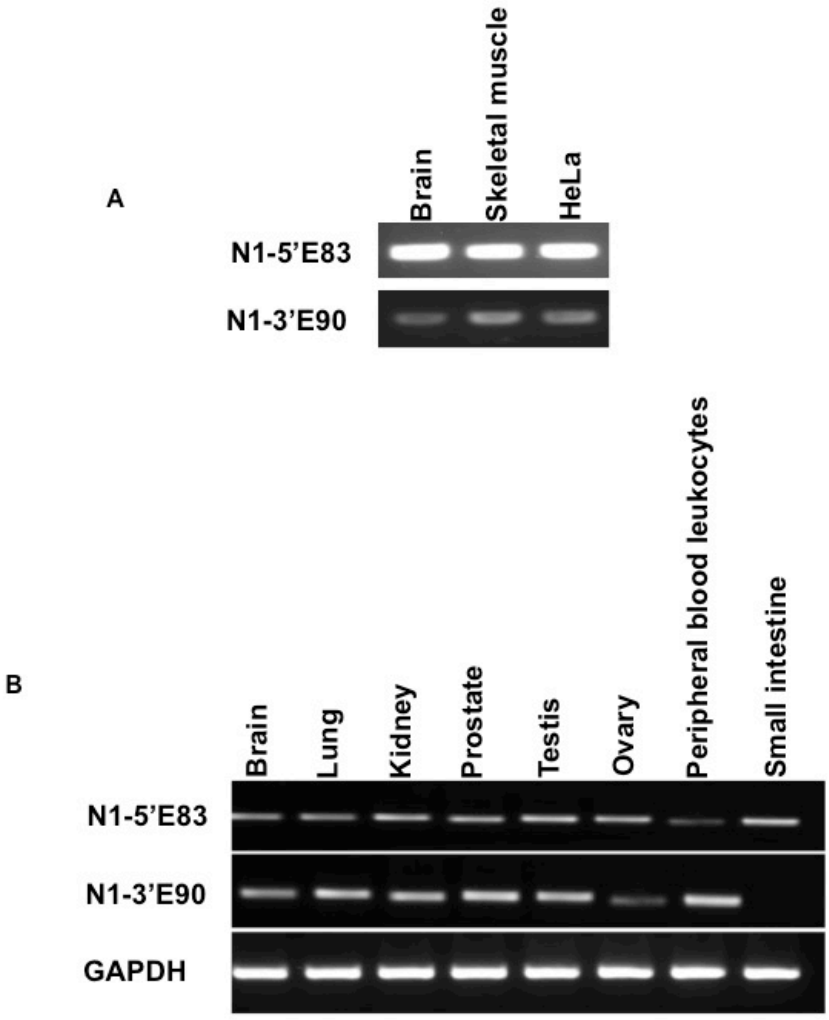

Figure 3.19 Identification of N1-5'E83 and N1-3'E90. To identify additional UTRs which could generate nesprin-1 variants recognized by the nesprin-1 N4 variants, 5' and 3' RACE was preformed downstream of exon 84 and upstream of exon 87 respectively, to identify additional UTRs which could account for nesprin-1 isoform diversity . A) 5'RACE using reverse primers designed in exon 83 amplified a PCR product in brain, skeletal muscle and HeLa cDNA libraries corresponding to N1-5'E83. 3'RACE using forward primers designed in exon 90 amplified a PCR product in brain, skeletal muscle and HeLa cDNA libraries corresponding to N1-3'E90. B) N1-5'E83 and N1-3'E90 were detected in a wide range of tissues by RT-PCR.

Table 3.4 Nesprin-1 N4 variants generated by alternative transcription. By combining the three unique 5'UTRs and two 3'UTRs clustered around the nesprin-1 N4 epitope, it is possible to generate 6 nesprin-1 variants. This table enlists the UTR combinations used to generate nesprin-1 SR variants in Figure 3.20.

Isoform	5'UTR	3'UTR	Mw (kDa)	Accession No.
$p31^{Nesp1}$	N1-5'E83	N1-3'E87	31	JQ740785
$p23^{Nesp1}$	N1-5'E84	N1-3'E87	23	JQ754364
$p12^{Nesp1}$	$1\beta_1$	N1-3'E87	12	JQ754365
$p50^{Nesp1}$	N1-5'E83	N1-3'E90	50	JQ740784
$p41^{Nesp1}$	N1-5'E84	N1-3'E90	41	JQ740786
$p30^{Nesp1}$	$1\beta_1$	N1-3'E90	30	-

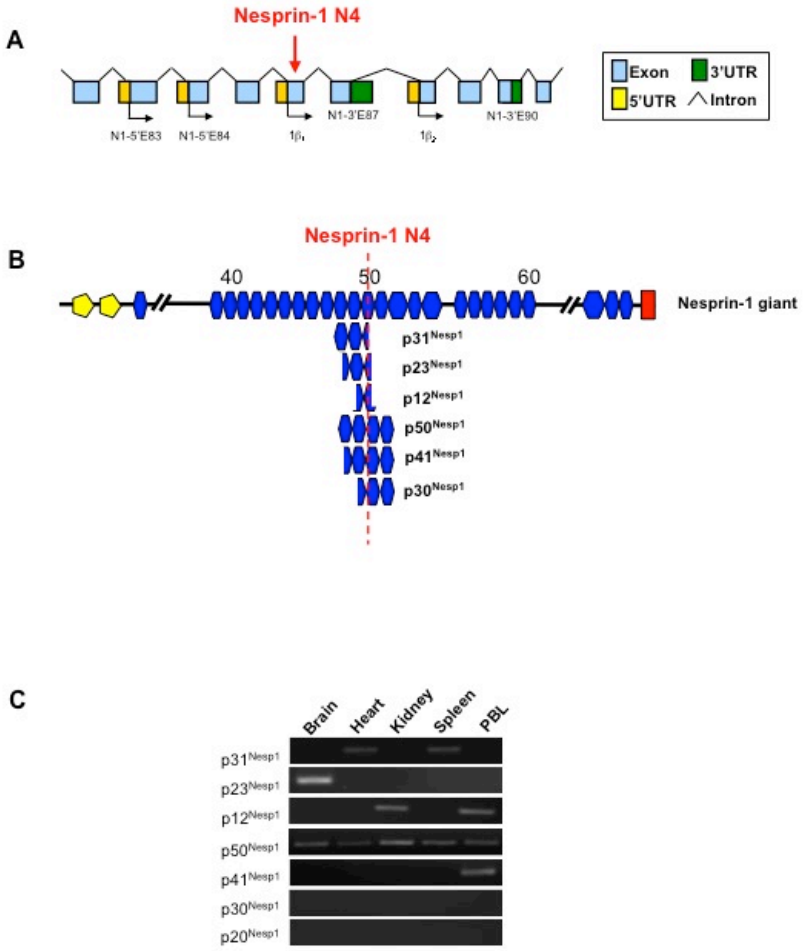

Figure 3.20 Nesprin-1 N4 variants generated by alternative transcription. A) Genomic map of nesprin-1 with the 5'UTRs and 3'UTRs clustered around the nesprin-1 N4 epitope. B) SR schematics of the 6 potential nesprin-1 N4 variants. C) RT-PCR on multiple tissue collection demonstrates the tissue specific nature of the nesprin-1 N4 variants.

3.2.7.5 p50^{Nesp1} is a microtubule nesprin-1 variant

p50^{Nesp1} is created through the utilization of the N1-5'E83 and N1-3'E90 UTRs. The 50 kDa variant composed of 4 SRs was detected in multiple tissues by RT-PCR (Figure 3.19). Flag-p50^{Nesp1} localized to fibrous structures that co-localized with α-Tubulin in U2OS cells suggesting that p50^{Nesp1} localizes to microtubules. Transfected cells also displayed α-Tubulin staining which appeared more structured and polymerized, resembling bundled microtubules [253] (Figure 3.21).

3.2.7.6 p41^{Nesp1} is a diffusive nesprin-1 variant

p41^{Nesp1} terminates with the same N1-3'E90 3'UTR as p50^{Nesp1} but initiates at N1-5'E84, making it approximately half a SR shorter at the N-terminus than p50^{Nesp1}. p41^{Nesp1} transcript appears to be a peripheral blood leukocytes specific nesprin-1 variant suggesting the protein may have a function in the immune response (Figure 3.20). Flag-p41^{Nesp1} localized diffusively within the cytosol when transfected into U2OS cells (Figure 3.21A). Therefore the localization of the protein was also examined in HDFs where it also displayed a similar diffusive localization pattern (Figure 3.22B).

3.2.7.7 p31^{Nesp1}, p23^{Nesp1} and p12^{Nesp1} are nucleolar nesprin-1 variants

p31^{Nesp1} initiates from N1-5'E83 and terminates with N1-3'E87 to create a 31 kDa variant composed of 2 and a half SRs. p31 ^{Nesp1} transcript expression is limited to kidneys and peripheral blood leukocytes by RT-PCR (Figure 3.19). Flag-p31^{Nesp1} localized diffusively within the cytosol when expressed in U2OS cells and localized to the nucleolus in HDFs (Figure 3.23, 3.24A).

p23^{Nesp1} is composed of 2 half SRs either side of a full SR as a result of utilizing N1-5'E84 and N1-3'E87. Expression of this 23 kDa variant was limited to the brain (Figure 3.20). Flag-p23Nesp1 localized diffusively within the cytosol when expressed in U2OS cells (Figure 3.23). However in HDFs the nesprin-1 variant localized to and disrupted nucleolar morphology, causing fibrillarin to redistribute into peri-nucleolar caps (Figure 3.24B).

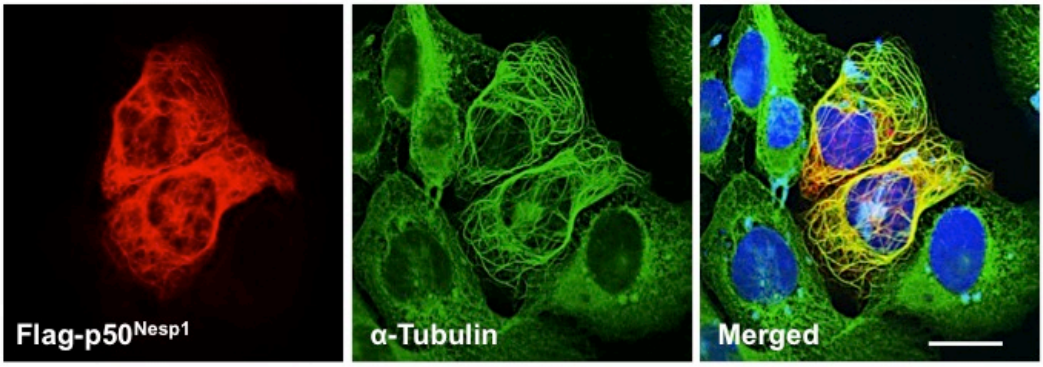

Figure 3.21 p50^{Nesp1} localizes to microtubules in U2OS cells. p50^{Nesp1} is created through the utilization of the N1-5'E83 and N1-3'E90 UTRs. The 50 kDa nesprin-1 variant localized to, and promoted microtubule bundling when a Flag-construct was transfected into U2OS cells. Image acquired using confocal microscopy. Scale bar = 10 μM.

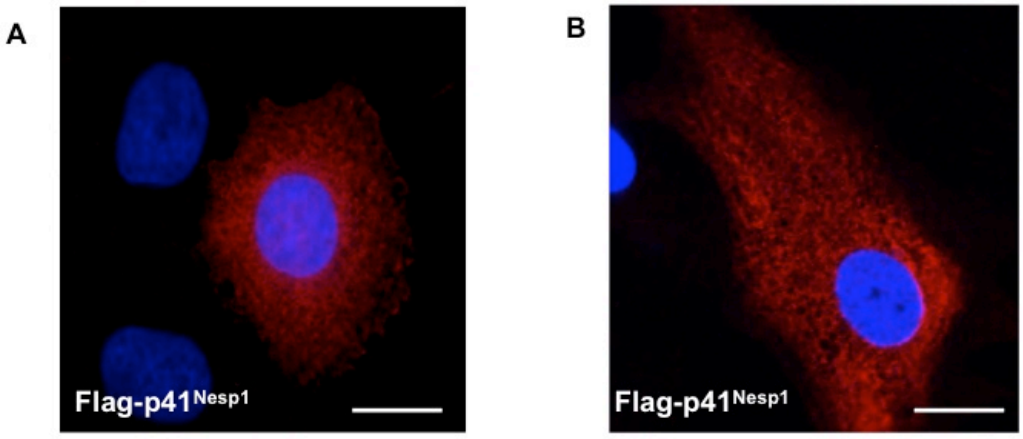

Figure 3.22 p41^{Nesp1} localizes diffusively in the cytosol of U2OS cells and HDFs. p41^{Nesp1} is created through the utilization of the N1-5'E84 and N1-3'E90 UTRs, to create a 41 kDa protein. A) Flag-p41^{Nesp1} localizes diffusively within the cytosol when transfected into U2OS cells. B) Therefore, its sub-cellular localization was examined in HDFs, where Flag-p41^{Nesp1} also localized diffusively within the cytosol. Images acquired using wide-field microscopy. Scale bars = 10 μM.

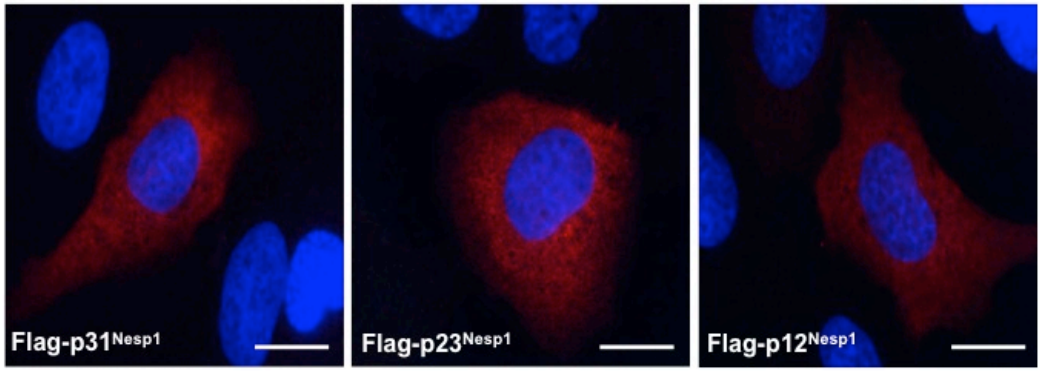

Figure 3.23 $p31^{Nesp1}$ $p23^{Nesp1}$ and $p12^{Nesp1}$ localizes diffusively in the cytosol of U2OS cells and HDFs. $p31^{Nesp1}$ $p23^{Nesp1}$ and $p12^{Nesp1}$ include the N1-3'E87 UTR however, $p31^{Nesp1}$ initiates with N1-5'E83, $p23^{Nesp1}$ with N1-5'E84 and $p12^{Nesp1}$ with the nesprin-1β1 5'UTR to generate 31 kDa, 23 kDa and 12 kDa proteins respectively. When Flag-constructs of the three variants are transfected into U2OS cells, they all localized diffusively within the cytosol. Images acquired using wide-field microscopy. Scale bars = 10 μM.

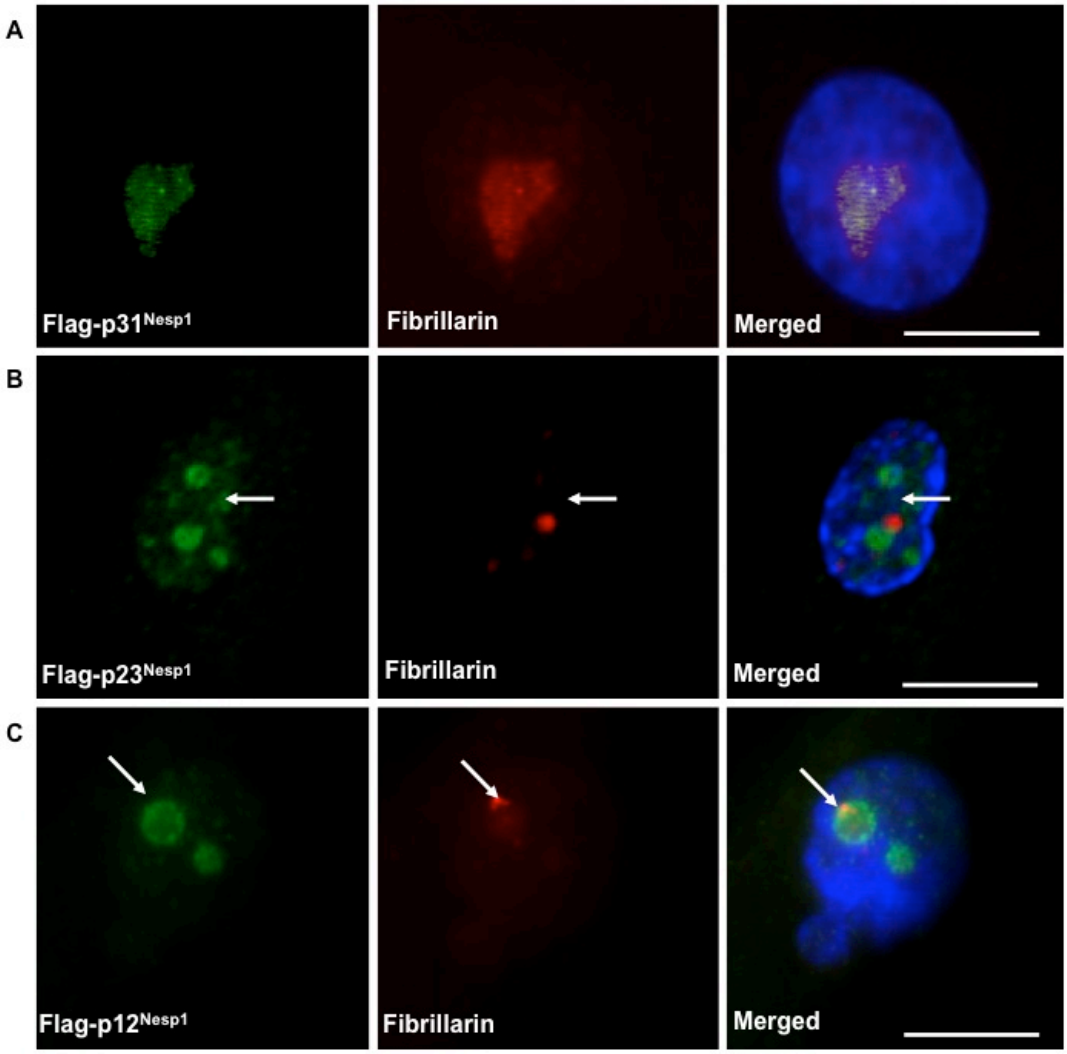

Figure 3.24 p31^{Nesp1}, p23^{Nesp1} and p12^{Nesp1} display nucleolar localizations in HDFs. p31^{Nesp1}, p23^{Nesp1} and p12^{Nesp1} all displayed cytoplasmic localizations when Flag-constructs were transfected into U2OS cells. Therefore the localization of their Flag-constructs were monitored in HDFs. A) Flag-p31^{Nesp1} co-localized with nucleolar marker fibrillarin at the nucleolus in HDFs. B) Flag-p23^{Nesp1} localized to the nucleolus, however re-distributed fibrillarin into nucleolar caps in HDFs C) Flag-p12^{Nesp1} also localized to the nucleolus, but also re-distributed fibrillarin into nucleolar caps in HDFs. This data suggests that nesprin-1 isoforms that terminate with N1-3'E87 may have nucleolar functions. Images acquired using confocal microscopy. Scale bars = 10 μM.

p12^{Nesp1} is the smallest nesprin-1 central rod isoform and is composed of 1 SR composed of 2 half SRs from adjacent repeats. p12^{Nesp1} initiates from the nesprin-1β1 5'UTR and terminates with the N1-3'E87 3'UTR, containing a coding region which spans over two coding exons. p12^{Nesp1} was detected in the kidney and peripheral blood leukocytes (Figure 3.20). Flag-p12^{Nesp1} localized diffusively within the cytosol when expressed in U2OS cells (Figure 3.23). However as with Flag-p31^{Nesp1}, in HDFs, Flag-p12^{Nesp1} localized to and disrupted nucleolar morphology, causing fibrillarin to redistribute into peri-nucleolar caps (Figure 3.24C). This data suggests that nesprin-1 isoforms that terminate with N1-3'E87 may have nucleolar functions.

3.2.7.8 p30 ^{Nesp1} failed to amplify from cDNA panel.

p30^{Nesp1} composed of 2 and a half SRs as a result of initiating from the nesprin-1b1 5'UTR and terminating with the N1-3'E90 3'UTR. The 30 kDa nesprin-1 variants could however not be amplified from any of the multiple tissue cDNA panel suggesting it is not expressed (Figure 3.20).

3.2.8. Nesprin-1 N4 bands represent newly identified nesprin-1 variants

To determine if any of the newly identified nesprin-1 variants were accountable for the many bands seen with the nesprin-1 N4 antibody, RT-PCR on cDNA isolated from U2OS cells and HDFs was performed to determine which N4 epitope containing variants were expressed in respective cell lines (Figure 3.25). The largest nesprin-1 variant with an accountable mRNA transcript was p50^{Nesp1} and was detected both by RT-PCR and Western blotting in large amounts from both U2OS cells and HDFs. Similarly p41^{Nesp1} and p31^{Nesp1} could be detected at both the mRNA level and protein level. The smaller nesprin-1 variants p12^{Nesp1} and p23^{Nesp1} were translated less abundantly relative to the bigger variants and displayed more of a cell specific expression. The transcription and translation products of p23^{Nesp1} were only present in HDFs whilst p12^{Nesp1} was specific to U2OS cells (Figure 3.25). Whereas many of the nesprin-1 N4 variants now appear accounted for, bands at ~130kDa, ~75kDa, ~37kDa and ~10kDa which remain unknown and will require further investigation. Furthermore, multiple nesprin-1 variants

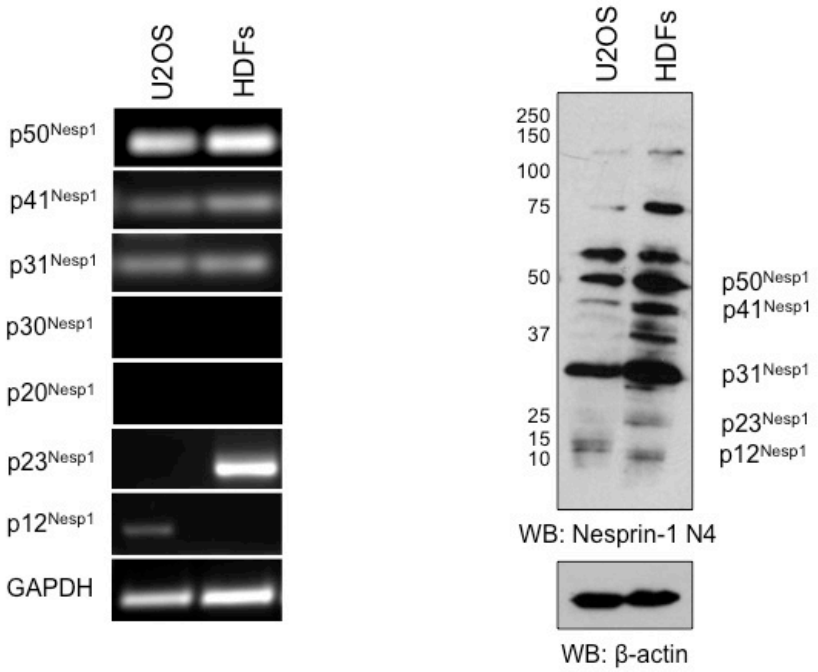

Figure 3.25 Detection of nesprin-1 N4 *in vitro*. To determine if any of the newly identified nesprin-1 variants were accountable for the many bands seen with the nesprin-1 N4 antibody, RT-PCR on cDNA isolated from U2OS cells and HDFs was performed to determine which N4 epitope containing variants were expressed in respective cell lines. RNA and protein lysates were harvested from the same experiment simultaneously. The Western blot used in this figure is the same as the one used in figure 3.16B. $p50^{Nesp1}$ was detected both by RT-PCR and Western blotting in large amounts from both U2OS cells and HDFs. Similarly $p41^{Nesp1}$ and $p31^{Nesp1}$ could be detected at both the mRNA level and protein level. $p12^{Nesp1}$ and $p23^{Nesp1}$ were translated less abundantly relative to the bigger variants and displayed more cell-type specific expression. The transcription and translation products of $p23^{Nesp1}$ were only present in HDFs, whilst $p12^{Nesp1}$ was specific to U2OS cells. Whereas many of the nesprin-1 N4 variants now appear accounted for, bands at ~130kDa, ~75kDa, ~37kDa and ~10kDa remain unknown and will require further investigation.

were knocked down in U2OS cells using siRNAs designed to target specific coding exons surrounding the nesprin-1 N4 epitope. Together with the peptide blocking experiments, this highlights the specificity of the multiple bands presented by the polyclonal antibody (Figure 3.17 and Chapter 4, figure 4.28).

3.2.9 Nesprin isoform expression is highly adaptable

To further confirm the validity of the novel variants, and because previous evidence indicates that nesprins have the ability to self-compensate, the effects of how knocking down a sub-set of transcripts would effect expression levels of variants encoded for by nearby transcripts was measured [191]. By designing an siRNA targeting exon 90 of nesprin-1 (si-90), it was possible to monitor by qRT-PCR the levels of transcripts terminating with N1-3'E87 and N1-3'E90 UTRs (Figure 3.26). In theory, si-90 should target all transcripts terminating with N1-3'E90, but have no effect on N1-3'E87 where the final coding exon is exon 87. As expected, si-90 significantly reduced levels of N1-3'E90 expression in U2OS cells, but more interestingly also significantly knocked down levels of the transcripts terminating with N1-3'E87. Furthermore, si-136 (targeting exon 136 of nesprin-1), an siRNA designed towards the KASH domain of nesprin-1 increased expression of N1-3'E87 transcripts, showing that perturbations in the expression of one transcript can influence expression of other downstream transcripts. Conversely, no change in N1-3'E90 was detected with si-136, however both si-90 and si-136 knocked down levels of nesprin-1 KASH expressing transcripts (Figure 3.26).

3.3 Discussion

3.3.1 Nesprins as adaptable, tissue specific, intracellular scaffolds

The potential combinations of nesprin-1 5'UTRs and 3'UTRs are multitudinous and would allow a vast array of nesprin-1 variants to be generated. Using alternative 5' and 3'UTRs, it is possible to generate at least 17 nesprin-1 KASH domain containing variants that may localize to the INM and/or the ONM (Figure 3.5). Likewise, 9 nesprin-1 CHD containing variants

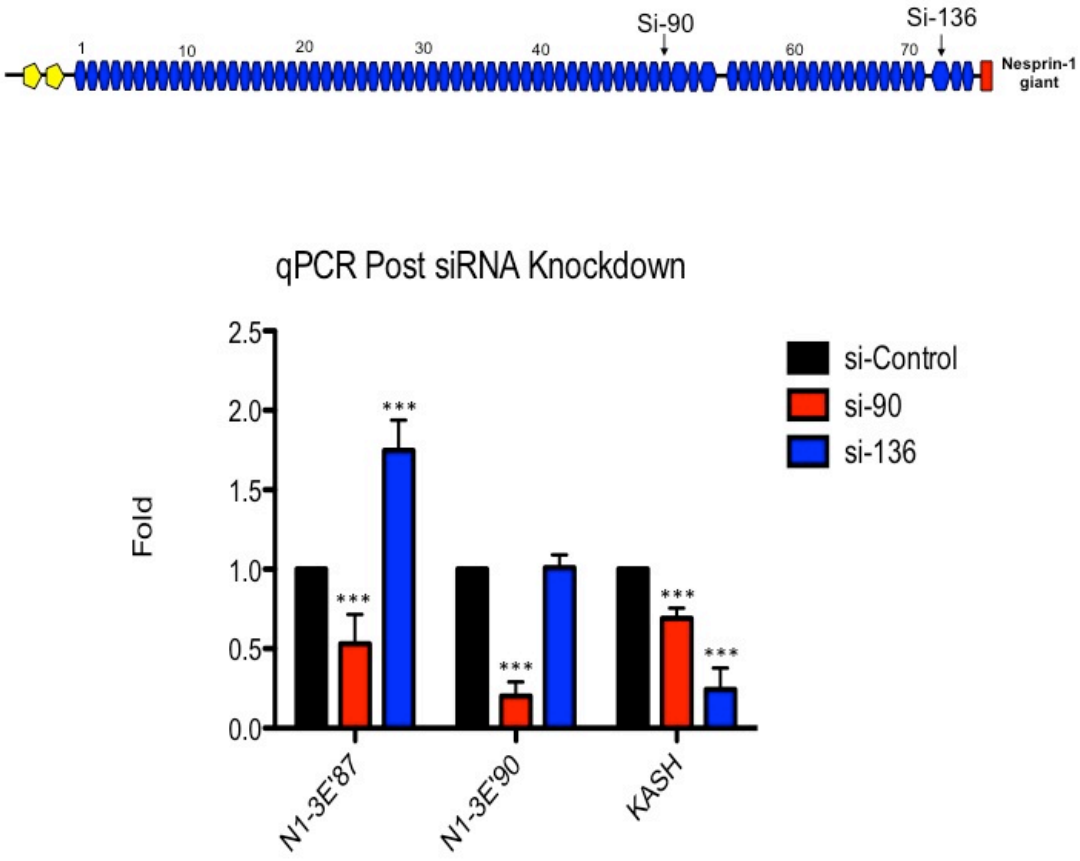

Figure 3.26 Nesprin-1 expression is highly adaptable. Previous evidence indicates that nesprins have the ability to self-compensate, therefore the effects of how knocking down a sub-set of transcripts would effect expression levels of variants encoded for by nearby transcripts was measured by qRT-PCR in U2OS cells. By designing an siRNA targeting exon 90 of nesprin-1 (si-90), it was possible to monitor by qRT-PCR, the levels of transcripts terminating with N1-3'E87 and N1-3'E90 UTRs in U2Os cells. In theory, si-90 should target all transcripts terminating with N1-3'E90 but have no effect on N1-3'E87. As expected, si-90 significantly reduced levels of N1-3'E90 expression in U2OS cells but more interestingly also significantly knocked down levels of the transcripts terminating with N1-3'E87. Furthermore, si-136 (targeting exon 136 of nesprin-1) increased expression of N1-3'E87 transcripts, showing that perturbations in the expression of one transcript can influence expression of other downstream transcripts. Conversely, no change in N1-3'E90 was detected with si-136, however both si-90 and si-136 knocked down levels of nesprin-1 KASH expressing transcripts. ***p<0.001; one-way ANOVA, Dunnett's *post hoc* test.

that range vastly in molecular weight have the potential to be generated by alternative UTRs (Figure 3.7). Although these variants were only briefly characterized, it is likely that they are expressed in a cell/tissue specific manner and are able to scaffold different sub-cellular compartments or protein complexes to the NE and actin cytoskeleton. Alternatively, these variants may be dynamically regulated, which would allow cells to fine-tune their nesprin isoform repertoire as needed to maintain and restore homeostasis following stress or to regulate tissue-specific signalling pathways [99,185]. As a proof of principle, adaptability in nesprin-1 transcription with a feedback loop was shown in figure 3.26. By using si-136 to knockdown a region of nesprin-1 near the KASH domain, an up regulation of N1-3'E87 UTR transcripts were observed. These observations are consistent with studies that have shown nesprin-2 CHD knockout mice display an altered expression pattern for specific nesprin-2 C-terminal isoforms in certain tissues to compensate for the loss of nesprin-2 giant or nesprin-2 actin binding domain isoforms [191]. These observations suggest that nesprin alternative transcript generation is highly flexible and more complex than a simplified tissue-specific expression model.

3.3.2 Generation, regulation and function of novel tissue specific nesprin variants via alternative initiation and alternative 3'end processing.

Multiple novel nesprin-1 variants were identified by RT-PCR using UTRs identified by 5' and 3' RACE, along with sequences identified previously by out laboratory (Table 3.1, Figures 3.9, 3,13, 3.19). RT-PCR was used to establish the existence of mRNA transcripts for full-length short isoforms (Figures 3.10, 3.14, 3.25). The multiple UTRs allow nesprin-1 to express a large number of sequence variants via alternate initiation and pre-mRNA 3'end processing and many of these were generated in a tissue specific manner (Figure 3.27 for updated nesprin-1 genomic map with new UTRs). Therefore, in addition to the novel UTR's verified in this study, it is likely that by performing RACE on a greater collection of cells/tissues it may be possible to identify further nesprin-1 UTRs. To date, the mechanisms of tissue specific

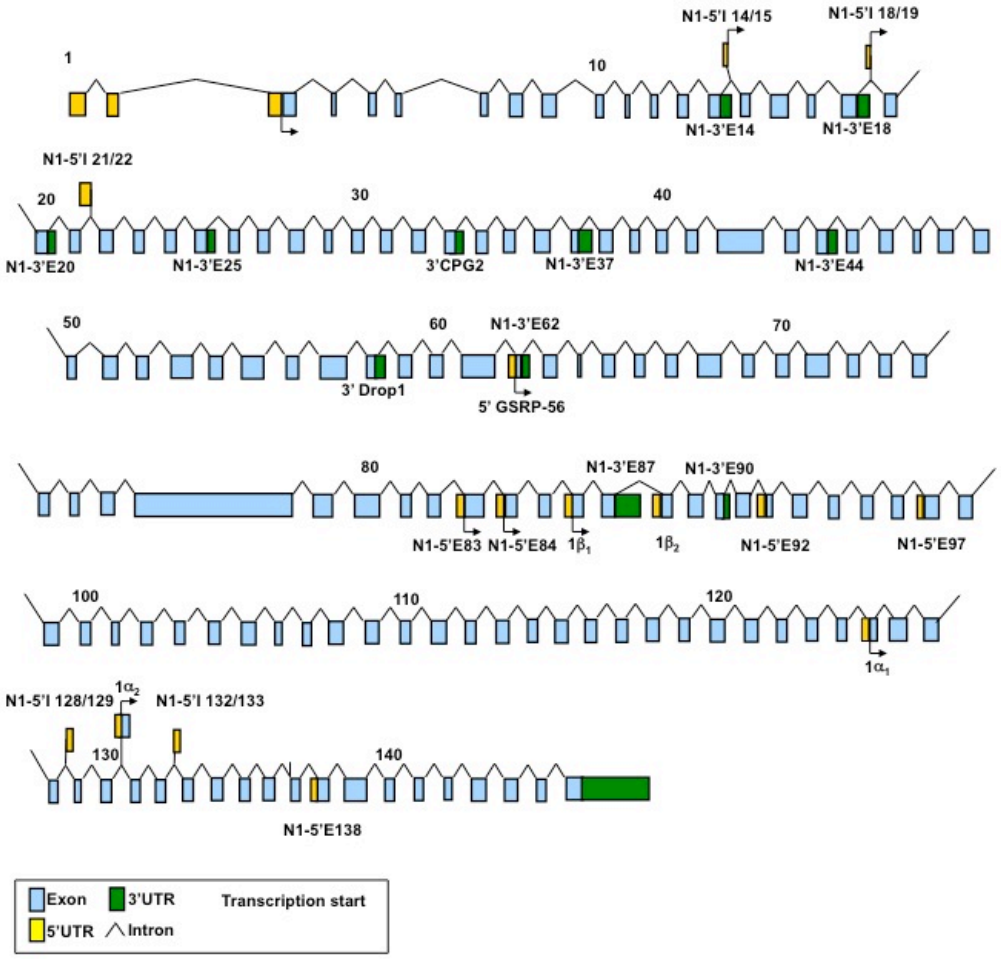

Figure 3.27 Nesprin-1 genomic map with new UTRs. Up to date genomic map of the nesprin-1 gene, highlighting the positions of the nesprin-1 UTRs identified in this chapter, and those previously identified though online databases.

generation of nesprin variants has not been studied. Analysis of the human transcriptome shows a direct correlation between alternative promoter use and alternative splicing [254]. Alternative promoters can produce mRNAs with different 5'UTRs that encode the same protein, distinct N-termini, and even different proteins from the same locus [255,256,257]. The identification of multiple novel 5'UTRs in nesprin-1 indicates the presence of several internal alternative promoters. The existence and regulation of alternative nesprin-1 promoters has not yet been explored but this study suggests that these promoters are utilised in a tissue specific manner. Furthermore, because many individual variants have unique pairs of 5' and 3'UTRs, additional control and regulation of variant expression can be maintained. The 5'UTR is an important regulator of mRNA translation and can contain regulatory motifs/sequences which affect the rate of translation as well as containing a kozak sequence upstream of the start codon which plays a major role in determining the translational strength of the transcript [258,259]. The 3'UTR of mRNA transcripts can play a role in mRNA localization, stability, and translation [260,261,262,263]. For example, binding of miRNAs to partially complementary sequences in the 3'UTR can result in de-adenylation and translational inhibition or destruction of the target mRNA [264]. Future work should focus on scanning the entire length of all the 5' and 3' UTRs for regulatory motifs, such as miRNA binding sites.

Importantly, many of the variants generated through alternative 3'end processing, generate unique peptide sequences that range in size from 8 amino acids in N1-3'E90 to 37 amino acids in N1-3'E14. It is highly likely that these sequences expose new functional domains that give the variants additional localization signals or motifs that play an important role in their function or localizations. For example, $p31^{Nesp1}$, $p23^{Nesp1}$ and $p12^{Nesp1}$ which terminate with N1-3'E87 have a unique C-terminal peptide sequence which may contribute to the nucleolar localization of these variants in HDFs. Furthermore, ELM analysis predicts a novel myristoylation site in the N-terminus of $p931KASH^{Nesp1}$, a post-translational modification which facilitates membrane anchoring, suggesting this variant of nesprin-1 may link membranous organelles to the NE [265,266]. ELM analysis also predicts multiple PKA, MAPK and CDK phosphorylation sites in the unique 37 amino

acids of p56CH^{Nesp1}, which may play a role in contributing to its different sub-cellular localizations observed in U2OS cells and HDFs. To further explore this hypothesis, yeast-2-hybrid analyses or co-immunoprecipitation assays should be performed to identify binding partners for specific nesprin-1 variants.

Post-translational modifications such as phosphorylation, sumoylation, and enzymatic cleavage may be partially responsible for the range of Western bands often visualized using the current crop of available nesprin antibodies [14,66,191]. Designing isoform-specific antibodies will help to distinguish between modifications and splicing.

3.3.3 Nesprin-1 variants display different sub-cellular localizations

In this chapter, I demonstrated that KASH-less nesprin-1 variants displayed sub-cellular localizations which varied depending on the cell lines they were expressed in (Figures 3.11, 3.12, 3.22, 3.23, 3.24, 4.17). In U2OS cells, p56CH^{Nesp1} localized to the nucleolus while the same protein localized along actin stress fibres and focal adhesions in HDFs (Figures 3.11, 3.12). The reasons behind the differential sub-cellular localizations currently remain a mystery, but could be partially regulated by the actin cytoskeleton. The nesprin-1 CHDs contain two nuclear localization signals which may be utilized in cells with low F-actin levels such as U2OS cells, but not in structural cells like HDFs where there is increased levels of cytoplasmic actin available for binding. Alternatively, potential p56CH^{Nesp1} phosphorylation events predicted by ELM analysis may occur in a tissue specific manner, which may contribute to the differences seen in localizations between the two cell types as described above. Similarly, differential sub-cellular localizations were seen when central rod isoforms p12^{Nesp1}, p23^{Nesp1} and p31^{Nesp1}, were transfected into U2OS and HDFs (Figures 3.23, 3.24). In U2OS cells, all isoforms displayed diffuse cytoplasmic localization, while in HDFs nucleolar localization was observed. Differences in post-translational modifications could vary between the two cell lines or the proteins may have different binding partners.

Chapter 4: Nesprin-1 Links P-bodies to Microtubules and is Required for miRISC

4.1 Introduction

In chapter 3, I identified novel nesprin-1 variants composed of SRs encoded by the central rod domain and demonstrated they have sub-cellular localizations beyond the NE. RT-PCR and Western blotting with the nesprin-1 N4 antibody, was used to demonstrate that these species are transcribed and translated into protein. In this chapter, nesprin-1 N4 variants are further characterized by monitoring their endogenous sub-cellular localizations, which show they match the sub-cellular localizations of ectopically expressed constructs.

This chapter of the thesis primarily focuses on the role of nesprin-1 in cytoplasmic RNA processing bodies (P-bodies), a localization confirmed for the nesprin-1 N4 antibody (see below). P-bodies are membrane-less cytoplasmic foci conserved in vertebrates and invertebrates as well as yeast, plants and trypanosomes. At the cellular level, P-bodies are dynamic aggregates of mRNA-protein complexes (mRNPs) that predominantly serve to store translationally silenced mRNAs and recruit mRNAs which are targeted for deadenylation and degradation by the decapping/Xrn1 pathways [267]. I show that nesprin-1 variant, $p50^{Nesp1}$, localizes to P-bodies and scaffolds them to microtubules. $p50^{Nesp1}$ was chosen to primarily be characterised because no SR proteins have previously been implicated in P-body biology, and this work significantly contributes to how microtubule based P-body attachment regulates cellular mRNA dynamics.

4.1.1 P-bodies as sites for mRNA decay

P-bodies play host to a range of proteins implicated in mRNA decay. Degradation of most mRNAs in eukaryotic cells is initiated by shortening and removal of the poly(A) tail which is mediated by deadenylating enzymes such as the Ccr4–Caf1 and Pan2– Pan3 complexes which localize to P-bodies [268]. Following deadenylation, mRNA can be degraded in either the 5'-3'

direction through the decapping pathway or 3'-5' direction via the exosome pathway [269].

P-bodies also contain the exoribonuclease Xrn1 together with the associated Lsm1–7 protein complex, which is believed to bind to mRNAs with short poly(A) tails [270,271]. P-bodies further contain the decapping enzyme Dcp2 together with many of its enhancers: Dcp1a, Dcp1b Edc3, Hedls, Pat1 and Rck/p54 [272,273,274,275]. The presence of all the proteins required for degrading mRNAs via the deadenylation–decapping–5′–3′ decay pathway in P-bodies suggest that these micro-environments are able to deal with mRNA degradation to a high efficiency. Exosome components, which mediate 3'-5' degradation localize to cytoplasmic granules distinct from P-bodies suggesting that the two major mRNA degradation pathways are spatially segregated within the cytoplasm [276,277]. Although the sequestration of mRNA degradation enzymes in P-bodies does not necessarily imply that mRNA degradation occurs within these microenvironments, four lines of evidence support the notion that P-bodies are mRNA degradation centers. 1) P-bodies disappear after inhibition of deadenylation by deletion of Ccr4 in *S. cerevisiae* or in cells depleted of Caf1, indicating that deadenylation is a requirement for P-body formation [273,278]. 2) Poly(A)-binding protein (PABP) is absent from P-bodies, suggesting that most of the mRNAs within P-bodies lack long poly(A) tails. Since deadenylation is the initial step of most mRNA decay pathways, this suggests that mRNAs located within P-bodies are already engaged in the degradation process [239]. 3) P-bodies increase in number and size when mRNA decay is inhibited in an Xrn1-deleted *S. cerevisiae* strain. The mRNA itself accumulates in P-bodies under these conditions, and the same was observed after knockdown of Xrn1 in human cells [269,273]. 4) mRNA decay intermediates could be trapped in *S. cerevisiae* P-bodies [273]. Taken together, these findings support a model where deadenylation is linked to the initial step by which mRNAs enter P-bodies. This model would further suggest that decapping and 5′–3′ decay of the mRNA subsequently occur within P-bodies, since mRNAs remain trapped and accumulate in P-bodies if these steps are inhibited [273]. However, it is important to note that not all mRNAs are degraded within P-bodies, as mRNAs can also exit P-bodies and re-initiate translation [279].

4.1.1.1 Non-sense Mediated decay (NMD)

mRNA transcripts which have premature termination codons (PTC) have a tendency to be rapidly degraded by the NMD pathway before they translate a truncated faulty protein. Many protein factors required for NMD appear to have transient localization to P-bodies in yeast, the essential NMD factors Upf (up-frameshift) 1, Upf2 and Upf3 have a diffuse cytoplasmic distribution, but accumulate in P-bodies when mRNA decay is inhibited as observed in Xrn1-, Dcp1- or Dcp2-deletion strains [280]. Similarly, human Upf1, Upf3 and Upf3X visibly accumulate in P-bodies only when NMD is inhibited by a chemical compound, that causes the hyperphosphorylation of Upf1 [281]. Additional factors required for NMD such as Smg (suppressor with a morphogenetic effect on genitalia) 5, Smg6 and Smg7 also localize to P-bodies [281,282]. More importantly, the PTC-containing mRNA itself is specifically recruited to P-bodies both in yeast and in human cell lines when Upf1 is locked in P-bodies by an NMD inhibitor [281]. Rather than being permanently associated with P-bodies, it appears that most NMD factors cycle through P-bodies as NMD substrates are delivered for degradation [282].

4.1.1.2 ARE (AU-rich-element) mediated decay (AMD)

AREs are found in the 3'UTR of many cytokine and proto-oncogene mRNAs, and by mediating rapid mRNA degradation they potently inhibit gene expression at the post-transcriptional level [283]. Bioinformatic approaches have estimated that 5–8% of all mRNAs may contain AREs, indicating that AMD is a widespread mode of regulating gene expression [284]. The three main mammalian inducers of AMD are TTP (tristetraprolin), BRF (butyrate response factor) 1 and BRF2 proteins. These proteins function as adaptors that connect ARE-containing mRNAs to the exosome as well as to the decapping 5′–3′ decay complex, thereby delivering the bound mRNAs to the general decay machinery [285,286]. TTP, BRF1 and BRF2 all localize to P-bodies with ARE-containing reporter mRNAs. The presence of ARE-containing mRNAs in P-bodies depends on the TTP/BRF proteins, suggesting that these proteins deliver bound mRNAs to P-bodies, or nucleate P-bodies once they bind to target mRNAs. Both ARE-containing mRNAs and TTP/BRF

proteins strongly accumulate in P-bodies when the general decay pathway is inhibited by the knockdown of Xrn1 or Dcp2 and therefore AMD factors appear to also associate transiently with P-bodies [287].

4.1.1.3 miRNA induced mRNA silencing

miRNAs silence gene expression by either repressing translation or by inducing decay of the mRNAs to which they are bound. miRNAs exert their function by recruiting RISC (RNA-induced silencing complex) to the mRNA. Many proteins that are associated with RISC and important for miRNA-mediated suppression localize to P- bodies. This includes all four human Argonaute (Ago) proteins, GW182 (TNRC6A) together with its two human paralogues TNRC6B and TNRC6C, as well as the RNA helicase Rck/p54 [243,288,289,290]. Both Rck/p54 and GW182 are essential for P-body formation [290,291]. An important function of GW182 protein is to target Ago proteins to P-bodies [292]. Using transfected reporters, it has been demonstrated that miRNAs and their target mRNAs specifically localize to P-bodies [288]. For example, endogenous CAT-1 (cationic amino acid transporter-1) mRNA together with miR-122 localizes to P-bodies in liver cells. CAT-1 mRNA associates with P-bodies under conditions where translation is suppressed by miR-122, yet the same mRNA is released from P-bodies when its translation is activated by amino acid starvation [293]. Importantly, studies in both *D. melanogaster* and mammalian cells conclude that P-body formation is the consequence rather than the cause of miRNA-mediated mRNA silencing. Indeed, when general mRNA silencing is prevented by knocking down components of the miRNA biogenesis pathway, this leads to the loss of P-bodies. Interestingly, re-introduction of siRNAs caused P-bodies to re-emerge, emphasizing that the pool of silenced mRNAs is a key determinant of P-body formation [294]. Similar to the studies with NMD and AMD targets, these results point towards a very dynamic model of P-body formation. In this flux-based model, P-bodies are formed and resolved according to the amount of mRNA that is subject to silencing, be it translational arrest or targeting for decay.

4.1.2 Stress Granules (SGs)

SGs are large aggregates of mRNAs, translation initiation factors and 40S ribosomal subunits that accumulate in the cytosol of cells undergoing translational arrest. SGs are formed in cells that have been exposed to different forms of stress such as heat shock, oxidative stress or energy deprivation [295]. Although P-bodies and SGs are distinct structures, there is strong evidence that the two compartments are functionally linked. SGs emerge next to P-bodies in *S. cerevisiae,* and in these cells the formation of SGs is dependent on the presence of P-bodies [296]. In mammalian cells however, P-bodies and SGs are formed independently, since abrogation of P-bodies does not hamper SG assembly and vice versa [239]. Transient contacts between P-bodies and SGs are frequently observed in mammalian cells suggesting that mRNPs may be exchanged between the two bodies. This would imply that cells may utilize dynamic compartments to regulate the flux of their mRNAs within the cytoplasm in response to environmental cues [239].

4.2 Results

4.2.1 Nesprin-1 N4 localizes endogenous nesprin-1 variants to the nucleolus and cytoplasmic foci

To identify the sub-cellular localization of endogenous nesprin-1 variants described in chapter 3, immunofluorescence microscopy using the nesprin-1 N4 antibody was performed on cultured U2OS cells and HDFs (Figure 4.1 A,B,C). In both cell lines, nesprin-1 N4 stained multiple cytoplasmic foci that varied in size and number between individual U2OS cells and HDFs.

Additionally, the antibody stained sub-nuclear compartments that co-localized with nucleolar marker fibrillarin (Figure 4.2). The nucleolar localizations of endogenous nesprin-1 appear to match the localizations of the novel transfected nesprin-1 variants identified in chapter 3. Both cell lines expressed nucleolar nesprin-1 variant $p31^{Nesp1}$, whilst $p12^{Nesp1}$ appears to be U2OS specific and $p23^{Nesp1}$ HDF specific (Figures 3.24, 3.26).

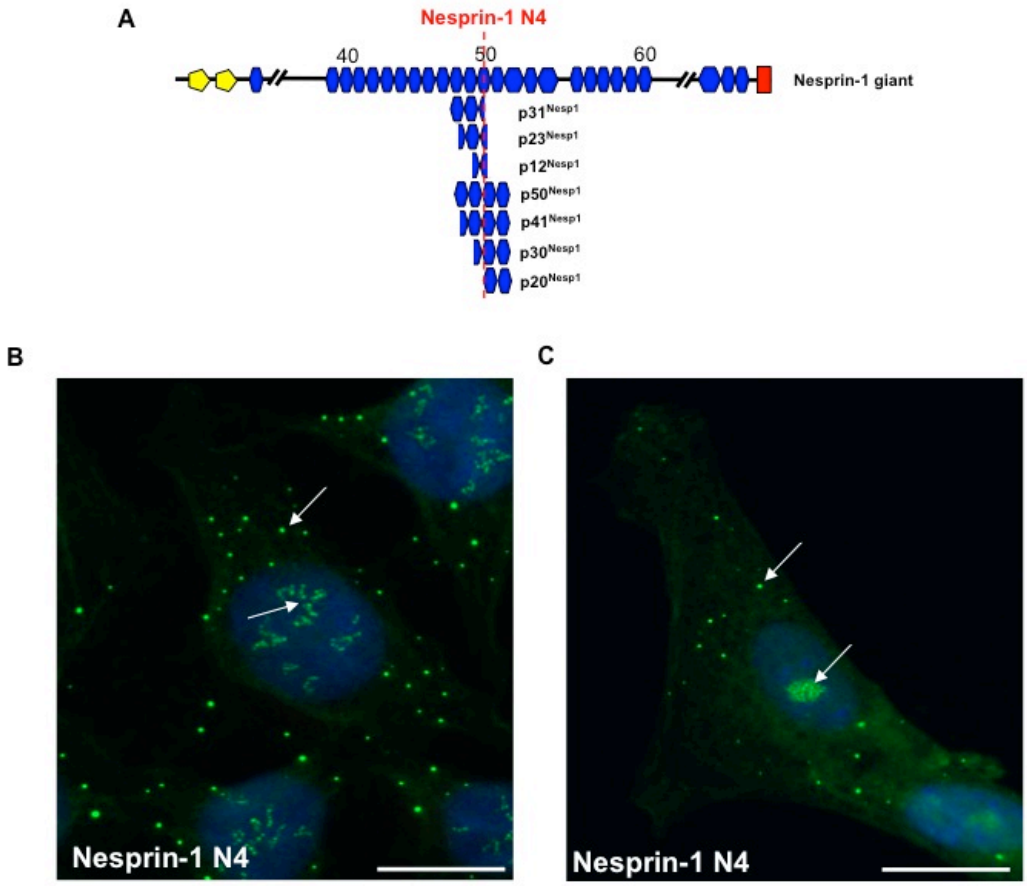

Figure 4.1. Endogenous nesprin-1 N4 variants localize to the nucleus and cytoplasmic foci. A) Schematic representation of nesprin-1 variants recognized by the nesprin-1 N4 antibody. B) Nesprin-1 N4 immunofluorescence microscopy on cultured U2OS cells stained numerous cytoplasmic foci and sub-nuclear structures. B) Nesprin-1 N4 immunofluorescence microscopy on cultured HDFs stained numerous cytoplasmic foci and sub-nuclear structures. Images acquired using wide-field microscopy. Scale bars = 10 μM.

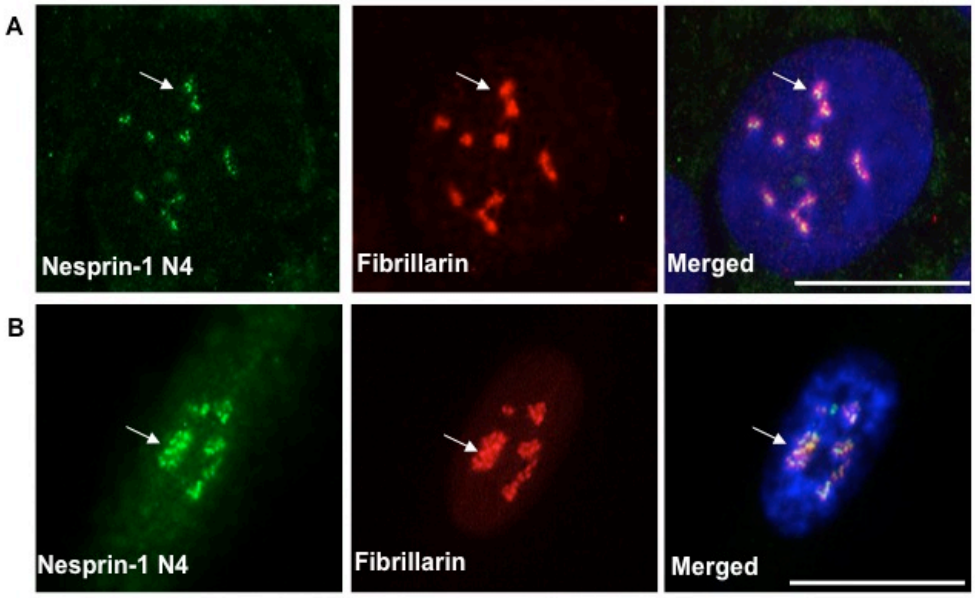

Figure 4.2. Endogenous nesprin-1 N4 variants localize to the nucleolus. Co-localization studies with nucleolar marker fibrillarin were performed to determine whether endogenous nesprin-1 matches localization of ectopically expressed nucleolar variants $p12^{Nesp1}$, $p23^{Nesp1}$ and $p31^{Nesp1}$ (Figure 3.24). A) Nesprin-1 N4 co-localized with fibrillarin in the nucleolus of U2OS cells. B) Nesprin-1 N4 co-localized with fibrillarin in the nucleolus of HDFs. Images acquired using confocal microscopy. Scale bars = 10 μM.

To determine whether the cytoplasmic foci and nucleolar staining were specific for the nesprin-1 N4 antibody, and not due to cross-reaction with other epitopes present in fixed cells, peptide blocking experiments were performed. All staining was diminished when the nesprin-1 N4 antibody was pre-blocked with its excess peptide and then used to stain U2OS cells, confirming the antibody stains genuine nesprin-1 proteins with the N4 epitope (Figure 4.3). To further confirm antibody specificity, siRNA knockdown experiments performed in the latter sections of this thesis eliminated certain nesprin-1 staining (Figure 4.28).

4.2.2 Nesprin-1 localizes to P-bodies

To identify the sub-cytoplasmic foci structures detected by the nesprin-1 N4 antibody, the online literature was scanned for potential proteins which localize as foci's within the cytosol. One group of proteins resembled those which belong to a family of RNA binding proteins which aggregate with RNA within the cytosol. These proteins localize in membrane-less compartments known as mRNA processing bodies (P-bodies) or stress-induced granules called stress granules (SGs) [291,297,298].

To ascertain if the nesprin-1 cytoplasmic foci could be P-bodies, nesprin-1 N4 was co-stained with a P-body marker, human enhancer of decapping large subunit (Hedls), in U2OS cells [299]. All the nesprin-1 foci co-localized with Hedls P-bodies confirming the presence of nesprin-1 in P-bodies (Figure 4.4).

Next, a series of experiments were carried out to compare the physical properties of nesprin-1 P-bodies. Oxidative stress is commonly used to not only induce P-body formation but also to promote assembly of (SGs) [239,299]. The number of Hedls-positive nesprin-1 foci substantially increased in U2OS cells exposed to sodium arsenite (0.5 mM) for one hour (Figure 4.5). Furthermore, a population of stressed cells displayed a loss of nucleolar nesprin-1 staining, indicating the nucleolar variants may be stress responsive. Immunostaining for eIF3-η which labels SGs in arsenite stressed U2OS cells failed to co-localize with the nesprin-1 foci suggesting that nesprin-1 is only present in P-bodies [239]. However the nesprin-1 foci did

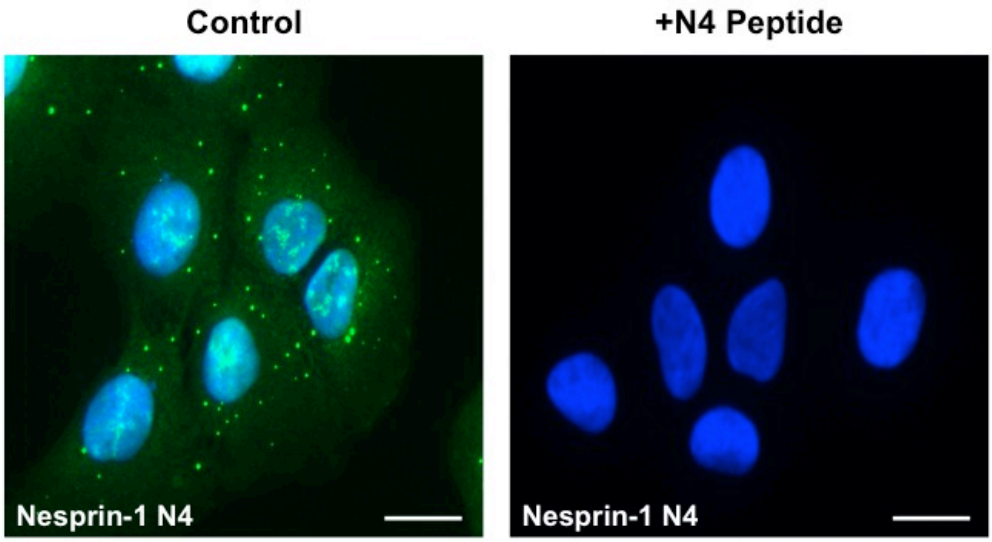

Figure 4.3. Nesprin-1 N4 staining is blocked by incubating antibody with purified N4 peptide. To determine whether the cytoplasmic foci and nucleolar staining were specific for the nesprin-1 N4 antibody, and not due to cross-reaction with other epitopes present in the fixed cells, peptide blocking experiments were performed. All staining was diminished when the nesprin-1 N4 antibody was pre-blocked with excess peptide and then used to stain U2OS cells, confirming the antibody stains genuine nesprin-1 proteins that posses the N4 epitope. Images acquired using wide-field microscopy. Scale bars = 10 μM.

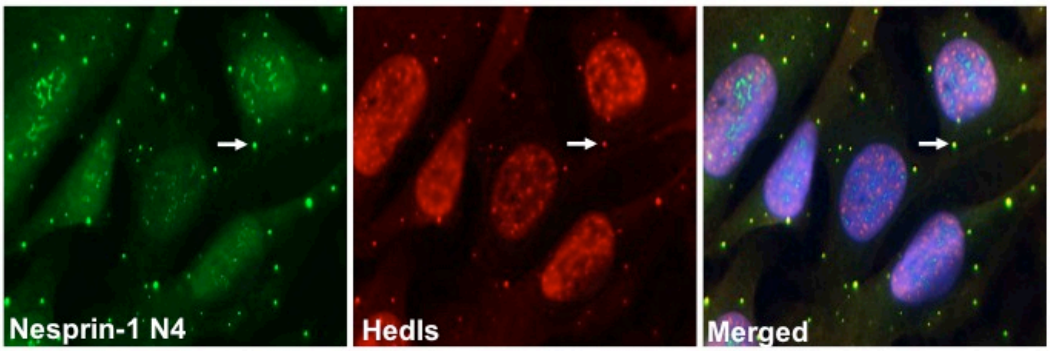

Figure 4.4. Nesprin-1 localizes to P-bodies. To determine if the cytoplasmic focis recognized by the nesprin-1 N4 antibody were P-bodies, confocal microscopy was performed with P-body marker Hedls on fixed U2OS cells. Every nesprin-1 N4 cytoplasmic foci co-localized with P-body marker Hedls in U2OS cells, confirming nesprin-1 P-body localization. Scale bars = 10 μM.

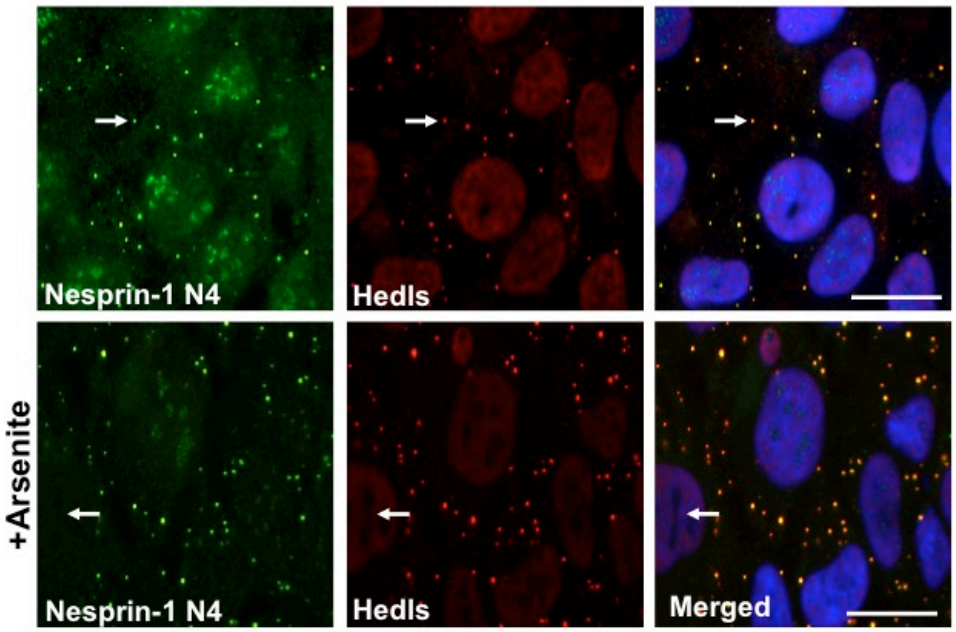

Figure 4.5. Oxidative stress induced Nesprin-1 N4 P-body formation. To induce oxidative stress, U2OS cells were treated with 0.05 mM sodium arsenite for 1 hour. Stressed cells displayed a greater number of nesprin-1 and Hedls P-bodies compared to untreated cells. Furthermore, a small population of U2OS cells lost nesprin-1 nucleolar staining. Images acquired using wide-field microscopy. Scale bars = 10 μM.

often juxtapose to the eIF3-η SGs, a typical phenomenon seen between the two types of RNA granules in stressed cells (Figure 4.6).

4.2.3 Nesprin-1 foci display P-body features

Previous work has demonstrated that P-bodies display three characteristics which facilitate their formation and disassembly. P-bodies not only significantly increase in number during stress, but also increase in number in response to nocodozole-mediated microtubule depolymerization [300]. The nesprin-1 and Hedls P-bodies greatly increased in number, but appeared smaller in size, when U2OS cells were treated with nocodozole for 1 hour (10 μg/ml), indicating that microtubules may adhere P-body mRNP complexes (Figure 4.7). Staining for α-tubulin, which became diffusely cytoplasmic in nocodazole treated cells, served as a positive control for microtubule de-polymerization (Figure 4.8).

Finally, the effect of P-body disruption on nesprin-1 foci was examined. Cycloheximide is a translational inhibitor that stabilizes the association of mRNA with polysomes, thereby depleting the availability of stalled mRNAs which are necessary for P-body formation [279]. As expected, Hedls and nesprin-1 foci's were eliminated in U2OS cells treated with cycloheximide (10 μg/ml) (Figure 4.7).

4.2.4 Nesprin-1 P-bodies co-localize with decapping factors and translational repressors

As described above, P-bodies are multi-functional microenvironments comprised of proteins and enzymes implicated in a host of cytoplasmic mRNA processing events such as mRNA decay and translational repression. To identify the groups of mRNP subsets nesprin-1 associate with, a panel of previously identified P-body components were transfected into U2OS cells and confocal microscopy was used to determine components nesprin-1 co-localized with in P-bodies.

Endogenous nesprin-1 P-bodies co-localized with the ectopic foci formed by the mRNA decapping co-factor Dcp1a-YFP and the translational

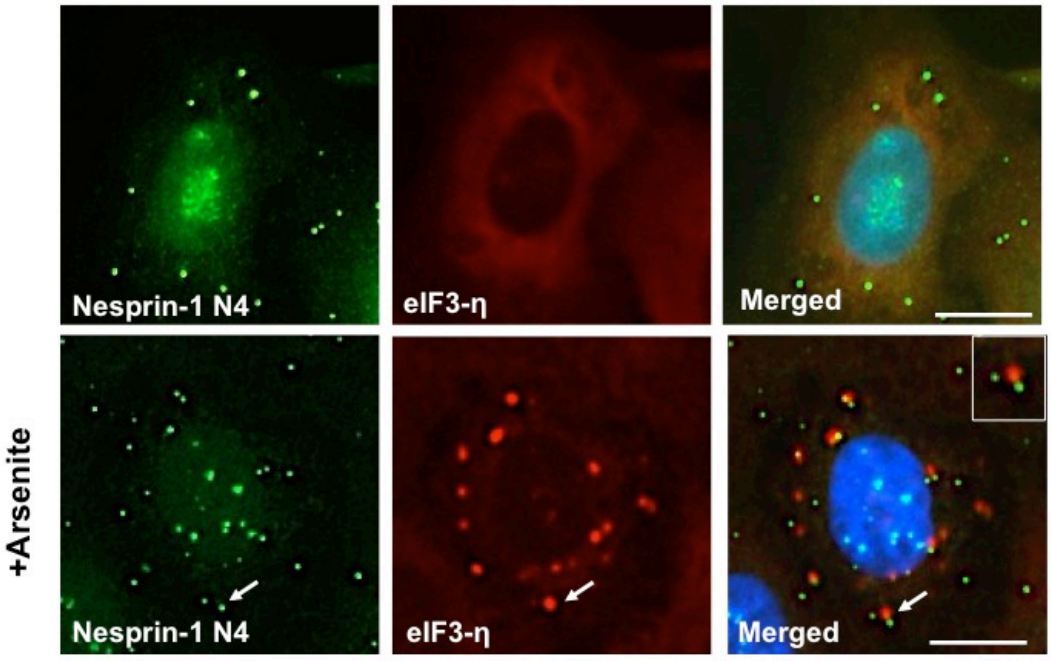

Figure 4.6. Nesprin-1 P-bodies juxtapose to stress induced stress granules (SGs). To induce oxidative stress, U2OS cells were treated with 0.05 mM sodium arsenite for 1 hour. eIF3-η SGs form following sodium arsenite exposure and juxtapose to nesprin-1 P-bodies in U2OS cells. Images acquired using confocal microscopy. Scale bars = 10 μM.

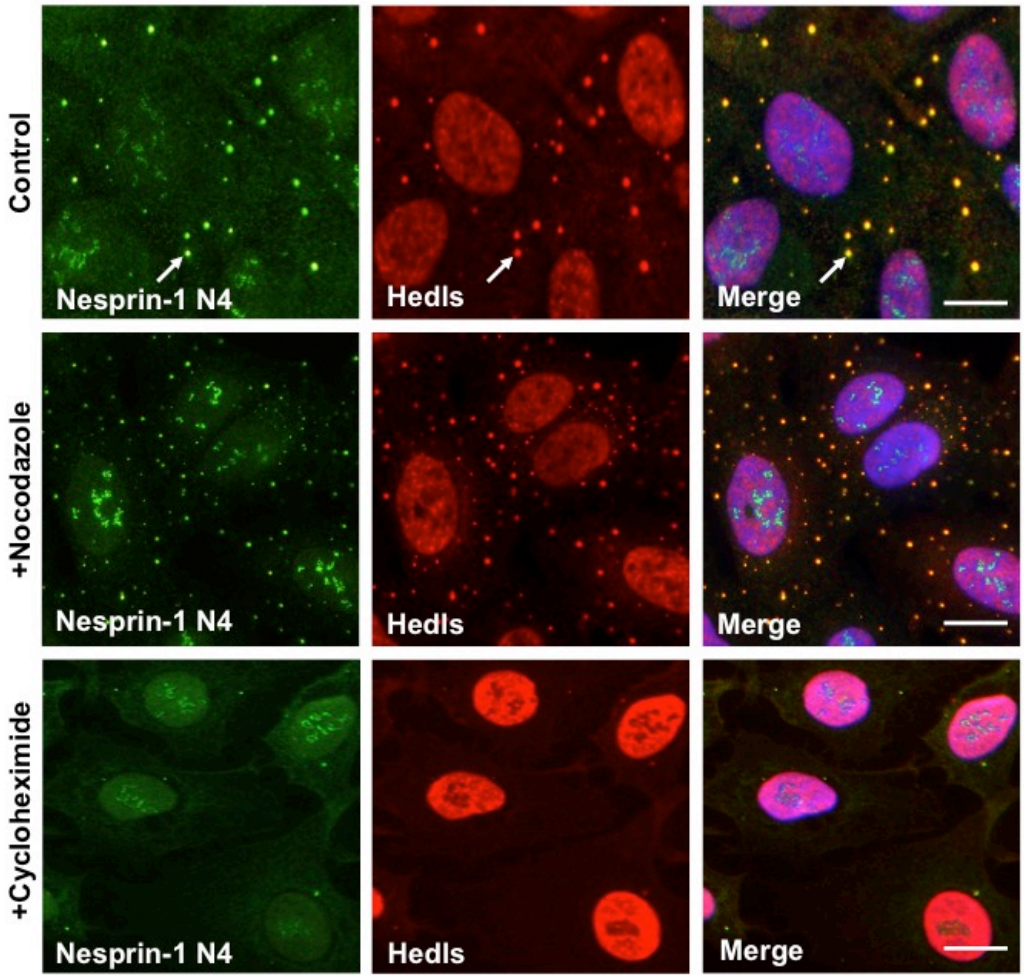

Figure 4.7. Nesprin-1 P-bodies display physical P-body properties. To determine the physical properties of nesprin-1 P-bodies, U2OS cells were treated with nocodazole (10 µg/ml) or cycloheximide (10 µg/ml) for 1 hour to depolymerize microtubules or induce translational repression respectively. Nesprin-1 P-bodies increased in number, however became smaller in size, following nocodazole-mediated microtubule disruption, suggesting microtubules may adhere mRNP complexes to P-bodies. P-bodies disassembled during cycloheximide-mediated translational arrest in U2OS cells, indicating P-bodies are dependent on mRNA availability. Images acquired using confocal microscopy. Scale bars = 10 µM.

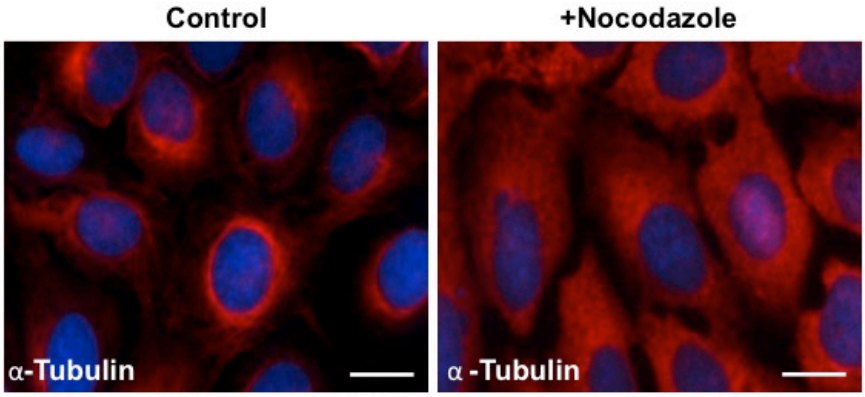

Figure 4.8. Nocodazole depolymerizes microtubules. α-Tubulin staining was used as a positive control to determine whether nocodazole treatment for 1 hour at 10 µg/ml could induce microtubule depolymerization in U2OS cells. Scale bars = 10 µM. Images acquired using confocal microscopy.

regulator RFP-Rck/p54 [269,290] (Figures 4.9 A,B). Similarly, transfected mRNA cap-binding translation factor, HA-eIF4E, and its inhibitor, HA-4E-T, both co-localized with endogenous nesprin-1 within cytoplasmic foci [301] (Figure 4.9 C,D). On the contrary, exogenous adenine/uridine rich element (ARE)-mediated decay factor, TTP-YFP, and pan-RISC regulator, GW182-GFP, formed multiple nesprin-1-negative P-bodies [302,303] (Figures 4.10 A,B).

4.2.5 Nesprin-1 variant p50^{Nesp1} exists in a complex with Rck/p54 and Dcp1a

These results indicate that P-body localized nesprin-1 may preferentially interact with cytoplasmic mRNA decapping factors such as Rck/p54 and Dcp1a. To further examine this possibility, endogenous nesprin-1 was immunoprecipitated from U2OS whole cell lysates and probed for mRNA decapping factors. Nesprin-1 pulled down complexes containing Dcp1a and its binding partner Rck/p54. Similarly, a rabbit polyclonal Rck/p54 antibody, used as a positive control, immunoprecipitated endogenous Rck/p54 and Dcp1a to the same degree as the nesprin-1 antibody, demonstrating the strength of nesprin-1 association with the two P-body proteins (Figure 4.11A).

To determine what nesprin-1 variant was involved in this complex and localized to P-bodies, a reverse co-immunoprecipitation (co-IP) experiment with a murine monoclonal Rck/p54 antibody was performed. This precipitated a 50kDa nesprin-1 variant corresponding to p50^{Nesp1}, a 4SR containing nesprin 1 variant (Figure 4.11B). To show this variant was indeed p50^{Nesp1}, 5 μg of lysate from U2OS cells transfected with untagged-p50^{Nesp1} was run on the same gel, which migrated the same distance as the endogenous product detected by the nesprin-1 N4 antibody.

To prove p50^{Nesp1} interacted with Dcp1a and Rck/p54, full-length p50^{Nesp1} along with the first 2 SRs (p50NT), final 2 SRs (p50CT) and individual SRs of p50^{Nesp1} were GST-tagged and incubated with whole cell lysates from U2OS cells. Endogenous Rck/p54 and Dcp1a pulled-down with full-length GST-p50^{Nesp1} and GST-p50NT. Interestingly, the first SR was able

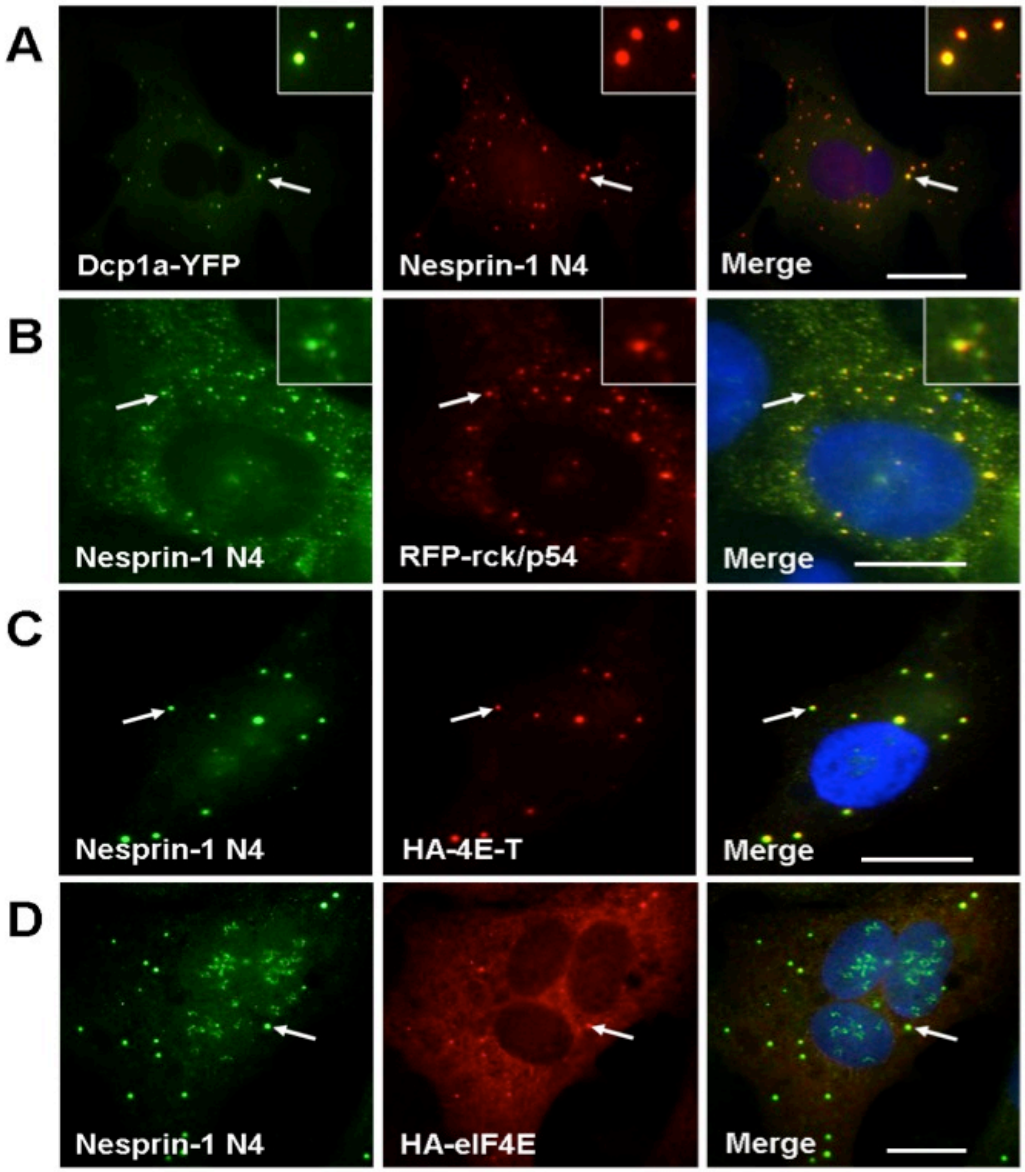

Figure 4.9. Nesprin-1 P-bodies co-localize with decapping factors and translational repressors in U2OS cells. To identify the group of mRNP subsets nesprin-1 was associated with, a panel of previously identified P-body components were transfected into U2OS cells and confocal microscopy was used to determine which components co-localized with nesprin-1 in P-bodies. Nesprin-1 P-bodies co-localized with ectopically expressed tagged-mRNA decapping factors and -translational repressors A) Dcp1a-YFP, B) RFP-Rck/p54, C) HA-4E-T and D) HA-eIF4E. White arrows label single co-localized bodies. Scale bars = 10 μM.

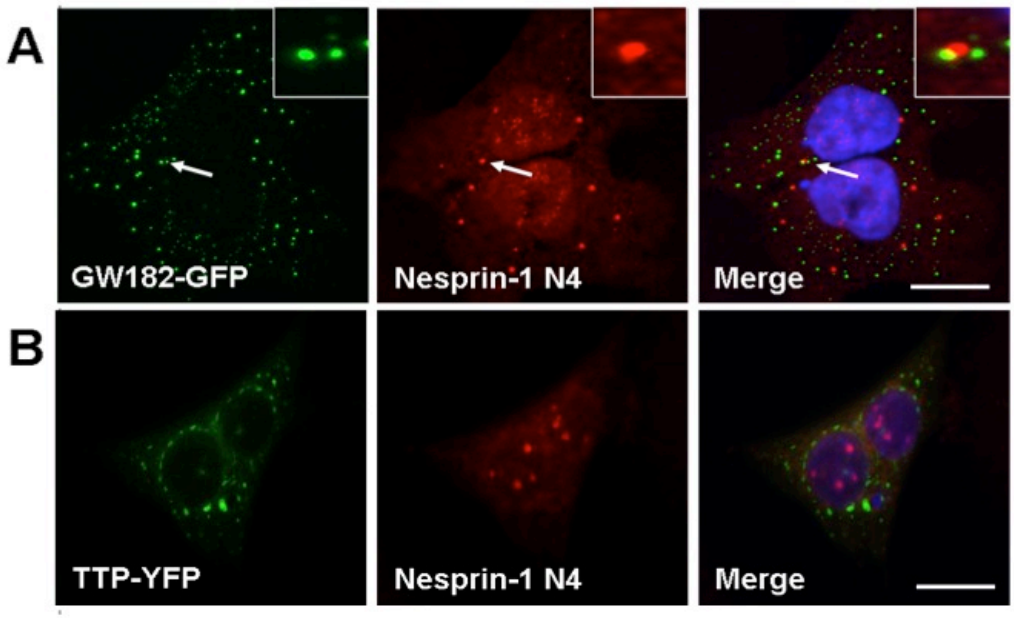

Figure 4.10. Nesprin-1 P-bodies do not co-localize with core RISC regulator and ARE-mediated decay factor in U2OS cells. Confocal microscopy failed to co-localize nesprin-1 P-bodies with ectopically expressed RISC regulator A) GW182-GFP, and ARE-mediated decay factor B) TTP-YFP. This data suggests that nesprin-1 may primarily associate with mRNA decapping factors and translational repressors. GW182-GFP bodies often juxtaposed to nesprin-1 bodies but failed to show complete co-localization. Scale bars = 10 μM.

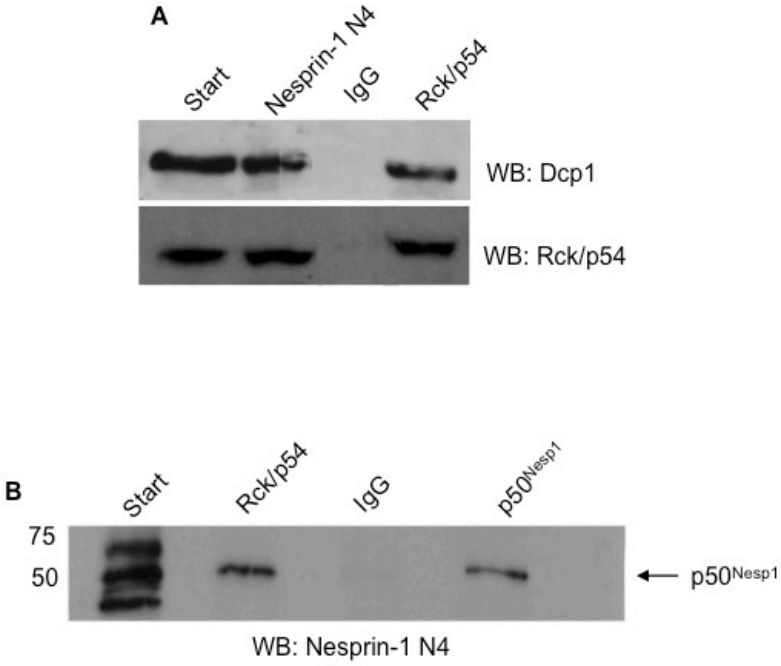

Figure 4.11. Dcp1 and Rck/p54 exist in a complex with p50^{Nesp1}. The co-localization data obtained from the previous experiments suggest P-body nesprin-1 may preferentially interact with mRNA decapping factors such as Rck/p54 and Dcp1a. A) To further examine this possibility, endogenous nesprin-1 was immunoprecipitated from U2OS whole cell lysates and probed for mRNA decapping factors. Nesprin-1 pulled down complexes containing Dcp1a and its binding partner Rck/p54. A rabbit anti-Rck/p54 antibody immunoprecipitated endogenous Rck/p54 and Dcp1a to the same degree as the nesprin-1 antibody and served as a positive control. B) To determine which nesprin-1 variant was involved in this complex and localized to P-bodies, a reverse co-immunoprecipitation experiment was performed with a mouse Rck/p54 antibody. This precipitated a 50kDa nesprin-1 variant corresponding to p50^{Nesp1}, a 4SR containing nesprin 1 variant. To show this variant was indeed p50^{Nesp1}, 5 μg of lysate from U2OS cells transfected with untagged p50^{Nesp1} was run on the same gel, which migrated the same distance as the endogenous product detected by the nesprin-1 N4 antibody.

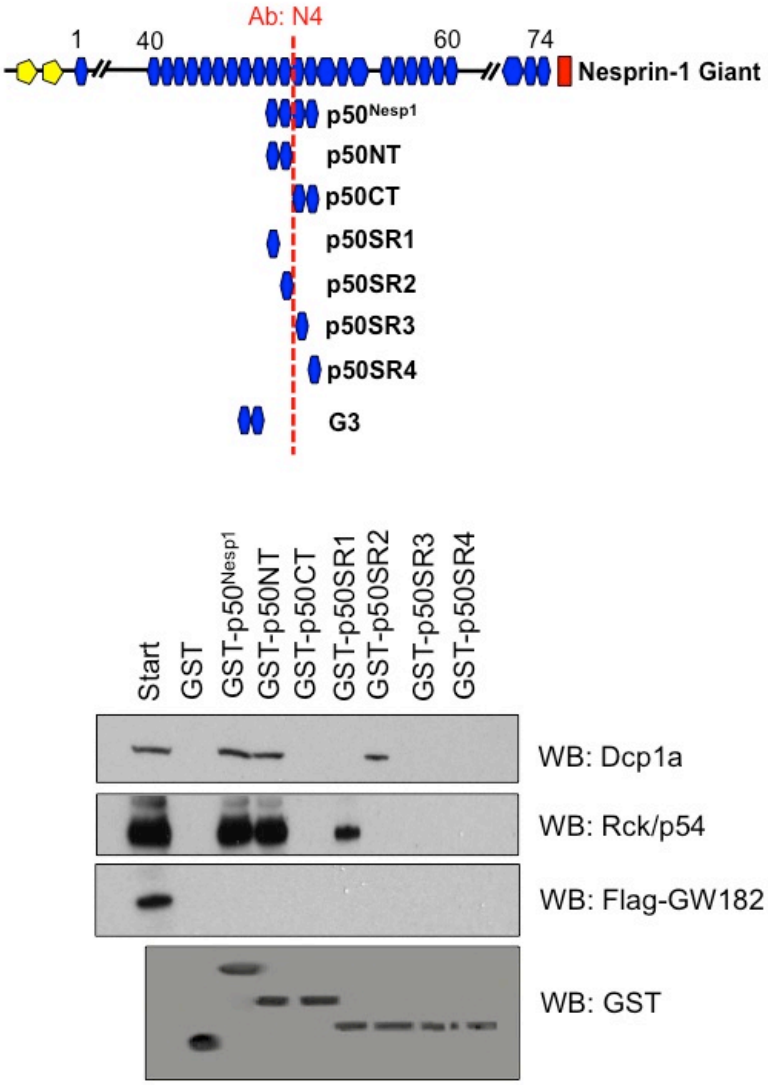

Figure 4.12. p50^{Nesp1} associates with Dcp1a and Rck/p54. GST pull-downs were performed to not only prove p50^{Nesp1} interacted with Dcp1a and Rck/p54, but to also map their binding regions. Both proteins were pulled-down with full length GST-p50^{Nesp1} and GST-p50NT, while Dcp1a interacted specifically with p50SR2 and Rck/p54 interaction was specific to p50SR1. Flag-GW182 failed to pull-down with p50^{Nesp1}, suggesting it is absent from the complex, consistent with the failure of GW182-GFP to co-localize with endogenous nesprin-1 N4.

to pull-down Rck/p54 but not Dcp1a (p50SR1), whilst the second SR pulled-down Dcp1a but not Rck/p54 (p50SR2) (Figure 4.12). Flag- GW182 failed to interact with GST- $p50^{Nesp1}$ or any of its deletion constructs, consistent with the failure of GW182-GFP to co-localize with endogenous nesprin-1 N4 (Figure 4.10A, 4.12).

When a flag-construct of the N-terminal SRs of $p50^{Nesp1}$ (Flag-p50NT) was transfected into U2OS cells, the construct displayed a diffusive localization pattern. However, the construct was drawn into ectopically formed foci in approximately 10% of transfected cells co-expressing YFP-Dcp1a or RFP-Rck/p54 (Figures 4.13, 4.14, 4.15). To prove that this was a specific localization and not an artifact of overexpression, YFP-Dcp1a and RFP-Rck/p54 were co-transfected with Flag-G3, a pair of negative control SRs downstream of the $p50^{Nesp1}$ SRs located in the giant isoform. No co-localization of the G3 SRs with the ectopically formed bodies in any of the co-transfected cells were observed, suggesting association of p50NT SRs with ectopic P-body proteins is a specific organization (Figures 4.13, 4.14, 4.15).

4.2.6 $p50^{Nesp1}$ localizes to microtubules and P-bodies

In chapter 3 the nesprin isoforms were shown to have different sub-cellular localizations in primary and transformed cell lines. To determine the localization of $p50^{Nesp1}$, a Flag-variant of full-length $p50^{Nesp1}$ was transfected into primary Vascular Smooth Muscle Cells (VSMCs), HDFs and U2OS cells. In VSMCs, $p50^{Nesp1}$ induced P-body formation, however in U2OS cells and HDFs the isoform formed fibrous structures that co-localized with α-tubulin, suggesting it additionally localizes to microtubules (Figure 4.16). Furthermore, these tubules displayed an enhanced polymerized structure, resembling microtubule bundling [253].

4.2.7 $p50^{Nesp1}$ interacts with microtubules *in vitro*

The microtubule coating of ectopically expressed $p50^{Nesp1}$ in U2OS cells suggests that this nesprin-1 variant may have attributes which make it a Microtubule Associated Protein (MAP). Therefore, *in vitro* microtubule binding assays were performed by incubating recombinant GST-tagged $p50^{Nesp1}$ and

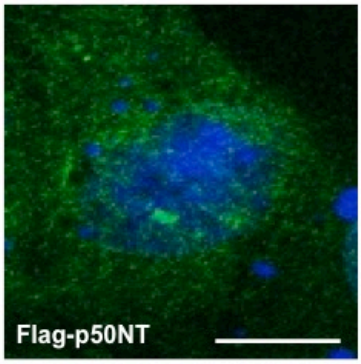

Figure 4.13. p50NT has a diffusive sub cellular localization pattern. To determine the sub-cellular localization of the P-body binding SRs, Flag-p50NT was transfected into U2OS cells. Flag staining revealed p50NT localized diffusively within U2OS cells. Image acquired using wide-field microscopy. Scale bar = 10 μM.

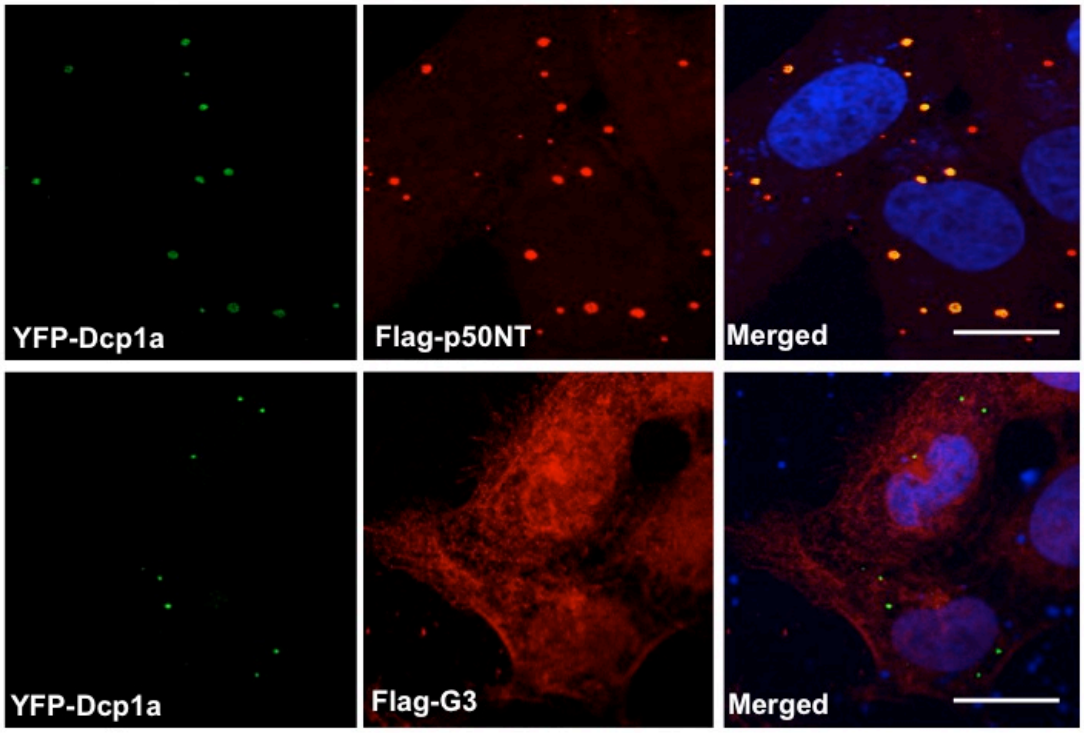

Figure 4.14. p50NT co-localizes with ectopically expressed YFP-Dcp1a. Flag-p50NT co-localizes with Dcp1a-YFP in ~10% of co-transfected U2OS cells, demonstrating a strong association with these SRs for Dcp1a . However, no co-localization of Dcp1a-YFP is seen in cells co-expressing negative control SRs Flag-G3. Images acquired using confocal microscopy. Scale bars = 10 μM.

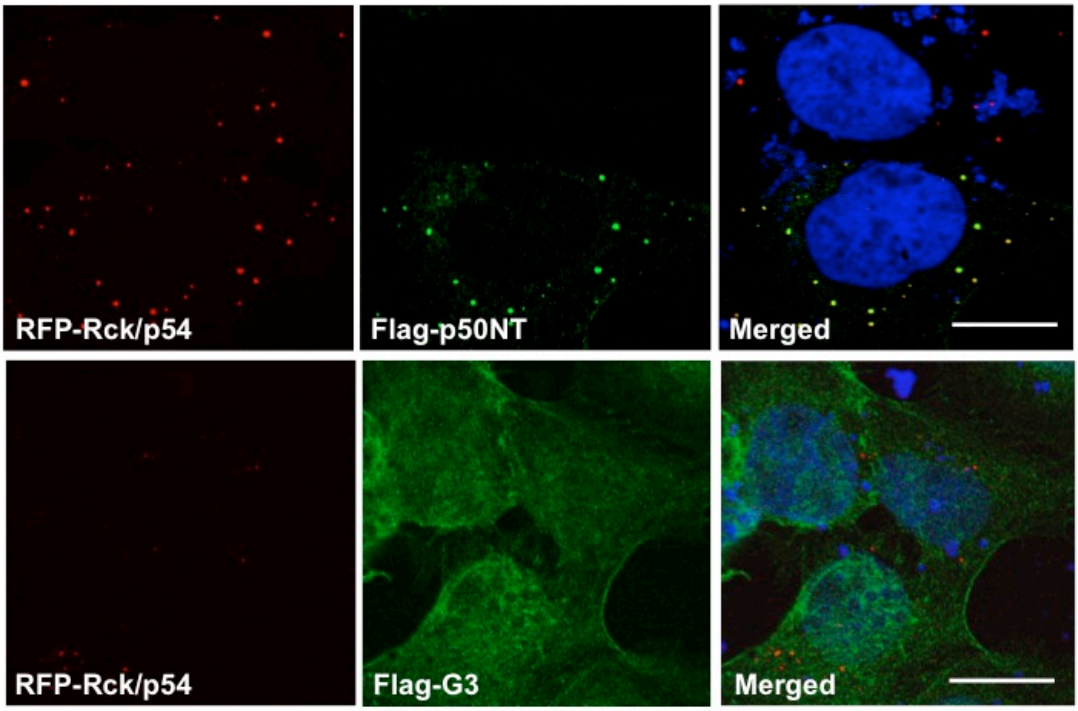

Figure 4.15. p50NT co-localizes with ectopically expressed RFP-Rck/p54. Flag-p50NT co-localizes with RFP-Rck/p54 in ~10% of co-transfected U2OS cells, demonstrating a strong association with these SRs for Rck/p54. However, no co-localization of RFP-Rck/p54 is seen in cells co-expressing negative control SRs Flag-G3. Images acquired using confocal microscopy. Scale bars = 10 μM.

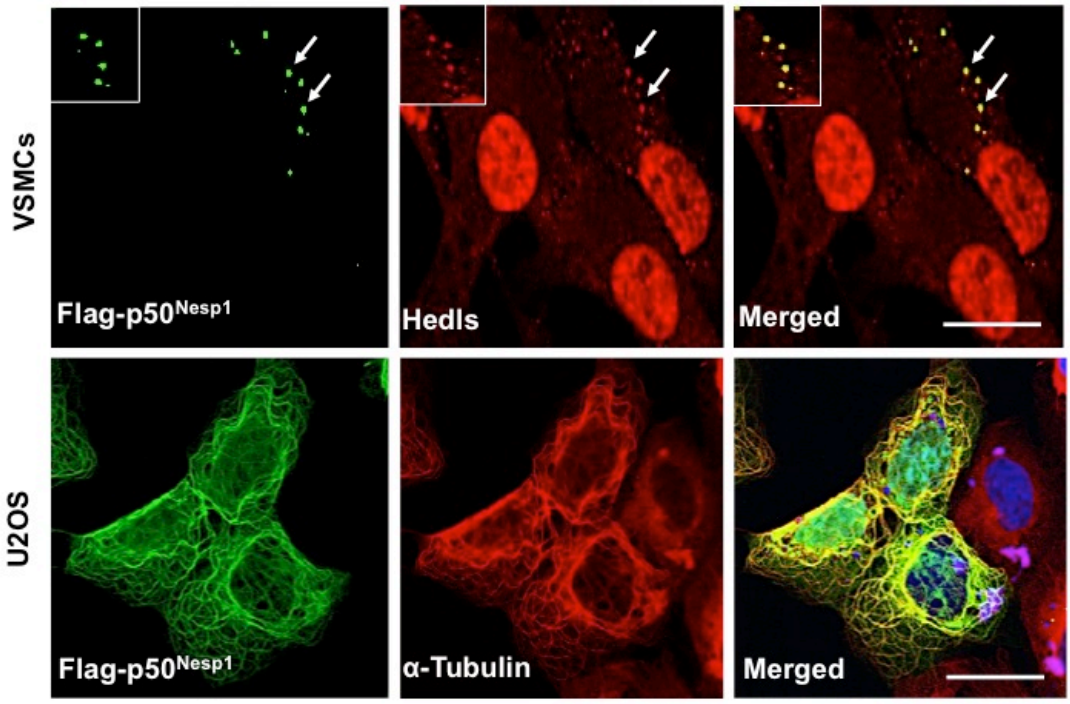

Figure 4.16. p50^{Nesp1} localizes to P-bodies and microtubules. To determine the sub-cellular localization of ectopically expressed p50^{Nesp1}, Flag-p50^{Nesp1} was transfected into primary vascular smooth muscle cells (VSMCs) and U2OS cells. In VSMCs, ectopically expressed p50^{Nesp1} localized to, and induced HedIs P-bodies. However in U2OS cells, the nesprin-1 variant localized to and bundled microtubules, consistent with nesprin-1 variants behaving distinctively in different cell lines as shown in chapter 3. Images acquired using confocal microscopy. Scale bars = 10 μM.

its deletion constructs with purified polymerized microtubules. To determine whether p50^{Nesp1} was capable of binding to microtubules directly, microtubules were pelleted by ultracentrifugation and the pellet and supernatant fractions were analysed by Western blotting. Full-length p50^{Nesp1} and p50CT pelleted after ultracentrifugation in the presence of microtubules, but not in their absence, suggesting a direct interaction exists between the final 2 SRs of p50^{Nesp1} and microtubules (Figure 4.17). However, SR3 and SR4 which make up p50CT, failed to pellet with microtubules indicating that the microtubule binding region of p50^{Nesp1} is shared between the two SRs. The P-body binding p50NT SRs remained in the supernatant upon ultracentrifugation in the presence and absence of microtubules, ruling out microtubule interaction with these SRs (Figure 4.17).

4.2.8 p50^{Nesp1} localizes microtubules in cells

To confirm that the C-terminal pair of SRs in p50^{Nesp1} could associate with microtubules in cells, a Flag construct of p50CT was expressed into U2OS cells. These SRs also promoted microtubule bundling in a similar manner to full length p50^{Nesp1}, confirming its activity as a MAP (Figure 4.18).

4.2.9 p50^{Nesp1} is a P-body-microtubule scaffold

The ability of p50^{Nesp1} to associate with P-body mRNP complexes through it first two SRs and microtubules through it final two SRs suggest this nesprin-1 variants may be a functional scaffold which links P-body mRNP complexes to the microtubule cytoskeleton. The p50^{Nesp1} binding domains are summarized in figure 4.19. The next set of experiments focus on thoroughly investigating whether p50^{Nesp1} is indeed a microtubule linker protein, and the implications associated with P-body and mRNA dynamics when this scaffold is disrupted.

4.2.10 p50CT knocks endogenous Rck/p54 off microtubules.

Next, P-body phenotype was examined in U2OS cells overexpressing Flag-p50^{Nesp1}, therefore p50^{Nesp1} binding partner Rck/p54 was stained for as an endogenous P-body marker. Rather than forming cytoplasmic foci,

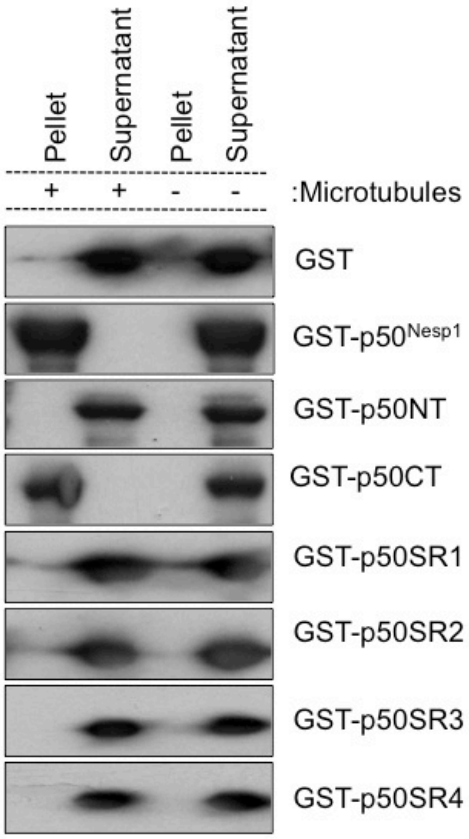

Figure 4.17. p50^{Nesp1} interacts directly with microtubules *in vitro*. Microtubule binding assays were performed by incubating purified p50^{Nesp1} constructs with polymerized microtubules in an eppendorf. The microtubules were pelleted by ultracentrifugation and analysed along with the supernatant by Western blotting with anti-GST. To control for the pelleting nature of p50^{Nesp1} constructs, ultracentrifugation was performed and pellets and supernatants were additionally analyzed in the absence of microtubules. p50^{Nesp1} and p50CT directly pelleted upon ultracentrifugation in the presence of microtubules, however remain in the supernatant when microtubules are absent, suggesting the final two SRs of p50^{Nesp1} give the protein the ability to directly associate with microtubules. All other constructs remain in the supernatant regardless of microtubule presences. The ability of p50^{Nesp1} to directly interact with microtubules confirms that this nesprin-1 variant is a microtubule associated protein (MAP).

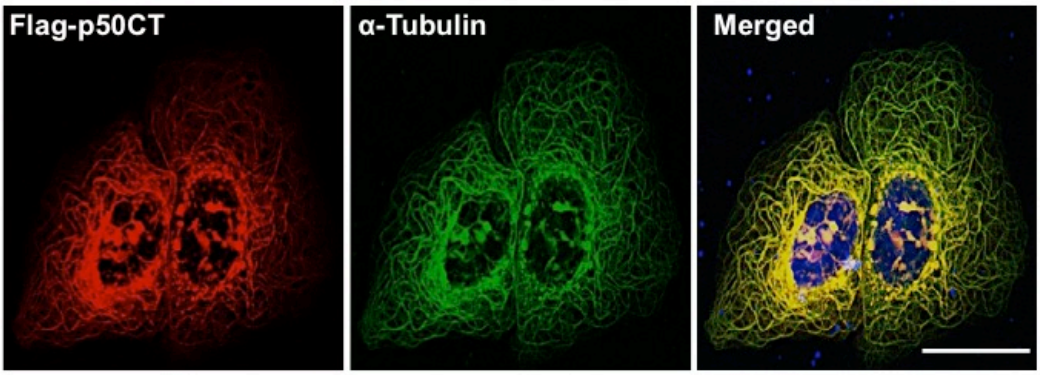

Figure 4.18. p50CT associates with microtubules in cells. To confirm that the C-terminal pair of SRs in p50^{Nesp1} could associate with microtubules *in vivo,* a Flag construct of p50CT was expressed into U2OS cells. These SRs co-localized with the microtubule network using confocal microscopy, and promoted microtubule bundling as seen with full-length p50^{Nesp1}. Scale bars = 10 μM.

Proteins	$p50^{Nesp1}$	p50NT	p50CT	p50SR1	p50SR2	p50SR3	p50SR4
Dcp1a	+	+	-	-	+	-	-
Rck/p54	+	+	-	+	-	-	-
Gw182	-	-	-	-	-	-	-
Microtubules	+	-	+	-	-	-	-

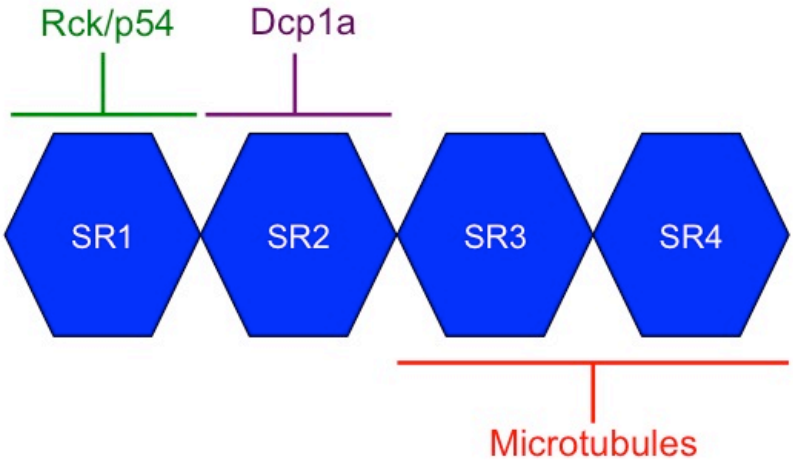

Figure 4.19. Summary of $p50^{Nesp1}$ binding domains. The ability of $p50^{Nesp1}$ to associate with P-body proteins, Rck/p54 and Dcp1a, through it first two SRs and microtubules through it final two SRs suggest this nesprin-1 variants may be a functional scaffold that links P-body mRNP complexes to the microtubule cytoskeleton

endogenous Rck/p54 co-localized to and coated the $p50^{Nesp1}$ bundled microtubules (Figure 4.20A). However, when endogenous Rck/p54 was stained in U2OS cells overexpressing Flag-p50CT, which lacks the Rck/p54 binding site, Rck/p54 coating along the microtubules was no longer observed and instead Rck/p54 positive P-bodies localized adjacent to the microtubules (Figure 4.20A). Furthermore, cells expressing Flag-$p50^{Nesp1}$ had enhanced expression of Rck/p54 and Dcp1a, whereas cells expressing Flag-p50CT had reduced expressions when compared to Flag-control transfected cells (Figure 4.20B). This data suggests that $p50^{Nesp1}$ may be a key regulator of P-body formation, by controlling the expression of P-body proteins and assembly of mRNP complexes in response to microtubule attachment. Alternatively, $p50^{Nesp1}$ may stabilize and/or protect P-body mRNP complexes by extending protein half-lives or protecting them from the cells degradation machinery.

I hypothesised that Flag-p50CT acts in a dominant negative manner, where it is able to displace endogenous $p50^{Nesp1}$ and mRNP complexes associated with it from microtubules (Figure 4.21). This dominant negative construct now provides an invaluable tool to allow $p50^{Nesp1}$ microtubule-associated P-body dynamics to be studied.

4.2.11 p50CT expression results in reduced P-body coverage

Previously, P-body dynamics have been shown to be regulated by the cytoskeleton, of which P-body movement is microtubule dependent [297]. As p50CT overexpression in U2OS cells was able to knock Rck/p54 bodies off microtubules, P-body mobility was initially examined. In collaboration with Dr. Daniel Soong (Divisional Microscopy Officer, King's College London), real-time tracking of DCP1a-YFP P-bodies in U2OS cells co-transfected with a control empty Flag-vector, Flag-$p50^{Nesp1}$ or Flag-p50CT was performed. Using a method originally described by Aizer et al., 2008, Dr. Soong tracked individual bodies using single particle tracking in each sample over a time-frame of 2 minutes and then determined the area covered by each body [297]. The area centroid of each tracked object was exported as a list of coodrinates and converted to .CEL format in a custom-written Mathematica (Wolfram Research, USA) notebook and .cel files were imported into the Chemotaxis

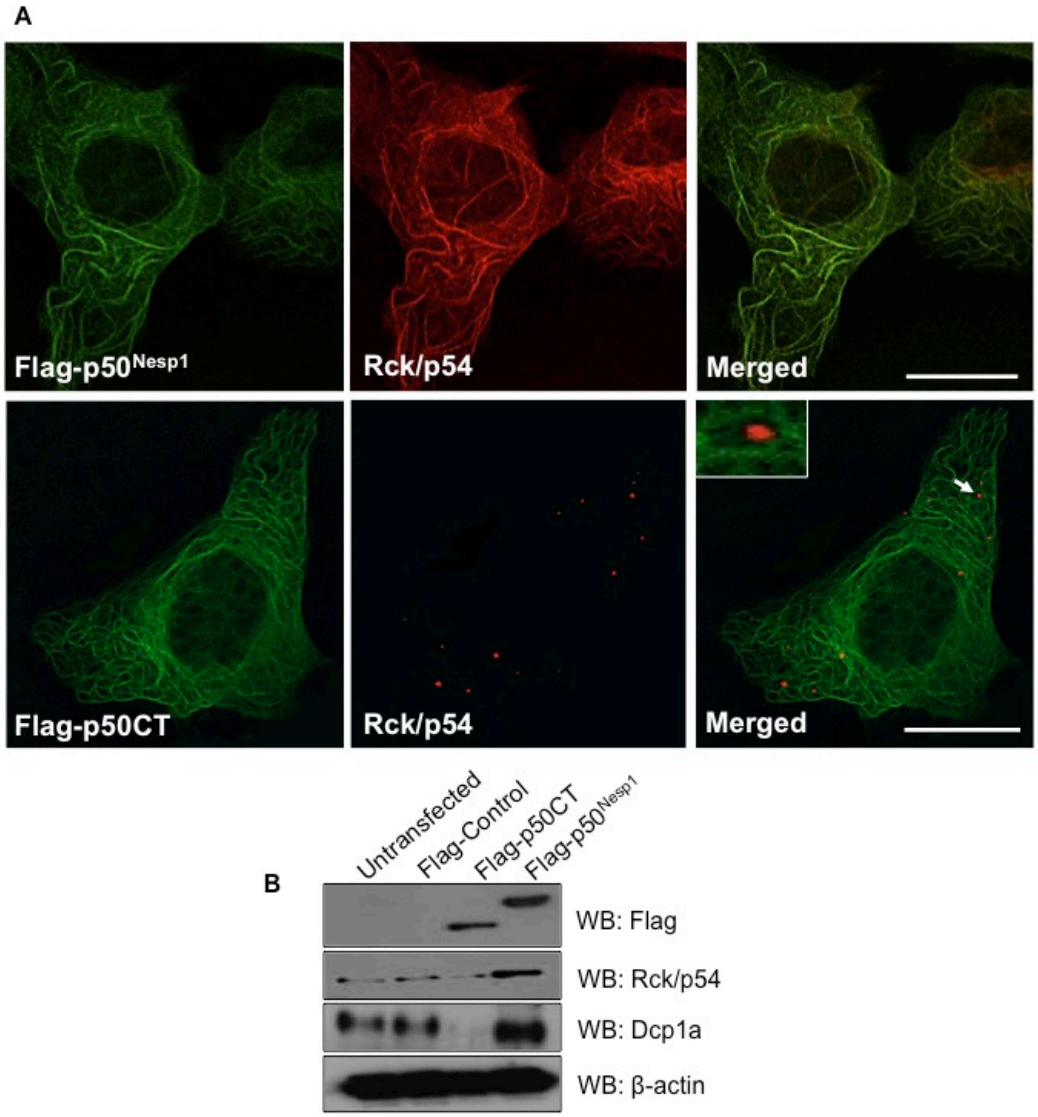

Figure 4.20. Rck/p54 associates with p50^{Nesp1} microtubules. A) To determine the effects overexpression of p50^{Nesp1} had on its P-body binding partners, U2OS cells overexpressing Flag-p50^{Nesp1} were stained for endogenous Rck/p54. Rather than forming cytoplasmic foci, Rck/p54 was recruited to Flag-p50^{Nesp1} bundled microtubules. Interestingly, Flag-p50CT which lacks the Rck/p54 binding site, was able to displace Rck/p54 from microtubules when overexpressed in U2OS cells, suggesting that Flag-p50CT may act as a dominant negative construct. Furthermore, cells expressing Flag-p50CT appeared to have reduced Rck/p54 staining. Images acquired using confocal microscopy. Scale bars = 10 μM. B) Western blotting lysate from cells overexpressing full-length Flag-p50^{Nesp1} and Flag-p50CT demonstrate increased expression of Rck/p54 and Dcp1a in Flag-p50^{Nesp1} overexpressing cells and reduced expression of Rck/p54 and Dcp1a in cells overexpressing Flag-p50CT.

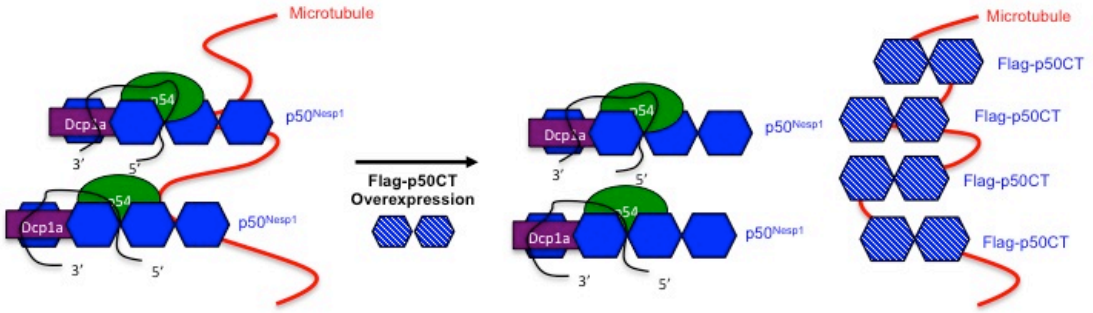

Figure 4.21. Working model: p50CT is able to displace endogenous P-bodies from microtubules. Flag-p50CT overexpression potentially acts in a dominant negative manner by displacing endogenous $p50^{Nesp1}$ associated P-bodies from microtubules in U2OS cells. As p50CT lacks binding sites for Rck/p54 and Dcp1a, it potentially knocks all $p50^{Nesp1}$ sub-complexes off microtubules and effects P-body-microtubule dynamics.

Analysis notebook V1.6 (Graham Dunn, King's College London) for analysis and statistical comparison. The videos generated from this experiment support the findings described by Aizer et al., 2008 and the concept that P-bodies localize to spatially confined regions within the cytosol [297]. The empty Flag-vector control cells (n=84) and Flag-p50^{Nesp1} (n=262) expressing cells covered areas of 0.0798μ and 0.0799μ while the cells expressing Flag-p50CT (n=116) covered a significantly reduced area averaging 0.0514μ, comparable to control Flag-vector cells treated with nocodozole (n=429) at 0.0501μ. However, no significant P-body area coverage was observed between the control Flag-vector cells treated with nocodozole and Flag-p50CT expressing cells, suggesting that overexpression of Flag-p50CT has a similar effect as nocodozole treatment (Figure 4.22).

To determine that U2OS cells co-expressing YFP-Dcp1a and the respective Flag-protein were being filmed, the culture dishes were fixed after filming and stained for anti-Flag. Every cell expressing Dcp1a-YFP was also expressing Flag-p50^{Nesp1} or Flag-p50CT, allowing easy selection for co-transfected cells. Interestingly, Flag-p50^{Nesp1} no longer localized to microtubules but instead co-localized with Dcp1a foci in P-bodies in co-transfected cells. Flag-p50CT however localized to microtubules with Dcp1a-YFP bodies located adjacent to the microtubules, providing further evidence for strong association between these P-body proteins and the N-terminal SRs of p50^{Nesp1} (Figure 4.23).

4.2.12 p50CT expressing cells have reduced P-body-stress granule connections and fail to disassemble stress granules post-stress

SGs are thought to be compartments where mRNAs are sorted before they juxtapose to P-bodies to allow mRNA transcript transferral for degradation or storage. Previous studies using nocodazole treatment have demonstrated that P-bodies and SGs associate in a microtubule dependent manner during stress and a single class of mRNA can be transferred between the two classes of granules [239,297]. Therefore, the dynamics of P-body-SG associations by displacing P-bodies from microtubules using exogenous p50CT was examined. Flag-Control or Flag-p50CT were transfected into U2OS cells with a β-globin mRNA containing the MS2-binding site in its

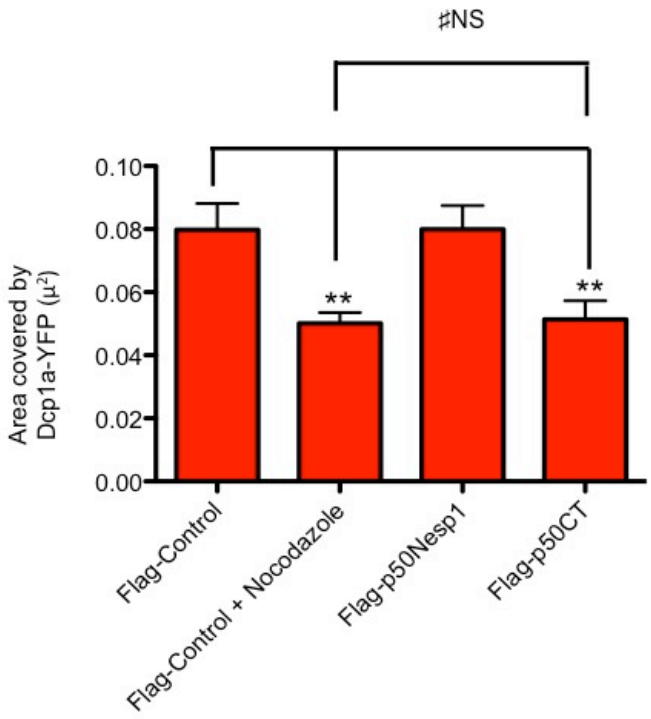

Figure 4.22. Real time tracking of Dcp1a-YFP P-bodies. Single particle tracking of Dcp1a-YFP bodies were performed by Dr. Daniel Soong (Divisional Microscopy Officer , King's College London) to determine the area covered by P-bodies in cells expressing Flag-control (n=83) , Flag-p50^{Nesp1} (n=262) and Flag-p50CT (n=116). Flag-control samples treated with 10 μg/ml nocodazole served as a positive control for reduced area coverage (n=429). Dcp1a-YFP P-bodies in Flag-p50CT cells have significantly reduced P-body movement when compared to control cells, however have no significant reduction when compared to control cells treated with nocodozole. All bodies within the cells were tracked over a period of 2 minutes. ♯NS=Not significant , **P=< 0.01; one-way ANOVA, Bonferroni *post hoc* test.

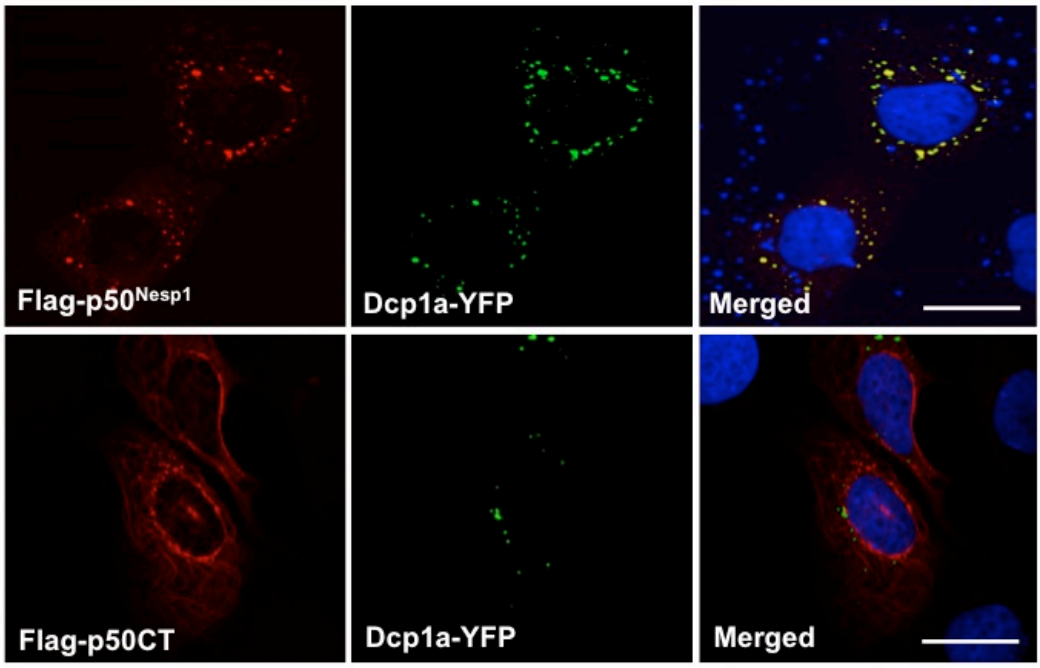

Figure 4.23. Cells expressing DCp1a-YFP also expressed Flag-tagged constructs. To determine that U2OS cells co-expressing YFP-Dcp1a and the respective Flag-protein were being filmed, the culture dishes were fixed after filming and stained for anti-Flag. Every cell expressing Dcp1a-YFP was also expressing Flag-p50^{Nesp1} or Flag-p50CT, allowing easy selection for co-transfected cells. Interestingly, Flag-p50^{Nesp1} no longer localized to microtubules, but instead co-localized with Dcp1a foci in P-bodies of co-transfected cells. However, Flag-p50CT localized to microtubules with Dcp1a-YFP located adjacent to the bodies, providing further evidence for strong association between these P-body proteins and the N-terminal SRs of p50^{Nesp1}. Images acquired using wide-field microscopy. Scale bars = 10 μM.

3'UTR (pEF-7B- MS2bs) together with a GFP-MS2 coat protein allowing the β-globin mRNA to be tracked with a GFP signal (Figure 4.24) [239]. Cells were then stressed with 2 μM hydrogen peroxide (H_2O_2) for 1 hour and stained for Rck/p54 P-bodies and PABP-1 labelling SGs. In co-transfected cells the β-globin reporter containing the MS2-binding site, bound to the GFP-MS2 protein with cytoplasmic GFP signal found in SGs and P-bodies. In control cells, frequent P-body-SG contacts were seen with the majority of the β-globin transcript detected in P-bodies (Figure 4.25 A,B,C). However in the Flag-p50CT expressing cells, association between P-bodies and SGs were almost non-existent and the GFP-signal for the tethered RNA accumulated solely in SGs, suggesting mRNA species stored in SGs were failing to be transferred into P-body compartments (Figure 4.25 A,B,C).

4.2.13 p50CT expressing cells fail to disassemble SGs during recovery

When U2OS cells were allowed to recover for 3 hours in H_2O_2 free growth media, the SGs in control cells disassembled and the β-globin mRNA localized to P-bodies. However in the Flag-p50CT expressing cells, the SGs failed to dissolve and accumulated the β-globin mRNA suggesting the cells were in a translationally repressed state (Figure 4.26).

4.2.14 Oxidative stress triggers cell death in Flag-p50CT expressing cells

The ability of Flag-p50CT U2OS cells to disassemble SGs during recovery suggests that these cells are locked in a translationally repressed state. To determine the phenotypic effect Flag-p50CT had on transfected cells post-stress, time-lapse microscopy was performed. U2OS cells were filmed from the start of recovery over a period of 16 hours. After approximately 8 hours into recovery, Flag-p50CT cells underwent extensive cell death suggesting that p50CT was harmful to cells once exposed to a stress agent (Figure 4.27A). Using MTT assays, Flag-p50CT expressing cells experienced mild cellular toxicity between 4-5 hours into recovery and severe toxicity after 7 hours, confirming the lethal effects of this construct post-stress exposure (Figure 4.27B).

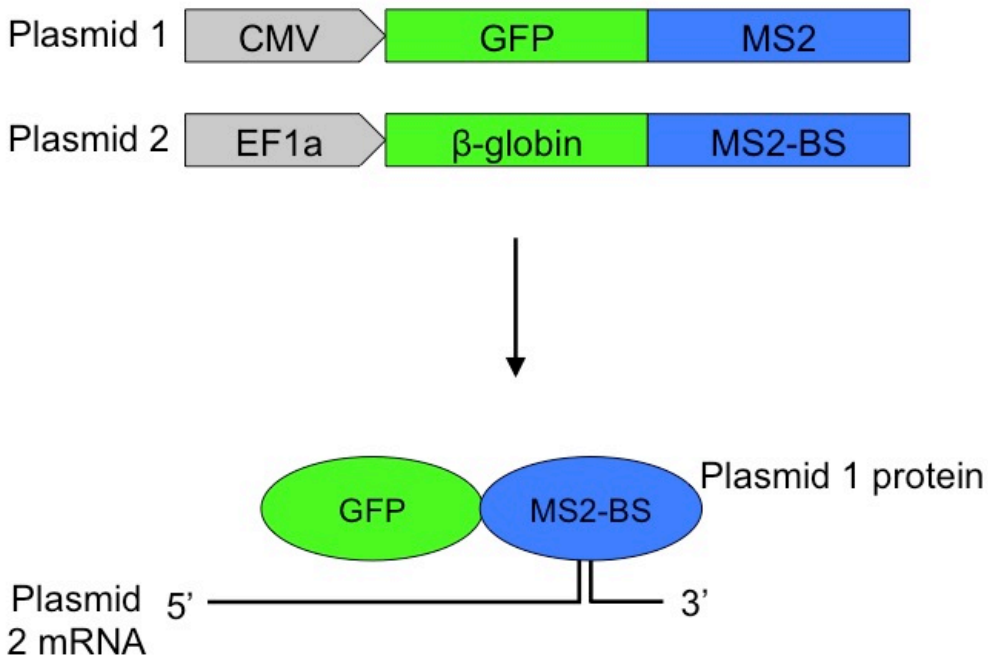

Figure 4.24. Detection of exogenous B-globin mRNA transcript. GFP-MS2 translated off plasmid 1 binds to the the MS2 binding site (MS2-BS) present in the β-globin transcript transcribed off plasmid 2. This allows the ectopic β-globin transcripts to be monitored using GFP signal and is an alternative to *in situ* hybridization.

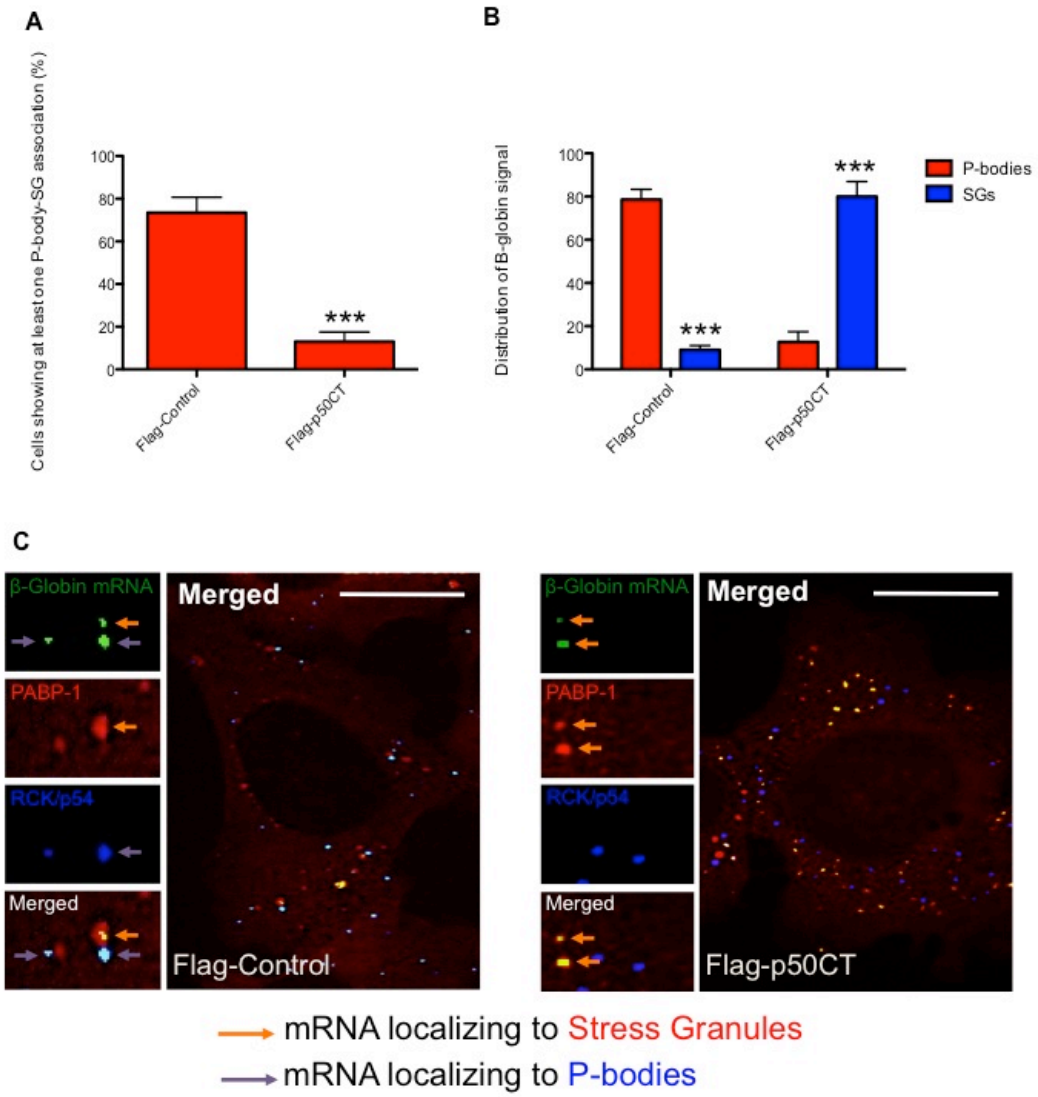

Figure 4.25. P-body attachment to microtubules is required for association with SGs and mRNA dynamics. A) Flag-p50CT expressing U2OS cells had fewer cells with at least one P-body-SG connection in response to H_2O_2 treatment (2μM, 1 hour). B) Flag-control U2OS cells accumulated more β-globin mRNA in P-bodies while Flag-p50CT cells had more mRNA in SGs, indicative of de-regulated mRNA sorting in response to H_2O_2 treatment. ***P=< 0.001, student t-test. C) Representative confocal images highlighting the data described above. PAPB-1 (red) was used to label SGs, Rck/p54 (blue) was used as a P-body marker. Orange arrows correspond to β-globin mRNA present in SGs, purple arrow correspond to β-globin mRNA present in P-bodies. Scale bars = 10 μM.

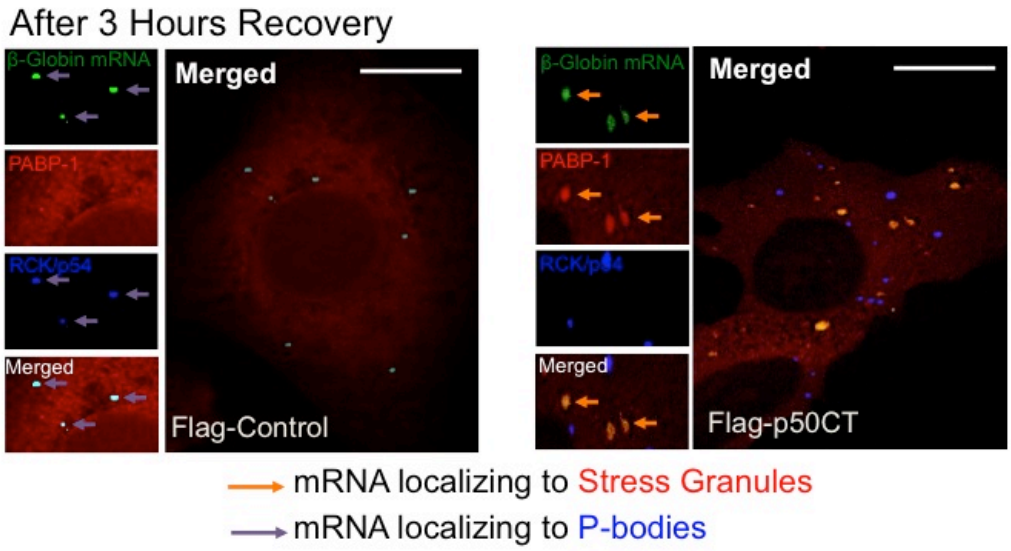

Figure 4.26. P-body attachment to microtubules is required for SG disassembly. Flag-p50CT U2OS cells fail to disassemble SGs 3 hours post-recovery. Cells were fixed and stained 3 hours after the removal of H_2O_2 containing media. PAPB-1 (red) was used to label SGs, Rck/p54 (blue) was used as a P-body marker. Orange arrows correspond to β-globin mRNA present in SGs, purple arrows correspond to β-globin mRNA present in P-bodies. Images acquired using confocal microscopy. Scale bars = 10 μM.

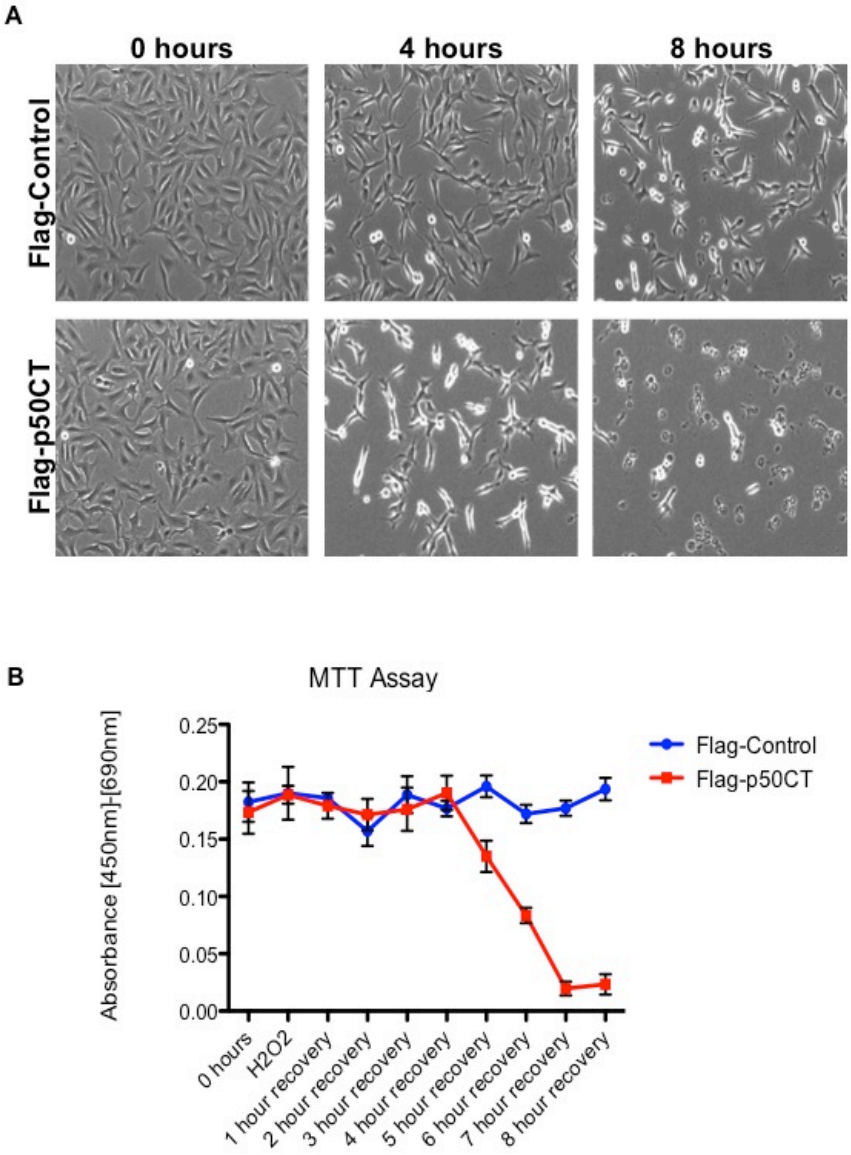

Figure 4.27. Flag-p50CT promotes cell death once exposed to stress. A) Time-lapse microscopy showing Flag-p50CT induces cell death in U2OS cells ~8 hours post H_2O_2 relief. B) MTT assay was used to determine cellular toxicity of Flag-p50CT. The Flag-p50CT transfected cells started displaying toxic features 4 hours into recovery, and total toxicity at ~7 hours.

4.2.15 p50^{Nesp1} knockdown eliminates P-bodies

By overexpressing p50^{Nesp1} and dominant negative p50CT, I have demonstarted the importance of nesprin-1 in P-body and mRNA dynamics. To further determine the role of p50^{Nesp1} in P-bodies, a knockdown approach was utilized to determine the effects of disrupting complete functionality of p50^{Nesp1}. A panel of siRNA oligos, si-83, si-86, si-90 and si-136, were designed to target exons 83, 86, 90 and 136 respectively, to knockdown the central SR rod of nesprin-1. si-86 was created in the same coding exon as the nesprin-1 N4 epitope but consistently induced cell death in a large proportion of transfected cells, therefore was excluded from further work. si-83 and si-90 were created towards the N- and C-terminal SRs of p50^{Nesp1} respectively, while si-136 was created towards the C-terminus of the nesprin-1 giant and designed as a negative control siRNA (Figure 4.28A).

qRT-PCR performed in chapter 3 demonstrated si-90 was capable of knocking down p50^{Nesp1} terminating N1-3'E90 UTR in U2OS cells (Figure 3.25). Western blotting confirmed that only si-83 and si-90 knocked-down p50^{Nesp1} , p41^{Nesp1} and the unknown ~75 kDa nesprin-1 variant, while si-136 had no effect on N4 variants in U2OS cells (Figure 4.28B). Nesprin-1 N4 and Hedls staining were used to assess P-body phenotype in U2OS cells 72 hours post-transfection (Figures 4.28C). Cells transfected with si-136 showed no differences in P-body phenotype when compared to control siRNA, indicating that KASH-domain nesprin-1 isoforms neither localize to nor directly regulate P-body formation. In contrast, si-83 and si-90 both eliminated nesprin-1 N4 and Hedls-positive P-bodies in up to 80% of transfected cells. Similarly, knockdown of Rck/p54 resulted in a similar % loss of P-bodies and served as a positive control (Figure 4.28D) [290].

4.2.16 p50^{Nesp1} knock-down attenuates miRISC function

The loss of macroscopic P-bodies does not necessarily imply loss of function of the mRNA processing pathways associated with these structures [290]. p50^{Nesp1} binding partner Rck/p54 is a component which regulates general miRNA-induced silencing complex (miRISC) mediated translational repression, therefore a CXCR4 miRISC luciferase reporter assay was used to

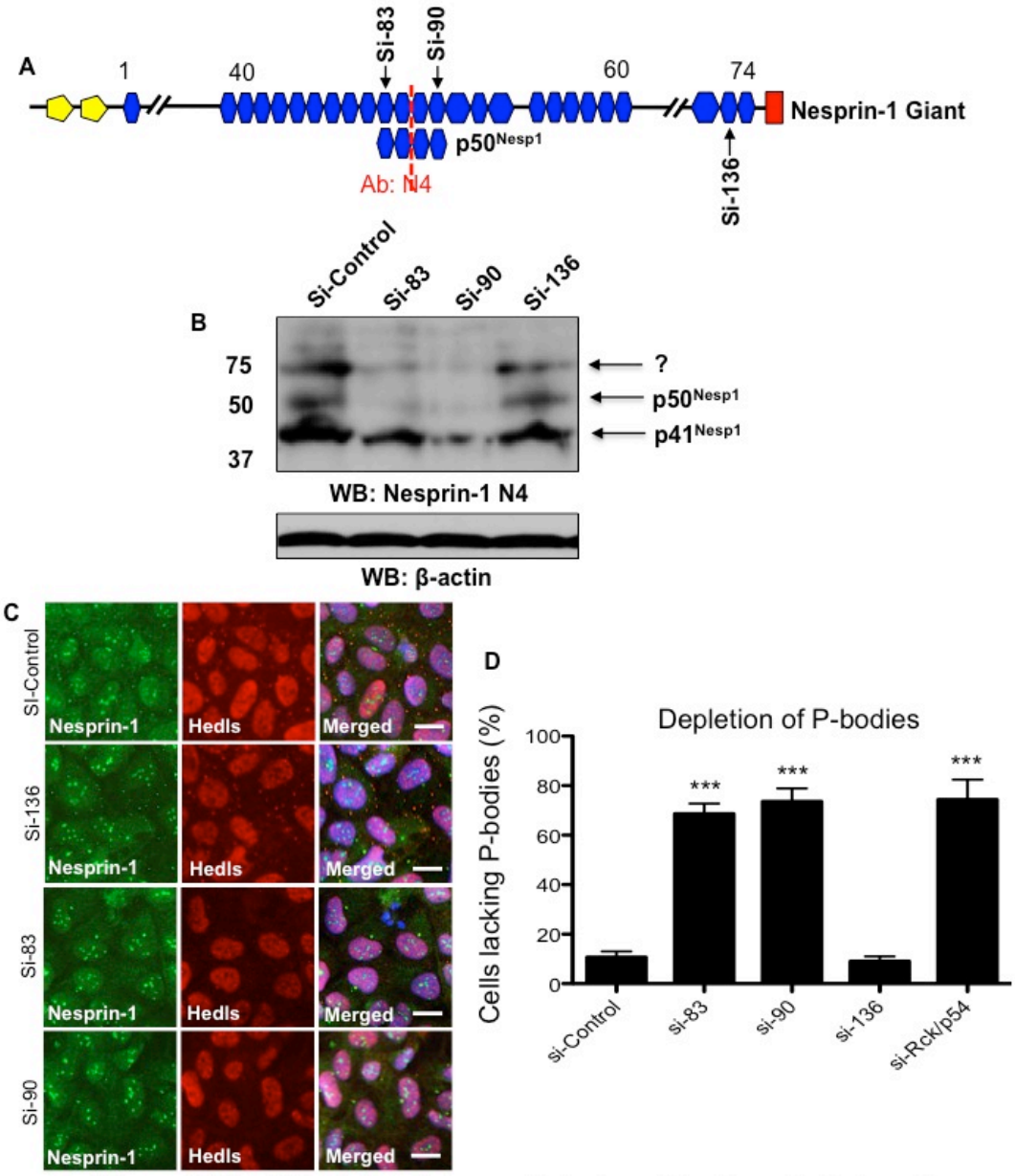

Figure 4.28 p50^{Nesp1} knockdown eliminates P-bodies. A) Schematic representation depicting the locations of the utilized siRNA oligos relative to nesprin-1 giant and p50^{Nesp1}. B) Western blots confirmed that si-83 and si-90 knocked-down p50^{Nesp1} while si-136 knockdown had comparable levels to si-Control. C) p50^{Nesp1} knockdown using si-90 and si-83 eliminated P-bodies from U2OS cells while si-136 had no effect as visualized by nesprin-1 N4 staining. Nesprin-1 remained associated with the nucleolus following knock-down. Images acquired using wide-field microscopy. Scale bars = 10 μM. D) Quantification of P-body depletion in nesprin-1 depleted cells. 200 cells were counted per treatment in each of three independent experiments. ***P=< 0.001; one-way ANOVA, Dunnett's *post hoc* test.

determine the effects of p50^{Nesp1} knock down on miRISC activity [245,290]. The pRL-TK6x vector encoding luciferase has 6 CXCR4 miRNA partially-complementary binding sites within its 3'UTR and becomes silenced when co-expressed with the CXCR4 miRNA (Figure 4.29A). However, concomitant knockdown of proteins involved in the miRISC pathway should reduce luciferase silencing and enhance relative luciferase and luminescent levels. Knockdown of positive control Rck/p54 and p50^{Nesp1} using si-83 and si-90, but not si-136, significantly decreased miRISC activity in U2OS cells compared to scrambled control suggesting, p50^{Nesp1} is required for efficient miRNA function (Figures 4.29B).

Next a Let-7 miRNA reporter construct which contains 4x Let-7 complementary sites (FF4LCS) for endogenous Let-7 was utilized as an additional tool to confirm p50^{Nesp1} as an essential miRNA silencing component [248]. As with the CXCR4 reporter, si-Rck/p54 and both si-83 and si-90, but not si-136, were sufficiently able to attenuate miRNA function of endogenous Let-7 in U2OS cells (Figure 4.30A). However, when this assay was performed in U2OS cells transfected with a miRNA reporter construct carrying a mutation in the target seed region of Let-7 (FFr4mLCS), rather than the WT FF4LCS construct, none of the p50^{Nesp1} targeting siRNAs or si-Rck/p54 were able to attenuate its silencing function relative to si-Control (Figure 4.30B). Instead, ~3 fold increase in luciferase activity was observed in si-Control cells transfected with FFr4mLCS compared to those transfected with FF4LCS.

4.2.17 SR1 and SR2 of p50^{Nesp1} are required for miRISC

To show miRISC attenuation was due to p50^{Nesp1} knock down and not depletion of other endogenous nesprin-1 variants eliminated by si-83 and si-90, a series of rescue experiments were performed using p50^{Nesp1} and p50^{Nesp1} constructs described throughout this chapter. The si-83 targeting nucleotides in full length p50^{Nesp1}, p50NT and p50SR1 were mutated so they could not be targeted for knockdown, however the codons still encoded for WT amino acids to not mutate the translated proteins.

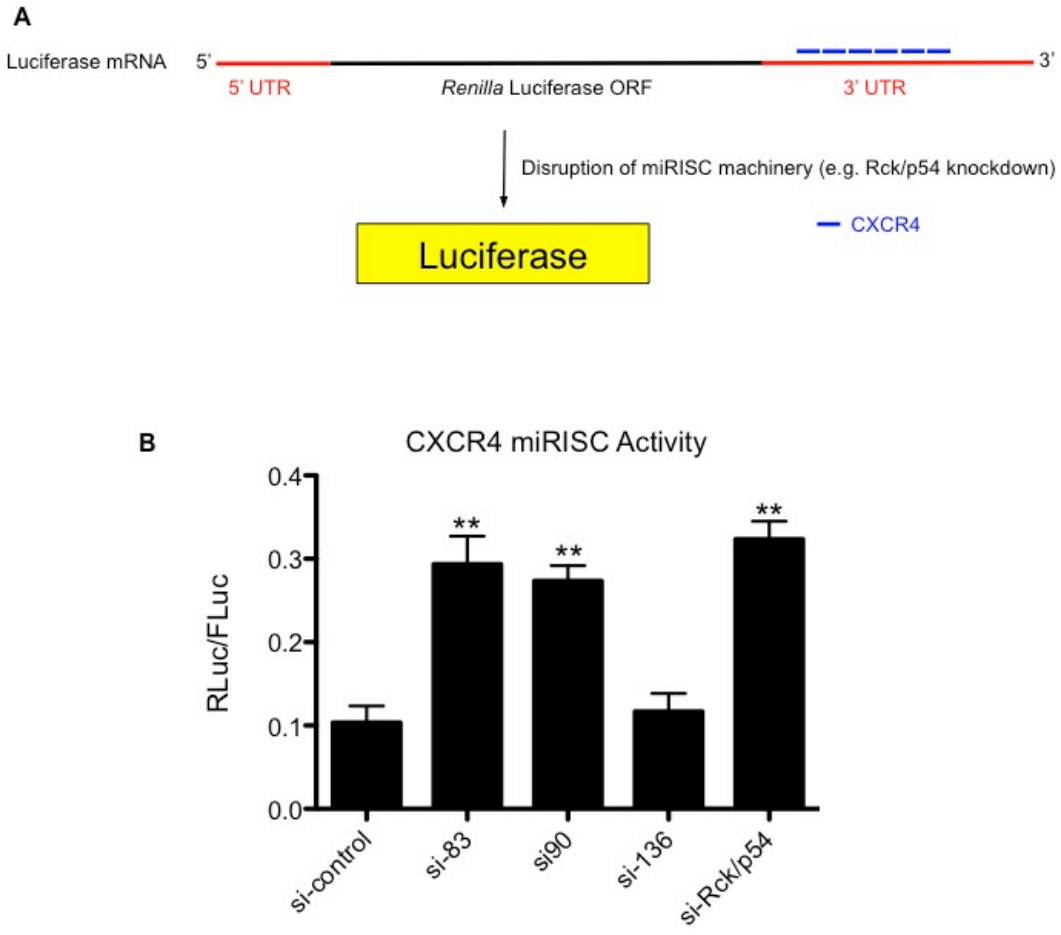

Figure 4.29. p50^{Nesp1} knockdown attenuates CXCR4 miRISC function. p50^{Nesp1} binding partner Rck/p54 is a component which regulates general miRNA-induced silencing complex (miRISC) mediated translational repression. Therefore, a CXCR4 luciferase reporter assay to measure miRISC activity was employed. A) The CXCR4 luciferase assay contains 6x CXCR4 miRNA binding sites in the 3'UTR of a plasmid encoding for luciferase and is used to measure general miRNA function. The CXCR4 miRNA suppresses luciferase expression in cells with functional RISC complexes. However, cells with core RISC proteins depleted (e.g. Rck/p54) fail to silence luciferase, resulting in protein translation. B) U2OS cells depleted of p50^{Nesp1} using si-83 or si-90 significantly attenuated miRISC function in the CXCR4 luciferase assay. Si-Rck/p54 served as a positive control. *Renilla* luciferase (Rluc) readings were normalized to *Firefly* luciferase (Fluc) readings. **P=< 0.01; one-way ANOVA, Dunnett's *post hoc* test.

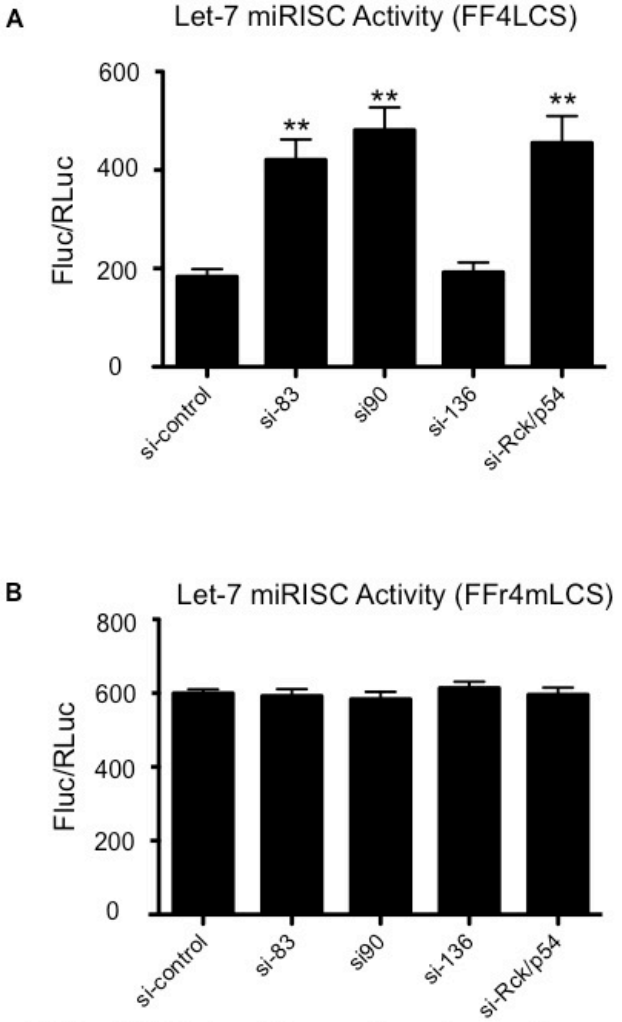

Figure 4.30. p50^{Nesp1} knockdown attenuates endogenous Let-7 miRISC function. A) FF4LCS reporter construct contains 4 miRNA binding sites for endogenous Let-7 miRNA. When this plasmid was transfected into U2OS cells depleted of p50^{Nesp1}, using si-83 and si-90, Let-7 suppression was attenuated. Si-Rck/p54 and si-136 served as positive and negative controls respectively. B) FFr4mLCS reporter construct carries a mutation in the target seed region of Let-7, making it resistant to Let-7 suppression. As expected, U2OS cells depleted of either p50^{Nesp1} or Rck/p54 were unable to attenuate repression relative to si-Control. *Firefly* luciferase (Fluc) readings were normalized to *Renilla* luciferase (Rluc) readings. **P=< 0.01; one-way ANOVA, Dunnett's *post hoc* test.

First, the CXCR4 miRISC reporter was used in the rescue experiments. Not only did over expression of $p50^{Nesp1}$ result in reduced luminescence, indicative of miRISC rescue, but a similar score was also achieved when p50NT was over expressed into si-83 transfected U2OS cells. Expression of $p50^{Nesp1}$ or p50NT in si-Rck/p54 transfected cells failed to rescue miRISC activity suggesting that both $p50^{Nesp1}$ and Rck/p54 are required for miRISC function. miRISC activity could not be rescued by overexpressing the microtubule binding p50CT or the individual SRs which make up $p50^{Nesp1}$ in s-83 transfected cells, suggesting that the two N-terminal SRs together make up the scaffold which complexes translationally-repressed mRNPs (Figures 4.31).

Next, the same rescue experiments were performed in U2OS cells transfected with FF4LCS or FFr4mLCS to measure Let-7 function. Once again, only expression of $p50^{Nesp1}$ or p50NT were able to significantly rescue the silencing function of endogenous Let-7 in U2OS cells transfected with si-83 and FF4LCS (Figure 4.32A). When mutant FFr4mLCS is transfected into U2OS cells, it failed to be suppressed by endogenous Let-7 under any of the knockdown and/or rescue conditions (Figure 4.32B). As expected, the Let-7 luciferase activity in FF4LCS transfected U2OS cells was repressed ~3 fold compared to FFr4mLCS in si-Control U2OS cells.

4.3 Discussion

In this chapter of the thesis, the nesprin-1 N4 antibody was used to determine the sub-cellular localization of endogenous nesprin-1 variants containing the N4 epitope described in chapter 3 (Figures 3.21, 3.22, 3.23, 3.24). Nesprin-1 variant $p50^{Nesp1}$ was shown to localize to P-bodies where it interacts with decapping proteins and translational repressors, Dcp1a and Rck/p54 (Figures 4.12, 4.13). More importantly, $p50^{Nesp1}$ provides a cytoskeletal-scaffold to P-bodies by acting as a microtubule-linker (Figure 4.33). Using recombinant $p50^{Nesp1}$ constructs, the N-terminal domains, SR1 and SR2, were shown to associate with P-body proteins Dcp1a and Rck/p54 in GST pull-down assays (Figure 4.13). Recombinant SR3 and SR4 in tandem could interact directly with microtubules *in vitro,* and furthermore

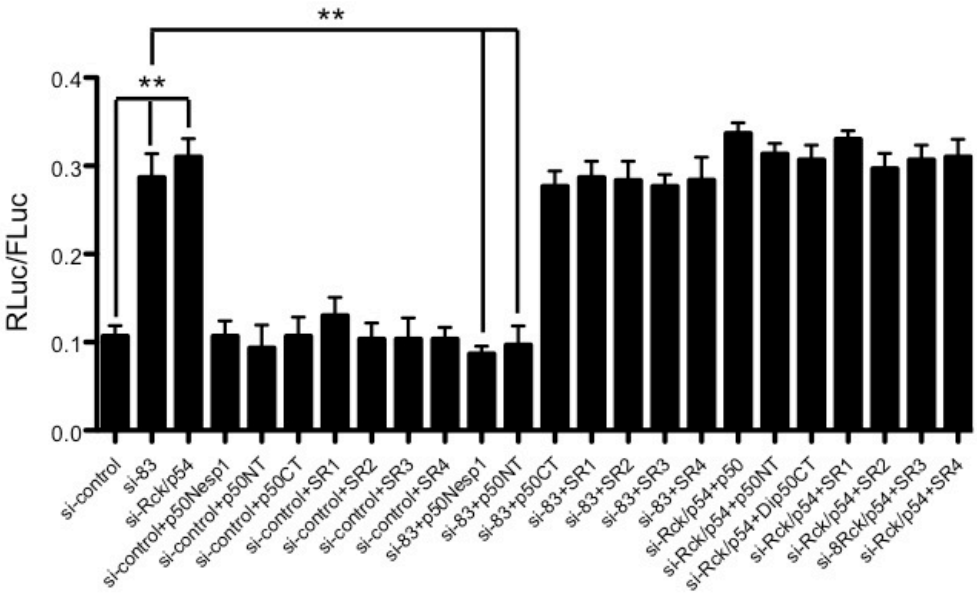

Figure 4.31. The N-terminal SRs of p50^{Nesp1} are required for CXCR4 miRNA silencing function. To show miRISC attenuation was due to p50^{Nesp1} knockdown, and not depletion of other endogenous nesprin-1 variants eliminated by si-83 and si-90, a series of rescue experiments were performed using p50^{Nesp1} and p50^{Nesp1} constructs described throughout this chapter. The si-83 targeting nucleotides in full-length Flag-p50^{Nesp1}, -p50NT and -p50SR1 were mutated so they could not be targeted for knockdown, however the codons still encoded for WT amino acids. Not only did Flag-p50^{Nesp1} overexpression result in reduced luminescence, indicative of miRISC rescue, but a similar score was also achieved when Flag-p50NT was over expressed into si-83 transfected U2OS cells. Overexpression of Flag-p50^{Nesp1} or -p50NT into si-Rck/p54 transfected cells failed to rescue miRISC activity, suggesting that both p50^{Nesp1} and Rck/p54 are required for miRISC function. miRISC activity could not be rescued by overexpressing the microtubule binding Flag-p50CT or the 4 individual SRs making up p50^{Nesp1} into s-83 transfected cells, suggesting that the two N-terminal SRs make up the scaffold which complexes miRNA translationally-repressed mRNPs. Si-Rck/p54 served as a positive control. *Renilla* luciferase (Rluc) readings were normalized to *Firefly* luciferase (Fluc) readings. **P=< 0.01; one-way ANOVA, Dunnett's *post hoc* test.

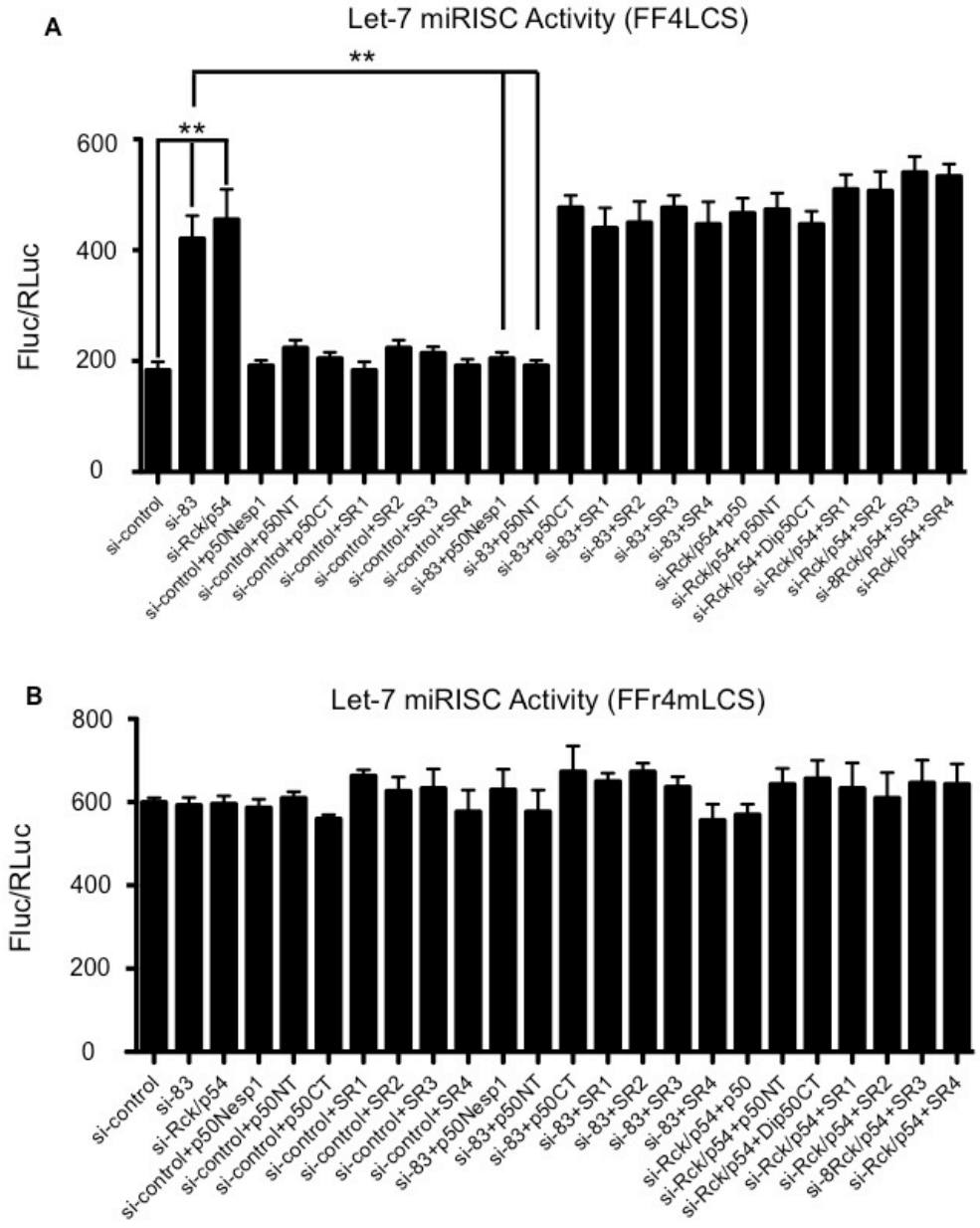

Figure 4.32. The N-terminal SRs of p50^{Nesp1} are required for Let-7 silencing function. As with the experiments performed in the previous figure, the Let-7 reporter constructs were utilized in the rescue experiments. A) Flag-p50^{Nesp1} and Flag-p50NT overexpression could rescue Let-7 suppression of FF4LCS in si-83 transfected U2OS cells. B) When mutant FFr4mLCS is transfected into U2OS cells, it failed to be suppressed by endogenous Let-7 under any of the knockdown and/or rescue conditions. *Firefly* luciferase (Fluc) readings were normalized to *Renilla* luciferase (Rluc) readings. **P=< 0.01; one-way ANOVA, Dunnett's *post hoc* test.

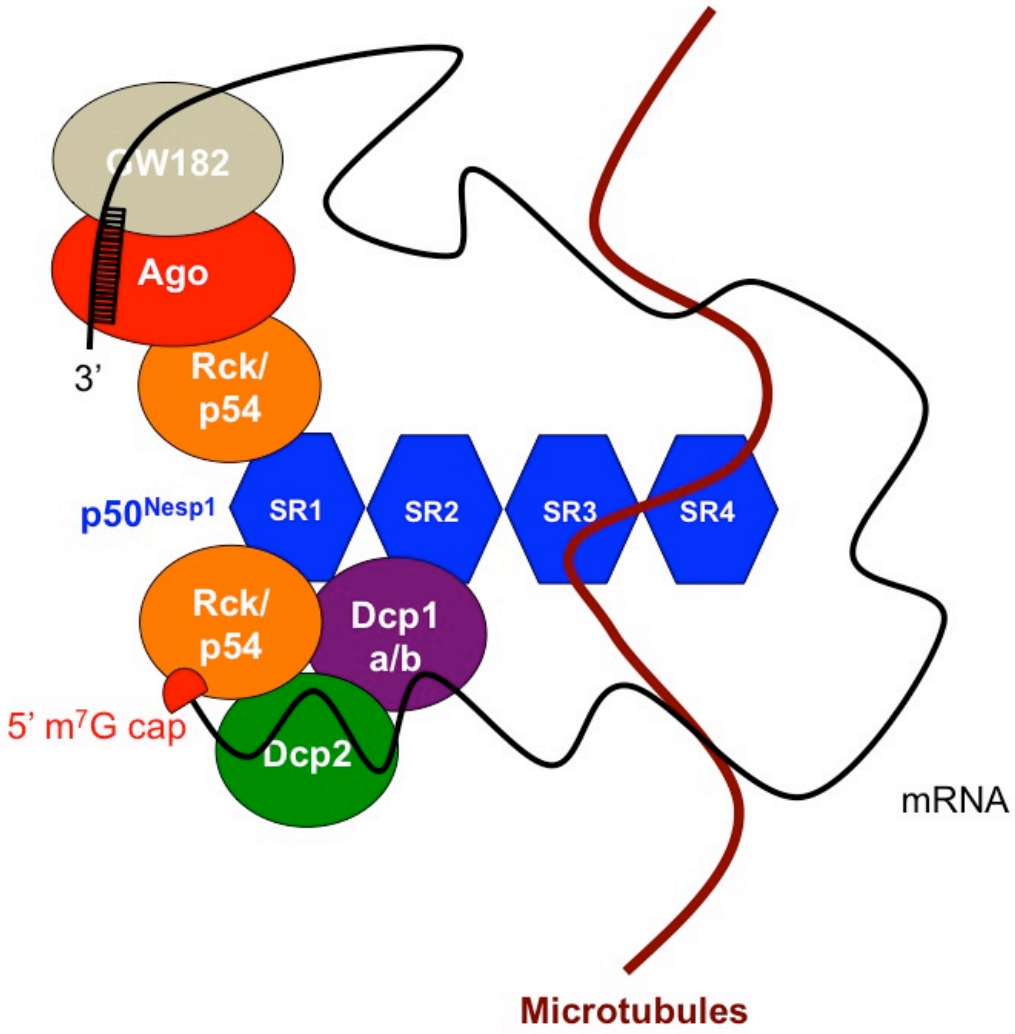

Figure 4.33. p50^{Nesp1} scaffolds P-bodies to microtubules. By potentially interacting with decapping factors (Dcp1a, Dcp1b, Dcp2, Rck/p54), translational repressors (Rck/p54) and miRISC components (Rck/p54, Ago, GW182) through SRs 1 and 2, and microtubules through SR 3 and 4, p50^{Nesp1} is able to scaffold P-body mRNP complexes to microtubule cytoskeleton.

promoted microtubule bundling in U2OS cells, strongly favouring p50^{Nesp1} as a MAP (Figure 4.18, 4.19). To confirm p50^{Nesp1} as a microtubule-P-body linker, full-length Flag-p50^{Nesp1} recruited Rck/p54 to microtubules bundles when expressed in U2OS cells. However when Flag-p50CT, which fails to bind to Rck/p54, was transfected into U2OS cells, no localization or association of Rck/p54 with the microtubules was observed (Figure 4.20). Moreover, the latter cells had defects in two microtubule-regulated processes; abrogated P-body movement and the failure of P-bodies to attach to SGs in stress-induced cells [297] (Figures 4.22, 4.25). The latter resulted in the failure of transferring GFP-labelled β-globin mRNA transcripts from SGs to P-bodies (Figure 4.26). Moreover, SGs were unable to resolve in the recovery phase and promoted cell death at around ~7 hours, suggesting the cells were locked in a translationally repressed state (Figure 4.27).

Furthermore, p50^{Nesp1} knockdown resulted in P-body loss, similar attributes to Rck/p54 [290], while p50^{Nesp1} promoted P-body formation when overexpressed in VSMCs and enhanced Rck/p54 and Dcp1a production in U2OS cells (Figures 4.17, 4.20). On the contrary, Rck/p54 and Dcp1a production was reduced in Flag-p50CT over expressing U2OS cells (Figure 4.20). This data suggests that expression of proteins associated with p50^{Nesp1} mRNP complexes may be dependent on them being attached to microtubules via nesprin-1, or expression of these proteins is governed by the availability of p50^{Nesp1} binding sites, which could help stabilize the proteins by providing a microtubule-scaffold, or protect them from the cells degradation machinery. Additionally, p50^{Nesp1} knockdown attenuated miRISC function of two independent reporter constructs, which could be recovered by overexpressing p50NT (Figures 4.29, 4.30, 4.31, 4.32). This data suggests that not only is p50^{Nesp1} required for stabilizing other P-body proteins by providing a microtubule-scaffold, but it maybe an essential component in silencing and transferring miRISC complexes around the cell.

4.3.1 p50^{Nesp1} scaffolds mRNP Dcp1a, Rck/p54 and miRISC complexes to microtubules

Transcribed and processed mRNAs are packaged into mRNP complexes and transferred from the nucleus into the cytosol, where the

destiny of the mRNA is decided. Once in the cytosol, mRNAs can be loaded onto ribsosomes for protein translation or they can be stored in a translationally repressed state for protein synthesis at a later point of the cells cycle. When the mRNA is no longer required for cellular function, signals can be sent to the cells mRNA degradation machinery for decay or alternatively for mRNA storage. When degradation occurs from the 5'cap end, the mRNA decapping machinery is required for cap removal, which initiates the events for mRNA degradation. The eukaryotic decapping machinery localizes to P-bodies and is comprised of the decapping enzyme Dcp2 and its two co-factors Dcp1a and Dcp1b [272]. Furthermore, proteins required for RNA-mediated silencing, translational repression and non-sense mediated decay such as GW182, Argounautes, Rck/p54, eIF4E and UPF proteins amongst many others also localize to P-bodies, suggesting P-bodies play a regulatory role in mRNA storage and degradation [267,304,305,306].

In this chapter, the first 2 SRs of $p50^{Nesp1}$ were able to interact with Dcp1a and Rck/p54, and were required for miRISC function, suggesting that $p50^{Nesp1}$ may act as a scaffold for these regulatory proteins (Figures 4.13, 4.30, 4.31). The final 2 SRs of $p50^{Nesp1}$ were shown to localize and interact directly with microtubules (Figures 4.18, 4.19). Because p50CT was unable to interact with Rck/p54 and Dcp1a, it was proposed as a potential dominant negative construct to disrupt P-body dynamics. Indeed when overexpressed, p50CT was able to knock endogenous Rck/p54 and Dcp1a-YFP off microtubules in U2OS cells, however the P-bodies remained in close proximity to the microtubules, presumably trying to re-attach (Figures 4.20, 4.23). Furthermore, these cells had abrogated P-body movement in their spatially confined regions, mimicking P-body detachment from microtubules as previously described [297]. The same study suggested that the erratic confined movement of P-bodies was due to the dynamic swaying nature of individual microtubule tracks, agreeing with the data provided in this chapter showing that this erratic movement is reduced when P-bodies are removed from microtubules (Figure 4.22). Microtubule attachment allows P-bodies to probe a greater cytosolic area and therefore increases the likelihood of colliding with RNAs that need to be degraded or translationally repressed in a miRNA-dependent or –independent manner for storage. Furthermore,

previous studies indicate that cytoplasmic mRNAs can be associated with and move rapidly along microtubules [307]. Therefore, P-bodies are more likely to encounter these mRNAs along their travel and sequester them through their membrane-less compartments for degradation and/or storage, signifying that P-body anchorage to microtubules is required for regulating cytosolic mRNA turnover events and translation.

4.3.2 p50^{Nesp1} promotes microtubule bundling.

Microtubules are required for a host of cellular processes, including spindle assembly for chromosome segregation, organelle positioning, polarized growth, cell migration, assembly of cilia and flagella, and intracellular transport [308]. In all these functions, it is crucial that the microtubule polymers are precisely organized. The variety of microtubule structures observed across different cell types require a diverse group of proteins to assemble, stabilize, and dynamically control microtubule tracks. MAPs, which include both molecular motors and non-motor proteins, regulate the global properties of microtubule structures by moving and cross-linking filaments. Previously, Protein Regulator of Cytokinesis 1 (PRC1, also know as MAP65) was the first protein shown to interact directly with microtubules via its SR domains [309]. Like p50^{Nesp1}, PRC1 promotes microtubule bundling, however bundles anti-parallel running tracks, by forming homodimers produced from opposing centrioles before chromosome segregation. Whether p50^{Nesp1} forms bundles with anti-parallel tracks, or those running in the same direction have yet to be determined. Furthermore, the mechanism of p50^{Nesp1}-mediated microtubule bundling has yet to be characterised, whether through N-terminal homodimerization events or through the recruitment of additional protein complexes. Interestingly, PRC1 works with various kinesins to organize microtubule bundles. For example, in mammalian cells, PRC1 is transported to the midzone of tracks by kif4, a kinesin-4 motor protein, before it detaches and promotes microtubule bundling. Previously, components of kinesin-1 and -2 have been identified to interact with SRs of nesprin-1 and nesprin-4 [69,82]. With SRs being structurally conserved, it is not unreasonable to assume multiple kinesin binding sites are

located throughout the nesprins, including domains within $p50^{Nesp1}$ [78]. Whether localization of $p50^{Nesp1}$ to specific points along tubule tracks is mediated via a similar mechanism to that of PRC1 would make an interesting hypothesis.

4.3.3 P-body-SG association is dependent on P-bodies being linked to microtubules

mRNA translation is the most energy consuming process that cells undergo, and during certain stress responses such as oxidative stress, UV exposure, hyperthermia and hypoxia, cells rapidly reprogram their translational machinery to produce proteins such as heat shock proteins and DNA repair enzymes necessary to deal with the stress for cell survival and to stop synthesis of housekeeping proteins [295,310,311,312,313,314]. During such times, SGs form and potentially aid in sorting non-essential transcripts into P-bodies, whilst loading essential transcripts for cell survival onto ribsosomes for translation. Previously, P-body-SG association has been shown to be microtubule dependent, where fluorescently labelled P-body and SG components lost connections in nocodozole treated cells [297]. This chapter shows that by knocking P-bodies off microtubules, using p50CT, its connections with SGs are abolished; suggesting P-body-SG connections are dependent on P-bodies being linked to microtubules (Figure 4.25). Both SGs and P-bodies are attached to the microtubule cytoskeleton, however P-body detachment could substantially reduce the number of collisions with SGs. Furthermore, the data in this chapter shows that there was an inability to transfer mRNA transcripts from SGs to P-bodies using a β-globin mRNA reporter, confirming that transfer of species between the two bodies is dependent on P-bodies being attached to microtubules (Figure 4.25). U2OS cells expressing p50CT were unable to disassemble SGs in the recovery phase signifying that SG disassembly is somehow dependent on P-bodies being attached to microtubules (Figure 4.26). Currently the mechanism for SG disassembly remains unclear, but one plausible explanation is that P-bodies are unable to transfer specific protein and/or RNA components during stress that may act as disassembly stimuli for SGs entering a recovery period. Previous studies have also highlighted impairment of SGs in nocodozole

treated cells, suggesting microtubules play an important role in SG dissolution and mRNA processing during stress responses [315].

Chapter 5: Identification of Matrin-3 as a novel miRISC and P-body Protein

5.1 Introduction

So far a candidate approach has been used to identify Rck/p54 and Dcp1a as $p50^{Nesp1}$ binding partners, based on their ability to co-localize with endogenous nesprin-1 foci using confocal microscopy. Although Rck/p54 is a novel miRISC component, nesprin-1 foci failed to co-localize and interact with ectopically expressed GW182, a silencing protein considered to be core for miRISC function [290,302]. These data suggest that $p50^{Nesp1}$ may be part of a GW182 independent sub-silencing complex that has yet to be identified. Therefore to further characterize proteins associated with $p50^{Nesp1}$ miRISC function and also proteins that could be associated with microtubule-based P-body dynamics, in this chapter an attempt is made to identify novel nesprin-1 binding partners. By using stringent conditions, co-immunoprecipitation experiments were performed which identified a host of RNA binding proteins associated with nesprin-1. Of these binding partners, Matrin-3 was identifed as a new novel miRISC component that localizes to P-bodies and the nuclear matrix.

5.1.1 Matrin-3 is an integral component of nuclear matrix

Matrin-3 is a 95kDa protein which is predicted by SMART program to consists of two RNA binding domains (RBDs) which are flanked by two zinc finger (ZnF) motifs. The purpose of these domains in matrin-3 remains unknown and the functional biology of matrin-3 is limited to the DNA damage response, RNA editing and cell survival [316,317,318,319]. Matrin-3 is an RNA binding protein that abundantly localizes to the nuclear matrix and is required for cell survival [317,318,320]. Although matrin-3 was identified and cloned two decades ago, its potential roles in the nucleus have only recently begun to emerge through the identification of novel binding partners. Yeast-2-hybrid data suggest that matrin-3 may play a role in a number of key nuclear processes including chromatin remodelling, RNA processing, transcription, translation, DNA replication and repair, translation, and apoptosis [246,316].

Matrin-3 is an RNA binding protein which has been shown to stabilize a group of mRNA transcripts as well as associate with hyperedited RNA, implying its RNA binding domains are likely to have functional roles in novel RNA processing events [319,321]. More interestingly, matrin-3 has been identified as a novel splicing factor and depletion of matrin-3 in HeLa cells results in the de-regulation of cassette exon splicing in a wide range of mRNA transcripts (Professor Chris Smith, Biochemistry Department, University of Cambridge, unpublished data).

5.1.2 Matrin-3 associated diseases

5.1.2.1 Autosomal-Dominant Distal Myopathy

Matrin-3 has been implicated in multiple diseases, however the underlying defective signalling pathways involving matrin-3 remain to be characterized. A genomic screen identified a S85C matrin-3 point mutation in patients suffering from a form of autosomal-dominant distal myopathy with vocal cord and pharyngeal weakness (VCPDM) [322]. Distal myopathies are a group of genetic muscle disorders, and the S85C point mutations resulted in weakened distal muscles of the upper and the lower limbs, with some patients suffering from mild cardiac hypertrophy. Furthermore, these patients displayed myofibre degeneration and a substantial amount of muscle was replaced by fat and connective tissue. At the cellular level these patients had degenerative nuclei, a typical characteristic displayed by multiple myopathies.

5.1.2.2 Down's syndrome

Down's syndrome (DS) is the most frequent genetic (trisomy 21) cause of mental retardation caused by meiotic defects resulting in an extra chromosome 21. Although known for more than a hundred years, the underlying pathomechanisms for the phenotype and abnormal brain functions remain elusive. Protein expression studies found that matrin-3 expression levels were significantly reduced in fetal DS brain relative to control [323]. The trisomic effect of chromosome 21 is not thought to directly have any effects on matrin-3 expression, which is encoded by a gene on chromosome 5. However, dysfunctions in regulatory elements such as miRNAs or proteins

which stabilize matrin-3 may be impaired and as a consequence result in abrogated matrin-3 function.

5.1.2.3 DGAP105

A 5-year old male with multiple congenital anomalies, including posteriorly rotated ears, webbed neck, congenital heart defects, mental retardation and mild hypertelorism was described (Developmental Genome Anatomy Project (DGAP), Harvard University, Unpublished data). A chromosomal translocation of the matrin-3 3'UTR on chromosome 5 to chromosome 1 (t1;5) is believed to be the underlying cause of these symptoms. Matrin-3 is strongly expressed throughout the developing heart, and also in the nuclei of adult and embryonic skeletal muscle, smooth muscle, vascular endothelial cells, and in the developing lung, brain and kidney, suggesting a requirement for matrin-3 function in development and muscle function. The 3'UTR of mRNA transcripts can play a role in mRNA localization, stability, and translation [262]. For example, binding of miRNAs to partially complementary sequences in the 3'UTR can result in de-adenylation and translational inhibition or destruction of the target mRNA [264]. With matrin-3 containing potential miRNA binding sites in its 3'UTR, defects in matrin-3 expression could be a cause of the phenotype observed in DGAP105 [324].

5.2 Results

5.2.1 Identification of p50^{Nesp1} specific binding partners

To further characterize protein complexes associated with p50^{Nesp1} functions in miRISC and P-body dynamics, U2OS cells were transfected with Flag-p50^{Nesp1} or an empty control Flag vector and stringent co-immunoprecipitations (co-IPs) were performed with anti-Flag to purify p50^{Nesp1} associated protein complexes. Precipitated protein complexes were denatured by boiling in β-mercaptoethanol loading buffer and separated by SDS-PAGE. Silver staining of the gel identified multiple bands in the Flag-p50^{Nesp1} co-IP, however these bands were also present in the negative control

co-IP suggesting no p50^{Nesp1} specific protein complexes were purified (Figure 5.1).

5.2.2 Generation of nesprin-1 N5 antibody.

The failure to identify p50^{Nesp1} specific binding partners using anti-Flag co-IPs suggested another approach would be required for characterizing p50^{Nesp1} associated proteins. Performing a yeast-2-hybrid screen using p50^{Nesp1} as bait would have been the ideal option, as it would have identified both strong and weak p50^{Nesp1} interacting partners. Instead, an approach to identify endogenous binding partners was used by performing co-IPs with nesprin-1 N4. However to identify nesprin-1 specific binding partners, nesprin-1 N5 was created against nesprin-1 amino acids *QTIRQAENRLSKLNQA* (amino acids 5510-5525 of nesprin-1 giant). These amino acids are located downstream of the nesprin-1 N4 epitope, however are still encoded for by exon 86 and present in SR50 of nesprin-1.

5.2.3 Nesprin-1 N5 stains p50^{Nesp1} P-bodies and the nuclear matrix but recognizes non-specific species by Western blotting.

In theory, nesprin-1 N5 should localize the nesprin-1 variants to the nucleolus and P-bodies, and detect the same bands on a Western blot as nesprin-1 N4. Indeed, nesprin-1 N5 did stain P-bodies in U2OS cells as well as strongly staining the nuclear matrix, which the nesprin-1 N4 antibody stains weakly (Figure 5.2A). However, the antibody did not localize any nesprin-1 variants to the nucleolus.

To determine if nesprin-1 N5 recognized p50^{Nesp1} P-body complexes, co-IPs with nesprin-1 N5 were performed on U2OS cell lysates. The lysates were then probed for endogenous p50^{Nesp1} binding partners Rck/p54 and Dcp1a, which precipitated strongly with nesprin-1 N5 (Figure 5.2B). Nesprin-1 N4 and Rck/p54 co-IPs were performed alongside nesprin-1 N5 as positive controls, which also pulled down Rck/p54 and Dcp1a.

Next, co-IPs were performed with nesprin-1 C2 and nesprin-1 CH2, which served as additional negative controls. Nesprin-1 C2 and nesprin-1 CH2 antibodies are described in chapter 3 and target the nesprin-1 KASH

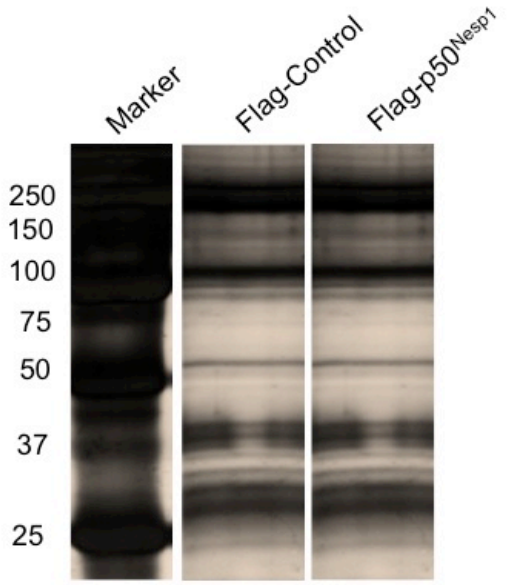

Figure 5.1. Purification of p50^{Nesp1} protein complexes. To identify p50^{Nesp1} specific binding partners, Flag-p50^{Nesp1} was transfected in U2OS cells and protein complexes were purified using anti-Flag antibody. Flag-control transfection served as a negative control. Both co-IPs were separated by SDS-PAGE and protein bands from both samples were visualized by silver staining. Both samples appeared to purify bands of the same molecular weight suggesting the Flag-p50^{Nesp1} co-IP was unsuccessful.

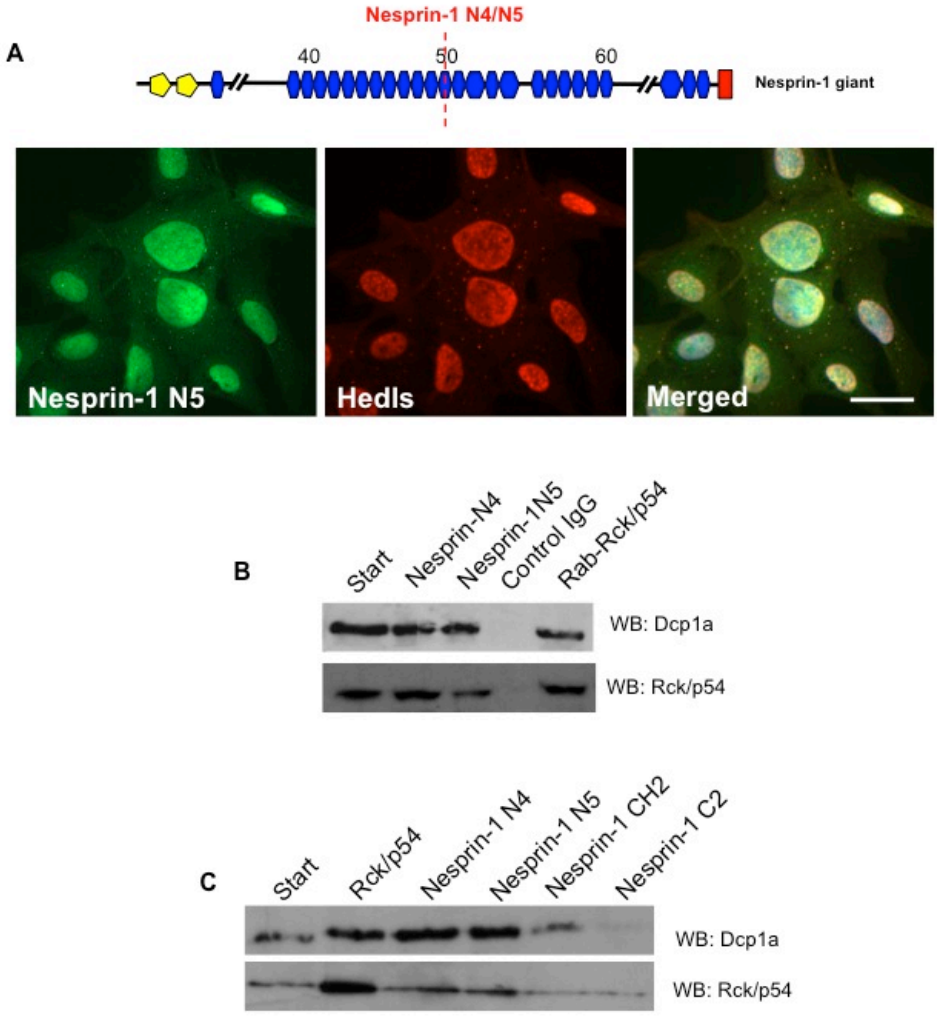

Figure 5.2. Nesprin-1 N5 stains P-bodies in U2OS cells. Nesprin-1 N5 was created against nesprin-1 amino acids *QTIRQAENRLSKLNQA* (amino acids 5510-5525 of nesprin-1 giant). These amino acids are located downstream of the nesprin-1 N4 epitope, however are still encoded for by exon 86 and present in SR50. A) Nesprin-1 N5 stains P-bodies that co-localize with Hedls using confocal microscopy in U2OS cells. Additionally, nesprin-1 N5 strongly stained the nuclear matrix. Scale bar = 10 μM. B) To determine if nesprin-1 N5 recognized $p50^{Nesp1}$ P-body complexes, co-IPs with nesprin-1 N5 were performed on U2OS cell lysates. The lysates were then probed for endogenous $p50^{Nesp1}$ binding partners Rck/p54 and Dcp1a, which precipitated strongly with nesprin-1 N5. Nesprin-1 N4 and Rck/p54 co-IPs were performed alongside nesprin-1 N5 as positive controls. C) The co-IP experiments were repeated with nesprin-1 CH2 and nesprin-1 C2, which served as additional negative controls. Both antibodies precipitated weak background signals, however did not co-IP Rck/p54 and Dcp1a to the same extent as nesprin-1 N4 and N5.

domain and nesprin-1 CHDs respectively, domains absent in $p50^{Nesp1}$ (Figures 3.6, 3.8). Although both antibodies precipitated with Rck/p54 and Dcp1a, the amount detected was substantially reduced relative to the nesprin-1 N4 and nesprin-1 N5 antibodies. (Figure 5.2C)

To confirm specificity of the nesprin-1 N5 antibody, peptide blocking experiments were performed, which diminished nuclear matrix staining and P-body staining when the N5 antibody was pre-blocked by the N5 peptide via immunofluorescence microscopy (Figure 5.3).

When nesprin-1 N5 was used for Western blotting, the antibody detected different molecular weight bands in different experiments that were not reproducible from U2OS whole cell lysates. Furthermore, the bands failed to be attenuated in peptide blocking experiments, suggesting the antibody was unsuitable for Western blotting (Figure 5.4).

5.2.4 Identification of novel nesprin-1 N4/N5 binding partners

Although the nesprin-1 N5 antibody is not suitable for Western blotting, it does appear to recognize nesprin-1 P-body complexes suggesting it may be suitable for co-IPs when used with adequate controls. Therefore, co-IPs on untransfected U2OS cells were performed with both nesprin-1 N4 and N5 antibodies in tandem to identify endogenous nesprin-1 binding partners. The advantage of this approach over a yeast-2-hybrid is that it would obtain binding partners for other nesprin-1 variants as well as $p50^{Nesp1}$, allowing the function of other nesprin-1 variants to be identified.

Purified nesprin-1 N4 and N5 complexes from U2OS cells were separated by SDS-PAGE and silver staining identified several bands present in the nesprin-1 N4 and N5 purification but absent in the negative control IgG (Figure 5.5). Mass spectrometry performed by Dr. Xiaoke Yin (Professor Mayr laboratory, King's College London) was used to identify all the bands stained from both the nesprin-1 and negative control co-IPs. Any proteins identified from the nesprin-1 co-IPs and the control IgG co-IPs were subtracted and only proteins that co-IP with both nesprin-1 antibodies were considered for further investigation. Interestingly the majority of proteins identified were nuclear components involved in RNA processing (Matrin-3,

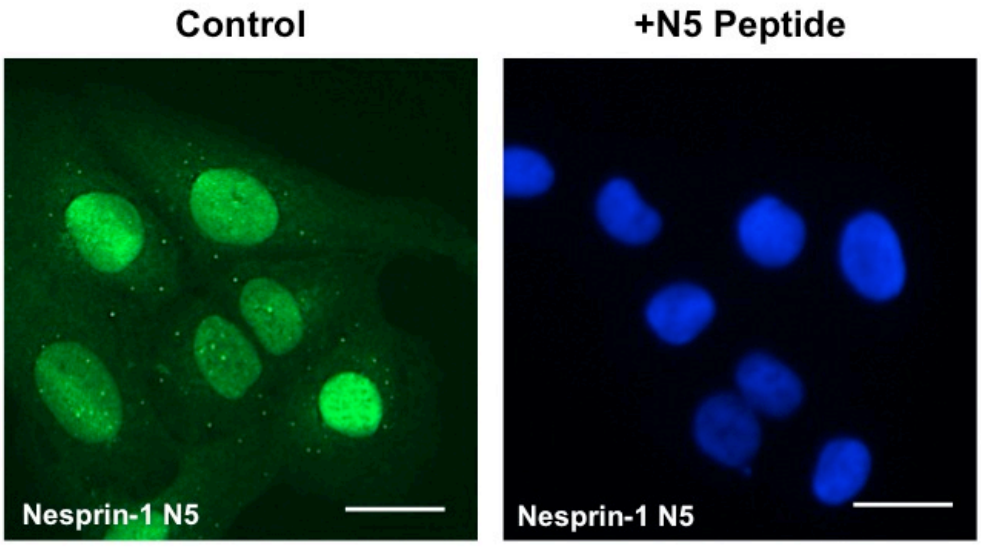

Figure 5.3. Nesprin-1 N5 P-bodies and nuclear matrix stain are blocked by the N5 peptide. To confirm specificity of nesprin-1 N5 antibody, peptide blocking experiments were performed, which diminished nuclear matrix staining and P-body staining when the N5 antibody was pre-blocked by the N5 peptide via immunofluorescence microscopy. Images acquired using wide-field microscopy. Scale bars = 10 μM.

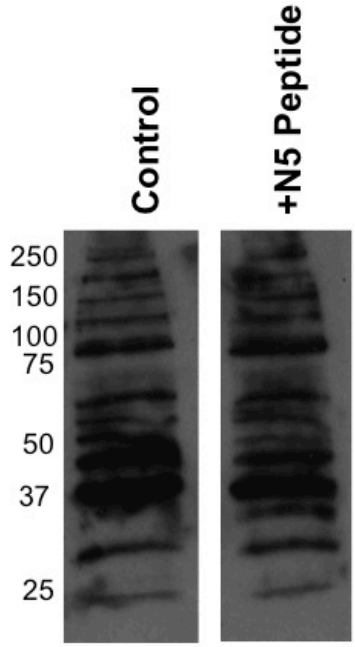

Figure 5.4. Nesprin-1 N5 Western bands fail to be blocked by the N5 peptide. When nesprin-1 N5 was used on Western blotting, the antibody detected different molecular weight bands in different experiments that were not reproducible from U2OS whole cell lysate. Furthermore, the bands failed to be attenuated in peptide blocking experiments, suggesting the antibody was unsuitable for Western blotting.

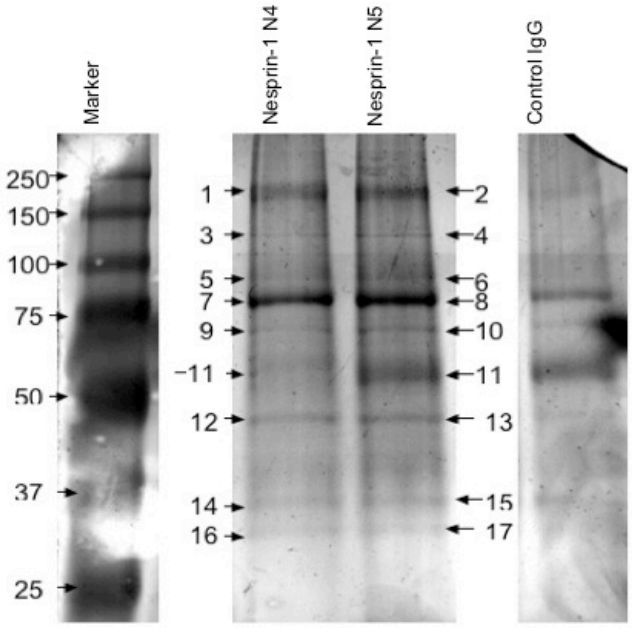

Figure 5.5. Purification of protein complexes associated with nesprin-1 N4/ N5 variants. Nesprin-1 N4 and N5 were used to co-IP endogenous nesprin-1 N4/N5 variants and protein complexes associated with them. A non-specific control IgG rabbit polyclonal antibody was used as a negative control. co-IPs were separated by SDS-PAGE and protein bands from all samples were visualized by silver staining. Nine bands were present in the nesprin-1 N4 and N5 lanes which were excised along with all the bands in the control IgG lane. The identify of all proteins in the nesprin-1 N4 and N5 co-IPs were identified by mass spectrometry performed by Dr. Xiaoke Yin (Mayr lab, King's College London) and are summarized in table 5.1. The numbered arrows in the nesprin-1 N4 and N5 lanes (1-17) correspond to the numbers in the 'Number' column of table 5.1.

PSF, DDx5, hnRNP A2/B1) although some cytoplasmic proteins were also identified (HSP90, 40S ribosomal protein SA, Creatine kinase). Remarkably, NE protein importin-β and cytoskeletal protein actin were also purified, suggesting larger nesprin-1 N4/N5 variants may also be associated with the LINC complex (Table 5.1).

5.2.5 Validation of nesprin-1 binding partners

The nuclear nature of many of these binding proteins suggests that they may preferentially interact with nesprin-1 variants other than P-body $p50^{Nesp1}$. Therefore, to narrow down the binding regions of these proteins to nesprin-1, GST constructs covering a wider range of SRs in the vicinity of the nesprin-1 N4/N5 epitopes were created (Figure 5.6A).

GST pull-downs were performed on U2OS lysates using four different GST clones. The pull-down products were then probed for some of the binding partners obtained from mass spectrometry such as matrin-3, DDx5, PCNA and importin-β. Matrin-3 interacted specifically with GST-G4, whilst PCNA had a strong association with SRs in GST-G3. Although DDx5 and importin- β appeared to have strong attraction for GST in general, DDx5 had an enhanced attraction for the SRs attached to GST-G3 (Figure 5.6B). Of the four GST constructs, only GST-G4 contains SRs which overlap with $p50^{Nesp1}$ while the rest of the constructs contain SRs downstream of SR48. The ability of matrin-3 to interact with SRs in GST-G4 suggest it is the most likely binding partner to associate with $p50^{Nesp1}$ complexes.

5.2.6 Identifying new miRISC components

In Chapter 4, $p50^{Nesp1}$ was identified as a protein required for miRISC function using the CXCR4 and Let-7 miRISC reporter constructs (Figures 4.29, 4.30, 4.31, 4.32). Interestingly, $p50^{Nesp1}$ failed to interact with core silencing protein GW182 suggesting that $p50^{Nesp1}$ may scaffold silencing complexes independent of GW182. Therefore to further characterize the $p50^{Nesp1}$ silencing complex, the CXCR4 and Let-7 luciferase assays were performed on cells depleted of either Importin-β, DDx5, hnRNPA2/B1, PCNA or matrin-3. Cells depleted of Importin-β, DDx5, hnRNPA2/B1 or PCNA

Table 5.1. Nesprin-1 binding partners identified by mass spectrometry. Proteins from excised bands in figure 5.5 are listed below. The numbers represent the numbered bands in Figure 5.5

Number	Protein	Protein Accession Number
1,2	Matrin-3	NP_001181884.1
1,2	PTB-Associated Splicing Factor (PSF)	CAA50283.1
3,4	Ubiquitin-Like Modifier-Activating Enzyme 1	NP_003325.2
5,6	Heat Shock Protein 90 (HSP90)	BAA13431.1
5,6	Importin Subunit Beta-1	NP_002256.2
7,8	78 kDa Glucose Regulated Protein	NP_005338.1
7,8	Heat Shock Cognate 71 kDa Protein	NP_006588.1
7,8	DDx5	NP_004387.1
9,10	60 kDa Heat Shock Protein, Mitochondrial	NP_002147.2
11	40S Ribosomal Protein SA	NP_002286.2
11	Creatine Kinase B-type	NP_001814.2
11	Histone H4	NP_778224.1
12,13	40S Ribosomal Protein S3	NP_000996.2
12,13	Actin, Cytoplasmic 1	NP_001092.1
14,15	hnRNP A2/B1	BAA06032.1 /BAA06031.1
14,15	14-3-3 Protein Epsilon	NP_006752.1
16,17	Proliferating Cell Nuclear Antigen	NP_002583.1

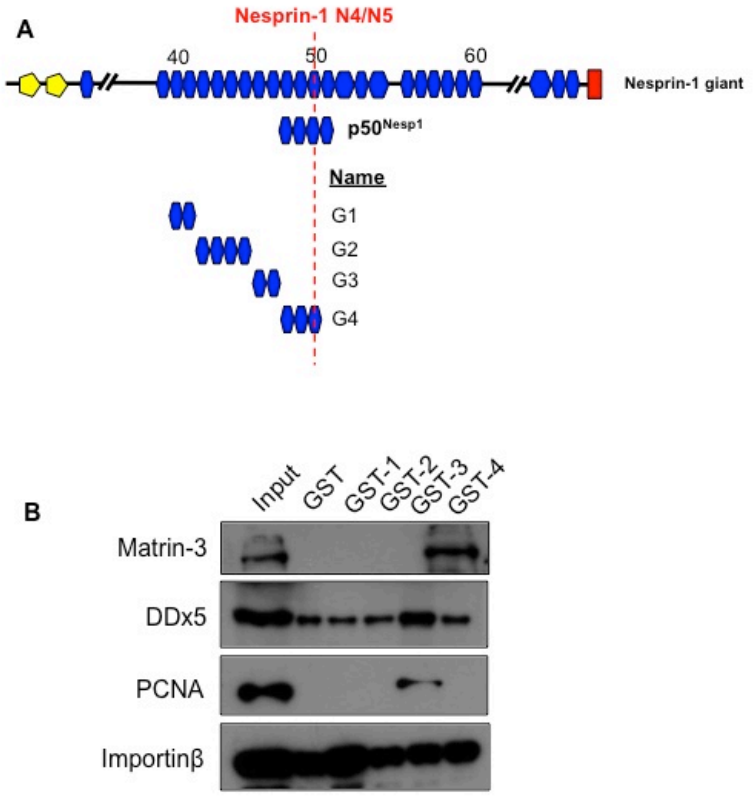

Figure 5.6. Validation of nesprin-1 binding partners. To validate nesprin-1 binding partners, GST pull-downs were performed with GST-tagged nesprin-1 constructs. A) Schematic representation of GST clones created to narrow down the binding regions of potential nesprin-1 binding partners. Only GST-G4 contains SRs which overlap with $p50^{Nesp1}$. B) GST pull-downs were performed on U2OS whole cell lysates. Matrin-3 had a strong association with GST-G4 SRs while DDx5 and PCNA interacted strongly with GST-G3 SRs. Importin-β was pulled-down with all the GST clones including GST, indicative of a strong association with GST in general. The ability of matrin-3 to interact with SRs in GST-G4 suggest it is the most likely binding partner to associate with $p50^{Nesp1}$ complexes.

(knockdowns determined by qRT-PCR, Figure 5.7A) failed to show any significant changes in the CXCR4 luciferase reading compared to control cells, signifying these proteins are not required for RNA silencing. Cells lacking matrin-3 had increased luciferase activity suggesting they had attenuated miRISC to similar levels observed in $p50^{Nesp1}$, GW182 and Rck/p54 depleted U2OS cells (Figure 5.7B). Similar observations were achieved when U2OS cells were transfected with the FF4LCS construct to measure endogenous Let-7 function (Figure 5.8A). However, endogenous Let-7 was unable to attenuate the silencing of FFr4mLCS mutant construct in any of the knockdown conditions (Figure 5.8B).

5.2.7 Matrin-3 localizes to P-bodies

The requirement for matrin-3 in miRISC function and the lack of understanding in general matrin-3 biology through the literature suggested matrin-3 warranted further investigation. To determine the sub-cellular localization of matrin-3, antibodies targeting the N-terminal and C-terminal ends (matrin-3N and matrin-3C, respectively obtained from Abcam) of the protein were used to stain U2OS cells for endogenous matrin-3 (Figure 5.9A,B,C). Both the antibodies stained the nuclear matrix, while matrin-3N additionally stained cytoplasmic foci that co-localized with Hedls protein, suggesting an N-terminal matrin-3 isoform or cleavage product may localize to P-bodies (Figure 5.9B,C).

5.2.8 Matrin-3 foci display typical P-body characteristics

In chapter 4, I demonstrated that nesprin-1 P-bodies were induced in response to oxidative stress and microtubule depolymerisation, and they disassembled in cells that had no free pool of cytoplasmic mRNAs (Figures 4.6, 4.8) . To determine whether matrin-3 P-bodies behaved in a similar manner, they were examined in response to arsenite, nocodozole and cycloheximide. The number of matrin-3- foci increased following arsenite-induced oxidative stress and nocodozole mediated microtubule depolymerisation, whilst being eliminated in cells treated with the translational inhibitor cycloheximide (Figure 5.10).

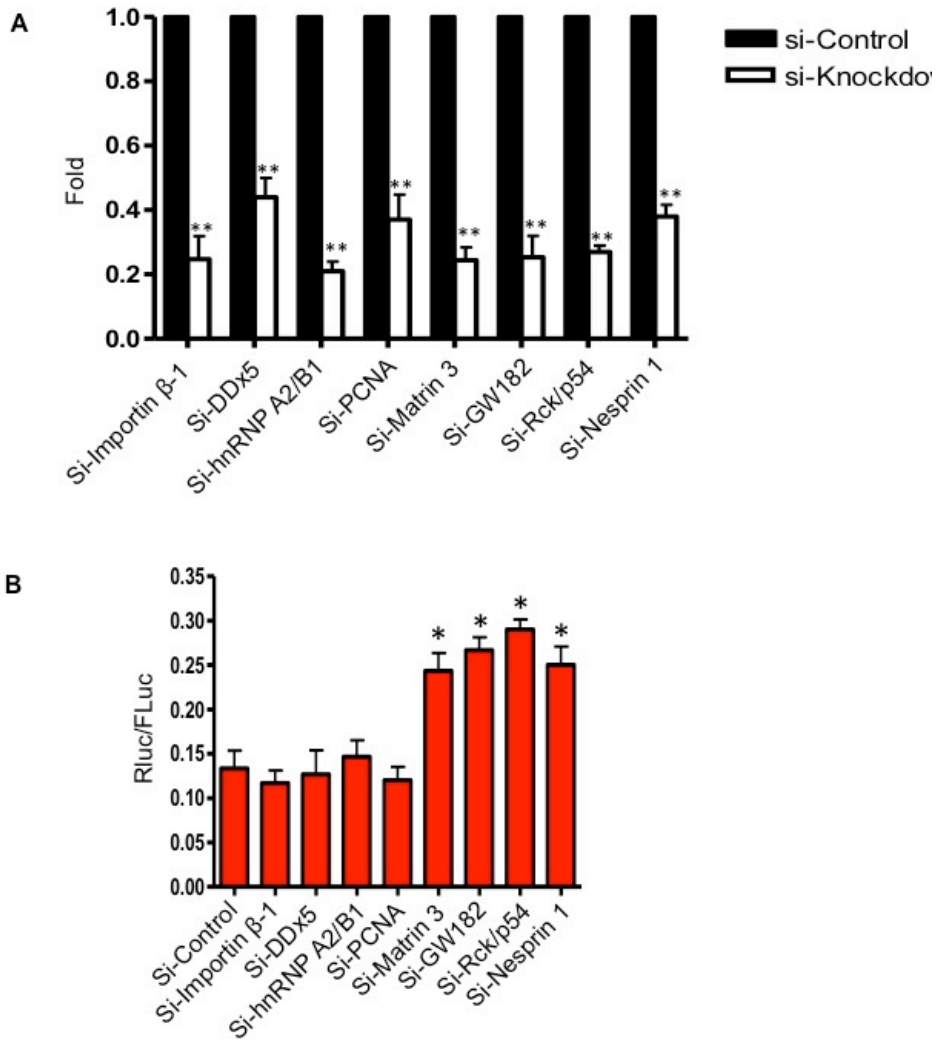

Figure 5.7. Matrin-3 is required for CXCR4 miRISC function. To further characterize the p50^{Nesp1} silencing complex the CXCR4 miRISC assay was performed in U2OS cell depleted of multiple nesprin-1 binding partners. A) qRT-PCR was used to determine knockdown of transcripts in cells transfected with siRNAs. Significant knockdown in levels of importin-β, DDx5, hnRNP A2/B1, PCNA, Matrin-3, GW182, Rck/p54 and nesprin-1 (primers designed across exons 89-90) was observed. **P=< 0.01; Student t-test. B) CXCR4 miRISC assay was performed on cells depleted of importin-β-1, DDx5, hnRNPA2/B1, PCNA and matrin-3. Matrin-3 knockdown resulted in attenuation of miRNA function. GW182, Rck/p54 and si-90 for p50^{Nesp1} served as positive controls. *Renilla* luciferase (Rluc) readings were normalized to *Firefly* luciferase (Fluc) readings. *p<0.05; one-way ANOVA, Dunnett's *post hoc* test.

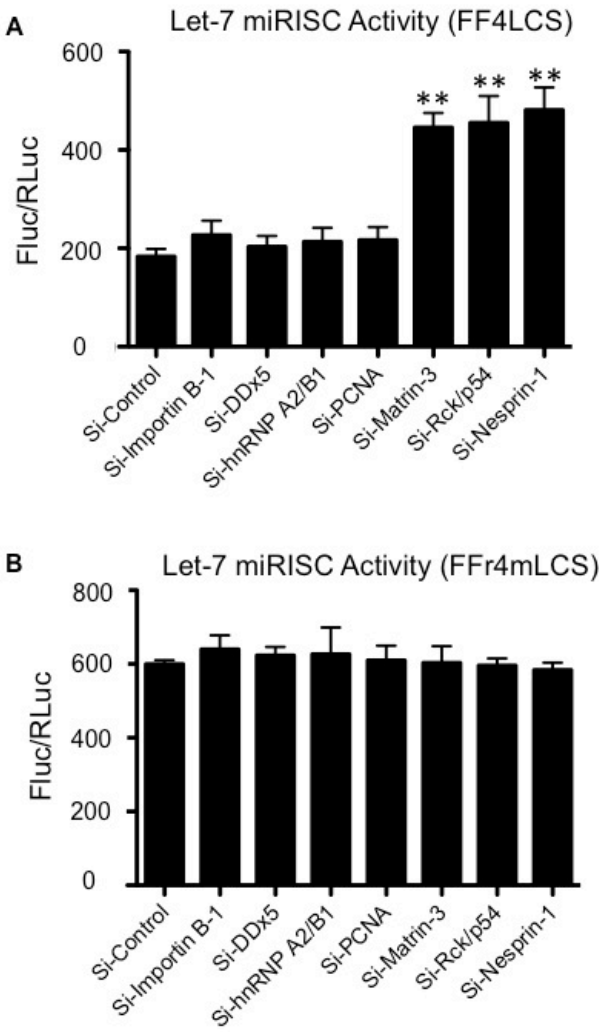

Figure 5.8. Matrin-3 is required for Let-7 miRISC function. A) Matrin-3 knockdown attenuates the silencing function of endogenous Let-7 on FF4LCS. Importin-β-1, DDx5 or hnRNP A2/B1 knockdown did not significantly enhance luciferase readings. Si-Rck/p54 and si-90 for $p50^{Nesp1}$ served as positive controls. B) When mutant FFr4mLCS is transfected into U2OS cells, it failed to be suppressed by endogenous Let-7 under any of the knockdown conditions compared to control cells. *Firefly* luciferase (Fluc) readings were normalized to *Renilla* luciferase (Rluc) readings. **P=< 0.01; one-way ANOVA, Dunnett's *post hoc* test.

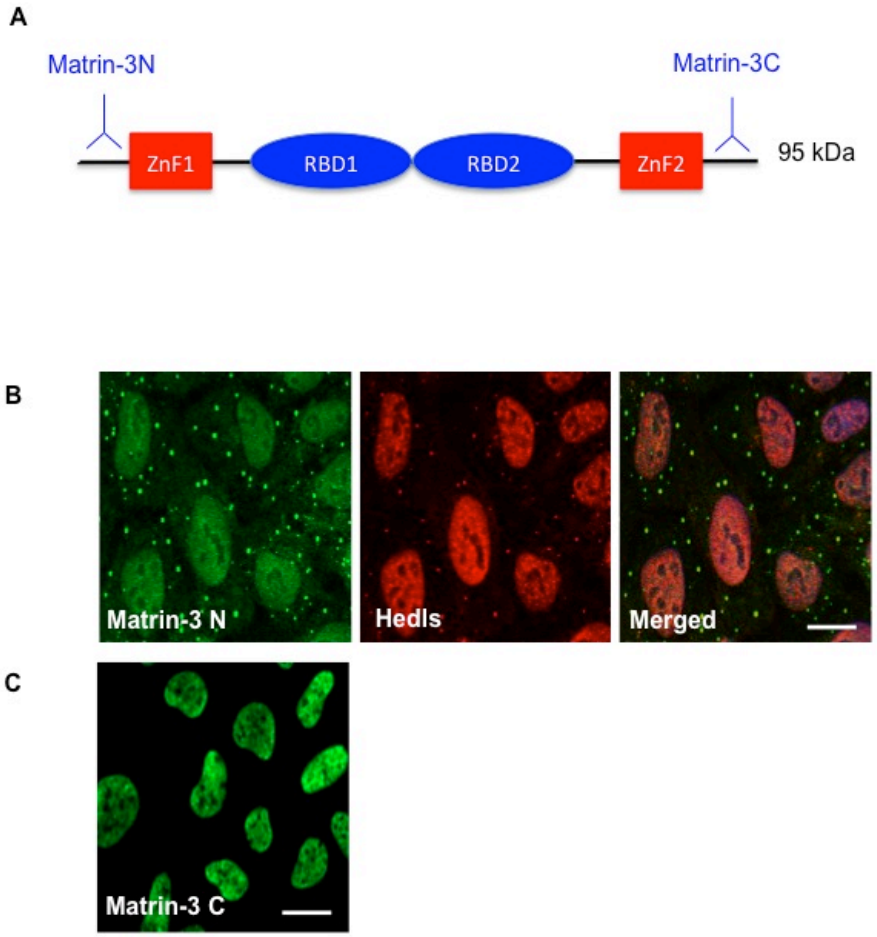

Figure 5.9. Matrin-localizes to P-bodies. To examine the sub-cellular localization of matrin-3, antibodies targeting the N-terminal and C-terminal ends (matrin-3N and matrin-3C, respectively obtained from Abcam) of the protein were used to stain U2OS cells for endogenous matrin-3 A) Schematic representation of matrin-3 domains determined using SMART prediction software with the position of the matrin-3N and C-terminal matrin-3C antibodies. B) Matrin-3N stains the nucleus and cytoplasmic foci which co-localize with P-body marker Hedls in U2OS cells. C) Matrin-3C stains only the nucleus in U2OS cells, suggesting a matrin-3 isoform or cleavage product exists which localizes to P-bodies. ZnF = Zinc finger motif, RBD = RNA binding domain motif. Images acquired using confocal microscopy. Scale bars = 10 μM.

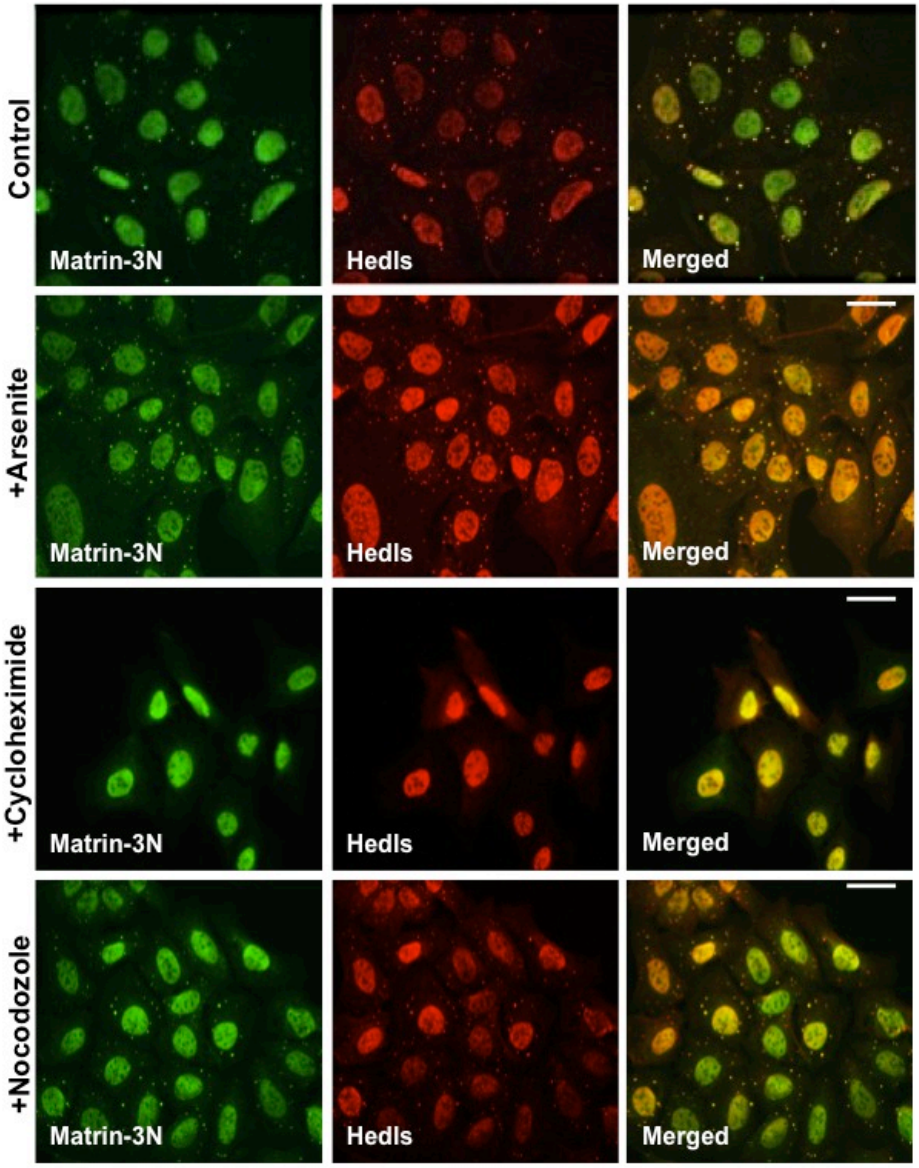

Figure 5.10. Matrin-3 foci display P-body characteristics. To determine the physical properties of matrin-3 foci, P-body formation and depletion was examined in response to cell stress, mRNA-ribosomal trapping and microtubule disruption. Matrin-3 P-bodies increased in number in response to arsenite-induced stress and nocodozole-mediate microtubule disruption. Matrin-3 foci disassemble in response to cycloheximide-mediated translational arrest. Hedls staining was used as a positive control. Images acquired using wide-field microscopy. Scale bars = 10 μM.

5.2.9 Matrin-3 co-localizes and interacts with a host of P-body components

To determine the post-transcriptional mRNA pathways matrin-3 was involved in, U2OS cells were transfected with tagged -GW182, -Rck/p54, -Dcp1a, and -eIF4E, and co-localizations with matrin-3N were examined by confocal microscopy. Unlike $p50^{Nesp1}$, matrin-3 co-localized with all the P-body markers including GW182-GFP (Figure 5.11). This data along with the functional domains present in matrin-3, suggest it might be involved in a more extensive range of post-translational mRNA processing events relative to $p50^{Nesp1}$.

Next, to determine what protein complexes matrin-3 was physically associated with, co-IPs were performed with U2OS cells ectopically expressing Flag-GW182 and HA-eIF4E in the absence and presence of RNAase A. Matrin-3 immunoprecipitated both proteins, in a RNA independent manner, suggesting these interactions were protein-protein dependent. Furthermore, matrin-3 co-purified with endogenous Argounaute-2 (Ago2), Rck/p54 and Dcp1a of which the matrin-3 – Argounaute-2 association occurred in an RNA dependent manner. P-body proteins did not precipitate with the C-terminal nuclear matrix staining matrin-3 antibody, suggesting interactions with GW182, eIF4E, Dcp1a, Rck/p54 and Argounaute-2 were specific to P-body matrin-3. Western blotting with PTB-associated splicing factor (PSF) served as a positive control for matrin-3 purified complexes (Figure 5.12) [319].

5.2.10 A 50 kDa matrin-3 variant localizes to P-bodies

Next, studies were undertaken to examine whether nuclear and cytosolic matrin-3 shared a common pool of the protein. Western blotting on U2OS cytosolic and nuclear fractions isolated using a hypotonic buffer showed differences in matrin-3 molecular weights between the two compartments. The previously identified novel 95kDa matrin-3 appeared in the nuclear pool only, while a smaller 50kDa band was present in the cytosolic fraction (Figure 5.13A). Furthermore, endogenous Ago2, Rck/p54 and Dcpa1a co-immunoprecipitated only with the small 50 kDa matrin-3 while

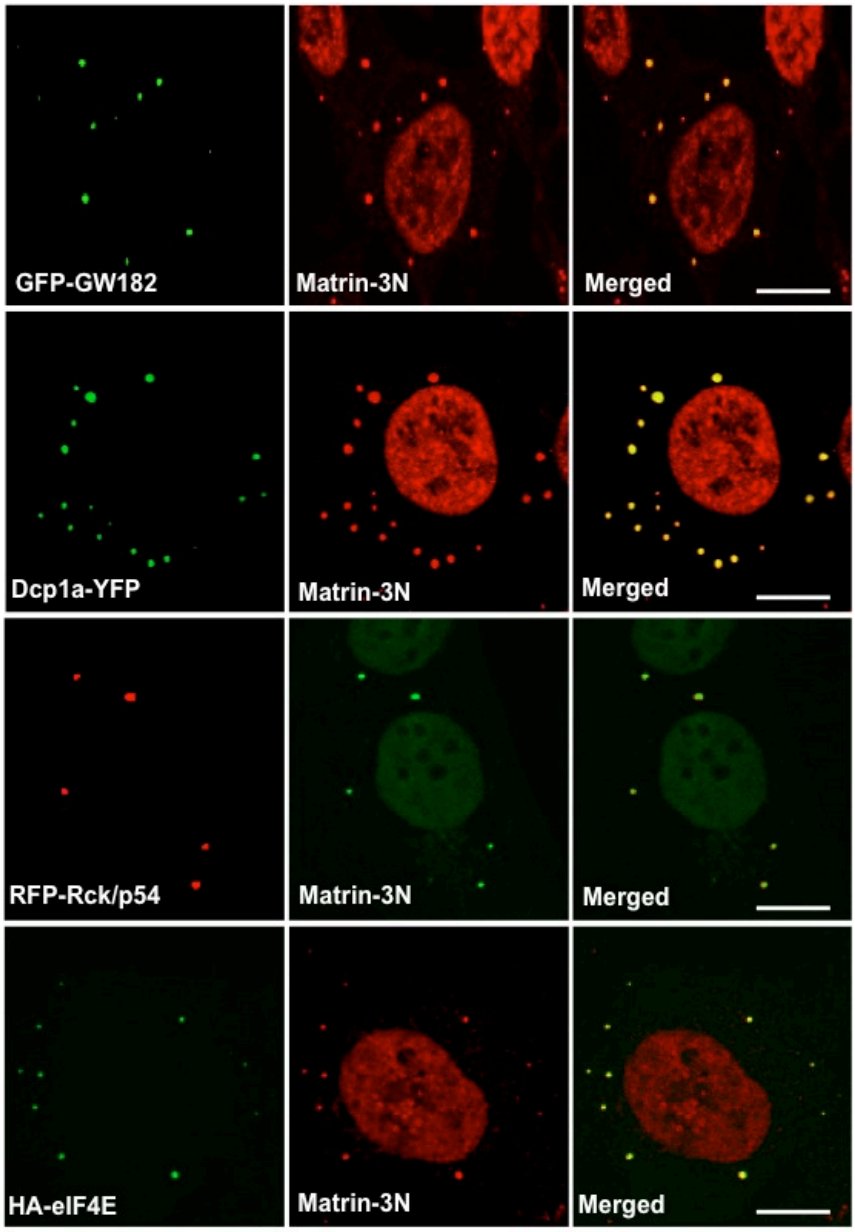

Figure 5.11. Matrin-3 foci localize with ectopically expressed P-body proteins. To identify the post-transcriptional mRNA pathways matrin-3 was involved in, U2OS cells were transfected with tagged GW182, Rck/p54, Dcp1a, and eIF4E and co-localizations with matrin-3N were examined by confocal microscopy. Unlike endogenous $p50^{Nesp1}$ cytoplasmic foci, matrin-3N foci co-localized with ectopically expressed GFP-GW182. Matrin-3N foci additionally also co-localized with decapping factors and translational repressors Dcp1a-YFP, RFP-Rck/p54 and HA-eIF4E. Scale bars = 10 μM.

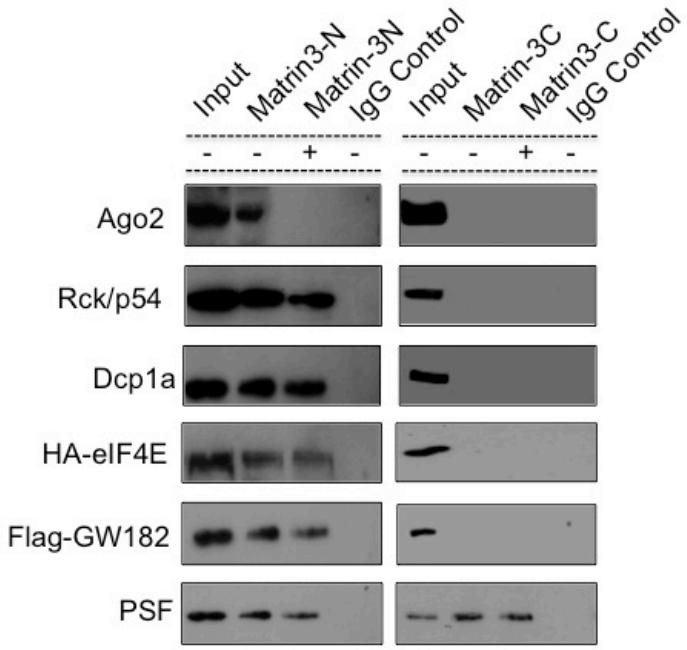

Figure 5.12. Matrin-3N co-IPs endogenous and exogenous P-body proteins. P-body proteins associated with matrin-3 were examined by co-IPs to further characterize matrin-3 protein complexes. Matrin-3N co-IPs with endogenous Argounaute-2 (Ago2), Rck/p54 and Dcp1a of which the matrin-3-Ago2 interaction is abolished in RNAaseA treated lysate, suggesting that the interaction is RNA dependent. Matrin-3N also co-IPs exogenously tagged eIF4E and GW182. Matrin-3C failed to co-IP any endogenous or exogenous P-body proteins suggesting that P-body proteins do not associate with nuclear matrin-3. Western blotting for PTB-associated splicing factor (PSF) served as a positive control for co-IPs and RNAase A treatment for matrin-3N and matrin-3C purifications.

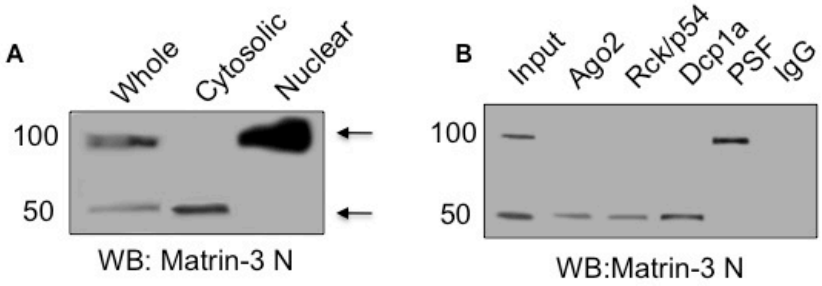

Figure 5.13. A 50 kDa matrin-3 band identified on Western blot associates with P-bodies. Western blotting and co-IPs from U2OS cells were used to examine whether nuclear and cytosolic matrin-3 shared a common pool of the protein. A) Western blotting on cytoplasmic and nuclear fractions obtained from U2OS cells with matrin-3N demonstrates that the antibody recognizes two species. A nuclear band of ~100 kDa is seen in the nuclear fraction, that represents matrin-3 described in the literature, and an additional band is seen in the cytosolic fraction at ~50 kDa. B) P-body proteins Ago2, Rck/p54 and Dcp1a co-IP with the cytosolic band, suggesting a 50kDa matrin-3 isoform or cleavage product localizes to P-bodies. PSF co-IP served as a positive control and associated with nuclear matrin-3.

PSF, a known binding partner of matrin-3 used as a positive control, only co-immunopreicpitated with the 95kDa nuclear matrin-3 (Figure 5.13B). A protein BLAST of the matrin-3N peptide sequence revealed no overlap with any other protein sequences on the database suggesting the antibody is specifically targeting matrin-3.

To identify whether the 50kDa band was a novel isoform/splice variant, cleavage product or a non-specific protein recognized by the N-terminal antibody, siRNAs were created against the N-terminal and C-terminal (si-N and si-C, respectively) ORF of matrin-3. Si-M3N knocked down both the 95kDa and 50kDa bands on a Western blot while also eliminating nuclear matrix and P-body matrin-3 staining in U2OS cells, while si-M3C eliminated nuclear matrin-3 but failed to have any effect on P-body matrin-3 staining, suggesting a unique novel N-terminal matrin-3 splice variant exists in P-bodies (Figure 5.14A,B).

5.2.11 Multiple potential matrin-3 splice variants exist

The data obtained so far suggests that P-body matrin-3 possibly has the same coding sequence and therefore same 5' mRNA end as nuclear matrin-3, with the two transcripts only differing in the 3' end. Therefore, to try and identify a new novel matrin-3 splice variant, 3'RACE was performed to obtain a new cDNA end that could correspond to P-body matrin-3 using HeLa, Brain and Skeletal muscle cDNA libraries. Primers sets were designed to target the first coding exon of matrin-3, which is recognized by the N-terminal antibody. Although 3'RACE worked successfully with identifying new nesprin-1 cDNA ends, no PCR amplicons were produced for matrin-3, including nuclear matrin-3.

Due to limitations with RACE, such as its inability to detect transcripts which may have long UTRs and therefore long cDNA ends, the EST and ensemble databases were screened to see if novel sequences were available which could represent the ~50 kDa matrin-3 protein. The EST database was initially scanned for cassette exons which could generate matrin-3 variants through alternative splicing, followed by searching for sequences that could provide new 3' termination sites. Searches through the EST database failed

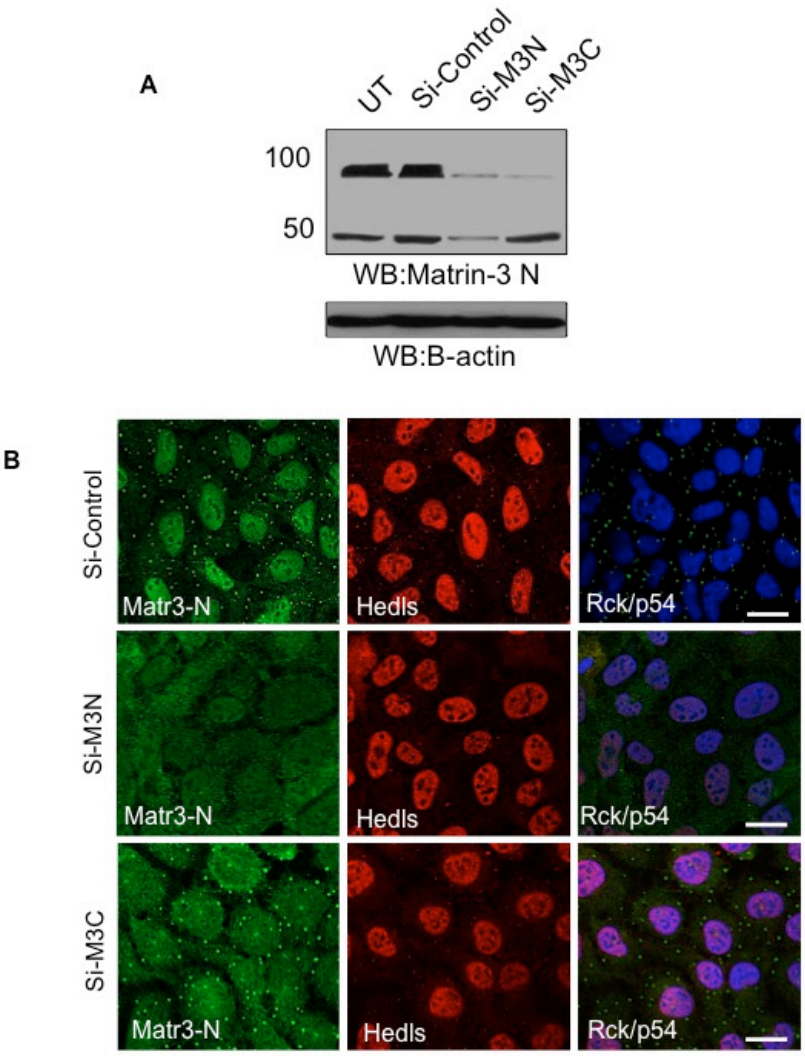

Figure 5.14. 50 kDa matrin-3 P-body protein represents a matrin-3 isoform. A) To determine whether the 50 kDa band detected by matrin-3N was a matrin-3 isoform, cleavage product or non-specific detection, matrin-3 was knocked down using siRNAs designed against the N-terminus of matrin-3 (si-M3N) or the C-terminus (si3C). Si-M3N knocked down both the 50 kDa and 100 kDa bands suggesting the small 50 kDa band is a product generated from a transcript transcribed off the matrin-3 gene. Si-M3C only eliminated the 100 kDa band, with no changes in expression levels of the 50 kDa product suggesting that the 50kDa is not a cleavage product and has to be a novel matrin-3 isoform. B) si-M3N eliminated both nuclear and P-body staining in U2OS cells, while si-M3C only eliminated nuclear staining. Si-M3N additionally eliminated Hedls staining, suggesting that matrin-3 may be a core P-body protein. Images acquired using wide-field microscopy. Scale bars = 10 μM.

to provide any novel findings in either case. The Ensemble database contained a matrin-3 clone *MATR3-011* which encoded a 47 kDa protein that contained the N-terminal matrin-3 antibody epitope. This transcript had the same 5'UTR as nuclear matrin-3 but contained no terminating 3' end, suggesting the *MATR3-011* may be an incomplete sequence and difficult to validate. Other matrin-3 sequences in the Ensemble database produced protein products which lacked the matrin-3 N-terminal antibody epitope or as with *MATR-011,* had no identifiable 3'end.

5.2.12 Matrin 3 ZnF1 and RBD1 form nuclear and cytoplasmic foci

The inability to identify any novel nucleotide sequences which could correspond to P-body matrin-3, implied a cloning approach to identify P-body localizing and interacting domains would be required as an alternative. The staining of P-body foci with the N-terminal antibody and siRNA knockdown of the 50 kDa band with si-M3N suggests P-body matrin-3 is likely to retain its N-terminal domains assuming no unusual alternative splicing events occur. Therefore, matrin-3 N-terminal truncation constructs were created by introducing stop codons after every major domain of GFP-matrin-3 using site directed mutagenesis (Figure 5.15).

GFP-833 encodes matrin-3 amino acids 1-833, GFP-798 encodes matrin-3 amino acids 1-798, GFP-567 encodes matrin-3 amino acids 1-567, GFP-469 encodes matrin-3 amino acids 1-469, GFP-399 encodes matrin-3 amino acids 1-399, GFP-322 encodes matrin-3 amino acids 1-332 and GFP-288 encodes matrin-3 amino acids 1-288 (Figure 5.15A). GFP-matrin-3, GFP-833, GFP-798 and GFP-567 all showed nuclear matrix localization in U2OS cells, while removal of the second RBD in GFP-469 induced cytoplasmic and nuclear foci formation. Subsequent truncation constructs eliminated cytoplasmic foci localization, however still localized to nuclear foci as seen in GFP-399 and GFP-322. The N-terminal uncharacterized motif of GFP-288 localized diffusely throughout the cell (Figure 5.15B).

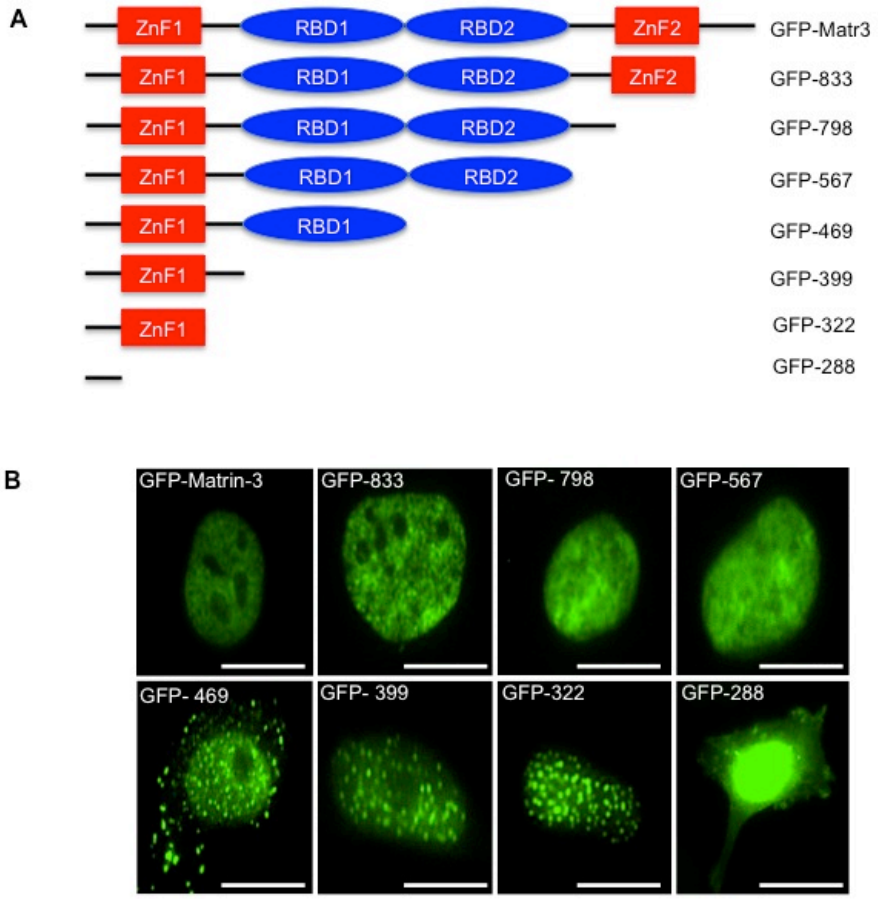

Figure 5.15 Cloning of N-terminal matrin-3 GFP constructs. The staining of P-body foci with the N-terminal antibody and siRNA knockdown of the 50 kDa band with si-M3N suggests P-body matrin-3 is likely to retain its N-terminal domains. Therefore, matrin-3 N-terminal truncation constructs were created by introducing stop codons after every major domain of GFP-matrin-3 using site directed mutagenesis. A) Schematic representation of N-terminal matrin-3 truncation clones and predicted molecular weights. B) GFP-matrin-3 and truncated constructs to GFP-567 localized to the nuclear matrix. Removal of RBD2 resulted in the formation of cytoplasmic foci in GFP-469, which were eliminated when RBD1 was removed in GFP-399. GFP-399 and GFP-322 localize to the nuclear matrix and formed nuclear speckles. The uncharacterized motif in GFP-288 localized diffusively around the cell. Transfection were carried out in U2OS cells and images were acquired using wide-field microscopy. Scale bars = 10 μM.

5.2.13 Matrin 3 ZnF1 and RBD1 localize to P-bodies

To characterise the cytoplasmic foci structures formed by the 52 kDa GFP-469 matrin-3 construct, confocal microscopy was used to determine whether these structures co-localized with P-body markers Hedls, Rck/p54, eIF4E, GW182 and $p50^{Nesp1}$ (Figure 5.16). GFP-469 cytoplasmic foci strongly co-localized with endogenous Hedls and Rck/p54 and ectopically expressed HA-eIF4E and Flag-GW182 in U2OS cells, suggesting GFP-469 cytoplasmic foci resemble P-bodies (Figure 5.16A,B,C,D). Although GFP-469 did co-localize with some endogenous nesprin-1 N4 foci, the majority showed no co-localization with a minority of bodies showing juxtaposed localization (Figure 5.16E). The nuclear foci formed by GFP-469 failed to co-localize with any P-body markers, suggesting they represent different sub-cellular structures.

5.2.14 Matrin 3 ZnF1 and RBD1 interact with P-body components

To determine whether matrin-3-469 (matr3-469) also contained binding sites for P-body proteins, the construct was cloned into a GST vector and pull-down experiments were performed. GST-matr3-469 pulled down endogenous Rck/p54, Ago2 and Dcp1a from U2OS whole cell lysates suggesting that matr-469 has all the relevant domains for P-body localization and interactions. Furthermore, this construct was able to interact with exogenous GW182 and eIF4E obtained from U2OS cells transfected with Flag-GW182 and HA-eIF4E (Figure 5.17).

5.2.15 Matrin-3 mutation S85C attenuates tethering function and interactions with eIF4E, Dcp1a and Rck/p54

Recently a S85C missense mutation in matrin-3 was reported to be a cause of an adult-onset progressive autosomal-dominant distal myopathy with vocal cord and pharyngeal weakness (VCPDM) [325] (See section *5.1.1.1.1*). Currently the effects of this point mutation on cells are unknown due to a lack of knowledge behind matrin-3 function. Although muscle diseases are often associated with structural proteins, I wanted to investigate whether this mutation had any effect on mRNA processing associated with P-body matrin-3.

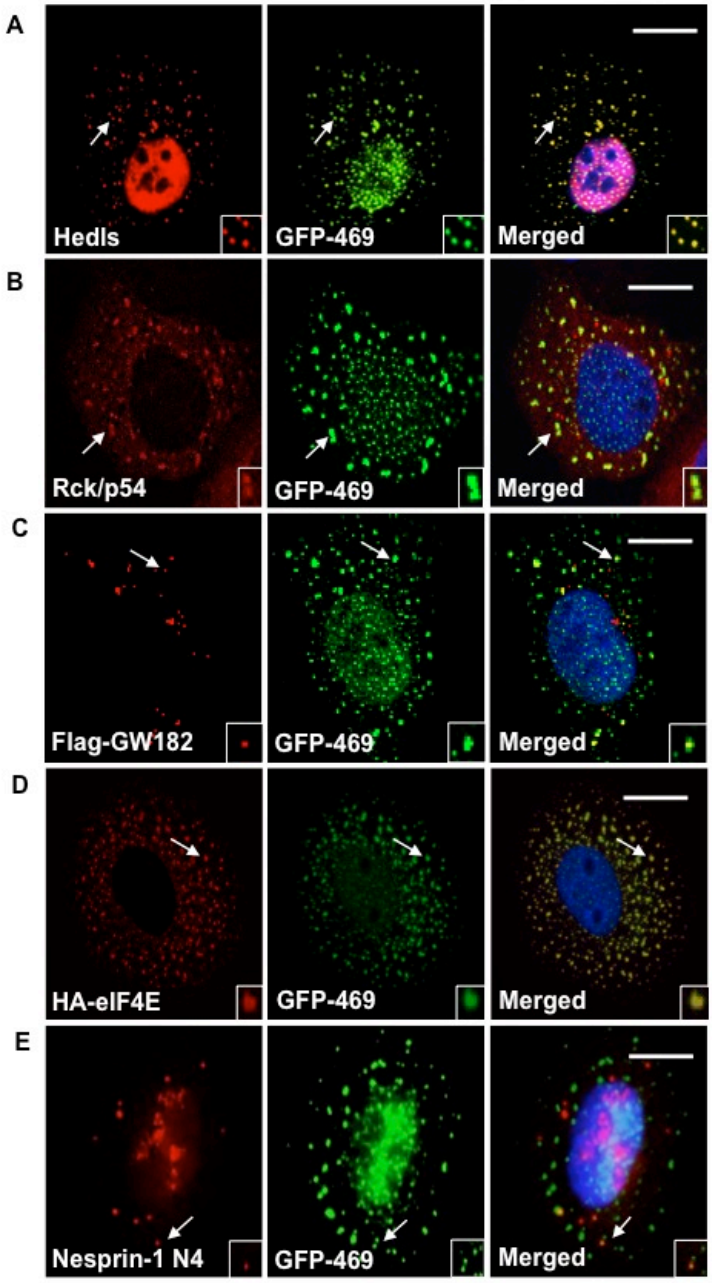

Figure 5.16 GFP-469 localizes to P-bodies. To determine whether GFP-469 cytoplasmic foci resembled P-bodies, transfected cells were stained with endogenous A) Hedls, B) Rck/p54 and exogenous C) Flag-GW182 and D) HA eIF4E. Every GFP-469 foci co-localized with the the four P-body proteins. E) When GFP-439 cells were stained for nesprin-1 N4 P-bodies, only a small number of foci co-localized, with the majority showing no co-localization and a minority of bodies showing juxtaposed localization. Images acquired using confocal microscopy. Scale bars = 10 μM.

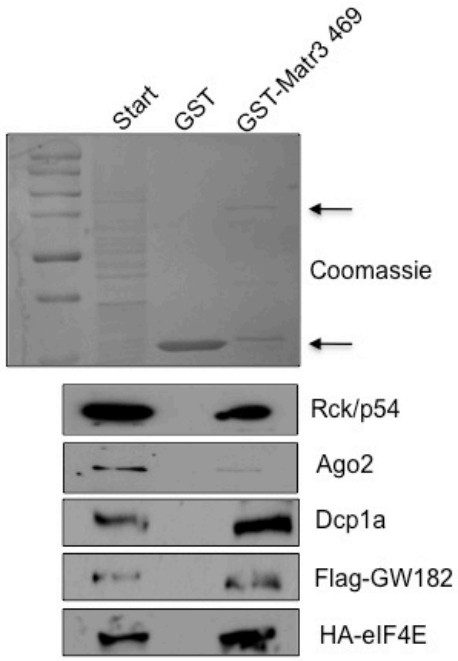

Figure 5.17 Matr3-469 interacts with P-body proteins. To determine whether matrin-3-469 (matr3-469) also contained the binding sites for P-body proteins, matr3-469 was GST-tagged and used in pull-down experiments with whole cell lysates from U2OS cells. GST-matr3-469 pulled down endogenous Rck/p54, Argounaute-2 and Dcp1a, as well as exogenous Flag-GW182 and HA-eIF4E.

To examine whether protein-protein interactions were effected as a result of this mutation, the S85C mutation and a control S85A mutation were introduced into GST-tagged matr3-469 and protein-protein interactions were examined with GW182, Ago2, eIF4E, Dcp1a and Rck/p54. Interactions with GW182 and Ago2 were unaltered while a weakened interaction was observed with eIF4E, Dcp1a and Rck/p54. The control S85A mutation showed the same degree of interaction as the WT, suggesting that the missense mutation to cysteine negates the interaction rather than the serine being absolutely required (Figure 5.18A,B).

Next the ability of the WT, S85C and S85A mutants to silence a β-globin reporter construct in a tethering assay was examined. To do this WT, S85C and S85A matr3-469 were cloned into pc1-λN-V5 and tethered to a luciferase tagged β-globin reporter construct (pRLTK-globin-boxB) in U2OS cells [326]. The λN-peptide has a high affinity for the boxB sites within the luciferase-tagged β-globin transcript, allowing β-globin suppression to be measured by luminescence in response to the recruitment of matr3-469. All three matr3-469 constructs significantly reduced luciferase expression by direct tethering, however the S85C mutant showed impaired reduction relative to the WT and the S85A control, suggesting VCDPM patients may have mRNA silencing defects in muscle. Rck/p54 tethering served as a positive control and expression levels of all constructs were determined by Western blotting for the V5-tag (Figure 5.18C,D).

5.3 Discussion

5.3.1 Nesprin-1 variants may be involved in a wide range of RNA processing events

The initial aim of this chapter was to further characterise the role of $p50^{Nesp1}$ in miRISC silencing and P-body dynamics. As the purification of $p50^{Nesp1}$ using Flag-based co-IPs in U2OS cell transfected with Flag-$p50^{Nesp1}$ was unsuccessful, an alternative approach was used to identify binding partners. The generation of nesprin-1 N5 not only further proves the existence of nesprin-1 within P-bodies, but provides a valuable tool for

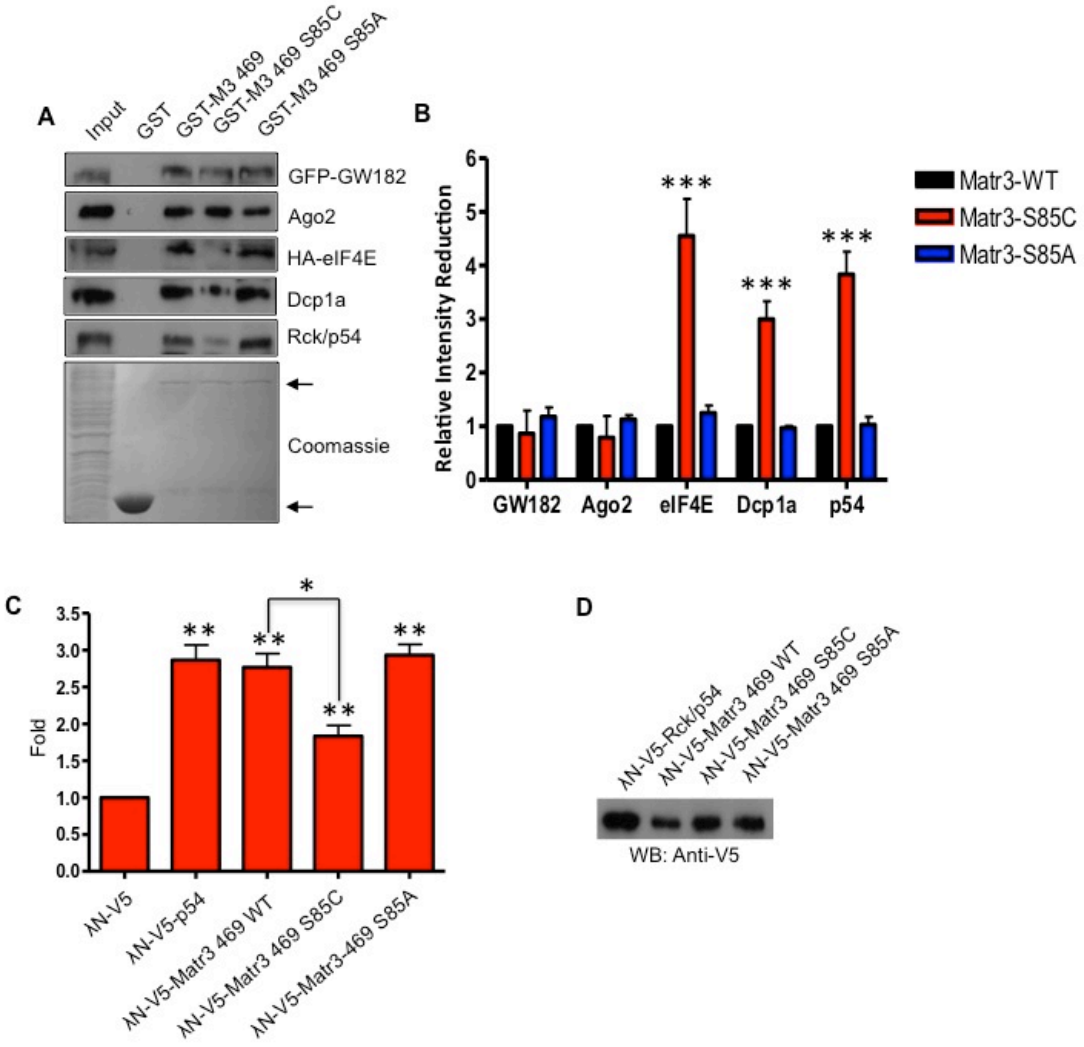

Figure 5.18 Matrin-3 S85C mutation causing VCPDM have defects in interactions with P-body proteins and mRNA silencing. A) GST pull-downs performed with matr3-469 WT, S85C and S85A demonstrate reduced interactions with eIF4E, Dcp1a and Rck/p54 translational repressors and decapping factors. B) Densitometry was performed to quantify strength of interactions of GST-matr3-469 with P-body proteins from three independent GST pull-down experiments. ***p<0.001; one-way ANOVA, Dunnett's *post hoc* test. C) To determine whether matr3-469 could silence mRNA transcripts in a miRNA independent manner, matr3-469 was tethered to a β-globin tagged luciferase construct and silencing was measured in response to luminescence. All three matr3-469 constructs significantly reduced luciferase expression by direct tethering, however the S85C mutant showed impaired reduction relative to the WT and the S85A control suggesting VCDPM patients may have mRNA silencing defects in muscle. Rck/p54 tethering served as a positive control. D) Expression levels of all constructs were determined by western blotting for the V5 tag. *p<0.05, **p<0.01; one-way ANOVA, Bonferroni's *post hoc* test.

characterizing other nesprin-1 variants (Figure 5.3). Like many other antibodies available on the market, it remains unsuitable for Western blotting and therefore fails to identify the molecular weights of P-body and nuclear matrix nesprin-1 variants. Nesprin-1 N5 failed to stain nucleolar structures recognized by nesprin-1 N4 and Flag-constructs, however this could be due to a number of reasons including epitope masking. Instead of performing a yeast-2-hybrid screen to identify $p50^{Nesp1}$ binding partners, purified protein complexes associated with all nesprin-1 N4/N5 variants using co-IPs were performed. Interestingly, this method yielded a range of binding partners primarily involved in RNA processing.

Many of the potential binding partners have previously been shown to be involved in transcription (DDx5, PSF) [327,328,329,330,331], alternative splicing (PSF, DDx5, hnRNP A2/B1) [332,333,334,335], DNA replication/damage repair (PCNA, Matrin-3) [336,337], transport (Importin, hnRNP A2/B1) [338,339,340,341,342] and protein chaperoning (HSP90) [343], further highlighting the capabilities of nesprin-1 as a multi-functional protein through generation of diverse isoforms. Although this chapter focused on identifying new miRISC associated binding partners, functional assays in transcription, splicing and transport involving the function of newly identified binding partners can be used to gain further insight into nesprin-1 function. Furthermore, future work should try and attempt to match binding partners to each of the individual nesprin-1 isoforms so the function of each individual isoform can be determined.

5.3.2 Matrin-3 as a novel P-body and miRISC component

Using co-localization studies along with co-IPs, a ~50 kDa cytosolic matrin-3 splice variant was shown to associate with P-body proteins (Figure 5.13). However, matrin-3 P-body localization was only observed with an antibody created against an N-terminal peptide of the protein, but not with an antibody targeting the C-terminal end (Figure 5.9). The ability to abolish P-bodies and a 50kDa matrin-3 Western band using a siRNA targeting the N-terminal region of the protein but not the C-terminal region, implies that at least two splice variants of the protein exist, one which localizes to the nuclear

matrix and another which localizes to P-bodies (Figure 5.14). Using RACE and online databases, attempts were made to identify novel mRNA sequences which could code for P-body matrin-3. However due to the multiple limitations with RACE and lack of novel online sequences, the transcribed product encoding P-body matrin-3 could not be identified. The constant addition of new sequences to online databases will hopefully reveal possible clues to help identify the true coding sequence of this matrin-3 species in the future.

As an alternative approach, matrin-3 N-terminal truncation constructs were created in order to identify the major domains required for matrin-3 P-body localization (Figure 5.15). Matr3-469 which terminates after the first RBD, encodes a 52 kDa construct and co-localize with Hedls, Rck/p54, GW182 and eiF4E (Figure 5.16). Interestingly, rather than co-localizing with endogenous $p50^{Nesp1}$, the majority of matr3-469 foci showed a juxtaposed localization, indicatinf that overexpression of this construct may act in a dominant negative manner to remove nesprin-1 from P-bodies. Although this phenomena requires further investigation it would be interesting to determine whether matr3-469 promotes nesprin-1 localization to SGs which display a similar juxtaposition to P-bodies in stressed cells (Figures 5.16, 4.7). Additionally, it would be interesting to see what effect this construct has on P-body dynamics such an P-body movement and their ability to associate with SGs, particularly if matr3-469 is able to remove endogenous nesprin-1 from P-bodies.

The degree of alignment which exists between matr3-469 and the actual ~50kDa matrin-3 isoform has yet to be determined, but P-body localization through truncation constructs suggests that RBD1 is necessary for localization, as its removal resulted in disappearance of P-bodes (Figure 5.15). Although matrin-3 has been studied for a number of years now, the biological function of this apparent multi-functional protein has yet to be determined, let alone the role of the various RNA binding and zinc finger domains that exist within the protein.

5.3.3 Matrin-3 silencing and Autosomal-dominant distal myopathy

Not only did matr3-469 localize to P-bodies, but it was also able to interact with P-body proteins and silence a luciferase reporter construct through direct tethering (Figures 5.16, 5.17, 5.18). Furthermore, when a S85C mutation causing autosomal dominant distal myopathy was introduced into matr3-469, interactions with certain P-body proteins and silencing function of matrin-3 was significantly hindered (Figure 5.18). Although myopathies are normally associated with structural defects, this data suggests that the silencing ability of matrin-3 could also be a contributing factor [146]. As well as abrogating interactions with Rck/p54, Dcp1a and eIF4E, the next set of experiments should take a closer look at whether interactions with cytoskeletal proteins are also effected, which could effect how P-bodies migrate and how silenced mRNAs are transported to distant cellular sites in muscle cells. Ideally work performed on skin fibroblasts and/or muscle biopsies obtained from patients will allow the effects of mRNA silencing to be properly studied, as they will allow mRNA silencing to be studied on endogenous P-body matrin-3 mutant rather than an artificial constructs.

Chapter 6: Summary and Future Directions

6.1 Thesis Summary

Nesprins were originally identified as giant SR proteins which scaffold the NE to components of the cytoskeleton [67,68,69]. Nesprins are characterized by N-terminal cytoskeletal-binding motifs followed by a flexible SR rod that terminates with a C-terminal KASH domain, promoting NE localization. Initial studies concentrated on the interactions between nesprins and nuclear lamina associated proteins, such as lamin A/C and emerin, which are mutated in a class of devastating diseases known as nuclear envelopathies. Although nesprin mutations have been identified in nuclear envelopathies, more recent studies have implicated nesprins in diseases not directly linked to the NE, such as bipolar disorder and cancers [202,232]. Previous work conducted by our laboratory, and the work presented in this thesis, confirmed that alternative transcript generation produces multiple tissue- and organelle-specific nesprin-1 variants with roles beyond the NE.

In **chapter 3**, the true extent of nesprin-1 isoform diversity was determined. Initially, Western blots on whole cell lysates of U2OS cells and HDFs using antibodies targeting the nesprin-1 CHD, KASH domain and a SR present in the central rod domain was preformed (Figures 3.6, 3.8, 3.16). Unsurprisingly, all the antibodies detected multiple bands of various molecular weights suggesting various nesprin-1 isoforms exist that contain specific domains. Although some of these bands could be assigned to specific nesprin-1 variants based on the identification of novel 5' and 3' UTRs previously discovered by our laboratory, many were unidentifiable (Figures 3.5, 3.7, 3.18). Therefore, 5' and 3' RACE analysis was performed using nesprin-1 specific primers to detect new UTRs that could help identify new novel isoforms. By alternatively combining the newly identified UTRs with pre-existing ends, it became possible to identify almost every band detected by nesprin-1 antibodies on a Western blot (Figures 3.10, 3.14, 3.20). Many small nesprin-1 variants were verified by RT-PCR on cDNA isolated from multiple tissues and cell lines, which demonstrated nesprin-1 expression specificity. When the small nesprin-1 variants were flag-tagged and examined

in vitro, they localized to multiple sub-cellular compartments such as actin-stress fibres, focal adhesions, cytoplasmic granules, microtubules, P-bodies, nucleolus and the cytosol (Figures 3.11, 3.12, 3.15, 3.21, 3.22, 3.23, 3.24, 4.17). Interestingly, the localization of the ectopically expressed nesprin-1 variants appeared to be cell-type specific, suggesting individual isoforms may have distinctive functions in different cell types.

In **chapter 4,** variants generated within the central rod region of nesprin-1 were further examined. To determine their endogenous localizations, immunofluorescence microscopy was performed with the nesprin-1 N4 antibody on cultured U2OS cells and HDFs (Figure 4.1). Nesprin-1 N4 labelled the nucleolus and multiple cytoplasmic foci that co-localized with mRNA decapping factors and translational repressors in P-bodies (Figures 4.2, 4.10). Not only did $p50^{Nesp1}$ co-IP with Rck/p54 P-body protein, but it also localized to P-bodies when ectopically expressed in VSMCs, strongly linking $p50^{Nesp1}$ to P-bodies (Figures 4.10, 4.12). Interestingly, $p50^{Nesp1}$ localized to and recruited Rck/p54 to microtubules when ectopically expressed in U2OS cells suggesting it may scaffold/link P-bodies to microtubules (Figure 4.20). Indeed, when the final two SRs of $p50^{Nesp1}$ (p50CT), which were demonstrated to have microtubule binding capabilities (Figure 4.18), were transfected into U2OS cells they were able to act in a dominant negative manner and displace P-bodies from microtubules (Figure 4.20). The displacement of P-bodies from microtubules resulted in reduced P-body movement as demonstrated by live-cell imaging using single particle tracking (Figure 4.22). Furthermore, it stopped P-bodies from associating with SGs and blocked β-globin mRNA transfer from SGs to P-bodies during the stress response, resulting in the accumulation of β-globin mRNA within SGs (Figure 4.25). Additionally, SGs were unable to dissemble during recovery which resulted in cellular toxicity and cell death (Figures 4.26, 4.27). Finally, P-body phenotype in response to siRNA-mediated $p50^{Nesp1}$ knockdown was examined. Elimination of $p50^{Nesp1}$ resulted in P-body loss and attenuated miRISC function, which could be rescued by overexpression of the first two SRs of p50Nesp1, measured by a luciferase reporter assays (Figures 4.28, 4.29, 4.30, 4.31, 4.32). Interestingly $p50^{Nesp1}$ failed to interact

with GW182, a core miRISC protein, suggesting that $p50^{Nesp1}$ may scaffold GW182 independent miRSIC complexes.

To gain further insight into the $p50^{Nesp1}$ sub-silencing complex, nesprin-1 binding partners were identified and validated in **chapter 5** using co-IP and GST pull-down experiments (Figures 5.5, 5.6, Table 5.1). Interestingly, the majority of binding partners identified were RNA binding proteins associated with nuclear events, including matrin-3. In this chapter, an additional matrin-3 isoform was found to localize to P-bodies and be a component required for efficient miRISC function (Figures 5.7, 5.8, 5.9, 5.11). Although the identity of the matrin-3 P-body isoform remains elusive, P-body localizing domains were identified (Figures 5.15, 5.16). When a P-body matrin-3 constructs was tethered to a luciferase reporter construct, it was able to induce luciferase repression, which was significantly hampered when a single point mutation (S85C), previously described in a form of autosomal dominant distal myopathy, was introduced (Figure 5.18). Furthermore, the S85C mutated construct had weakened interactions with core P-body proteins Rck/p54, Dcp1a and eIF4E, indicating myopathy patients may have hampered mRNA processing functions (Figure 5.18).

6.2 Discussion and future directions

6.2.1 Nesprins are cellular scaffolds and linkers

Originally nesprins were identified as members of the LINC complex that connect the NE to components of the cytoskeleton. The importance of nuclear-cytoskeletal scaffolding has been widely studied using nesprin animal models, dnKASH constructs and siRNA-mediated knockdown experiments described in Chapter 1.

In addition to functions of nesprins as nuclear-cytoskeletal couplers, scaffolding roles have been identified for nesprins beyond the NE through the generation of KASH-less nesprin variants. GSRP-56, CPG2 and Drop1 are three KASH-less nesprin-1 variants with identifiable transcripts, whereas KASH-less nesprin-2 has been shown as an important mediator of ERK1/2

signalling [207,208,222,232]. In this thesis I have identified additional nesprin-1 variants, which not only act as potential cytoskeletal scaffolds, but may also have cell/tissue specific nuclear scaffolding functions.

6.2.2 Nespin-1 in nuclear scaffolding

In chapter 3 I identified 3 nucleolar nesprin-1 variants terminating with the N1-3'E87 UTR (Figure 3.20). The largest isoform, $p31^{Nesp1}$ composed of 2 and a half SRs, localized to the nucleolus without hampering nucleolar morphology in HDFs. However, when the two shorter nucleolar variants $p23^{Nesp1}$ and $p12^{Nesp1}$ composed of 2 SRs and 1 SR respectively, were transfected into HDFs, they caused fibrillarin to re-distribute into nucleolar cap structures (Figures 3.24). Segregation of nucleolar components into cap structures occurs under some physiological conditions of transcriptional arrest, which can be mimicked by transcriptional arrest using actinomycin D or cellular stress [378,379]. The ability of the two smaller nesprin-1 variants to induce cap formation without the application of stress or translational inhibitors implies that they may be crucial nucleolar organizer, or stress-induced nucleolar signalling proteins. As the primary function of SRs is to mediate protein-protein interactions, it is difficult to speculate what nucleolar proteins these nesprin-1 variants scaffold without identifying binding partners. Future work regarding these nucleolar variants should involve identifying binding partners for each of the 3 nucleolar variants terminating with the N1-3'E87 UTR. Undoubtedly $p31^{Nesp1}$ is expected to scaffold a greater number of proteins than $p23^{Nesp1}$ and $p12^{Nesp1}$. Therefore identifying binding partners for $p31^{Nesp1}$, via a yeast-2-hybrid screen, and then mapping their binding sites to the individual SRs of $p31^{Nesp1}$, $p23^{Nesp1}$ and $p12^{Nesp1}$ would be the most efficient strategy in identifying binding partners for all three variants, assuming the structural properties of the C-terminal ends remain unchanged as the protein truncates. The nucleolus is classically known to be a site of rRNA assembly, however mass spectrometry on purified nucleoli has revealed over 700 proteins related to cell cycle regulation, DNA damage repair, mRNA processing and miRNA biogenesis in the nucleolus, suggesting it has additional roles [380,381]. The unique tissue specific expression patterns of

the three nesprin-1 variants suggest they may influence nucleolar organization and function in a tissue specific manner (Figure 3.20).

Previously a group of nuclear matrix proteins, mostly RNA binding proteins, have been shown to re-localize from the nuclear matrix to nucleolar cap during transcriptional inhibition [379]. Matrin-3 binding protein PSF (which may also interact with nesprin-1 nuclear variants, (Table 5.1) was one of the proteins shown to re-localize to nucleolar caps under these conditions. Although the matrin-3 binding site in nesprin-1 needs to be narrowed down further, potentially all three nucleolar nesprin-1 variants have the ability to associate with matrin-3. Future work should therefore focus on determining whether these nucleolar nesprin-1 variants are capable of interacting with nuclear matrin-3. If they fail to interact, then further extensive RACE will need to be performed to identify additional nesprin-1 variants associated with matrin-3 nuclear function.

Finally p56CH^{Nesp1}, which is composed of both nesprin-1 CHDs and a single SR, was shown to localize to the nucleolus in U2OS cells suggesting multiple nesprin-1 variants generated across the nesprin-1 gene may posses signals to promote nucleolar localization (Figure 3.11). Interestingly, the ability of a CHD variant to localize to the nucleolus suggests it may play a role in linking the nucleolus to nuclear F-actin in U2OS cells. Although the function of nuclear F-actin in transcription and chromatin re-modelling has been well established, the literature shows no link between it and the nucleolus, therefore making an interesting path to pursue [382].

6.2.3 Nesprin-1 in cytoskeletal scaffolding

In addition to nuclear scaffolds, p56CH^{Nesp1} and p50^{Nesp1} were identified as ubiquitously expressed components associated with the cytoskeleton in a cell specific manner suggesting, nesprin-1 variants have functions as cytoskeletal scaffolds.

6.2.3.1 p56CH^{Nesp1} in cell adhesion and migration

Although p56CH^{Nesp1} was shown to localize to the nucleolus in U2OS cells, it strongly associated with actin stress fibres in HDFs (figures 3.11, 3.12).

The ability of p56CH^{Nesp1} to also strongly associate with focal adhesions in HDFs suggest it may play a role in cell migration and adhesion (Figure 3.12). Often knockdown studies with time-lapse microscopy are performed to study the function of proteins in cell motility. However designing siRNAs against the CHDs of nesprin-1 would target global knockdown of all CHD containing nesprin-1 variants with probable drastic F-actin organization throughout the cell. The alternative 3' end processing of the p56CH^{Nesp1} transcript provides it with a unique 37 amino acid peptide sequence absent in the nesprin-1 giant and other nesprin-1 variants, which could be utilised for targeting with siRNAs to specifically knockdown p56CH^{Nesp1}. Furthermore, the large peptide sequence makes an ideal target for synthesizing p56CH^{Nesp1} specific antibodies, which will allow the endogenous localization of the variant to be distinguished in multiple cell lines. SRs generally mediate protein-protein interactions, and with p56CH^{Nesp1} containing a single SR and a long unique peptide sequence it would be interesting to determine what protein(s) associate with the C-terminal end of p56CH^{Nesp1}. Therefore, future studies should focus on the identification of p56CH^{Nesp1} binding partners followed by knockdown experiments to see if disruption of p56CH^{Nesp1} complexes effects F-actin organization and cell migration.

6.2.3.2 Nesprin-1 variants as a microtubule scaffold

In chapter 4, the final two SRs of p50^{Nesp1} were shown to directly interact with microtubules and therefore any nesprin-1 variants which terminates with the N1-3'E90 UTR would retain these the C-terminal SRs and microtubule binding capabilities. Figure 6.1 highlights all potential nesprin-1 variants which could terminate with N1-3'E90 UTR and scaffold various protein complexes to the microtubule cytoskeleton. The variants terminating with this UTR are both large and small, with the largest variant pCH661^{Nesp1} also retaining the N-terminal CHDs suggesting it could act as a microtubule – actin cross linker. The other large variants include pCH620^{Nesp1}, pCH579^{Nesp1} and pCH292^{Nesp1} which posses numerous SRs. Nesprin isoforms tend to be expressed in a tissue/cell specific manner and therefore these microtubule associated protein (MAP) variants could link multiple tissue-specific protein

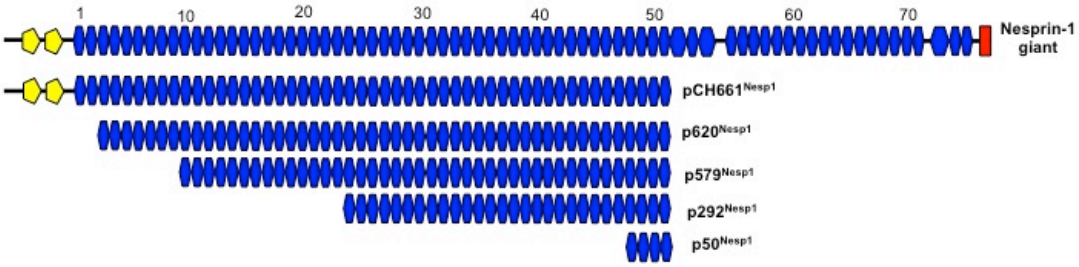

Figure 6.1. Microtubule associated nesprin-1 variants. By alternatively initiating transcripts with the different nesprin-1 5'UTRs and terminating with the the nesprin-1 N1-3'E90 3'UTR, it is possible to create multiple different microtubule associated nesprin-1 variants. The tissue specific expression pattern of the individual 5'UTRs suggest that these variants are likely to be expressed in a tissue specific manner.

complexes to microtubules, regulating transport of intra-cellular complexes within the cell. Validation of the large variants by RT-PCR would be difficult and therefore other methods such as Northern blotting should be utilized in future experiments to confirm their expression. Components of kinesin-1 and 2 have been identified to interact with SRs of nesprin-1 and nesprin-4 [69,82]. With SRs being conserved, it is not unreasonable to assume multiple kinesin binding sites are located throughout the nesprins [78].

Previously, 5 unique mutations were identified in the nesprin-1 gene which resulted in a form of autosomal recessive cerebellar ataxia (ARCA1) [13]. Two of these mutations 306434A-G and 310067A-G, located in splice acceptor sites of introns 81 and 84 of the nesprin-1 gene respectively, abrogated correct splicing of the gene, resulting in premature termination of the protein. Both mutations would result in pre-mature termination of the larger variants and de-regulate signalling pathways of protein complexes associated with nesprin- MAP variants. Identification of binding partners for SRs downstream of the nesprin-1 MAP domain will further aid in the understanding the protein complexes and signalling pathways associated with these nesprin-1 variants.

6.2.3.3 p50^{Nesp1} as a P-body microtubule scaffold

p50^{Nesp1} is the first SR-containing protein to date identified as a novel P-body component. Importantly, p50^{Nesp1} fulfils nesprins role as an intra-cellular scaffold by linking P-bodies to microtubules. Although SR3 and SR4 of p50^{Nesp1} are accountable for microtubule linkage, it appears that SR1 and SR2 of the protein provide functionality by interacting with enzymes and co-factors required for mRNA decapping, translational repression and miRISC (Figure 4.33).

In chapter 5, attempts were made to identify p50^{Nesp1} binding partners. Although matrin-3 was identified as a binding partner and miRISC regulator, the screen did not provide any other useful clues in further dissecting p50^{Nesp1} associated protein complexes. Rather than providing a list of cytoplasmic RNA binding proteins, the co-IP screen revealed nuclear RNA binding proteins as preferential binding partners. This suggests that either nuclear

nesprin-RNA complexes are more abundant than cytosolic nesprin-RNA complexes within U2OS cells, or the nesprin-1 N4 and N5 antibodies have a stronger affinity for associating with nuclear nesprin-1. Nonetheless, this data along with the ability of $p50^{Nesp1}$ to associate with Rck/p54 and Dcp1a suggest that SRs present around the nesprin-1 N4/N5 epitope may have a high affinity for RNA binding proteins. To overcome this issue, SR1 and SR2 of $p50^{Nesp1}$ should be incorporated into a yeast-2-hybrid screen which will pick up both strong and weak interacting RNA binding partners and help further characterize the $p50^{Nesp1}$ complex.

As described above, the 310067A-G (in splice acceptor site of intron 84) ARCA1 mutant would result in pre-mature termination of $p50^{Nesp1}$ and may be a possible contributor to the ataxia phenotype observed by the patient. Previously, mutations in P-body proteins have been described in neurodegenerative diseases. For example, the Huntington protein (Htt), mutated in Huntington's disease, was identified as an Argounate-2 binding protein, which localizes to, and is necessary for, the formation and function of P-bodies, as determined by siRNA knock-down of Htt and expression of dominant-negative disease-causing mutants [383]. Furthermore, ataxin-2, mutated in a related neurodegenerative disorder spinocerebellar ataxia type 2 (SCA2), interacts with the $p50^{Nesp1}$ binding partner Rck/p54 and localizes to both P-bodies and SGs [306,384]. Whether any of the ARCA1 patients, in particular 310067A-G, have defects in P-body dynamics such as assembly, motility, hindered SG connections and mRNA transfer, would provide a plausible explanation behind the disease.

6.3 Concluding remarks

In this thesis I have identified a vast range of diverse tissue specific nesprin-1 isoforms, with the majority still needing to be experimentally characterized. Although this thesis has contributed significantly to the nesprin field, there still remains a large uncertainty into the plethora of functions for nesprins as both cellular scaffolds and signalling proteins. For example, the other nesprin genes, in particular nesprins-2, are sure to have similar levels of isoform complexity and diversity to nesprin-1, suggesting much more needs to be done in understanding nesprin biology.

Bibliography

1. Rabkin SW, Tsang MY (2008) The action of nitric oxide to enhance cell survival in chick cardiomyocytes is mediated through a cGMP and ERK1/2 pathway while p38 mitogen-activated protein kinase-dependent pathways do not alter cell death. Exp Physiol 93: 834-842.
2. Coulombe PA, Wong P (2004) Cytoplasmic intermediate filaments revealed as dynamic and multipurpose scaffolds. Nat Cell Biol 6: 699-706.
3. Rodriguez OC, Schaefer AW, Mandato CA, Forscher P, Bement WM, et al. (2003) Conserved microtubule-actin interactions in cell movement and morphogenesis. Nat Cell Biol 5: 599-609.
4. Djinovic-Carugo K, Gautel M, Ylanne J, Young P (2002) The spectrin repeat: a structural platform for cytoskeletal protein assemblies. FEBS Lett 513: 119-123.
5. Warren DT, Zhang Q, Weissberg PL, Shanahan CM (2005) Nesprins: intracellular scaffolds that maintain cell architecture and coordinate cell function? Expert Rev Mol Med 7: 1-15.
6. Mellad JA, Warren DT, Shanahan CM (2011) Nesprins LINC the nucleus and cytoskeleton. Curr Opin Cell Biol 23: 47-54.
7. Youssoufian H, McAfee M, Kwiatkowski DJ (1990) Cloning and chromosomal localization of the human cytoskeletal alpha-actinin gene reveals linkage to the beta-spectrin gene. Am J Hum Genet 47: 62-72.
8. Beggs AH, Byers TJ, Knoll JH, Boyce FM, Bruns GA, et al. (1992) Cloning and characterization of two human skeletal muscle alpha-actinin genes located on chromosomes 1 and 11. J Biol Chem 267: 9281-9288.
9. Honda K, Yamada T, Endo R, Ino Y, Gotoh M, et al. (1998) Actinin-4, a novel actin-bundling protein associated with cell motility and cancer invasion. J Cell Biol 140: 1383-1393.
10. Kaplan JM, Kim SH, North KN, Rennke H, Correia LA, et al. (2000) Mutations in ACTN4, encoding alpha-actinin-4, cause familial focal segmental glomerulosclerosis. Nat Genet 24: 251-256.
11. Mohapatra B, Jimenez S, Lin JH, Bowles KR, Coveler KJ, et al. (2003) Mutations in the muscle LIM protein and alpha-actinin-2 genes in

dilated cardiomyopathy and endocardial fibroelastosis. Mol Genet Metab 80: 207-215.

12. Puckelwartz MJ, Kessler EJ, Kim G, Dewitt MM, Zhang Y, et al. (2010) Nesprin-1 mutations in human and murine cardiomyopathy. J Mol Cell Cardiol 48: 600-608.
13. Gros-Louis F, Dupre N, Dion P, Fox MA, Laurent S, et al. (2007) Mutations in SYNE1 lead to a newly discovered form of autosomal recessive cerebellar ataxia. Nat Genet 39: 80-85.
14. Zhang Q, Bethmann C, Worth NF, Davies JD, Wasner C, et al. (2007) Nesprin-1 and -2 are involved in the pathogenesis of Emery Dreifuss muscular dystrophy and are critical for nuclear envelope integrity. Hum Mol Genet 16: 2816-2833.
15. Ikeda Y, Dick KA, Weatherspoon MR, Gincel D, Armbrust KR, et al. (2006) Spectrin mutations cause spinocerebellar ataxia type 5. Nat Genet 38: 184-190.
16. Lecomte MC, Garbarz M, Grandchamp B, Feo C, Gautero H, et al. (1989) Sp alpha I/78: a mutation of the alpha I spectrin domain in a white kindred with HE and HPP phenotypes. Blood 74: 1126-1133.
17. Guetarni D, Roux AF, Alloisio N, Morle F, Ducluzeau MT, et al. (1990) Evidence that expression of Sp alpha I/65 hereditary elliptocytosis is compounded by a genetic factor that is linked to the homologous alpha-spectrin allele. Hum Genet 85: 627-630.
18. Whitfield CF, Follweiler JB, Lopresti-Morrow L, Miller BA (1991) Deficiency of alpha-spectrin synthesis in burst-forming units-erythroid in lethal hereditary spherocytosis. Blood 78: 3043-3051.
19. Basseres DS, Duarte AS, Hassoun H, Costa FF, Saad ST (2001) beta-Spectrin S(ta) Barbara: a novel frameshift mutation in hereditary spherocytosis associated with detectable levels of mRNA and a germ cell line mosaicism. Br J Haematol 115: 347-353.
20. Palek J, Liu SC, Liu PY, Prchal J, Castleberry RP (1981) Altered assembly of spectrin in red cell membranes in hereditary pyropoikilocytosis. Blood 57: 130-139.

21. Liu SC, Palek J, Prchal J, Castleberry RP (1981) Altered spectrin dimer-dimer association and instability of erythrocyte membrane skeletons in hereditary pyropoikilocytosis. J Clin Invest 68: 597-605.
22. Bonilla E, Samitt CE, Miranda AF, Hays AP, Salviati G, et al. (1988) Duchenne muscular dystrophy: deficiency of dystrophin at the muscle cell surface. Cell 54: 447-452.
23. Lewit-Bentley A, Rety S (2000) EF-hand calcium-binding proteins. Curr Opin Struct Biol 10: 637-643.
24. Kretsinger RH, Nockolds CE (1973) Carp muscle calcium-binding protein. II. Structure determination and general description. J Biol Chem 248: 3313-3326.
25. Burridge K, Nuckolls G, Otey C, Pavalko F, Simon K, et al. (1990) Actin-membrane interaction in focal adhesions. Cell Differ Dev 32: 337-342.
26. Choi CK, Vicente-Manzanares M, Zareno J, Whitmore LA, Mogilner A, et al. (2008) Actin and alpha-actinin orchestrate the assembly and maturation of nascent adhesions in a myosin II motor-independent manner. Nat Cell Biol 10: 1039-1050.
27. Schultheiss T, Choi J, Lin ZX, DiLullo C, Cohen-Gould L, et al. (1992) A sarcomeric alpha-actinin truncated at the carboxyl end induces the breakdown of stress fibers in PtK2 cells and the formation of nemaline-like bodies and breakdown of myofibrils in myotubes. Proc Natl Acad Sci U S A 89: 9282-9286.
28. Chi RJ, Simon AR, Bienkiewicz EA, Felix A, Keller TC, 3rd (2008) Smooth muscle titin Zq domain interaction with the smooth muscle alpha-actinin central rod. J Biol Chem 283: 20959-20967.
29. Byers TJ, Husain-Chishti A, Dubreuil RR, Branton D, Goldstein LS (1989) Sequence similarity of the amino-terminal domain of Drosophila beta spectrin to alpha actinin and dystrophin. J Cell Biol 109: 1633-1641.
30. Dubreuil RR, Byers TJ, Sillman AL, Bar-Zvi D, Goldstein LS, et al. (1989) The complete sequence of Drosophila alpha-spectrin: conservation of structural domains between alpha-spectrins and alpha-actinin. J Cell Biol 109: 2197-2205.
31. Viel A (1999) Alpha-actinin and spectrin structures: an unfolding family story. FEBS Lett 460: 391-394.

32. Marchesi VT, Steers E, Jr. (1968) Selective solubilization of a protein component of the red cell membrane. Science 159: 203-204.
33. Winkelmann JC, Leto TL, Watkins PC, Eddy R, Shows TB, et al. (1988) Molecular cloning of the cDNA for human erythrocyte beta-spectrin. Blood 72: 328-334.
34. Huebner K, Palumbo AP, Isobe M, Kozak CA, Monaco S, et al. (1985) The alpha-spectrin gene is on chromosome 1 in mouse and man. Proc Natl Acad Sci U S A 82: 3790-3793.
35. Stabach PR, Morrow JS (2000) Identification and characterization of beta V spectrin, a mammalian ortholog of Drosophila beta H spectrin. J Biol Chem 275: 21385-21395.
36. Stankewich MC, Tse WT, Peters LL, Ch'ng Y, John KM, et al. (1998) A widely expressed betaIII spectrin associated with Golgi and cytoplasmic vesicles. Proc Natl Acad Sci U S A 95: 14158-14163.
37. Berghs S, Aggujaro D, Dirkx R, Jr., Maksimova E, Stabach P, et al. (2000) betaIV spectrin, a new spectrin localized at axon initial segments and nodes of ranvier in the central and peripheral nervous system. J Cell Biol 151: 985-1002.
38. McMahon AP, Giebelhaus DH, Champion JE, Bailes JA, Lacey S, et al. (1987) cDNA cloning, sequencing and chromosome mapping of a non-erythroid spectrin, human alpha-fodrin. Differentiation 34: 68-78.
39. Wang DS, Shaw G (1995) The association of the C-terminal region of beta I sigma II spectrin to brain membranes is mediated by a PH domain, does not require membrane proteins, and coincides with a inositol-1,4,5 triphosphate binding site. Biochem Biophys Res Commun 217: 608-615.
40. Das A, Base C, Manna D, Cho W, Dubreuil RR (2008) Unexpected complexity in the mechanisms that target assembly of the spectrin cytoskeleton. J Biol Chem 283: 12643-12653.
41. Benz PM, Blume C, Moebius J, Oschatz C, Schuh K, et al. (2008) Cytoskeleton assembly at endothelial cell-cell contacts is regulated by alphaII-spectrin-VASP complexes. J Cell Biol 180: 205-219.

42. Nedrelow JH, Cianci CD, Morrow JS (2003) c-Src binds alpha II spectrin's Src homology 3 (SH3) domain and blocks calpain susceptibility by phosphorylating Tyr1176. J Biol Chem 278: 7735-7741.
43. Cohen CM, Foley SF (1980) Spectrin-dependent and -independent association of F-actin with the erythrocyte membrane. J Cell Biol 86: 694-698.
44. Cherry L, Menhart N, Fung LW (1999) Interactions of the alpha-spectrin N-terminal region with beta-spectrin. Implications for the spectrin tetramerization reaction. J Biol Chem 274: 2077-2084.
45. Hoffman EP, Brown RH, Jr., Kunkel LM (1987) Dystrophin: the protein product of the Duchenne muscular dystrophy locus. Cell 51: 919-928.
46. Ibraghimov-Beskrovnaya O, Ervasti JM, Leveille CJ, Slaughter CA, Sernett SW, et al. (1992) Primary structure of dystrophin-associated glycoproteins linking dystrophin to the extracellular matrix. Nature 355: 696-702.
47. Love DR, Hill DF, Dickson G, Spurr NK, Byth BC, et al. (1989) An autosomal transcript in skeletal muscle with homology to dystrophin. Nature 339: 55-58.
48. Rafael JA, Tinsley JM, Potter AC, Deconinck AE, Davies KE (1998) Skeletal muscle-specific expression of a utrophin transgene rescues utrophin-dystrophin deficient mice. Nat Genet 19: 79-82.
49. Matsumura K, Ervasti JM, Ohlendieck K, Kahl SD, Campbell KP (1992) Association of dystrophin-related protein with dystrophin-associated proteins in mdx mouse muscle. Nature 360: 588-591.
50. Broderick MJ, Winder SJ (2005) Spectrin, alpha-actinin, and dystrophin. Adv Protein Chem 70: 203-246.
51. Amann KJ, Renley BA, Ervasti JM (1998) A cluster of basic repeats in the dystrophin rod domain binds F-actin through an electrostatic interaction. J Biol Chem 273: 28419-28423.
52. Amann KJ, Guo AW, Ervasti JM (1999) Utrophin lacks the rod domain actin binding activity of dystrophin. J Biol Chem 274: 35375-35380.
53. Rybakova IN, Ervasti JM (1997) Dystrophin-glycoprotein complex is monomeric and stabilizes actin filaments in vitro through a lateral association. J Biol Chem 272: 28771-28778.

54. Ruhrberg C, Watt FM (1997) The plakin family: versatile organizers of cytoskeletal architecture. Curr Opin Genet Dev 7: 392-397.
55. Koster J, Geerts D, Favre B, Borradori L, Sonnenberg A (2003) Analysis of the interactions between BP180, BP230, plectin and the integrin alpha6beta4 important for hemidesmosome assembly. J Cell Sci 116: 387-399.
56. Koster J, van Wilpe S, Kuikman I, Litjens SH, Sonnenberg A (2004) Role of binding of plectin to the integrin beta4 subunit in the assembly of hemidesmosomes. Mol Biol Cell 15: 1211-1223.
57. Jefferson JJ, Ciatto C, Shapiro L, Liem RK (2007) Structural analysis of the plakin domain of bullous pemphigoid antigen1 (BPAG1) suggests that plakins are members of the spectrin superfamily. J Mol Biol 366: 244-257.
58. Sonnenberg A, Liem RK (2007) Plakins in development and disease. Exp Cell Res 313: 2189-2203.
59. Leung CL, Sun D, Liem RK (1999) The intermediate filament protein peripherin is the specific interaction partner of mouse BPAG1-n (dystonin) in neurons. J Cell Biol 144: 435-446.
60. Choi HJ, Park-Snyder S, Pascoe LT, Green KJ, Weis WI (2002) Structures of two intermediate filament-binding fragments of desmoplakin reveal a unique repeat motif structure. Nat Struct Biol 9: 612-620.
61. Nikolic B, Mac Nulty E, Mir B, Wiche G (1996) Basic amino acid residue cluster within nuclear targeting sequence motif is essential for cytoplasmic plectin-vimentin network junctions. J Cell Biol 134: 1455-1467.
62. Meng JJ, Bornslaeger EA, Green KJ, Steinert PM, Ip W (1997) Two-hybrid analysis reveals fundamental differences in direct interactions between desmoplakin and cell type-specific intermediate filaments. J Biol Chem 272: 21495-21503.
63. Leung CL, Sun D, Zheng M, Knowles DR, Liem RK (1999) Microtubule actin cross-linking factor (MACF): a hybrid of dystonin and dystrophin that can interact with the actin and microtubule cytoskeletons. J Cell Biol 147: 1275-1286.

64. Sun D, Leung CL, Liem RK (2001) Characterization of the microtubule binding domain of microtubule actin crosslinking factor (MACF): identification of a novel group of microtubule associated proteins. J Cell Sci 114: 161-172.

65. Slep KC, Rogers SL, Elliott SL, Ohkura H, Kolodziej PA, et al. (2005) Structural determinants for EB1-mediated recruitment of APC and spectraplakins to the microtubule plus end. J Cell Biol 168: 587-598.

66. Zhang Q, Skepper JN, Yang F, Davies JD, Hegyi L, et al. (2001) Nesprins: a novel family of spectrin-repeat-containing proteins that localize to the nuclear membrane in multiple tissues. J Cell Sci 114: 4485-4498.

67. Zhang Q, Ragnauth C, Greener MJ, Shanahan CM, Roberts RG (2002) The nesprins are giant actin-binding proteins, orthologous to Drosophila melanogaster muscle protein MSP-300. Genomics 80: 473-481.

68. Wilhelmsen K, Litjens SH, Kuikman I, Tshimbalanga N, Janssen H, et al. (2005) Nesprin-3, a novel outer nuclear membrane protein, associates with the cytoskeletal linker protein plectin. J Cell Biol 171: 799-810.

69. Roux KJ, Crisp ML, Liu Q, Kim D, Kozlov S, et al. (2009) Nesprin 4 is an outer nuclear membrane protein that can induce kinesin-mediated cell polarization. Proc Natl Acad Sci U S A 106: 2194-2199.

70. Castresana J, Saraste M (1995) Does Vav bind to F-actin through a CH domain? FEBS Lett 374: 149-151.

71. Gimona M, Djinovic-Carugo K, Kranewitter WJ, Winder SJ (2002) Functional plasticity of CH domains. FEBS Lett 513: 98-106.

72. Winder SJ, Hemmings L, Maciver SK, Bolton SJ, Tinsley JM, et al. (1995) Utrophin actin binding domain: analysis of actin binding and cellular targeting. J Cell Sci 108 (Pt 1): 63-71.

73. Fukami K, Sawada N, Endo T, Takenawa T (1996) Identification of a phosphatidylinositol 4,5-bisphosphate-binding site in chicken skeletal muscle alpha-actinin. J Biol Chem 271: 2646-2650.

74. Foisner R, Feldman B, Sander L, Wiche G (1991) Monoclonal antibody mapping of structural and functional plectin epitopes. J Cell Biol 112: 397-405.

75. Bonet-Kerrache A, Fabbrizio E, Mornet D (1994) N-terminal domain of dystrophin. FEBS Lett 355: 49-53.
76. Mejean C, Lebart MC, Roustan C, Benyamin Y (1995) Inhibition of actin-dystrophin interaction by inositide phosphate. Biochem Biophys Res Commun 210: 152-158.
77. Winder SJ, Kendrick-Jones J (1995) Calcium/calmodulin-dependent regulation of the NH2-terminal F-actin binding domain of utrophin. FEBS Lett 357: 125-128.
78. Simpson JG, Roberts RG (2008) Patterns of evolutionary conservation in the nesprin genes highlight probable functionally important protein domains and isoforms. Biochem Soc Trans 36: 1359-1367.
79. Smith FJ, Eady RA, Leigh IM, McMillan JR, Rugg EL, et al. (1996) Plectin deficiency results in muscular dystrophy with epidermolysis bullosa. Nat Genet 13: 450-457.
80. Postel R, Ketema M, Kuikman I, de Pereda JM, Sonnenberg A (2011) Nesprin-3 augments peripheral nuclear localization of intermediate filaments in zebrafish. J Cell Sci 124: 755-764.
81. Young KG, Kothary R (2008) Dystonin/Bpag1 is a necessary endoplasmic reticulum/nuclear envelope protein in sensory neurons. Exp Cell Res 314: 2750-2761.
82. Fan J, Beck KA (2004) A role for the spectrin superfamily member Syne-1 and kinesin II in cytokinesis. J Cell Sci 117: 619-629.
83. Zhang X, Lei K, Yuan X, Wu X, Zhuang Y, et al. (2009) SUN1/2 and Syne/Nesprin-1/2 complexes connect centrosome to the nucleus during neurogenesis and neuronal migration in mice. Neuron 64: 173-187.
84. Speicher DW, Marchesi VT (1984) Erythrocyte spectrin is comprised of many homologous triple helical segments. Nature 311: 177-180.
85. Baron MD, Davison MD, Jones P, Critchley DR (1987) The sequence of chick alpha-actinin reveals homologies to spectrin and calmodulin. J Biol Chem 262: 17623-17629.
86. Darras BT, Koenig M, Kunkel LM, Francke U (1988) Direct method for prenatal diagnosis and carrier detection in Duchenne/Becker muscular

dystrophy using the entire dystrophin cDNA. Am J Med Genet 29: 713-726.

87. Koenig M, Monaco AP, Kunkel LM (1988) The complete sequence of dystrophin predicts a rod-shaped cytoskeletal protein. Cell 53: 219-228.
88. Liu J, Zheng Q, Deng Y, Cheng CS, Kallenbach NR, et al. (2006) A seven-helix coiled coil. Proc Natl Acad Sci U S A 103: 15457-15462.
89. Parry DA, Dixon TW, Cohen C (1992) Analysis of the three-alpha-helix motif in the spectrin superfamily of proteins. Biophys J 61: 858-867.
90. Harper SQ, Crawford RW, DelloRusso C, Chamberlain JS (2002) Spectrin-like repeats from dystrophin and alpha-actinin-2 are not functionally interchangeable. Hum Mol Genet 11: 1807-1815.
91. Kapiloff MS, Schillace RV, Westphal AM, Scott JD (1999) mAKAP: an A-kinase anchoring protein targeted to the nuclear membrane of differentiated myocytes. J Cell Sci 112 (Pt 16): 2725-2736.
92. Soukoulis V, Reddy S, Pooley RD, Feng Y, Walsh CA, et al. (2005) Cytoplasmic LEK1 is a regulator of microtubule function through its interaction with the LIS1 pathway. Proc Natl Acad Sci U S A 102: 8549-8554.
93. Devarajan P, Stabach PR, Mann AS, Ardito T, Kashgarian M, et al. (1996) Identification of a small cytoplasmic ankyrin (AnkG119) in the kidney and muscle that binds beta I sigma spectrin and associates with the Golgi apparatus. J Cell Biol 133: 819-830.
94. Starr DA, Fischer JA (2005) KASH 'n Karry: the KASH domain family of cargo-specific cytoskeletal adaptor proteins. Bioessays 27: 1136-1146.
95. McGee MD, Rillo R, Anderson AS, Starr DA (2006) UNC-83 IS a KASH protein required for nuclear migration and is recruited to the outer nuclear membrane by a physical interaction with the SUN protein UNC-84. Mol Biol Cell 17: 1790-1801.
96. Stewart-Hutchinson PJ, Hale CM, Wirtz D, Hodzic D (2008) Structural requirements for the assembly of LINC complexes and their function in cellular mechanical stiffness. Exp Cell Res 314: 1892-1905.
97. Crisp M, Liu Q, Roux K, Rattner JB, Shanahan C, et al. (2006) Coupling of the nucleus and cytoplasm: role of the LINC complex. J Cell Biol 172: 41-53.

98. Hetzer MW (2010) The nuclear envelope. Cold Spring Harb Perspect Biol 2: a000539.
99. Kandert S, Luke Y, Kleinhenz T, Neumann S, Lu W, et al. (2007) Nesprin-2 giant safeguards nuclear envelope architecture in LMNA S143F progeria cells. Hum Mol Genet 16: 2944-2959.
100. Mekhail K, Moazed D (2010) The nuclear envelope in genome organization, expression and stability. Nat Rev Mol Cell Biol 11: 317-328.
101. Gerace L, Huber MD (2012) Nuclear lamina at the crossroads of the cytoplasm and nucleus. J Struct Biol 177: 24-31.
102. Grunwald D, Singer RH (2012) Multiscale dynamics in nucleocytoplasmic transport. Curr Opin Cell Biol 24: 100-106.
103. Gruenbaum Y, Margalit A, Goldman RD, Shumaker DK, Wilson KL (2005) The nuclear lamina comes of age. Nat Rev Mol Cell Biol 6: 21-31.
104. Holmer L, Worman HJ (2001) Inner nuclear membrane proteins: functions and targeting. Cell Mol Life Sci 58: 1741-1747.
105. Chu A, Rassadi R, Stochaj U (1998) Velcro in the nuclear envelope: LBR and LAPs. FEBS Lett 441: 165-169.
106. Schirmer EC, Florens L, Guan T, Yates JR, 3rd, Gerace L (2003) Nuclear membrane proteins with potential disease links found by subtractive proteomics. Science 301: 1380-1382.
107. Korfali N, Wilkie GS, Swanson SK, Srsen V, de Las Heras J, et al. (2012) The nuclear envelope proteome differs notably between tissues. Nucleus 3: 552-564.
108. Fisher DZ, Chaudhary N, Blobel G (1986) cDNA sequencing of nuclear lamins A and C reveals primary and secondary structural homology to intermediate filament proteins. Proc Natl Acad Sci U S A 83: 6450-6454.
109. Aebi U, Cohn J, Buhle L, Gerace L (1986) The nuclear lamina is a meshwork of intermediate-type filaments. Nature 323: 560-564.
110. Machiels BM, Zorenc AH, Endert JM, Kuijpers HJ, van Eys GJ, et al. (1996) An alternative splicing product of the lamin A/C gene lacks exon 10. J Biol Chem 271: 9249-9253.

111. Lin F, Worman HJ (1993) Structural organization of the human gene encoding nuclear lamin A and nuclear lamin C. J Biol Chem 268: 16321-16326.
112. Weber K, Plessmann U, Traub P (1990) Protein chemical analysis of purified murine lamin B identifies two distinct polypeptides B1 and B2. FEBS Lett 261: 361-364.
113. Maison C, Pyrpasopoulou A, Theodoropoulos PA, Georgatos SD (1997) The inner nuclear membrane protein LAP1 forms a native complex with B-type lamins and partitions with spindle-associated mitotic vesicles. EMBO J 16: 4839-4850.
114. Dechat T, Korbei B, Vaughan OA, Vlcek S, Hutchison CJ, et al. (2000) Lamina-associated polypeptide 2alpha binds intranuclear A-type lamins. J Cell Sci 113 Pt 19: 3473-3484.
115. Lin F, Morrison JM, Wu W, Worman HJ (2005) MAN1, an integral protein of the inner nuclear membrane, binds Smad2 and Smad3 and antagonizes transforming growth factor-beta signaling. Hum Mol Genet 14: 437-445.
116. Goldman RD, Gruenbaum Y, Moir RD, Shumaker DK, Spann TP (2002) Nuclear lamins: building blocks of nuclear architecture. Genes Dev 16: 533-547.
117. Vergnes L, Peterfy M, Bergo MO, Young SG, Reue K (2004) Lamin B1 is required for mouse development and nuclear integrity. Proc Natl Acad Sci U S A 101: 10428-10433.
118. Coffinier C, Chang SY, Nobumori C, Tu Y, Farber EA, et al. (2010) Abnormal development of the cerebral cortex and cerebellum in the setting of lamin B2 deficiency. Proc Natl Acad Sci U S A 107: 5076-5081.
119. Dechat T, Pfleghaar K, Sengupta K, Shimi T, Shumaker DK, et al. (2008) Nuclear lamins: major factors in the structural organization and function of the nucleus and chromatin. Genes Dev 22: 832-853.
120. Stewart C, Burke B (1987) Teratocarcinoma stem cells and early mouse embryos contain only a single major lamin polypeptide closely resembling lamin B. Cell 51: 383-392.

121. Rober RA, Weber K, Osborn M (1989) Differential timing of nuclear lamin A/C expression in the various organs of the mouse embryo and the young animal: a developmental study. Development 105: 365-378.
122. Sullivan T, Escalante-Alcalde D, Bhatt H, Anver M, Bhat N, et al. (1999) Loss of A-type lamin expression compromises nuclear envelope integrity leading to muscular dystrophy. J Cell Biol 147: 913-920.
123. Nikolova V, Leimena C, McMahon AC, Tan JC, Chandar S, et al. (2004) Defects in nuclear structure and function promote dilated cardiomyopathy in lamin A/C-deficient mice. J Clin Invest 113: 357-369.
124. Sinensky M, Fantle K, Trujillo M, McLain T, Kupfer A, et al. (1994) The processing pathway of prelamin A. J Cell Sci 107 (Pt 1): 61-67.
125. Ragnauth CD, Warren DT, Liu Y, McNair R, Tajsic T, et al. (2010) Prelamin A acts to accelerate smooth muscle cell senescence and is a novel biomarker of human vascular aging. Circulation 121: 2200-2210.
126. Goldman RD, Shumaker DK, Erdos MR, Eriksson M, Goldman AE, et al. (2004) Accumulation of mutant lamin A causes progressive changes in nuclear architecture in Hutchinson-Gilford progeria syndrome. Proc Natl Acad Sci U S A 101: 8963-8968.
127. Bridger JM, Kill IR (2004) Aging of Hutchinson-Gilford progeria syndrome fibroblasts is characterised by hyperproliferation and increased apoptosis. Exp Gerontol 39: 717-724.
128. Scaffidi P, Misteli T (2006) Lamin A-dependent nuclear defects in human aging. Science 312: 1059-1063.
129. Liu B, Wang J, Chan KM, Tjia WM, Deng W, et al. (2005) Genomic instability in laminopathy-based premature aging. Nat Med 11: 780-785.
130. Goldberg M, Harel A, Brandeis M, Rechsteiner T, Richmond TJ, et al. (1999) The tail domain of lamin Dm0 binds histones H2A and H2B. Proc Natl Acad Sci U S A 96: 2852-2857.
131. Martins SB, Eide T, Steen RL, Jahnsen T, Skalhegg BS, et al. (2000) HA95 is a protein of the chromatin and nuclear matrix regulating nuclear envelope dynamics. J Cell Sci 113 Pt 21: 3703-3713.
132. Lee KK, Haraguchi T, Lee RS, Koujin T, Hiraoka Y, et al. (2001) Distinct functional domains in emerin bind lamin A and DNA-bridging protein BAF. J Cell Sci 114: 4567-4573.

133. Lattanzi G, Columbaro M, Mattioli E, Cenni V, Camozzi D, et al. (2007) Pre-Lamin A processing is linked to heterochromatin organization. J Cell Biochem 102: 1149-1159.
134. Moir RD, Spann TP, Herrmann H, Goldman RD (2000) Disruption of nuclear lamin organization blocks the elongation phase of DNA replication. J Cell Biol 149: 1179-1192.
135. Maraldi NM, Lattanzi G (2005) Linkage of lamins to fidelity of gene transcription. Crit Rev Eukaryot Gene Expr 15: 277-294.
136. Markiewicz E, Dechat T, Foisner R, Quinlan RA, Hutchison CJ (2002) Lamin A/C binding protein LAP2alpha is required for nuclear anchorage of retinoblastoma protein. Mol Biol Cell 13: 4401-4413.
137. Dorner D, Vlcek S, Foeger N, Gajewski A, Makolm C, et al. (2006) Lamina-associated polypeptide 2alpha regulates cell cycle progression and differentiation via the retinoblastoma-E2F pathway. J Cell Biol 173: 83-93.
138. Mariappan I, Gurung R, Thanumalayan S, Parnaik VK (2007) Identification of cyclin D3 as a new interaction partner of lamin A/C. Biochem Biophys Res Commun 355: 981-985.
139. Heessen S, Fornerod M (2007) The inner nuclear envelope as a transcription factor resting place. EMBO Rep 8: 914-919.
140. Ivorra C, Kubicek M, Gonzalez JM, Sanz-Gonzalez SM, Alvarez-Barrientos A, et al. (2006) A mechanism of AP-1 suppression through interaction of c-Fos with lamin A/C. Genes Dev 20: 307-320.
141. Capanni C, Mattioli E, Columbaro M, Lucarelli E, Parnaik VK, et al. (2005) Altered pre-lamin A processing is a common mechanism leading to lipodystrophy. Hum Mol Genet 14: 1489-1502.
142. Van Berlo JH, Voncken JW, Kubben N, Broers JL, Duisters R, et al. (2005) A-type lamins are essential for TGF-beta1 induced PP2A to dephosphorylate transcription factors. Hum Mol Genet 14: 2839-2849.
143. Pan D, Estevez-Salmeron LD, Stroschein SL, Zhu X, He J, et al. (2005) The integral inner nuclear membrane protein MAN1 physically interacts with the R-Smad proteins to repress signaling by the transforming growth factor-{beta} superfamily of cytokines. J Biol Chem 280: 15992-16001.

144. Frock RL, Kudlow BA, Evans AM, Jameson SA, Hauschka SD, et al. (2006) Lamin A/C and emerin are critical for skeletal muscle satellite cell differentiation. Genes Dev 20: 486-500.
145. Varela I, Cadinanos J, Pendas AM, Gutierrez-Fernandez A, Folgueras AR, et al. (2005) Accelerated ageing in mice deficient in Zmpste24 protease is linked to p53 signalling activation. Nature 437: 564-568.
146. Maraldi NM, Capanni C, Cenni V, Fini M, Lattanzi G (2011) Laminopathies and lamin-associated signaling pathways. J Cell Biochem 112: 979-992.
147. Andres V, Gonzalez JM (2009) Role of A-type lamins in signaling, transcription, and chromatin organization. J Cell Biol 187: 945-957.
148. Lammerding J, Lee RT (2005) The nuclear membrane and mechanotransduction: impaired nuclear mechanics and mechanotransduction in lamin A/C deficient cells. Novartis Found Symp 264: 264-273; discussion 273-268.
149. Broers JL, Kuijpers HJ, Ostlund C, Worman HJ, Endert J, et al. (2005) Both lamin A and lamin C mutations cause lamina instability as well as loss of internal nuclear lamin organization. Exp Cell Res 304: 582-592.
150. Broers JL, Peeters EA, Kuijpers HJ, Endert J, Bouten CV, et al. (2004) Decreased mechanical stiffness in LMNA-/- cells is caused by defective nucleo-cytoskeletal integrity: implications for the development of laminopathies. Hum Mol Genet 13: 2567-2580.
151. Lammerding J, Kamm RD, Lee RT (2004) Mechanotransduction in cardiac myocytes. Ann N Y Acad Sci 1015: 53-70.
152. Lammerding J, Schulze PC, Takahashi T, Kozlov S, Sullivan T, et al. (2004) Lamin A/C deficiency causes defective nuclear mechanics and mechanotransduction. J Clin Invest 113: 370-378.
153. Lammerding J, Hsiao J, Schulze PC, Kozlov S, Stewart CL, et al. (2005) Abnormal nuclear shape and impaired mechanotransduction in emerin-deficient cells. J Cell Biol 170: 781-791.
154. Haque F, Lloyd DJ, Smallwood DT, Dent CL, Shanahan CM, et al. (2006) SUN1 interacts with nuclear lamin A and cytoplasmic nesprins to provide a physical connection between the nuclear lamina and the cytoskeleton. Mol Cell Biol 26: 3738-3751.

155. Zhou Z, Du X, Cai Z, Song X, Zhang H, et al. (2012) Structure of Sad1-UNC84 homology (SUN) domain defines features of molecular bridge in nuclear envelope. J Biol Chem 287: 5317-5326.
156. Chen L, Lee L, Kudlow BA, Dos Santos HG, Sletvold O, et al. (2003) LMNA mutations in atypical Werner's syndrome. Lancet 362: 440-445.
157. De Sandre-Giovannoli A, Chaouch M, Kozlov S, Vallat JM, Tazir M, et al. (2002) Homozygous defects in LMNA, encoding lamin A/C nuclear-envelope proteins, cause autosomal recessive axonal neuropathy in human (Charcot-Marie-Tooth disorder type 2) and mouse. Am J Hum Genet 70: 726-736.
158. Fatkin D, MacRae C, Sasaki T, Wolff MR, Porcu M, et al. (1999) Missense mutations in the rod domain of the lamin A/C gene as causes of dilated cardiomyopathy and conduction-system disease. N Engl J Med 341: 1715-1724.
159. Puckelwartz MJ, Kessler E, Zhang Y, Hodzic D, Randles KN, et al. (2009) Disruption of nesprin-1 produces an Emery Dreifuss muscular dystrophy-like phenotype in mice. Hum Mol Genet 18: 607-620.
160. Helbling-Leclerc A, Bonne G, Schwartz K (2002) Emery-Dreifuss muscular dystrophy. Eur J Hum Genet 10: 157-161.
161. Raffaele Di Barletta M, Ricci E, Galluzzi G, Tonali P, Mora M, et al. (2000) Different mutations in the LMNA gene cause autosomal dominant and autosomal recessive Emery-Dreifuss muscular dystrophy. Am J Hum Genet 66: 1407-1412.
162. Eriksson M, Brown WT, Gordon LB, Glynn MW, Singer J, et al. (2003) Recurrent de novo point mutations in lamin A cause Hutchinson-Gilford progeria syndrome. Nature 423: 293-298.
163. Hegele RA, Cao H, Frankowski C, Mathews ST, Leff T (2002) PPARG F388L, a transactivation-deficient mutant, in familial partial lipodystrophy. Diabetes 51: 3586-3590.
164. Bushby K (2009) Diagnosis and management of the limb girdle muscular dystrophies. Pract Neurol 9: 314-323.
165. Navarro CL, De Sandre-Giovannoli A, Bernard R, Boccaccio I, Boyer A, et al. (2004) Lamin A and ZMPSTE24 (FACE-1) defects cause nuclear

disorganization and identify restrictive dermopathy as a lethal neonatal laminopathy. Hum Mol Genet 13: 2493-2503.

166. Padiath QS, Saigoh K, Schiffmann R, Asahara H, Yamada T, et al. (2006) Lamin B1 duplications cause autosomal dominant leukodystrophy. Nat Genet 38: 1114-1123.

167. Hegele RA, Cao H, Liu DM, Costain GA, Charlton-Menys V, et al. (2006) Sequencing of the reannotated LMNB2 gene reveals novel mutations in patients with acquired partial lipodystrophy. Am J Hum Genet 79: 383-389.

168. Waterham HR, Koster J, Mooyer P, Noort Gv G, Kelley RI, et al. (2003) Autosomal recessive HEM/Greenberg skeletal dysplasia is caused by 3 beta-hydroxysterol delta 14-reductase deficiency due to mutations in the lamin B receptor gene. Am J Hum Genet 72: 1013-1017.

169. Mislow JM, Holaska JM, Kim MS, Lee KK, Segura-Totten M, et al. (2002) Nesprin-1alpha self-associates and binds directly to emerin and lamin A in vitro. FEBS Lett 525: 135-140.

170. Wheeler MA, Davies JD, Zhang Q, Emerson LJ, Hunt J, et al. (2007) Distinct functional domains in nesprin-1alpha and nesprin-2beta bind directly to emerin and both interactions are disrupted in X-linked Emery-Dreifuss muscular dystrophy. Exp Cell Res 313: 2845-2857.

171. Malone CJ, Misner L, Le Bot N, Tsai MC, Campbell JM, et al. (2003) The C. elegans hook protein, ZYG-12, mediates the essential attachment between the centrosome and nucleus. Cell 115: 825-836.

172. King MC, Lusk CP, Blobel G (2006) Karyopherin-mediated import of integral inner nuclear membrane proteins. Nature 442: 1003-1007.

173. Malone CJ, Fixsen WD, Horvitz HR, Han M (1999) UNC-84 localizes to the nuclear envelope and is required for nuclear migration and anchoring during C. elegans development. Development 126: 3171-3181.

174. Kracklauer MP, Banks SM, Xie X, Wu Y, Fischer JA (2007) Drosophila klaroid encodes a SUN domain protein required for Klarsicht localization to the nuclear envelope and nuclear migration in the eye. Fly (Austin) 1: 75-85.

175. Tsujikawa M, Omori Y, Biyanwila J, Malicki J (2007) Mechanism of positioning the cell nucleus in vertebrate photoreceptors. Proc Natl Acad Sci U S A 104: 14819-14824.
176. Wang N, Tytell JD, Ingber DE (2009) Mechanotransduction at a distance: mechanically coupling the extracellular matrix with the nucleus. Nat Rev Mol Cell Biol 10: 75-82.
177. Zhang J, Felder A, Liu Y, Guo LT, Lange S, et al. (2010) Nesprin 1 is critical for nuclear positioning and anchorage. Hum Mol Genet 19: 329-341.
178. Khatau SB, Hale CM, Stewart-Hutchinson PJ, Patel MS, Stewart CL, et al. (2009) A perinuclear actin cap regulates nuclear shape. Proc Natl Acad Sci U S A 106: 19017-19022.
179. Lu W, Schneider M, Neumann S, Jaeger VM, Taranum S, et al. (2012) Nesprin interchain associations control nuclear size. Cell Mol Life Sci.
180. Ketema M, Sonnenberg A (2011) Nesprin-3: a versatile connector between the nucleus and the cytoskeleton. Biochem Soc Trans 39: 1719-1724.
181. Verstraeten VL, Renes J, Ramaekers FC, Kamps M, Kuijpers HJ, et al. (2011) Reorganization of the nuclear lamina and cytoskeleton in adipogenesis. Histochem Cell Biol 135: 251-261.
182. Ketema M, Wilhelmsen K, Kuikman I, Janssen H, Hodzic D, et al. (2007) Requirements for the localization of nesprin-3 at the nuclear envelope and its interaction with plectin. J Cell Sci 120: 3384-3394.
183. Morgan JT, Pfeiffer ER, Thirkill TL, Kumar P, Peng G, et al. (2011) Nesprin-3 regulates endothelial cell morphology, perinuclear cytoskeletal architecture, and flow-induced polarization. Mol Biol Cell 22: 4324-4334.
184. Vander Heyden AB, Naismith TV, Snapp EL, Hodzic D, Hanson PI (2009) LULL1 retargets TorsinA to the nuclear envelope revealing an activity that is impaired by the DYT1 dystonia mutation. Mol Biol Cell 20: 2661-2672.
185. Randles KN, Lam le T, Sewry CA, Puckelwartz M, Furling D, et al. (2010) Nesprins, but not sun proteins, switch isoforms at the nuclear envelope during muscle development. Dev Dyn 239: 998-1009.

186. Starr DA, Han M (2002) Role of ANC-1 in tethering nuclei to the actin cytoskeleton. Science 298: 406-409.
187. Lee KK, Starr D, Cohen M, Liu J, Han M, et al. (2002) Lamin-dependent localization of UNC-84, a protein required for nuclear migration in Caenorhabditis elegans. Mol Biol Cell 13: 892-901.
188. Zhang X, Xu R, Zhu B, Yang X, Ding X, et al. (2007) Syne-1 and Syne-2 play crucial roles in myonuclear anchorage and motor neuron innervation. Development 134: 901-908.
189. Hale CM, Shrestha AL, Khatau SB, Stewart-Hutchinson PJ, Hernandez L, et al. (2008) Dysfunctional connections between the nucleus and the actin and microtubule networks in laminopathic models. Biophys J 95: 5462-5475.
190. Salpingidou G, Smertenko A, Hausmanowa-Petrucewicz I, Hussey PJ, Hutchison CJ (2007) A novel role for the nuclear membrane protein emerin in association of the centrosome to the outer nuclear membrane. J Cell Biol 178: 897-904.
191. Dawe HR, Adams M, Wheway G, Szymanska K, Logan CV, et al. (2009) Nesprin-2 interacts with meckelin and mediates ciliogenesis via remodelling of the actin cytoskeleton. J Cell Sci 122: 2716-2726.
192. Lee SE, Kim JH, Kim NH (2007) Inactivation of MAPK affects centrosome assembly, but not actin filament assembly, in mouse oocytes maturing in vitro. Mol Reprod Dev 74: 904-911.
193. Chancellor TJ, Lee J, Thodeti CK, Lele T (2010) Actomyosin tension exerted on the nucleus through nesprin-1 connections influences endothelial cell adhesion, migration, and cyclic strain-induced reorientation. Biophys J 99: 115-123.
194. Guilak F, Tedrow JR, Burgkart R (2000) Viscoelastic properties of the cell nucleus. Biochem Biophys Res Commun 269: 781-786.
195. Caille N, Thoumine O, Tardy Y, Meister JJ (2002) Contribution of the nucleus to the mechanical properties of endothelial cells. J Biomech 35: 177-187.
196. Anno T, Sakamoto N, Sato M (2012) Role of nesprin-1 in nuclear deformation in endothelial cells under static and uniaxial stretching conditions. Biochem Biophys Res Commun 424: 94-99.

197. Lombardi ML, Jaalouk DE, Shanahan CM, Burke B, Roux KJ, et al. (2011) The interaction between nesprins and sun proteins at the nuclear envelope is critical for force transmission between the nucleus and cytoskeleton. J Biol Chem 286: 26743-26753.
198. Perry RL, Rudnick MA (2000) Molecular mechanisms regulating myogenic determination and differentiation. Front Biosci 5: D750-767.
199. Berkes CA, Tapscott SJ (2005) MyoD and the transcriptional control of myogenesis. Semin Cell Dev Biol 16: 585-595.
200. Brosig M, Ferralli J, Gelman L, Chiquet M, Chiquet-Ehrismann R (2010) Interfering with the connection between the nucleus and the cytoskeleton affects nuclear rotation, mechanotransduction and myogenesis. Int J Biochem Cell Biol 42: 1717-1728.
201. Attali R, Warwar N, Israel A, Gurt I, McNally E, et al. (2009) Mutation of SYNE-1, encoding an essential component of the nuclear lamina, is responsible for autosomal recessive arthrogryposis. Hum Mol Genet 18: 3462-3469.
202. Green EK, Grozeva D, Forty L, Gordon-Smith K, Russell E, et al. (2012) Association at SYNE1 in both bipolar disorder and recurrent major depression. Mol Psychiatry.
203. Taranum S, Vaylann E, Meinke P, Abraham S, Yang L, et al. (2012) LINC complex alterations in DMD and EDMD/CMT fibroblasts. Eur J Cell Biol 91: 614-628.
204. Emery AE (1989) Emery-Dreifuss syndrome. J Med Genet 26: 637-641.
205. Rankin J, Ellard S (2006) The laminopathies: a clinical review. Clin Genet 70: 261-274.
206. Zhang Q, Ragnauth CD, Skepper JN, Worth NF, Warren DT, et al. (2005) Nesprin-2 is a multi-isomeric protein that binds lamin and emerin at the nuclear envelope and forms a subcellular network in skeletal muscle. J Cell Sci 118: 673-687.
207. Warren DT, Tajsic T, Mellad JA, Searles R, Zhang Q, et al. (2010) Novel nuclear nesprin-2 variants tether active extracellular signal-regulated MAPK1 and MAPK2 at promyelocytic leukemia protein nuclear bodies and act to regulate smooth muscle cell proliferation. J Biol Chem 285: 1311-1320.

208. Kobayashi Y, Katanosaka Y, Iwata Y, Matsuoka M, Shigekawa M, et al. (2006) Identification and characterization of GSRP-56, a novel Golgi-localized spectrin repeat-containing protein. Exp Cell Res 312: 3152-3164.

209. Mislow JM, Kim MS, Davis DB, McNally EM (2002) Myne-1, a spectrin repeat transmembrane protein of the myocyte inner nuclear membrane, interacts with lamin A/C. J Cell Sci 115: 61-70.

210. Pare GC, Easlick JL, Mislow JM, McNally EM, Kapiloff MS (2005) Nesprin-1alpha contributes to the targeting of mAKAP to the cardiac myocyte nuclear envelope. Exp Cell Res 303: 388-399.

211. Dodge-Kafka KL, Soughayer J, Pare GC, Carlisle Michel JJ, Langeberg LK, et al. (2005) The protein kinase A anchoring protein mAKAP coordinates two integrated cAMP effector pathways. Nature 437: 574-578.

212. Pare GC, Bauman AL, McHenry M, Michel JJ, Dodge-Kafka KL, et al. (2005) The mAKAP complex participates in the induction of cardiac myocyte hypertrophy by adrenergic receptor signaling. J Cell Sci 118: 5637-5646.

213. Dodge KL, Khouangsathiene S, Kapiloff MS, Mouton R, Hill EV, et al. (2001) mAKAP assembles a protein kinase A/PDE4 phosphodiesterase cAMP signaling module. EMBO J 20: 1921-1930.

214. Priori SG, Napolitano C, Tiso N, Memmi M, Vignati G, et al. (2001) Mutations in the cardiac ryanodine receptor gene (hRyR2) underlie catecholaminergic polymorphic ventricular tachycardia. Circulation 103: 196-200.

215. Apel ED, Lewis RM, Grady RM, Sanes JR (2000) Syne-1, a dystrophin- and Klarsicht-related protein associated with synaptic nuclei at the neuromuscular junction. J Biol Chem 275: 31986-31995.

216. Luo ZG, Wang Q, Zhou JZ, Wang J, Luo Z, et al. (2002) Regulation of AChR clustering by Dishevelled interacting with MuSK and PAK1. Neuron 35: 489-505.

217. Okada K, Inoue A, Okada M, Murata Y, Kakuta S, et al. (2006) The muscle protein Dok-7 is essential for neuromuscular synaptogenesis. Science 312: 1802-1805.

218. Grady RM, Starr DA, Ackerman GL, Sanes JR, Han M (2005) Syne proteins anchor muscle nuclei at the neuromuscular junction. Proc Natl Acad Sci U S A 102: 4359-4364.

219. DeChiara TM, Bowen DC, Valenzuela DM, Simmons MV, Poueymirou WT, et al. (1996) The receptor tyrosine kinase MuSK is required for neuromuscular junction formation in vivo. Cell 85: 501-512.

220. Nedivi E, Hevroni D, Naot D, Israeli D, Citri Y (1993) Numerous candidate plasticity-related genes revealed by differential cDNA cloning. Nature 363: 718-722.

221. Nedivi E, Fieldust S, Theill LE, Hevron D (1996) A set of genes expressed in response to light in the adult cerebral cortex and regulated during development. Proc Natl Acad Sci U S A 93: 2048-2053.

222. Cottrell JR, Borok E, Horvath TL, Nedivi E (2004) CPG2: a brain- and synapse-specific protein that regulates the endocytosis of glutamate receptors. Neuron 44: 677-690.

223. Gough LL, Fan J, Chu S, Winnick S, Beck KA (2003) Golgi localization of Syne-1. Mol Biol Cell 14: 2410-2424.

224. Gough LL, Beck KA (2004) The spectrin family member Syne-1 functions in retrograde transport from Golgi to ER. Biochim Biophys Acta 1693: 29-36.

225. Aridor M, Bannykh SI, Rowe T, Balch WE (1995) Sequential coupling between COPII and COPI vesicle coats in endoplasmic reticulum to Golgi transport. J Cell Biol 131: 875-893.

226. Haraguchi K, Hayashi T, Jimbo T, Yamamoto T, Akiyama T (2006) Role of the kinesin-2 family protein, KIF3, during mitosis. J Biol Chem 281: 4094-4099.

227. Yamazaki H, Nakata T, Okada Y, Hirokawa N (1995) KIF3A/B: a heterodimeric kinesin superfamily protein that works as a microtubule plus end-directed motor for membrane organelle transport. J Cell Biol 130: 1387-1399.

228. Chan TA, Glockner S, Yi JM, Chen W, Van Neste L, et al. (2008) Convergence of mutation and epigenetic alterations identifies common genes in cancer that predict for poor prognosis. PLoS Med 5: e114.

229. Schuebel KE, Chen W, Cope L, Glockner SC, Suzuki H, et al. (2007) Comparing the DNA hypermethylome with gene mutations in human colorectal cancer. PLoS Genet 3: 1709-1723.
230. Sjoblom T, Jones S, Wood LD, Parsons DW, Lin J, et al. (2006) The consensus coding sequences of human breast and colorectal cancers. Science 314: 268-274.
231. Tessema M, Belinsky SA (2008) Mining the epigenome for methylated genes in lung cancer. Proc Am Thorac Soc 5: 806-810.
232. Marme A, Zimmermann HP, Moldenhauer G, Schorpp-Kistner M, Muller C, et al. (2008) Loss of Drop1 expression already at early tumor stages in a wide range of human carcinomas. Int J Cancer 123: 2048-2056.
233. Smith UM, Consugar M, Tee LJ, McKee BM, Maina EN, et al. (2006) The transmembrane protein meckelin (MKS3) is mutated in Meckel-Gruber syndrome and the wpk rat. Nat Genet 38: 191-196.
234. Kyttala M, Tallila J, Salonen R, Kopra O, Kohlschmidt N, et al. (2006) MKS1, encoding a component of the flagellar apparatus basal body proteome, is mutated in Meckel syndrome. Nat Genet 38: 155-157.
235. Meloche S, Pouyssegur J (2007) The ERK1/2 mitogen-activated protein kinase pathway as a master regulator of the G1- to S-phase transition. Oncogene 26: 3227-3239.
236. Bernardi R, Pandolfi PP (2007) Structure, dynamics and functions of promyelocytic leukaemia nuclear bodies. Nat Rev Mol Cell Biol 8: 1006-1016.
237. Luke Y, Zaim H, Karakesisoglou I, Jaeger VM, Sellin L, et al. (2008) Nesprin-2 Giant (NUANCE) maintains nuclear envelope architecture and composition in skin. J Cell Sci 121: 1887-1898.
238. Smith ER, Zhang XY, Capo-Chichi CD, Chen X, Xu XX (2011) Increased expression of Syne1/nesprin-1 facilitates nuclear envelope structure changes in embryonic stem cell differentiation. Dev Dyn 240: 2245-2255.
239. Kedersha N, Stoecklin G, Ayodele M, Yacono P, Lykke-Andersen J, et al. (2005) Stress granules and processing bodies are dynamically linked sites of mRNP remodeling. J Cell Biol 169: 871-884.

240. Wilczynska A, Aigueperse C, Kress M, Dautry F, Weil D (2005) The translational regulator CPEB1 provides a link between dcp1 bodies and stress granules. J Cell Sci 118: 981-992.

241. Dostie J, Ferraiuolo M, Pause A, Adam SA, Sonenberg N (2000) A novel shuttling protein, 4E-T, mediates the nuclear import of the mRNA 5' cap-binding protein, eIF4E. EMBO J 19: 3142-3156.

242. Okumara K, Nogami M, Matsushima Y, Matsumura K, Nakamura K, et al. (1998) Mapping of human DNA-binding nuclear protein (NP220) to chromosome band 2p13.1-p13.2 and its relation to matrin 3. Biosci Biotechnol Biochem 62: 1640-1642.

243. Eystathioy T, Jakymiw A, Chan EK, Seraphin B, Cougot N, et al. (2003) The GW182 protein colocalizes with mRNA degradation associated proteins hDcp1 and hLSm4 in cytoplasmic GW bodies. RNA 9: 1171-1173.

244. Landthaler M, Gaidatzis D, Rothballer A, Chen PY, Soll SJ, et al. (2008) Molecular characterization of human Argonaute-containing ribonucleoprotein complexes and their bound target mRNAs. RNA 14: 2580-2596.

245. Doench JG, Petersen CP, Sharp PA (2003) siRNAs can function as miRNAs. Genes Dev 17: 438-442.

246. Zeitz MJ, Malyavantham KS, Seifert B, Berezney R (2009) Matrin 3: chromosomal distribution and protein interactions. J Cell Biochem 108: 125-133.

247. Choe J, Cho H, Lee HC, Kim YK (2010) microRNA/Argonaute 2 regulates nonsense-mediated messenger RNA decay. EMBO Rep 11: 380-386.

248. Lytle JR, Yario TA, Steitz JA (2007) Target mRNAs are repressed as efficiently by microRNA-binding sites in the 5' UTR as in the 3' UTR. Proc Natl Acad Sci U S A 104: 9667-9672.

249. Rajgor D, Mellad JA, Autore F, Zhang Q, Shanahan CM (2012) Multiple novel nesprin-1 and nesprin-2 variants act as versatile tissue-specific intracellular scaffolds. PLoS One 7: e40098.

250. Culligan KG, Mackey AJ, Finn DM, Maguire PB, Ohlendieck K (1998) Role of dystrophin isoforms and associated proteins in muscular dystrophy (review). Int J Mol Med 2: 639-648.
251. Torelli S, Ferlini A, Obici L, Sewry C, Muntoni F (1999) Expression, regulation and localisation of dystrophin isoforms in human foetal skeletal and cardiac muscle. Neuromuscul Disord 9: 541-551.
252. Roper K, Gregory SL, Brown NH (2002) The 'spectraplakins': cytoskeletal giants with characteristics of both spectrin and plakin families. J Cell Sci 115: 4215-4225.
253. Umeyama T, Okabe S, Kanai Y, Hirokawa N (1993) Dynamics of microtubules bundled by microtubule associated protein 2C (MAP2C). J Cell Biol 120: 451-465.
254. Xin D, Hu L, Kong X (2008) Alternative promoters influence alternative splicing at the genomic level. PLoS One 3: e2377.
255. Pecci A, Viegas LR, Baranao JL, Beato M (2001) Promoter choice influences alternative splicing and determines the balance of isoforms expressed from the mouse bcl-X gene. J Biol Chem 276: 21062-21069.
256. Shmelkov SV, Jun L, St Clair R, McGarrigle D, Derderian CA, et al. (2004) Alternative promoters regulate transcription of the gene that encodes stem cell surface protein AC133. Blood 103: 2055-2061.
257. Quelle DE, Zindy F, Ashmun RA, Sherr CJ (1995) Alternative reading frames of the INK4a tumor suppressor gene encode two unrelated proteins capable of inducing cell cycle arrest. Cell 83: 993-1000.
258. Vagner S, Waysbort A, Marenda M, Gensac MC, Amalric F, et al. (1995) Alternative translation initiation of the Moloney murine leukemia virus mRNA controlled by internal ribosome entry involving the p57/PTB splicing factor. J Biol Chem 270: 20376-20383.
259. Melefors O, Hentze MW (1993) Iron regulatory factor--the conductor of cellular iron regulation. Blood Rev 7: 251-258.
260. Eldad N, Yosefzon Y, Arava Y (2008) Identification and characterization of extensive intra-molecular associations between 3'-UTRs and their ORFs. Nucleic Acids Res 36: 6728-6738.

261. Aronov S, Aranda G, Behar L, Ginzburg I (2001) Axonal tau mRNA localization coincides with tau protein in living neuronal cells and depends on axonal targeting signal. J Neurosci 21: 6577-6587.
262. Tanguay RL, Gallie DR (1996) Translational efficiency is regulated by the length of the 3' untranslated region. Mol Cell Biol 16: 146-156.
263. Loya A, Pnueli L, Yosefzon Y, Wexler Y, Ziv-Ukelson M, et al. (2008) The 3'-UTR mediates the cellular localization of an mRNA encoding a short plasma membrane protein. RNA 14: 1352-1365.
264. Mathonnet G, Fabian MR, Svitkin YV, Parsyan A, Huck L, et al. (2007) MicroRNA inhibition of translation initiation in vitro by targeting the cap-binding complex eIF4F. Science 317: 1764-1767.
265. Utsumi T, Sato M, Nakano K, Takemura D, Iwata H, et al. (2001) Amino acid residue penultimate to the amino-terminal gly residue strongly affects two cotranslational protein modifications, N-myristoylation and N-acetylation. J Biol Chem 276: 10505-10513.
266. Koutelou E, Sato S, Tomomori-Sato C, Florens L, Swanson SK, et al. (2008) Neuralized-like 1 (Neurl1) targeted to the plasma membrane by N-myristoylation regulates the Notch ligand Jagged1. J Biol Chem 283: 3846-3853.
267. Eulalio A, Behm-Ansmant I, Izaurralde E (2007) P bodies: at the crossroads of post-transcriptional pathways. Nat Rev Mol Cell Biol 8: 9-22.
268. Temme C, Zaessinger S, Meyer S, Simonelig M, Wahle E (2004) A complex containing the CCR4 and CAF1 proteins is involved in mRNA deadenylation in Drosophila. EMBO J 23: 2862-2871.
269. Cougot N, Babajko S, Seraphin B (2004) Cytoplasmic foci are sites of mRNA decay in human cells. J Cell Biol 165: 31-40.
270. Ingelfinger D, Arndt-Jovin DJ, Luhrmann R, Achsel T (2002) The human LSm1-7 proteins colocalize with the mRNA-degrading enzymes Dcp1/2 and Xrnl in distinct cytoplasmic foci. RNA 8: 1489-1501.
271. Chowdhury A, Mukhopadhyay J, Tharun S (2007) The decapping activator Lsm1p-7p-Pat1p complex has the intrinsic ability to distinguish between oligoadenylated and polyadenylated RNAs. RNA 13: 998-1016.

272. van Dijk E, Cougot N, Meyer S, Babajko S, Wahle E, et al. (2002) Human Dcp2: a catalytically active mRNA decapping enzyme located in specific cytoplasmic structures. EMBO J 21: 6915-6924.
273. Sheth U, Parker R (2003) Decapping and decay of messenger RNA occur in cytoplasmic processing bodies. Science 300: 805-808.
274. Fenger-Gron M, Fillman C, Norrild B, Lykke-Andersen J (2005) Multiple processing body factors and the ARE binding protein TTP activate mRNA decapping. Mol Cell 20: 905-915.
275. Yamochi T, Ohnuma K, Hosono O, Tanaka H, Kanai Y, et al. (2008) SSA/Ro52 autoantigen interacts with Dcp2 to enhance its decapping activity. Biochem Biophys Res Commun 370: 195-199.
276. Lebreton A, Tomecki R, Dziembowski A, Seraphin B (2008) Endonucleolytic RNA cleavage by a eukaryotic exosome. Nature 456: 993-996.
277. Schmid M, Jensen TH (2008) The exosome: a multipurpose RNA-decay machine. Trends Biochem Sci 33: 501-510.
278. Zheng D, Ezzeddine N, Chen CY, Zhu W, He X, et al. (2008) Deadenylation is prerequisite for P-body formation and mRNA decay in mammalian cells. J Cell Biol 182: 89-101.
279. Brengues M, Teixeira D, Parker R (2005) Movement of eukaryotic mRNAs between polysomes and cytoplasmic processing bodies. Science 310: 486-489.
280. Sheth U, Parker R (2006) Targeting of aberrant mRNAs to cytoplasmic processing bodies. Cell 125: 1095-1109.
281. Durand S, Cougot N, Mahuteau-Betzer F, Nguyen CH, Grierson DS, et al. (2007) Inhibition of nonsense-mediated mRNA decay (NMD) by a new chemical molecule reveals the dynamic of NMD factors in P-bodies. J Cell Biol 178: 1145-1160.
282. Unterholzner L, Izaurralde E (2004) SMG7 acts as a molecular link between mRNA surveillance and mRNA decay. Mol Cell 16: 587-596.
283. Shaw G, Kamen R (1986) A conserved AU sequence from the 3' untranslated region of GM-CSF mRNA mediates selective mRNA degradation. Cell 46: 659-667.

284. Bakheet T, Williams BR, Khabar KS (2003) ARED 2.0: an update of AU-rich element mRNA database. Nucleic Acids Res 31: 421-423.
285. Chen CY, Gherzi R, Ong SE, Chan EL, Raijmakers R, et al. (2001) AU binding proteins recruit the exosome to degrade ARE-containing mRNAs. Cell 107: 451-464.
286. Stoecklin G, Mayo T, Anderson P (2006) ARE-mRNA degradation requires the 5'-3' decay pathway. EMBO Rep 7: 72-77.
287. Franks TM, Lykke-Andersen J (2007) TTP and BRF proteins nucleate processing body formation to silence mRNAs with AU-rich elements. Genes Dev 21: 719-735.
288. Liu J, Valencia-Sanchez MA, Hannon GJ, Parker R (2005) MicroRNA-dependent localization of targeted mRNAs to mammalian P-bodies. Nat Cell Biol 7: 719-723.
289. Sen GL, Blau HM (2005) Argonaute 2/RISC resides in sites of mammalian mRNA decay known as cytoplasmic bodies. Nat Cell Biol 7: 633-636.
290. Chu CY, Rana TM (2006) Translation repression in human cells by microRNA-induced gene silencing requires RCK/p54. PLoS Biol 4: e210.
291. Yang Z, Jakymiw A, Wood MR, Eystathioy T, Rubin RL, et al. (2004) GW182 is critical for the stability of GW bodies expressed during the cell cycle and cell proliferation. J Cell Sci 117: 5567-5578.
292. Behm-Ansmant I, Rehwinkel J, Doerks T, Stark A, Bork P, et al. (2006) mRNA degradation by miRNAs and GW182 requires both CCR4:NOT deadenylase and DCP1:DCP2 decapping complexes. Genes Dev 20: 1885-1898.
293. Bhattacharyya SN, Habermacher R, Martine U, Closs EI, Filipowicz W (2006) Relief of microRNA-mediated translational repression in human cells subjected to stress. Cell 125: 1111-1124.
294. Pauley KM, Eystathioy T, Jakymiw A, Hamel JC, Fritzler MJ, et al. (2006) Formation of GW bodies is a consequence of microRNA genesis. EMBO Rep 7: 904-910.
295. Anderson P, Kedersha N (2008) Stress granules: the Tao of RNA triage. Trends Biochem Sci 33: 141-150.

296. Buchan JR, Muhlrad D, Parker R (2008) P bodies promote stress granule assembly in Saccharomyces cerevisiae. J Cell Biol 183: 441-455.

297. Aizer A, Brody Y, Ler LW, Sonenberg N, Singer RH, et al. (2008) The dynamics of mammalian P body transport, assembly, and disassembly in vivo. Mol Biol Cell 19: 4154-4166.

298. Moser JJ, Fritzler MJ, Rattner JB (2011) Repression of GW/P body components and the RNAi microprocessor impacts primary ciliogenesis in human astrocytes. BMC Cell Biol 12: 37.

299. Yu JH, Yang WH, Gulick T, Bloch KD, Bloch DB (2005) Ge-1 is a central component of the mammalian cytoplasmic mRNA processing body. RNA 11: 1795-1802.

300. Sweet TJ, Boyer B, Hu W, Baker KE, Coller J (2007) Microtubule disruption stimulates P-body formation. RNA 13: 493-502.

301. Andrei MA, Ingelfinger D, Heintzmann R, Achsel T, Rivera-Pomar R, et al. (2005) A role for eIF4E and eIF4E-transporter in targeting mRNPs to mammalian processing bodies. RNA 11: 717-727.

302. Ding L, Han M (2007) GW182 family proteins are crucial for microRNA-mediated gene silencing. Trends Cell Biol 17: 411-416.

303. Lykke-Andersen J, Wagner E (2005) Recruitment and activation of mRNA decay enzymes by two ARE-mediated decay activation domains in the proteins TTP and BRF-1. Genes Dev 19: 351-361.

304. Parker R, Sheth U (2007) P bodies and the control of mRNA translation and degradation. Mol Cell 25: 635-646.

305. Jakymiw A, Pauley KM, Li S, Ikeda K, Lian S, et al. (2007) The role of GW/P-bodies in RNA processing and silencing. J Cell Sci 120: 1317-1323.

306. Affaitati A, de Cristofaro T, Feliciello A, Varrone S (2001) Identification of alternative splicing of spinocerebellar ataxia type 2 gene. Gene 267: 89-93.

307. Blower MD, Feric E, Weis K, Heald R (2007) Genome-wide analysis demonstrates conserved localization of messenger RNAs to mitotic microtubules. J Cell Biol 179: 1365-1373.

308. Vale RD (2003) The molecular motor toolbox for intracellular transport. Cell 112: 467-480.
309. Subramanian R, Wilson-Kubalek EM, Arthur CP, Bick MJ, Campbell EA, et al. (2010) Insights into antiparallel microtubule crosslinking by PRC1, a conserved nonmotor microtubule binding protein. Cell 142: 433-443.
310. Anderson P, Kedersha N (2009) Stress granules. Curr Biol 19: R397-398.
311. Kedersha N, Anderson P (2007) Mammalian stress granules and processing bodies. Methods Enzymol 431: 61-81.
312. Anderson P, Kedersha N (2006) RNA granules. J Cell Biol 172: 803-808.
313. Anderson P, Kedersha N (2002) Stressful initiations. J Cell Sci 115: 3227-3234.
314. Kedersha N, Anderson P (2002) Stress granules: sites of mRNA triage that regulate mRNA stability and translatability. Biochem Soc Trans 30: 963-969.
315. Nadezhdina ES, Lomakin AJ, Shpilman AA, Chudinova EM, Ivanov PA (2010) Microtubules govern stress granule mobility and dynamics. Biochim Biophys Acta 1803: 361-371.
316. Salton M, Lerenthal Y, Wang SY, Chen DJ, Shiloh Y (2010) Involvement of Matrin 3 and SFPQ/NONO in the DNA damage response. Cell Cycle 9: 1568-1576.
317. Przygodzka P, Boncela J, Cierniewski CS (2011) Matrin 3 as a key regulator of endothelial cell survival. Exp Cell Res 317: 802-811.
318. Giordano G, Sanchez-Perez AM, Montoliu C, Berezney R, Malyavantham K, et al. (2005) Activation of NMDA receptors induces protein kinase A-mediated phosphorylation and degradation of matrin 3. Blocking these effects prevents NMDA-induced neuronal death. J Neurochem 94: 808-818.
319. Zhang Z, Carmichael GG (2001) The fate of dsRNA in the nucleus: a p54(nrb)-containing complex mediates the nuclear retention of promiscuously A-to-I edited RNAs. Cell 106: 465-475.
320. Belgrader P, Dey R, Berezney R (1991) Molecular cloning of matrin 3. A 125-kilodalton protein of the nuclear matrix contains an extensive acidic domain. J Biol Chem 266: 9893-9899.

321. Salton M, Elkon R, Borodina T, Davydov A, Yaspo ML, et al. (2011) Matrin 3 binds and stabilizes mRNA. PLoS One 6: e23882.
322. Senderek J GS, Krieger M, Guergueltcheva V, Urtizberea A, Roos A, Elbracht M, Stendel C, Tournev I, Mihailova V, Feit H, Tramonte J, Hedera P, Crooks K, Bergmann C, Rudnik-Schöneborn S, Zerres K, Lochmüller H, Seboun E, Weis J, Beckmann JS, Hauser MA, Jackson CE. (2009) Autosomal-dominant distal myopathy associated with a recurrent missense mutation in the gene encoding the nuclear matrix protein, matrin 3. Am J Hum Genet Apr;84: 511-518.
323. Bernert G FM, Lubec G. (2002) Manifold decreased protein levels of matrin 3, reduced motor protein HMP and hlark in fetal Down's syndrome brain. Proteomics Dec;2: 1752-1757.
324. Bimpaki EI, Iliopoulos D, Moraitis A, Stratakis CA (2010) MicroRNA signature in massive macronodular adrenocortical disease and implications for adrenocortical tumourigenesis. Clin Endocrinol (Oxf) 72: 744-751.
325. Senderek J, Garvey SM, Krieger M, Guergueltcheva V, Urtizberea A, et al. (2009) Autosomal-dominant distal myopathy associated with a recurrent missense mutation in the gene encoding the nuclear matrix protein, matrin 3. Am J Hum Genet 84: 511-518.
326. Pillai RS, Artus CG, Filipowicz W (2004) Tethering of human Ago proteins to mRNA mimics the miRNA-mediated repression of protein synthesis. RNA 10: 1518-1525.
327. Bates GJ, Nicol SM, Wilson BJ, Jacobs AM, Bourdon JC, et al. (2005) The DEAD box protein p68: a novel transcriptional coactivator of the p53 tumour suppressor. EMBO J 24: 543-553.
328. Caretti G, Schiltz RL, Dilworth FJ, Di Padova M, Zhao P, et al. (2006) The RNA helicases p68/p72 and the noncoding RNA SRA are coregulators of MyoD and skeletal muscle differentiation. Dev Cell 11: 547-560.
329. Mathur M, Tucker PW, Samuels HH (2001) PSF is a novel corepressor that mediates its effect through Sin3A and the DNA binding domain of nuclear hormone receptors. Mol Cell Biol 21: 2298-2311.

330. Urban RJ, Bodenburg Y, Kurosky A, Wood TG, Gasic S (2000) Polypyrimidine tract-binding protein-associated splicing factor is a negative regulator of transcriptional activity of the porcine p450scc insulin-like growth factor response element. Mol Endocrinol 14: 774-782.
331. Urban RJ, Bodenburg YH, Wood TG (2002) NH2 terminus of PTB-associated splicing factor binds to the porcine P450scc IGF-I response element. Am J Physiol Endocrinol Metab 283: E423-427.
332. Patton JG, Porro EB, Galceran J, Tempst P, Nadal-Ginard B (1993) Cloning and characterization of PSF, a novel pre-mRNA splicing factor. Genes Dev 7: 393-406.
333. Liu ZR (2002) p68 RNA helicase is an essential human splicing factor that acts at the U1 snRNA-5' splice site duplex. Mol Cell Biol 22: 5443-5450.
334. Hutchison S, LeBel C, Blanchette M, Chabot B (2002) Distinct sets of adjacent heterogeneous nuclear ribonucleoprotein (hnRNP) A1/A2 binding sites control 5' splice site selection in the hnRNP A1 mRNA precursor. J Biol Chem 277: 29745-29752.
335. Martinez-Contreras R, Cloutier P, Shkreta L, Fisette JF, Revil T, et al. (2007) hnRNP proteins and splicing control. Adv Exp Med Biol 623: 123-147.
336. Hoege C, Pfander B, Moldovan GL, Pyrowolakis G, Jentsch S (2002) RAD6-dependent DNA repair is linked to modification of PCNA by ubiquitin and SUMO. Nature 419: 135-141.
337. Salton M, Lerenthal Y, Wang SY, Chen DJ, Shiloh Y (2010) Involvement of matrin 3 and SFPQ/NONO in the DNA damage response. Cell Cycle 9.
338. Harel A, Forbes DJ (2004) Importin beta: conducting a much larger cellular symphony. Mol Cell 16: 319-330.
339. Levesque K, Halvorsen M, Abrahamyan L, Chatel-Chaix L, Poupon V, et al. (2006) Trafficking of HIV-1 RNA is mediated by heterogeneous nuclear ribonucleoprotein A2 expression and impacts on viral assembly. Traffic 7: 1177-1193.

340. Hoek KS, Kidd GJ, Carson JH, Smith R (1998) hnRNP A2 selectively binds the cytoplasmic transport sequence of myelin basic protein mRNA. Biochemistry 37: 7021-7029.
341. Ainger K, Avossa D, Diana AS, Barry C, Barbarese E, et al. (1997) Transport and localization elements in myelin basic protein mRNA. J Cell Biol 138: 1077-1087.
342. Carson JH, Worboys K, Ainger K, Barbarese E (1997) Translocation of myelin basic protein mRNA in oligodendrocytes requires microtubules and kinesin. Cell Motil Cytoskeleton 38: 318-328.
343. Pearl LH, Prodromou C (2006) Structure and mechanism of the Hsp90 molecular chaperone machinery. Annu Rev Biochem 75: 271-294.
344. Vlcek S, Dechat T, Foisner R (2001) Nuclear envelope and nuclear matrix: interactions and dynamics. Cell Mol Life Sci 58: 1758-1765.
345. Matlin AJ, Clark F, Smith CW (2005) Understanding alternative splicing: towards a cellular code. Nat Rev Mol Cell Biol 6: 386-398.
346. Will CL, Luhrmann R (2011) Spliceosome structure and function. Cold Spring Harb Perspect Biol 3.
347. Jurica MS, Moore MJ (2003) Pre-mRNA splicing: awash in a sea of proteins. Mol Cell 12: 5-14.
348. Grabowski PJ, Black DL (2001) Alternative RNA splicing in the nervous system. Prog Neurobiol 65: 289-308.
349. Modrek B, Lee C (2002) A genomic view of alternative splicing. Nat Genet 30: 13-19.
350. Graveley BR (2001) Alternative splicing: increasing diversity in the proteomic world. Trends Genet 17: 100-107.
351. Smith CW, Porro EB, Patton JG, Nadal-Ginard B (1989) Scanning from an independently specified branch point defines the 3' splice site of mammalian introns. Nature 342: 243-247.
352. Faustino NA, Cooper TA (2003) Pre-mRNA splicing and human disease. Genes Dev 17: 419-437.
353. Pagani F, Baralle FE (2004) Genomic variants in exons and introns: identifying the splicing spoilers. Nat Rev Genet 5: 389-396.

354. Caceres JF, Kornblihtt AR (2002) Alternative splicing: multiple control mechanisms and involvement in human disease. Trends Genet 18: 186-193.

355. Shen H, Green MR (2004) A pathway of sequential arginine-serine-rich domain-splicing signal interactions during mammalian spliceosome assembly. Mol Cell 16: 363-373.

356. Shen H, Kan JL, Green MR (2004) Arginine-serine-rich domains bound at splicing enhancers contact the branchpoint to promote prespliceosome assembly. Mol Cell 13: 367-376.

357. Graveley BR (2000) Sorting out the complexity of SR protein functions. RNA 6: 1197-1211.

358. Ring HZ, Lis JT (1994) The SR protein B52/SRp55 is essential for Drosophila development. Mol Cell Biol 14: 7499-7506.

359. Xu X, Yang D, Ding JH, Wang W, Chu PH, et al. (2005) ASF/SF2-regulated CaMKIIdelta alternative splicing temporally reprograms excitation-contraction coupling in cardiac muscle. Cell 120: 59-72.

360. Jumaa H, Wei G, Nielsen PJ (1999) Blastocyst formation is blocked in mouse embryos lacking the splicing factor SRp20. Curr Biol 9: 899-902.

361. Ding JH, Xu X, Yang D, Chu PH, Dalton ND, et al. (2004) Dilated cardiomyopathy caused by tissue-specific ablation of SC35 in the heart. EMBO J 23: 885-896.

362. Krecic AM, Swanson MS (1999) hnRNP complexes: composition, structure, and function. Curr Opin Cell Biol 11: 363-371.

363. Houben F, De Vos WH, Krapels IP, Coorens M, Kierkels GJ, et al. (2012) Cytoplasmic localization of PML particles in laminopathies. Histochem Cell Biol.

364. Gromak N, Rideau A, Southby J, Scadden AD, Gooding C, et al. (2003) The PTB interacting protein raver1 regulates alpha-tropomyosin alternative splicing. EMBO J 22: 6356-6364.

365. Llorian M, Schwartz S, Clark TA, Hollander D, Tan LY, et al. (2010) Position-dependent alternative splicing activity revealed by global profiling of alternative splicing events regulated by PTB. Nat Struct Mol Biol 17: 1114-1123.

366. Rideau AP, Gooding C, Simpson PJ, Monie TP, Lorenz M, et al. (2006) A peptide motif in Raver1 mediates splicing repression by interaction with the PTB RRM2 domain. Nat Struct Mol Biol 13: 839-848.

367. Kumaran RI, Muralikrishna B, Parnaik VK (2002) Lamin A/C speckles mediate spatial organization of splicing factor compartments and RNA polymerase II transcription. J Cell Biol 159: 783-793.

368. Vecerova J, Koberna K, Malinsky J, Soutoglou E, Sullivan T, et al. (2004) Formation of nuclear splicing factor compartments is independent of lamins A/C. Mol Biol Cell 15: 4904-4910.

369. Spector DL, Lamond AI (2011) Nuclear speckles. Cold Spring Harb Perspect Biol 3.

370. Bauren G, Wieslander L (1994) Splicing of Balbiani ring 1 gene pre-mRNA occurs simultaneously with transcription. Cell 76: 183-192.

371. Neugebauer KM, Roth MB (1997) Distribution of pre-mRNA splicing factors at sites of RNA polymerase II transcription. Genes Dev 11: 1148-1159.

372. Listerman I, Sapra AK, Neugebauer KM (2006) Cotranscriptional coupling of splicing factor recruitment and precursor messenger RNA splicing in mammalian cells. Nat Struct Mol Biol 13: 815-822.

373. Cmarko D, Verschure PJ, Martin TE, Dahmus ME, Krause S, et al. (1999) Ultrastructural analysis of transcription and splicing in the cell nucleus after bromo-UTP microinjection. Mol Biol Cell 10: 211-223.

374. Lai MC, Lin RI, Tarn WY (2003) Differential effects of hyperphosphorylation on splicing factor SRp55. Biochem J 371: 937-945.

375. Huang S, Spector DL (1992) U1 and U2 small nuclear RNAs are present in nuclear speckles. Proc Natl Acad Sci U S A 89: 305-308.

376. Ali GS, Prasad KV, Hanumappa M, Reddy AS (2008) Analyses of in vivo interaction and mobility of two spliceosomal proteins using FRAP and BiFC. PLoS One 3: e1953.

377. Sleeman JE, Ajuh P, Lamond AI (2001) snRNP protein expression enhances the formation of Cajal bodies containing p80-coilin and SMN. J Cell Sci 114: 4407-4419.

378. Reynolds RC, Montgomery PO, Hughes B (1964) Nucleolar "Caps" Produced by Actinomycin D. Cancer Res 24: 1269-1277.
379. Shav-Tal Y, Blechman J, Darzacq X, Montagna C, Dye BT, et al. (2005) Dynamic sorting of nuclear components into distinct nucleolar caps during transcriptional inhibition. Mol Biol Cell 16: 2395-2413.
380. Olson MO, Hingorani K, Szebeni A (2002) Conventional and nonconventional roles of the nucleolus. Int Rev Cytol 219: 199-266.
381. Andersen JS, Lyon CE, Fox AH, Leung AK, Lam YW, et al. (2002) Directed proteomic analysis of the human nucleolus. Curr Biol 12: 1-11.
382. de Lanerolle P, Johnson T, Hofmann WA (2005) Actin and myosin I in the nucleus: what next? Nat Struct Mol Biol 12: 742-746.
383. Savas JN, Makusky A, Ottosen S, Baillat D, Then F, et al. (2008) Huntington's disease protein contributes to RNA-mediated gene silencing through association with Argonaute and P bodies. Proc Natl Acad Sci U S A 105: 10820-10825.
384. Nonhoff U, Ralser M, Welzel F, Piccini I, Balzereit D, et al. (2007) Ataxin-2 interacts with the DEAD/H-box RNA helicase DDX6 and interferes with P-bodies and stress granules. Mol Biol Cell 18: 1385-1396.

Appendix I: Multiple Novel Nesprin-1 and Nesprin-2 Variants Act as Versatile Tissue-Specific Intracellular Scaffolds

OPEN ACCESS Freely available online

PLoS one

Multiple Novel Nesprin-1 and Nesprin-2 Variants Act as Versatile Tissue-Specific Intracellular Scaffolds

Dipen Rajgor[1☯], Jason A. Mellad[1☯], Flavia Autore[2], Qiuping Zhang[1], Catherine M. Shanahan[1]*

1 Cardiovascular Division, James Black Centre, King's College London, London, United Kingdom, **2** The Randall Division of Cell and Molecular Biophysics, New Hunt's House, King's College London, London, United Kingdom

Abstract

Background: Nesprins (Nuclear envelope spectrin-repeat proteins) are a novel family of giant spectrin-repeat containing proteins. The nesprin-1 and nesprin-2 genes consist of 146 and 116 exons which encode proteins of ~1mDa and ~800 kDa is size respectively when all the exons are utilised in translation. However emerging data suggests that the nesprins have multiple alternative start and termination sites throughout their genes allowing the generation of smaller isoforms.

Results: In this study we set out to identify novel alternatively transcribed nesprin variants by screening the EST database and by using RACE analysis to identify cDNA ends. These two methods provided potential hits for alternative start and termination sites that were validated by PCR and DNA sequencing. We show that these alternative sites are not only expressed in a tissue specific manner but by combining different sites together it is possible to create a wide array of nesprin variants. By cloning and expressing small novel nesprin variants into human fibroblasts and U2OS cells we show localization to actin stress-fibres, focal adhesions, microtubules, the nucleolus, nuclear matrix and the nuclear envelope (NE). Furthermore we show that the sub-cellular localization of individual nesprin variants can vary depending on the cell type, suggesting any single nesprin variant may have different functions in different cell types.

Conclusions: These studies suggest nesprins act as highly versatile tissue specific intracellular protein scaffolds and identify potential novel functions for nesprins beyond cytoplasmic-nuclear coupling. These alternate functions may also account for the diverse range of disease phenotypes observed when these genes are mutated.

Citation: Rajgor D, Mellad JA, Autore F, Zhang Q, Shanahan CM (2012) Multiple Novel Nesprin-1 and Nesprin-2 Variants Act as Versatile Tissue-Specific Intracellular Scaffolds. PLoS ONE 7(7): e40098. doi:10.1371/journal.pone.0040098

Editor: Krishna Sharma, University of Missouri-Columbia, United States of America

Received March 12, 2012; **Accepted** May 31, 2012; **Published** July 2, 2012

Funding: Medical Research Council and the British Heart Foundation provided funding for this study. The funders had no role in study design, data collection and analysis, decision to publish, or preparation of the manuscript.

Competing Interests: The authors have declared that no competing interests exist.

* E-mail: cathy.shanahan@kcl.ac.uk

☯ These authors contributed equally to this work.

Introduction

Nuclear envelope (NE) spectrin-repeat proteins, or nesprins, are a novel family of nuclear and cytoskeletal proteins with rapidly expanding roles as intracellular scaffolds and linkers [1,2,3,4]. Nesprins are characterized by a central extended spectrin-repeat (SR) rod domain and a C-terminal Klarsicht/ANC-1/Syne homology (KASH) transmembrane domain, which acts as a NE targeting motif. At the NE, via interactions with the Sun-domain family of proteins and the nuclear lamina, nesprins on both the inner and outer nuclear membrane form the linker of the nucleoskeleton and cytoskeleton (LINC) complex [5,6]. This complex requires the giant nesprin-1 (~1 MDa) and nesprin-2 (~800 kDa) isoforms, which possess a pair of N-terminal calponin homology domains, which bind directly to F-actin [7,8]. Nesprin-3 (~110 kDa) and nesprin-4 (~43 kDa) are smaller family members with more divergent spectrin-repeats. These lack the N-terminal CH domains of nesprin-1 and -2 and via SRs interact with intermediate filaments and microtubules respectively [3,4,9].

Disruption of the LINC complex via mutations in nesprin-1 and -2 or their binding partners, such as emerin and lamin A/C, give rise to Emery Dreifuss Muscular Dystrophy (EDMD) [6,10,11,12,13,14,15,16,17]. However, emerging evidence implicates nesprin-1 and -2 in several other unrelated diseases, including schizophrenia, epithelial cancers and autosomal recessive cerebellar ataxia (ARCA1), which are not characterized by NE defects [18,19,20]. It is likely that these non-canonical roles for nesprin are mediated by alternative transcription that has been shown to generate multiple tissue-specific nesprin variants that lack either the CH domain, the KASH domain or both and localize to a number of subcellular compartments [2,21]. For example, nesprin-1 has been shown to localize to the Golgi apparatus and over-expression of dominant-negative nesprin-1 fragments composed of SRs within the central rod domain disrupt Golgi organization and function [22,23,24]. Nesprin-1 isoform Drop1, which consists of the N-terminal CH domain and SRs but lacks the KASH domain, is significantly down regulated in epithelial cancer and may play a role in chromatin organization [16,25,26]. Furthermore, the brain-specific nesprin-1 isoform, candidate plasticity gene 2 (cpg2), consists solely of SRs and localizes to the neuronal postsynaptic endocytic zone surrounding dendritic spines where it regulates clathrin-mediated uptake and recycling of chemokine receptors [27,28].

In order to assess further the extent of alternate nesprin functionality, in this study we set out to identify novel nesprin variants by identifying 5′UTRs and 3′UTRs transcribed from the nesprin-1 and nesprin-2 genes. We provide evidence that both nesprin-1 and -2 undergo alternative splicing and express multiple tissue specific variants generated by alternate initiation and termination and that the sub-cellular localization of these variants is cell type dependent. We also provide a unifying nomenclature system for nesprin variants and their UTRs.

Results

Identification of Novel Nesprin-1 and Nesprin-2 UTRs

We adopted two approaches to identify *bone fide* novel 5′ and 3′UTRs. We first performed 5′ and 3′ RACE from HeLa, Skeletal Muscle and Brain cDNA libraries using multiple gene specific nesprin primers and nested primers designed towards the end of a range of exons throughout the nesprin gene. Many PCRs produced non-specific or no amplicons (data not shown) however, products for multiple UTRs as retained introns were detected (Figure 1A). For nesprin-1 we identified N1-5′E83, a novel 5′UTR where the first coding exon utilised is exon 83. Multiple nesprin-1 3′UTRs were detected in a tissue/cell specific manner where the last coding exons were either exons 14, 44, 82, 90 or 106 (N1-3′E14, N1-3′E44, N1-3′E82, N1-3′E90 and N1-3′E106 respectively). Similarly N2-3′E50 and N2-3′E90 are two novel nesprin-2 3′UTRs also identified by RACE. The stop codons for isoforms terminating with these novel 3′ ends were found in retained intronic sequences between the last coding exon and the exon thereafter. In nesprin variants using these 3′ ends the 'retained intron' resulted in the addition of unique amino acids followed by a stop codon that were absent from the giant isoforms. Downstream of the stop codon will be a polyA signal followed by a polyadenylation site. For example, variants terminating with the N1-3′E90 UTR contain eight codons before the stop codon in the retained intron between exon 90 and exon 91. Thus variants terminating with this 3′UTR possess a novel 8 amino acid peptide sequence, 'AGAGYPHQ*', which is absent in the giant isoform (Figure 1B).

Due to limitations with RACE analysis we next screened available databases for novel nesprin cDNA transcripts. The NCBI expressed sequence tag database (EST), which consists of one-shot sequences of cloned mRNA, was blasted with consecutive, 500 bp-overlapping 1 kb nesprin-1 and nesprin-2 sequences covering the entirety of the giant isoform cDNAs. Several novel UTRs were detected in the EST database screen, typically presenting as retained introns between two exons (Table 1). 5′UTRs were considered real if they contained an identifiable and viable Kozak sequence surrounding the first start codon. Only those 3′UTR sequences which already included a poly(A) tail or contained at least one poly(A) site downstream of the initial ORF termination codon, as determined by scanning with the polyAdq program or manually for non-canonical poly(A) signals, were considered for further study.

The majority of UTRs identified by RACE or through the EST screen were verified by PCR and DNA sequencing using a multi-tissue cDNA panel (Figures 1C,D. Table 1 contains a column showing the UTRs which have been verified by PCR). PCR primers were designed so that one primer was present within the UTR and the second within a constitutively present exon with at least one intervening intron sequence to control for genomic DNA contamination. Although many UTRs PCR amplified in a range of tissues, most were transcribed in a tissue specific manner suggesting they lead to the creation of tissue specific nesprin variants. The potential combinations of 5′ UTRs with 3′UTRs are extensive and would allow generation of many variants. Figures 2A and 3A provide an outline of the nesprin-1 and nesprin-2 UTRs across their respective genes with figures 2B and 3B highlighting proposed variants that could be created by a 'mix-and-match' approach *in vivo* for nesprin-1 and nesprin-2 respectively (Table S1 and Table S2 shows the UTRs that when combined generate these nesprin-1 and -2 variants respectively). The spectrin repeats (SRs) used in our schematics to represent nesprins are based on the predictions of SRs as previously described [29]. Many of the predicted nesprin variants are too large to be detected by conventional PCR and are therefore hypothetical. The smaller nesprin variants were however validated by PCR and are described below.

Although many variants could retain the KASH domain, there is a possibility of generating isoforms composed solely of SRs. Therefore, the identified nesprin variants were named according to their predicted molecular weights and the domains they possessed. For example, p56CH^{Nesp1} is a nesprin-1 variant of 56 kDa which has the N-terminal CH domains, p50^{Nesp1} is a 50 kDa nesprin-1 variant which lacks both the CH domains and the KASH domain and is composed of SRs, while p53KASH^{Nesp1} is a 53 kDa KASH containing variant lacking CH domains. Variants that lack the KASH domain due to alternative splicing events in and around the exons coding for the KASH domain have been described as ΔKASH variants (See below).

Nesprin KASH Isoforms

So far a number of KASH variants including the nesprin-1 and nesprin-2 α,β isoforms have been identified. In principle any of the 5′UTRs identified in this study could be utilised with the 3′UTR of the nesprin-1 giant to make KASH containing NE localized nesprin variants. Whilst most 5′UTRs are too distant from the KASH domain for PCR amplification we were able to verify p53KASH^{Nesp1} (Accession number JQ754366), the smallest nesprin-1 KASH containing isoform identified to date, with a molecular weight of 53 kDa. p53KASH^{Nesp1} uses the N1-5′E138 alternative start site which was detected in heart, spleen, lung, brain, prostate, PBL, small intestine (SI), ovary and liver cDNA (Figure 1C). Although full-length p53KASH^{Nesp1} could not be detected in a range of primary and transformed cell lines it was detected in tissues including heart, spleen and peripheral blood leukocytes (PBL) (Figure 4F). Flag-p53KASH^{Nesp1} cloned from heart cDNA confirmed NE localization when transfected into U2OS cells (Figure 4A,B).

Nesprin Calponin Homology Domain containing Isoforms

Next we set out to identify the sub-cellular localizations of KASH-less nesprin variants composed of SRs or CH domains. p56CH^{Nesp1} and p32CH^{Nesp2} are two nesprin CH-domain containing variants with a Mw suitable for PCR amplification and cloning (Accession numbers JQ740783 and JQ754367 respectively) (Figures 4A,E). p56CH^{Nesp1} initiates with the most upstream nesprin-1 UTR utilised by the nesprin-1 giant and terminates with N1-3′E14, encoding a protein that possesses the CH domains and the first SR of nesprin-1. p32CH^{Nesp2} terminates upstream of the first SR coding exon and is therefore the only known nesprin variant to date which lacks any SRs. Interestingly we observed differential sub-cellular localizations when p56CH^{Nesp1} was transfected into transformed and primary cell lines. In U2OS cells p56CH^{Nesp1} surprisingly localized to the nucleolus while in HDFs it associated with actin stress fibres and focal adhesions (Figure 4C,D). Whilst p56CH^{Nesp1} expression was ubiquitously detected in all cell lines examined, expression of

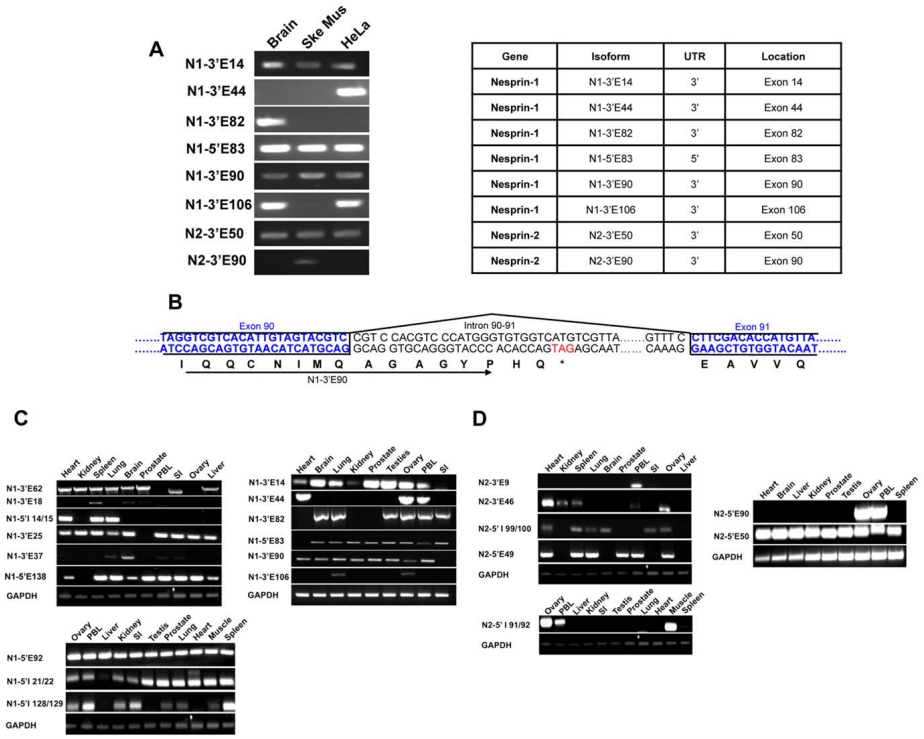

Gene	Isoform	UTR	Location
Nesprin-1	N1-3'E14	3'	Exon 14
Nesprin-1	N1-3'E44	3'	Exon 44
Nesprin-1	N1-3'E82	3'	Exon 82
Nesprin-1	N1-5'E83	5'	Exon 83
Nesprin-1	N1-3'E90	3'	Exon 90
Nesprin-1	N1-3'E106	3'	Exon 106
Nesprin-2	N2-3'E50	3'	Exon 50
Nesprin-2	N2-3'E90	3'	Exon 90

Figure 1. Identification of novel nesprin UTRs. A) cDNA ends identified by 3′ and 5′ RACE from Brain, Skeletal Muscle (SkeMus) and HeLa cDNA libraries. B) DNA sequencing results suggest that nesprin isoforms terminate with unique C-terminal ends absent from the giant isoforms as a result of intron retention. For example, isoforms utilising the N1-3′E90 UTR terminate with 'AGAGYPHQ' amino acids, giving it a unique fingerprint. Blue sequences show the coding regions of exons 90 and 91, black sequences show intronic regions and red sequence indicates a stop codon. C) Validation and tissue specificity of nesprin-1 UTRs identified on online databases and by RACE were confirmed by PCR amplification from a multiple tissue cDNA panel and DNA sequencing. Nesprin-1 PCRs were carried out when UTRs were identified on cDNA panels available at the time and are therefore organised into 3 separate sections. D) Validation and tissue specificity of nesprin-2 UTRs identified on online databases and by RACE were confirmed by PCR amplification from a multiple tissue cDNA panel and DNA sequencing. Nesprin-2 PCRs were carried out when UTRs were identified on cDNA panels available at the time and are therefore organised into 3 separate sections. Small Intestine and Peripheral Blood Lymphocytes have been abbreviated as 'SI' and 'PBL' respectively for all cDNA panels.
doi:10.1371/journal.pone.0040098.g001

p32CH^{Nesp2} was limited to PBL, MBs and U2OS cells (Figure 4F). Unlike p56CH^{Nesp1}, p32CH^{Nesp2} localized to focal adhesions when ectopically expressed in its native U2OS cells (Figure 4E).

Nesprin Central Rod Isoforms

Multiple 5′ and 3′ UTRs were identified in the nesprin-1 gene between exons 83 and 90, suggesting that it is a region where multiple variants are generated (Figure 5A). Using RACE we identified a 5′UTR where the first coding exon was exon 83 (N1-5′E83) and a 3′UTR where the final coding exon was exon 90 (N1-3′E90) (Figure 1A). Furthermore online databases revealed an additional 5′UTR associated with exon 84 (N1-5′E84) and a previously described Kazusa clone KIAA1262. The KIAA1262 sequence includes exons 77 to 87 and terminates in a 3′UTR where the final coding exon is exon 87 (N1-3′E87). The identification of these new UTRs together with the pre-existing nesprin-1$_{\beta1}$ and nesprin-1$_{\beta2}$ 5′UTRs confirms that this is a region of nesprin with the ability to generate multiple alternative transcripts (Figure 5A).

Hypothetically these UTRs could generate 7 nesprin-1 splice variants by alternative initiation and termination of the four 5′UTRs with the three 3′UTRs (Figure 5A). To test this, PCR amplification from 5′ to 3′UTRs were carried out in multiple tissue cDNA panels to see if any of the variant messages were transcribed. p50^{Nesp1} (Accession number JQ740784) expression was ubiquitous while expression of the p41^{Nesp1} (Accession number JQ740786), p31^{Nesp1}(Accession number JQ740785), p23^{Nesp1} (Accession number JQ754364) and p12^{Nesp1} (Accession

Table 1. UTRs identified through online databases.

Gene	UTR	5′ or 3′	Location	NCBI Accession	Verified by PCR
Nesprin-1	N1-5′I14/15	5′	Intron 14–15/	DA151121, CR933676, AK055440, BG197747, DB324328	+
Nesprin-1	N1-3′E18	3′	Exon 18	BC028616, DB545136, DB540697, DB538738	+
Nesprin-1	N1-5′I18/19	5′	Intron 18–19	DA337073	−
Nesprin-1	N1-3′E20	3′	Exon 20	DB540697, DB545136, DB538738	−
Nesprin-1	N1-5′I21/22	5′	Intron 21–22	DA337073	+
Nesprin-1	N1-3′E25	3′	Exon 25	DA151121, CR933676, AK055440, BG197747, DB324328	+
Nesprin-1	N1-3′E37	3′	Exon 37	AL713682	+
Nesprin-1	N1-5′E44	5′	Exon 44	DB300122	−
Nesprin-1	N1-3′E62	3′	Exon 62	BC039121,CA425673,AW300380, BG203678, BG210617, DB516174, CA441052, BX093712,CA312508, DB319424, AA227537,AI866946	+
Nesprin-1	N1-5′E84	5′	Exon 84	BU461222	−
Nesprin-1	N1-3′E87	3′	Exon 87	AB033088	−
Nesprin-1	N1-5′E92	5′	Exon 92	CJ462692, DA229059, DA227411, DA212433, DA509325, DB059554, DA802484, EE366817, DA241105, DA338782, DB289567, DA116814, DA493491	+
Nesprin-1	N1-5′E97	5′	Exon 97	BF740426, BF726175	−
Nesprin-1	N1-5′I128/129	5′	Intron 128–129	AK304825	+
Nesprin-1	N1-5′I132/133	5′	Intron 132–133	DA632075	−
Nesprin-1	N1-5′E138	5′	Exon 138	DA827648	+
Nesprin-2	N2-3′E9	3′	Exon 9	BC042134, BC071873	+
Nesprin-2	N2-3′E46	3′	Exon 46	BX648234	+
Nesprin-2	N2-5′E49	5′	Exon 49	BC036941, BI860943,AA247756	+
Nesprin-2	N2-5′E63	5′	Exon 63	CV571029	−
Nesprin-2	N2-5′I 91/92	5′	Intron 91–92	DA226447	+
Nesprin-2	N2-5′I 99/100	5′	Intron 99–100	DB089560, BM805144, DB088145, DA810994, DA725349, DA101036, DB152052, DA196319, DA706514, DA186088, DA106538, DA093934, DA334037, DA333629, DB063748, DA222451, DA230417, DA097798, DA094004, DA522676	+

Table listing all potential UTRs identified through available online databases.
doi:10.1371/journal.pone.0040098.t001

number JQ754365) variants was restricted to certain tissues. $p30^{Nesp1}$ and $p20^{Nesp1}$ failed to amplify and therefore are probably not expressed (Figure 5A). When $p50^{Nesp1}$ was expressed in U2OS cells it localized to and polymerized microtubules while all the other isoforms displayed a diffuse cytoplasmic and nuclear localization (Figure 5B for Flag- $p50^{Nesp1}$ and Flag- $p31^{Nesp1}$). All other isoforms are shown in Figure S1A). $p23^{Nesp1}$ and $p12^{Nesp1}$ both localized to and disrupted nucleolar morphology when expressed in HDFs, causing fibrillarin to redistribute into peri-nucleolar caps, while the slightly larger $p31^{Nesp1}$ localized with fibrillarin without affecting its localization (Figure 5C). When $p41^{Nesp1}$ was expressed in HDFs, it displayed diffuse cytoplasmic localization and also concentrated around the ER (Figure S1B).

Another central rod variant Nesprin-1 $p55^{Nesp1}$, is composed of a single SR and lacked both the CH and KASH domains (Figure 5D). $p55^{Nesp1}$ was detected in the kidney, spleen and PBL by PCR and displayed diffuse cytoplasmic localization when transfected into U2OS cells (Figure 5D).

Nesprin Isoform Expression is Highly Adaptable

To further confirm the validity of the novel variants and because previous evidence indicates that nesprins have the ability to self-compensate we decided to investigate how knocking down a sub-set of transcripts would effect expression levels of variants encoded by nearby transcripts [30]. By designing an siRNA targeting exon 90 (si-90) we were able to monitor by qRT-PCR the levels of transcripts terminating with N1-3′E87 and N1-3′E90 UTRs (Figure 6). In theory this siRNA should target all transcripts terminating with N1-3′E90 but have no effect on N1-3′E87 terminating transcripts as this termination site is located to the 5′ end on exon 87. As expected, si-90 significantly reduced levels of N1-3′E90 expression but more interestingly also significantly knocked down levels of the transcripts terminating with N1-3′E87. Furthermore si-136, an siRNA designed towards the KASH domain of nesprin-1 increased expression of N1-3′E87 transcripts, showing that perturbations in the expression of one transcript can influence expression of other downstream transcripts. Conversely no change in N1-3′E90 was detected with si-136, however both siRNAs knocked down levels of nesprin-1 KASH expressing transcripts (Figure 6).

Nesprin and Alternative Splicing of Cassette Exons

Next we set out to determine whether any of the 100 plus exons of the nesprin-1 and nesprin-2 genes have the ability to undergo alternative splicing to increase further variant diversity. As a starting point we used nesprin EST and nucleotide databases to look for potential splicing events which identified cassette exons 6′, 93 and 145 for nesprin-1 (Table 2). Exon 6′ is a potential isoform

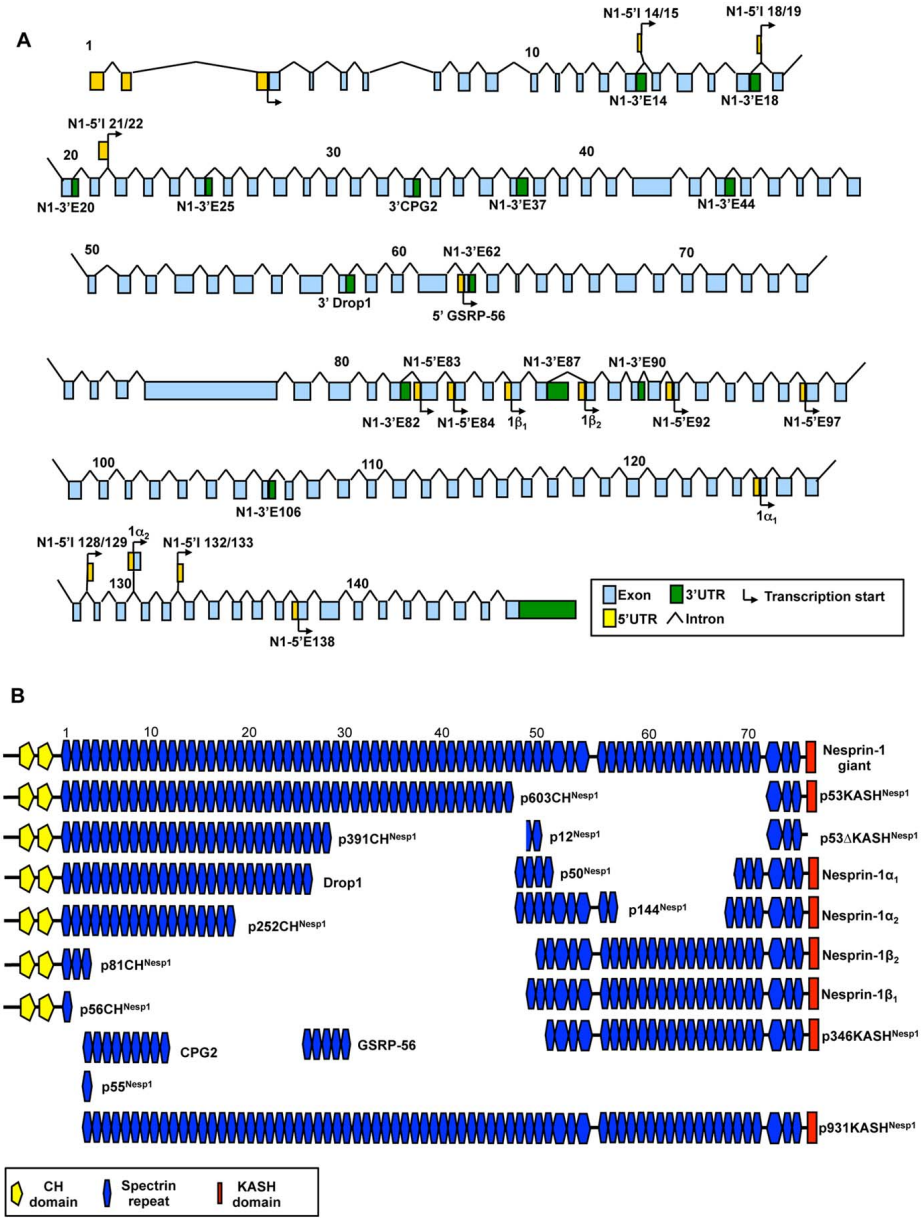
A
1
10
N1-5'I 14/15
N1-5'I 18/19
N1-3'E14
N1-3'E18
N1-5'I 21/22
20
30
40
N1-3'E20
N1-3'E25
3'CPG2
N1-3'E37
N1-3'E44
50
60
N1-3'E62
70
3' Drop1
5' GSRP-56
80
N1-5'E83
N1-3'E87
N1-3'E90
N1-3'E82
N1-5'E84
1β1
1β2
N1-5'E92
N1-5'E97
100
110
120
N1-3'E106
1α1
N1-5'I 128/129
1α2
N1-5'I 132/133
130
140
N1-5'E138
Exon
3'UTR
Transcription start
5'UTR
Intron
B
1
10
20
30
40
50
60
70
Nesprin-1 giant
p603CHNesp1
p53KASHNesp1
p391CHNesp1
p12Nesp1
p53ΔKASHNesp1
Drop1
p50Nesp1
Nesprin-1α1
p144Nesp1
Nesprin-1α2
p252CHNesp1
Nesprin-1β2
p81CHNesp1
Nesprin-1β1
p56CHNesp1
CPG2
GSRP-56
p346KASHNesp1
p55Nesp1
p931KASHNesp1
CH domain
Spectrin repeat
KASH domain

Figure 2. Potential nesprin-1 isoforms. A) Genomic map of the nesprin-1 gene highlighting the positions of the nesprin-1 UTRs identified to date. B) Proposed nesprin-1 isoforms created by alternative transcription. SRs are numbered and shown according to the scheme of *Simpson and Roberts 2008* and are shown to scale.
doi:10.1371/journal.pone.0040098.g002

or tissue specific coding region located between exons 6 and 7 and encodes a 7 amino acid peptide insert at the end of the first CH domain of nesprin-1 (See Figure S2A for nesprin-1 genomic map with cassette exon). Exon 93 contributes an additional 47 amino acids to a SR of the central rod domain while exon 145 encodes a peptide sequence at the C-terminal region of the KASH domain.

Several alternatively spliced exons, were also identified in nesprin-2 using the same data mining procedure, including cassette exons 101′, 107′ and 114 and 5′ alternatively spliced exons 110 to 113 (Table 2). Unlike nesprin-1, the identified exons were all located near the C-terminal half of the nesprin-2 giant. Splicing of exons 101′, 107′, 110 to 113 and 114 would alter the length of the coiled-coil regions surrounding the two SR preceding the KASH domain while removal of the first 31aa encoded by exon 113 would eliminate the final SR before the KASH domain. As with exon 6′ of nesprin-1, exon 101′ and 107′ of nesprin-2 represent coding regions which maybe isoform or tissue specific and are located between exons 101 to 102 and 107 to 108 respectively. (See Figure S2B for nesprin-2 genomic map with cassette exons).

To identify whether these splicing events did indeed take place we designed primers to exons either side of the cassette exons and carried out PCR analysis from U2OS and VSMC cDNA libraries (Figure 7A,B). For nesprin-1, two PCR products appeared from U2OS and VSMC libraries when PCR amplification was carried out across exon 93; the larger of the two bands included exon 93 and the smaller band with the exon excluded. Nesprin-2 splicing showed more tissue specificity than nesprin-1, with PCR products including and excluding cassette exon 107′ expressed in U2OS cells at equal quantities while in VSMCs exon 107′ was exclusively expressed with no band detected for transcripts with the exon excluded expressed. Furthermore in VSMCs, transcripts with exons 110–113 removed were detected as well as transcripts with the exons included, although transcripts with the exons included seem to be transcribed in greater abundance. U2OS cells only expressed transcripts with the exons included.

Although splicing of cassette exons 6′ of nesprin-1 and exon 28–31, 101′ and 114 for nesprin-2 failed to be detected in this set of PCRs, examination of a wider array of cells and tissues is required to determine whether the splicing events listed in the databases occur.

Nesprin ΔKASH Isoforms

The search for potential splicing events for nesprin also revealed splice events that eliminate the KASH domain. Alternative splicing of cassette exon 145 of nesprin-1, results in a frame shift that removes the KASH domain to create Nesprin-1ΔKASH (N1-ΔKASH) (Figure 8A). Though the same 3′UTR adjacent to exon 146 is shared between KASH domain and N1-ΔKASH sequences, the removal of exon 145 results in a change in the open reading frame of N1-ΔKASH variants and therefore they terminate with a novel 11aa tail: VHKRWLRFLPF rather than the RYTNGPPPL sequence utilized by KASH containing variants. Expression of N1-ΔKASH isoforms was detected in all tissue cDNA examined by PCR, suggesting that this splicing and resultant variants are ubiquitously expressed (Figure 8D). When the ΔKASH variant of $p53KASH^{Nesp1}$ ($p53\Delta KASH^{Nesp1}$) lacking exon 145 was transfected into U2OS cells it no longer resided at the NE, but instead displayed strong nuclear matrix localization and weak cytoplasmic staining (Figure 8A).

Unlike N1-ΔKASH, nesprin-2 possesses two mechanisms for creating ΔKASH variants (Figure 8B,C). Like nesprin-1, generation of N2-ΔKASH1 occurs via the removal of cassette exons 110 to 113 but uses the same 3′UTR as the KASH variant. This splicing event results in a change in the ORF and therefore N2-ΔKASH1 terminates with a GIAGHSATPPA amino acid sequence rather than the YPMLRYTNGPPPT sequence used by KASH containing isoforms. N2-ΔKASH2 is created by a novel 3′UTR immediately adjacent to the 3′ end of exon 115. N2-ΔKASH2 splicing truncates larger isoforms without generating a novel C-terminal peptide. The N2-ΔKASH1 splicing was predominantly detected in the brain and kidney with smaller amounts being amplified from the heart, where the lower band represents the removal of the cassette exons promoting N2-ΔKASH1 formation (Figure 8D). The N2-ΔKASH2 termination was detected in the heart and spleen only (Figure 8D).

Discussion

Nesprins as Adaptable, Tissue Specific, Intracellular Scaffolds

This study has demonstrated that nesprins, by generating variants via alternative transcriptional initiation and termination show localizations and therefore functions independent of their original description as NE linkers and scaffolds. Although nesprin-1 has the potential to generate more isoforms than nesprin-2, with more UTRs spread across the gene, the nesprin-2 isoforms are primarily N-terminal truncations that would retain the KASH domain. This suggests that nesprin-1 may have more functions beyond the NE than nesprin-2 or that sequences near the highly conserved C-terminus of nesprin-2 are important for cell function [29]. To our knowledge, the potential combinations of UTRs and exon splicing are unlimited. This combined with the ability of nesprins to dynamically regulate variant expression would allow cells to fine-tune their nesprin isoform repertoire as needed to maintain and restore homeostasis following stress or to regulate tissue-specific signalling pathways [31]. As a proof of principle we were able to show that nesprin transcription appears to be highly adaptable with a feedback loop regulating nesprin variant expression. For example we demonstrate using siRNAs that by knocking down a region of nesprin-1 near the KASH domain we were able to upregulate expression of N1-3′E87 UTR transcripts. Furthermore nesprin-2 CH domain knockout mice display an altered expression pattern for specific nesprin-2 C-terminal isoforms in certain tissues to compensate for the loss of nesprin-2 giant or nesprin-2 actin binding domain isoforms [30]. These observations suggest that nesprin alternative transcript generation is highly flexible and more complex than a simplified tissue-specific expression model.

Generation, Regulation and Function of Novel Tissue Specific Nesprin Variants via Alternative Initiation and Termination

Using 5′ and 3′RACE as well as sequences in the EST database, followed by PCR amplification and DNA sequencing, we identified multiple novel sequence variants for nesprin-1 and -2. RT-PCR was used to establish the existence of mRNA

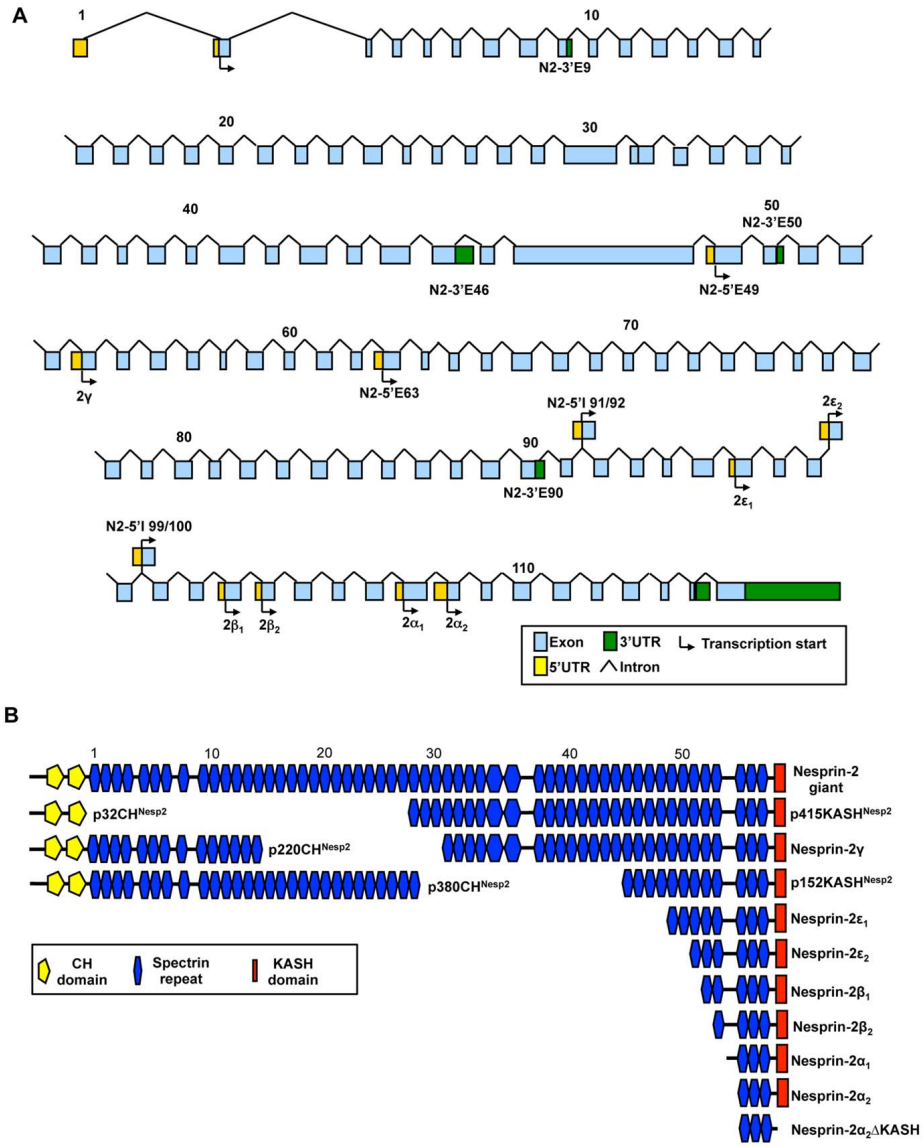

Figure 3. Potential nesprin-2 isoforms. A) Genomic map of the nesprin-2 gene highlighting the positions of the nesprin-1 UTRs identified to date. B) Proposed nesprin-2 isoforms created by alternative transcription. SRs are numbered and shown according to the scheme of *Simpson and Roberts 2008* and are shown to scale.
doi:10.1371/journal.pone.0040098.g003

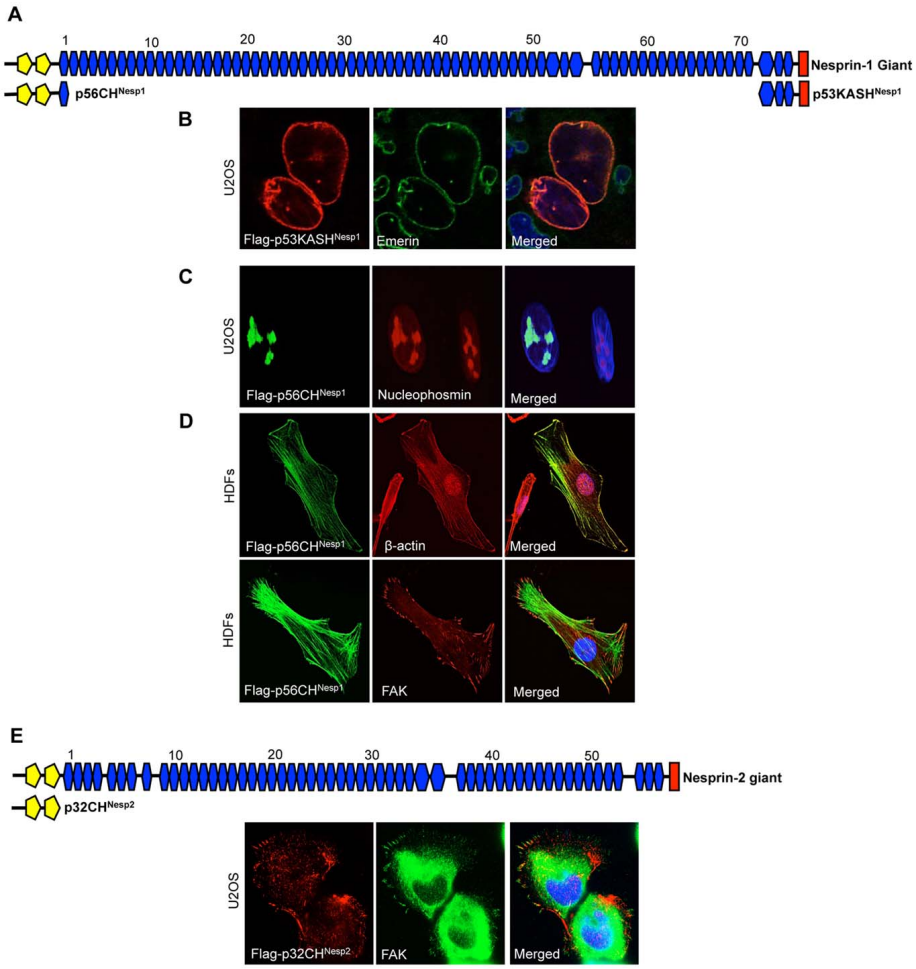
A
1
10
20
30
40
50
60
70
Nesprin-1 Giant
p56CH^Nesp1
p53KASH^Nesp1
B
U2OS
Flag-p53KASH^Nesp1
Emerin
Merged
C
U2OS
Flag-p56CH^Nesp1
Nucleophosmin
Merged
D
HDFs
Flag-p56CH^Nesp1
β-actin
Merged
HDFs
Flag-p56CH^Nesp1
FAK
Merged
E
1
10
20
30
40
50
Nesprin-2 giant
p32CH^Nesp2
U2OS
Flag-p32CH^Nesp2
FAK
Merged

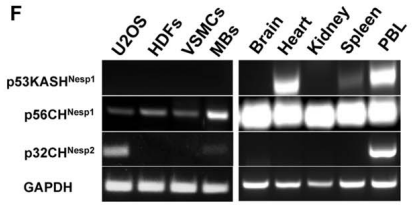
F
U2OS
HDFs
VSMCs
MBs
Brain
Heart
Kidney
Spleen
PBL
p53KASH^Nesp1
p56CH^Nesp1
p32CH^Nesp2
GAPDH

Figure 4. Cloning and expression of novel Nesprin KASH and CH isoforms. A) Schematic representation of p53KASH^{Nesp1} (Accession numberJQ754366) and p56CH^{Nesp1} (Accession number JQ740783) relative to the nesprin-1 giant. B) p53KASH^{Nesp1} localizes to the NE when transfected into U2OS cells. C) Nesprin-1 Flag-p56CH^{Nesp1} localized to the nucleolus when transfected into U2OS cells. D) Nesprin-1 Flag-p56CH^{Nesp1} localizes to actin stress fibres and with Focal Adhesion Kinase (FAK) at focal adhesions when transfected into Human Dermal Fibroblasts (HDFs). E) Nesprin-2 Flag-p32CH^{Nesp2} (Accession numberJQ754367) co-localized with FAK at focal adhesions when transfected into U2OS cells. F) p53KASH^{Nesp1} expression was not detected by PCR in U2OS, Human Dermal Fibroblasts (HDFs), Vascular Smooth Muscle Cells (VSMCs) or Myoblasts (MBs), however it was detected in the heart, spleen and peripheral blood leukocytes (PBL). p56CH^{Nesp1} was detected in all cells and tissues examined whereas p32CH^{Nesp2} was limited to U2OS cells, MBs and PBL.
doi:10.1371/journal.pone.0040098.g004

transcripts for full-length short isoforms or for the novel UTRs of potentially larger variants. The multiple UTRs allow nesprins to express a large number of sequence variants via alternate initiation and termination and many of these were generated in a tissue specific manner. Therefore, in addition to the novel UTR's verified in this study it is likely that by performing RACE in a greater collection of cells/tissues we may be able to identify further nesprin alternate initiation and termination sites.

To date, the mechanisms of tissue specific generation of nesprin variants has not been studied. Analysis of the human transcriptome shows a direct correlation between alternative promoter use and alternative splicing [32]. Alternative promoters can produce mRNAs with different 5′UTRs that encode the same protein, distinct N-termini, and even different proteins from the same locus [33,34,35,36]. The identification of multiple, novel 5′UTRs in both nesprin-1 and -2 indicated the presence of several internal alternative promoters. The existence and regulation of alternative nesprin promoters has not yet been explored but this study suggests that these promoters are utilised in a tissue specific manner. Furthermore, because many individual variants have unique pairs of 5′ and 3′UTRs, additional control and regulation of variant expression can be maintained. The 5′UTR is an important regulator of mRNA translation and can contain regulatory motifs/sequences which affect the rate of translation as well as containing a kozak sequence upstream of the start codon which plays a major role in determining the translational strength of the transcript [37,38]. The 3′UTR of mRNA transcripts can play a role in mRNA localization, stability, and translation [39,40,41,42]. For example, binding of miRNAs to partially complementary sequences in the 3′UTR can result in de-adenylation and translational inhibition or destruction of the target mRNA [43,44]. A RegRNA scan of both the nesprin 5′ and 3′UTRs for regulatory RNA motifs detected several potential miRNA binding sites which were transcript specific and could potentially regulate variant translation (data not shown).

Importantly, we showed that many of the variants generated through retained introns had generated unique peptide sequences. It is highly likely that these sequences expose new functional domains that give the variants additional localization signals or motifs that play an important role in their function. For example, ELM analysis predicts a novel retinoblastoma (Rb) interacting motif found in cell cycle regulatory proteins at the C-terminal end of p220CH^{Nesp2} while the N-terminus of p931KASH^{Nesp1} contains a potential N-myristoylation site, a post-translational modification which facilitates membrane anchoring [45,46,47]. ELM analysis also predicts multiple PKA, MAPK and CDK phosphorylation sites in the unique sequences of p32CH^{Nesp2}, p56CH^{Nesp1} and p55^{Nesp1}. To further explore this hypothesis yeast-2-hybrid analyses or co-immunoprecipitation assays will be required to identify binding partners for specific nesprin variants.

The ultimate validation for each proposed variant will be the detection of their translation and expression by western blotting. Post-translational modifications such as phosphorylation, sumoylation, and enzymatic cleavage may be partially responsible for the range of western bands often visualized using the currently available anti-nesprin antibodies [1,17,48]. Designing isoform-specific antibodies will help to distinguish between modifications and splicing.

Alternative Splicing of Cassette Exons may Diversify Nesprin Function and Localization

In addition to alternative initiation and termination, we showed that some of the cassette exons located in the EST database are indeed valid. It is unclear whether these splice events occur in multiple variants or are isoform specific but they are likely to substantially increase nesprin diversity, likely in a tissue specific manner. This notion was supported by the observation that while some splice events occurred in the majority of cell lines, some events seemed to be cell type specific. For example unlike the nesprin-1 ΔKASH which was detectable in all cells tested, the splicing event of cassette exons which generate nesprin-2 ΔKASH seem to be very tissue specific. Furthermore the ability for nesprin-2 to generate ΔKASH variants via 2 different mechanisms, one by the utilization of a unique 3′UTR and another by the splicing of exons 110–113 suggest that the C-terminal ends of the ΔKASH variants may serve unique tissue specific functions at sites away from the NE.

Although in this study we did not look specifically at the effects of structure, function and localization of nesprin variants with and without alternate splicing of the cassette exons we did show that some of these splicing events also created unique peptides. Nesprin-1 exon 93 encodes a unique 47 amino acid peptide sequence and nesprin-2 exon 107′ encodes a unique 23 amino acid peptide. Although these peptide sequences are not very large they may be capable of encoding novel localization signals or binding sites for interactions with other proteins. Our next aim will be to create nesprin variants with and without these exons so we can identify their putative roles in nesprin function.

However we were able to show that KASH-less nesprin isoforms displayed subcellular localizations which varied depending on the cell lines they were expressed in. In U2OS cells p56CH^{Nesp1} localized to the nucleolus while the same protein localized along actin cables and focal adhesions in HDFs. Currently we do not understand what determines this differential change in subcellular localizations but we speculate that the presence of endogenous p32CH^{Nesp2} at focal adhesions in U2OS cells (p32CH^{Nesp2} is not expressed in HDFs but is expressed in U2OS) is enough for p56CH^{Nesp1} function to become redundant at focal adhesions in U2OS. Furthermore we suspect that differences in the actin cytoskeleton may play a role in differential localization of p56CH^{Nesp1}. The nesprin-1 CH domains contain two nuclear localization signals which may be utilized in cells with low actin levels such as U2OS cells but not in structural cells such as HDFs where there is plenty of actin for the protein to bind to [49]. Alternatively, potential p56CH^{Nesp1} phosphorylation events predicted by ELM analysis may occur in a tissue specific manner which may contribute to the differences seen in localizations between the two cell types. Similarly differential sub-cellular localizations were seen when central rod isoforms p12^{Nesp1},

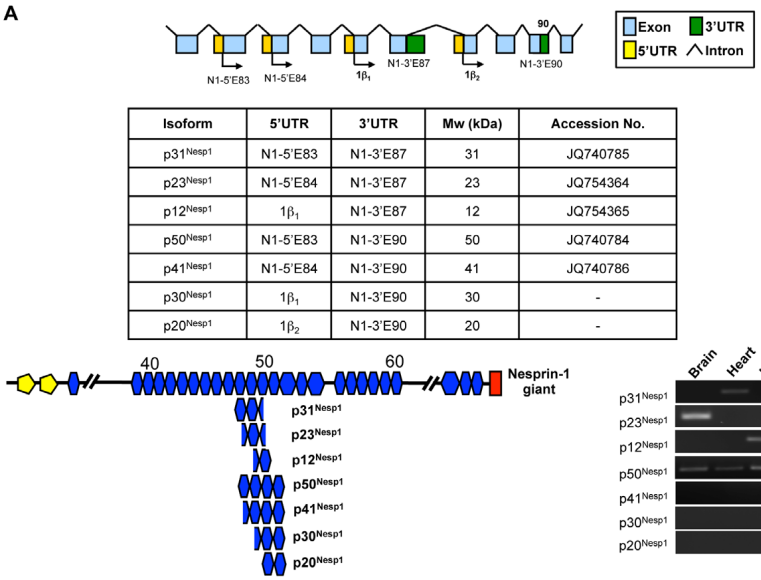

Isoform	5'UTR	3'UTR	Mw (kDa)	Accession No.
p31^{Nesp1}	N1-5'E83	N1-3'E87	31	JQ740785
p23^{Nesp1}	N1-5'E84	N1-3'E87	23	JQ754364
p12^{Nesp1}	1β_1	N1-3'E87	12	JQ754365
p50^{Nesp1}	N1-5'E83	N1-3'E90	50	JQ740784
p41^{Nesp1}	N1-5'E84	N1-3'E90	41	JQ740786
p30^{Nesp1}	1β_1	N1-3'E90	30	-
p20^{Nesp1}	1β_2	N1-3'E90	20	-

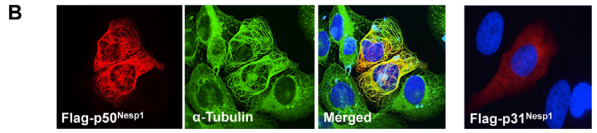

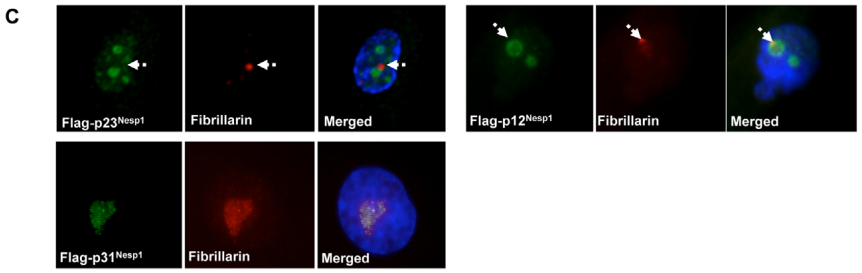

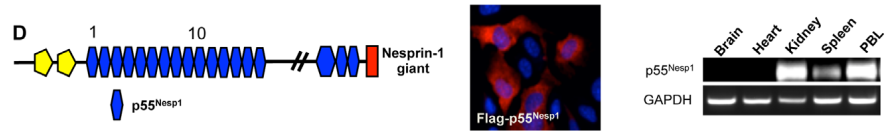

Figure 5. Nesprin-1 Central rod isoforms. A) Nesprin-1 isoforms p31^{Nesp1}, p23 ^{Nesp1}, p12 ^{Nesp1}, p50 ^{Nesp1}, p41 ^{Nesp1}, p30 ^{Nesp1} and p20 ^{Nesp1} are potential variants which could be generated through alternative initiation and termination using UTRs located between exons 83 and 90. All isoforms except p30^{Nesp1} and p20^{Nesp1} PCR amplified from at least one tissue examined. B) p50^{Nesp1} localized to and polymerized microtubules in U2OS cells. p31^{Nesp1} displayed a diffusive localization when transfected into U2OS cells. See Figure S1A for diffusive localization staining of p23^{Nesp1}, p12^{Nesp1} and p41^{Nesp1}. C) p23^{Nesp1} and p12^{Nesp1} promoted nucleolar cap formation in HDFs while p31^{Nesp1} localized to the nucleolus without causing any nucleolar disruption. D) p55^{Nesp1} localized diffusively around the cytosol when transfected into U2OS cells and was detected in the kidney, spleen and peripheral blood leukocytes (PBL) by PCR.
doi:10.1371/journal.pone.0040098.g005

p23^{Nesp1} and p31^{Nesp1}, were transfected into U2OS and HDFs. In U2OS cells all isoforms displayed diffuse cytoplasmic localization while in HDFs nucleolar localization was observed. Differences in post-translational modifications could vary between the two cell lines or the proteins may have different binding partners in each cell line which could contribute to differential localizations. Ultimately the localization of these isoforms would have to be monitored in cells that express the variant endogenously.

Isoforms and Disease

Multiple nesprin mutations have been identified in Emery Dreifuss Muscular Dystrophy (EDMD), Dilated Cardiomyopathies (DCM), autosomal recessive arthrogryposis (ARA) and autosomal recessive cerebellar ataxia (ARCA1) [15,17,18,50,51]. The nesprin mutations promoting EDMD and DCM presumably affect LINC nesprin variants resulting in abnormal nuclear morphology and function.

ARA is caused by an A to G mutation in a splice acceptor site, resulting in retention of intron 136 of nesprin-1 [51]. This mutation produces a premature stop codon and therefore the nesprin-1 giant, nesprin-1β and nesprin-1α isoforms should lack the KASH domain. Conversely these patients appeared to have no defects in nuclear morphology or lamin and emerin localization, suggesting other nesprin gene products or p53KASH^{Nesp1} which should not be effected by this mutation maybe enough to keep the nucleus intact.

ARCA1 is a neurological disease characterized by irregular gait and lack of limb coordination [18]. Five different mutations giving rise to ARCA1 were identified within the central spectrin rod of nesprin-1, upstream of the KASH variants identified so far. The A310067G mutation which effects the invariant A of the AG splice acceptor site at the junction of exon 85 and intron 84 results in the formation of a pre-mature stop codon and therefore will effect production of not only the p40, p50, p31 and p23 nesprin-1 proteins identified in this study but also other variants terminating with the N1-3′E87 and N1-3′E90 ends in there native tissues/cells. Although many diseases associated with nesprins so far suggest that NE nesprins are involved, ARCA1 patients appear to have no nuclear defects, suggesting that nesprin associated signalling pathways beyond the NE may be significantly hindered and potentially causative in the disease.

Materials and Methods

Identification of Novel UTRs

Rapid Amplification of cDNA Ends (RACE) on Brain, HeLa and Skeletal muscle Marathon-Ready cDNA libraries using the Advantage-2 PCR kit (Clontech) and gene specific primers was performed (Table S3). Resultant PCR fragments were cloned into pGEM-T easy vector (Promega) and sequenced (Gene Service). These sequences were then BLASTED against the human genome and novel cDNA ends were further analyzed.

Additional novel UTRs for nesprin-1 and nesprin-2 were identified by screening the NCBI expressed sequence tag (EST) database with consecutive, 500 bp-overlapping 1 kb Nesprin-1 and Nesprin-2 sequences covering the entirety of the giant isoform cDNAs. Tissue specificity of novel UTRs was determined by performing PCR amplification in a multiple tissue cDNA collection (Clontech). 30 PCR cycles were performed on 0.5 ul of cDNA followed by a further 15 cycles on 1 ul of the amplified

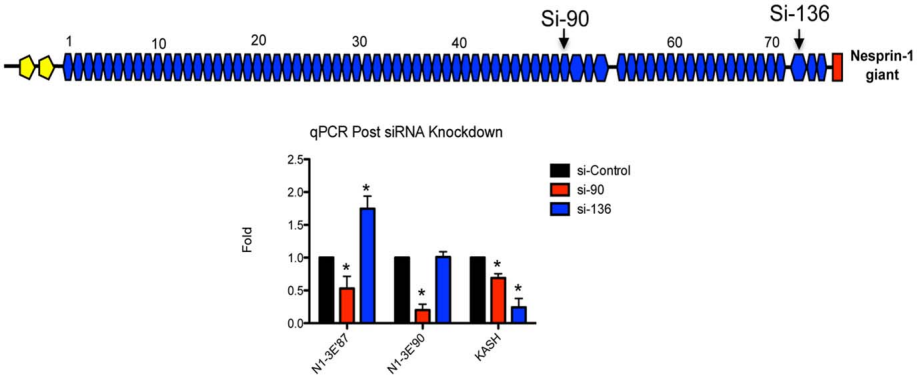

Figure 6. Nesprin-1 expression is highly adaptable. Expression levels of N1-3′E87, N1-3′E90 and nesprin-1 KASH domain were monitored post-siRNA knockdown using siRNAs targeting exons 90 and 136 of the nesprin-1 gene. As demonstrated si-136 increased expression of N1-3′E87 whereas si-90 reduced it's expression. *p<0.01, ANOVA analysis, 95% confidence interval.
doi:10.1371/journal.pone.0040098.g006

Table 2. Cassette exons identified through online databases.

Nesprin	Exon	Splicing	Peptide Sequence	Accession
Nesprin-1	Exon 6′	Cassette	SMHRGSP	CF552114
Nesprin-1	Exon 93	Cassette	MTAGRCHTLLSPVTEESGEEGTNSEISSPPACRSPSPVANTDASVNQ	DB289567, AK310977, CA425673, CA312508, DA809350, DB224830, DA493464
Nesprin-1	Exon 145	Cassette	VHKRWLRFLPF*	BX647837
Nesprin-2	Exons 28–31	Cassette	Premature stop codons	AU185086
Nesprin-2	Exon 101′	Cassette	PTHGVQQKYYLMMTKNAMFIREEVFQFFPMTMHFLFINVIFPKLGN CITIIIKGQDSRDPTSLQATTALAGLYQLGRQGSTARY	CR749324
Nesprin-2	Exon 107′	Cassette	DVEIPENPEAYLKMTTKTLKASS	NM_182914, DA044815, DB138084, DA868743
Nesprin-2	Exons 110–113	Cassette	IRASSPSKVQSSENYRRRGGDREQGPRQHTATALLPLKGGPGSPTPA AAPPAAAAPGLPAALLRRRLQLHSGQQLCPVLLPHAEVHQWATPH IEGIAGHSATPPA*	BM725084
Nesprin-2	Exon 114	Cassette	NPASPLPSFDEVDSGDQPPATSVPAPRAK	BE795270

An online scan of the EST and nucleotide databases indicated that the nesprin-1 and nesprin-2 genes underwent extensive alternative splicing and this was verified using PCR (Figure 7A,B).
*Represents a stop codon for nesprin-1 exon 145 and nesprin-2 exons 110–113.
doi:10.1371/journal.pone.0040098.t002

product. Specificity of the PCR products were validated by DNA sequencing. Primers used for UTR expression can be found in Table S4. Primers used for cassette exon splicing and detection of nesprin ΔKASH variants can be found in Tables S5 and S6 respectively.

Plasmids

Isoforms p53KASH^{Nesp1}, p56CH^{Nesp1} and p50^{Nesp1} were *Taq* PCR amplified from tissue cDNA and cloned into pGEM-T Easy. The pGEM-T plasmids were subsequently used as templates for *Pfu* amplification with primers containing restriction sites and ligated into pCMV-Tag2 vector. p53ΔKASH^{Nesp1} was cloned using inverse PCR with *Pfu* off the Flag-p53KASH^{Nesp1} vector while p50^{Nesp1} served as a template for the inverse PCR and creation of p41^{Nesp1} and p30^{Nesp1}. The Kazusa cDNA clone KIAA1262 served as a template for PCR amplification and cloning of p31^{Nesp1}, p23^{Nesp1} and p12^{Nesp1} into a pCMV-Tag2 (Clontech). p32CH^{Nesp2} was PCR amplified from *IMAGE clone* 5478637 and cloned into pCMV-Tag2 as described.

Tissue culture

Normal human dermal fibroblasts (HDF) and osteosarcoma cells (U2OS) were obtained from American Tissue Culture

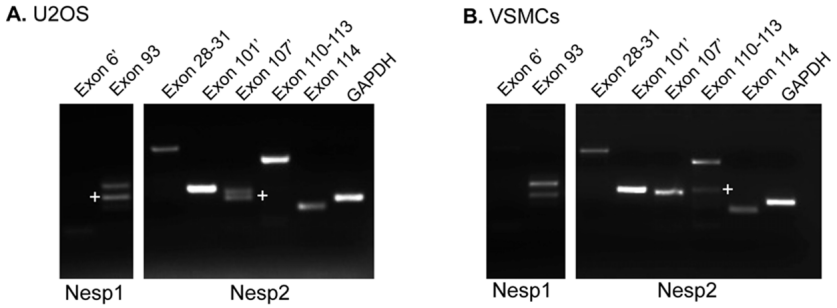

Figure 7. Identification of nesprin-1 and nesprin-2 splicing events. A) PCR amplification across splice sites was carried out from cDNA isolated from U2OS cells. Splicing of exon 93 for nesprin-1 was observed as was the splicing for nesprin-2 exon 107′. B) PCR amplification across splice sites was carried out from cDNA isolated from VSMCs. Splicing of exon 93 for nesprin-1 was observed. Exon 107′ was retained in all nesprin-2 transcripts while splicing of exons 110–113 was also observed in these cells. $^{+}$Represents bands with exon(s) excluded.
doi:10.1371/journal.pone.0040098.g007

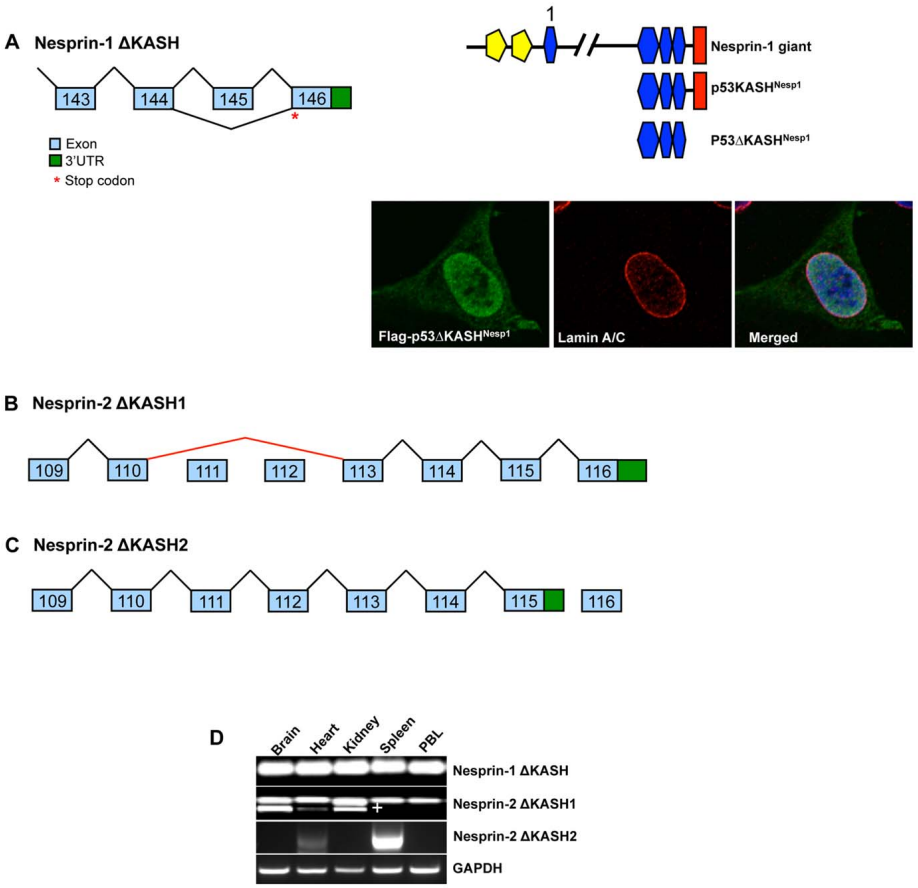

Figure 8. Generation of nesprin-1 and nesprin-2 ΔKASH variants. A) Nesprin-1ΔKASH is generated through the removal of cassette exon 145, resulting in disruption of the KASH domain. Ectopically expressed p53ΔKASH^{Nesp1} fails to localize to the NE in U2OS cells and is strongly concentrated within the nucleus and weakly in the cytosol. B) Nesprin-2ΔKASH1 is generated though the removal of exons 111–112 through the splicing event described in the previous section (splicing shown in red). C) Nesprin-2ΔKASH2 is generated through utilization of an alternative 3′UTR juxtaposed to exon 115. D) PCR-based tissue screen for ΔKASH variants shows that the removal of exon 145 for Nesprin-1ΔKASH is detected in a wide array of tissues. Nesprin-2ΔKASH1 splicing is detected pre-dominantly in the brain and kidney with small amounts also detected in the heart. $^{+}$denotes the spliced Nesprin-2ΔKASH1 product. Nesprin-2ΔKASH2 was detected in the heart and spleen only. Peripheral Blood Leukocytes (PBL).
doi:10.1371/journal.pone.0040098.g008

Collection (ATCC). The cells were passaged after reaching 70% confluency and maintained in DMEM complete media (Sigma) supplemented with 10 units/mL penicillin, 10 mg/mL streptomycin, 200 μM L-glutamine and 10% FBS.

Transfections

For Flag-tagged construct expression, 1×10^6 HDFs or U2OS cells were electroporated with 1 μg plasmid DNA using an Amaxa Nucleofector and cultured on coverslips for 16 hours.

Immunofluorescence

Cells were fixed for 5 minutes in 3.7% paraformaldehyde in PBS followed by 2 min permeabilization with 0.5% NP-40 in PBS. The coverslips were incubated with blocking solution (1% BSA) for 1 hour at RT. The primary antibodies were diluted in blocking solution and applied to the coverslips for 1 hour at RT, followed by a 1 hour RT incubation with fluorescent dye-conjugated secondary antibodies (Invitrogen) diluted in blocking solution. The coverslips were washed with PBS, mounted onto

slides with medium containing DAPI, and visualized using a Leica SP5 confocal microscope or a Zeiss Axioskop microscope.

siRNA Knockdown and qRT-PCR

U2OS cells were transfected with siRNAs for nesprin-1 or control siRNA using hiperfect transfection reagent (Quiagen) as described by the manufacturer. Three days post-transfection total RNA was obtained from cells using Triazole RNA STAT-60 and phenol chloroform extraction. 2 µg of total RNA was reverse transcribed using AMV Reverse Transcriptase (Promega) according to the manufacturer's instructions. qPCR was performed in a 20 µl reaction containing cDNA per 1× SYBR Green PCR master mix (Eurogentec) and 0.1 µM of each primer. PCR products were amplified, N1-3′E87 primers (forward, 5′-TCTCCAAGCTCAATCAGGCAGCAT -3′ and reverse, 5′-CACAGCCCTCTAAGTGTTGTGTCA -3′), N1-3′E90 primers (forward, 5′- AGTTGGACGTCTCAGTCTCAAGGA -3′ and reverse, 5′- TTTGATGGCTGAGCCCACACAATG -3′), KASH primers (forward, 5′-CGAGGCAAGTGTAGTCTCT-CACAG-3′ and reverse, 5′-AGGGCCATTCGTGTATCTGAG-CAT-3′) and GAPDH primers (forward, 5′-CGACCACTTTGT-CAAGCTC-3′ and reverse, 5′-CAAGGGTCTACATGGCAAC-3′). The cycling parameters were 94°C for 15 seconds followed by a single step annealing and extension at 60°C for 60 seconds. Amplifications were performed on RotorGene-3000 (Corbett). Fold changes between samples were calculated by the delta-delta CT method.

Supporting Information

Figure S1 Localizations of $p23^{Nesp1}$, $p12^{Nesp1}$ and $p41^{Nesp1}$. A) $p23^{Nesp1}$, $p12^{Nesp1}$ and $p41^{Nesp1}$ displayed diffusive cytoplasmic localization when transfected into U2OS cells. B) $p41^{Nesp1}$ displayed diffusive localization and concentrated around the ER when transfected into HDFs.
(TIF)

Figure S2 Schematics of nesprin-1 and nesprin-2 cassette exons. A) Nesprin-1 genomic map showing the location of nesprin-1 cassette exon 6′ (Red box). B) Nesprin-2 genomic map showing the location of nesprin-2 cassette exons 101' (orange box) and107' (Purple box).
(TIF)

Table S1 UTR combinations used to generate potential nesprin-1 variants. Nesprin-1 can generate multiple variants through the use of alternative UTRs in a 'mix-and-match' approach. The tables highlight the UTR pairs used to generate the potential isoforms described in Figures 2B.
(DOCX)

Table S2 UTR combinations used to generate potential nesprin-2 variants. Nesprin-2 can generate multiple variants through the use of alternative UTRs in a 'mix-and-match' approach. The tables highlight the UTR pairs used to generate the potential isoforms described in Figures 3B.
(DOCX)

Table S3 Primers used for 5′ and 3′ RACE. Primers and nested primers used for detection of novel nesprin-1 and nesprin-2 cDNA ends.
(DOCX)

Table S4 Primers used for UTR detection. Forward and reverse primers used for detection of novel nesprin-1 and nesprin-2 UTRs. Forward and reverse primers were separated by at least 1 coding exon to control for genomic contamination.
(DOCX)

Table S5 Primers used for detection of cassette exons. Forward and reverse primers used for detection of novel nesprin-1 and nesprin-2 cassette exons.
(DOCX)

Table S6 Primers used for the detection of ΔKASH variants. Forward and reverse primers used for detection of nesprin-1 and nesprin-2 ΔKASH variants.
(DOCX)

Author Contributions

Conceived and designed the experiments: DR JAM FA QZ CMS. Performed the experiments: DR JAM. Analyzed the data: DR JAM FA CMS. Contributed reagents/materials/analysis tools: DR JAM FA QZ CMS. Wrote the paper: DR.

References

1. Zhang Q, Skepper JN, Yang F, Davies JD, Hegyi L, et al. (2001) Nesprins: a novel family of spectrin-repeat-containing proteins that localize to the nuclear membrane in multiple tissues. J Cell Sci 114: 4485–4498.
2. Zhang Q, Ragnauth CD, Skepper JN, Worth NF, Warren DT, et al. (2005) Nesprin-2 is a multi-isomeric protein that binds lamin and emerin at the nuclear envelope and forms a subcellular network in skeletal muscle. J Cell Sci 118: 673–687.
3. Wilhelmsen K, Litjens SH, Kuikman I, Tshimbalanga N, Janssen H, et al. (2005) Nesprin-3, a novel outer nuclear membrane protein, associates with the cytoskeletal linker protein plectin. J Cell Biol 171: 799–810.
4. Roux KJ, Crisp ML, Liu Q, Kim D, Kozlov S, et al. (2009) Nesprin 4 is an outer nuclear membrane protein that can induce kinesin-mediated cell polarization. Proc Natl Acad Sci U S A 106: 2194–2199.
5. Crisp M, Liu Q, Roux K, Rattner JB, Shanahan C, et al. (2006) Coupling of the nucleus and cytoplasm: role of the LINC complex. J Cell Biol 172: 41–53.
6. Stewart-Hutchinson PJ, Hale CM, Wirtz D, Hodzic D (2008) Structural requirements for the assembly of LINC complexes and their function in cellular mechanical stiffness. Exp Cell Res 314: 1892–1905.
7. Zhang Q, Ragnauth C, Greener MJ, Shanahan CM, Roberts RG (2002) The nesprins are giant actin-binding proteins, orthologous to Drosophila melanogaster muscle protein MSP-300. Genomics 80: 473–481.
8. Zhen YY, Libotte T, Munck M, Noegel AA, Korenbaum E (2002) NUANCE, a giant protein connecting the nucleus and actin cytoskeleton. J Cell Sci 115: 3207–3222.
9. Ketema M, Wilhelmsen K, Kuikman I, Janssen H, Hodzic D, et al. (2007) Requirements for the localization of nesprin-3 at the nuclear envelope and its interaction with plectin. J Cell Sci 120: 3384–3394.
10. Hale CM, Shrestha AL, Khatau SB, Stewart-Hutchinson PJ, Hernandez L, et al. (2008) Dysfunctional connections between the nucleus and the actin and microtubule networks in laminopathic models. Biophys J 95: 5462–5475.
11. Lammerding J, Schulze PC, Takahashi T, Kozlov S, Sullivan T, et al. (2004) Lamin A/C deficiency causes defective nuclear mechanics and mechanotransduction. J Clin Invest 113: 370–378.
12. Lammerding J, Hsiao J, Schulze PC, Kozlov S, Stewart CL, et al. (2005) Abnormal nuclear shape and impaired mechanotransduction in emerin-deficient cells. J Cell Biol 170: 781–791.
13. Verstraeten VL, Ji JY, Cummings KS, Lee RT, Lammerding J (2008) Increased mechanosensitivity and nuclear stiffness in Hutchinson-Gilford progeria cells: effects of farnesyltransferase inhibitors. Aging Cell 7: 383–393.
14. Fairley EA, Kendrick-Jones J, Ellis JA (1999) The Emery-Dreifuss muscular dystrophy phenotype arises from aberrant targeting and binding of emerin at the inner nuclear membrane. J Cell Sci 112 (Pt 15): 2571–2582.
15. Puckelwartz MJ, Kessler E, Zhang Y, Hodzic D, Randles KN, et al. (2009) Disruption of nesprin-1 produces an Emery Dreifuss muscular dystrophy-like phenotype in mice. Hum Mol Genet 18: 607–620.
16. Raffaele Di Barletta M, Ricci E, Galluzzi G, Tonali P, Mora M, et al. (2000) Different mutations in the LMNA gene cause autosomal dominant and autosomal recessive Emery-Dreifuss muscular dystrophy. Am J Hum Genet 66: 1407–1412.

17. Zhang Q, Bethmann C, Worth NF, Davies JD, Wasner C, et al. (2007) Nesprin-1 and -2 are involved in the pathogenesis of Emery Dreifuss muscular dystrophy and are critical for nuclear envelope integrity. Hum Mol Genet 16: 2816–2833.
18. Gros-Louis F, Dupre N, Dion P, Fox MA, Laurent S, et al. (2007) Mutations in SYNE1 lead to a newly discovered form of autosomal recessive cerebellar ataxia. Nat Genet 39: 80–85.
19. Lindholm E, Ekholm B, Shaw S, Jalonen P, Johansson G, et al. (2001) A schizophrenia-susceptibility locus at 6q25, in one of the world's largest reported pedigrees. Am J Hum Genet 69: 96–105.
20. Tessema M, Willink R, Do K, Yu YY, Yu W, et al. (2008) Promoter methylation of genes in and around the candidate lung cancer susceptibility locus 6q23–25. Cancer Res 68: 1707–1714.
21. Warren DT, Tajsic T, Mellad JA, Searles R, Zhang Q, et al. (2010) Novel nuclear nesprin-2 variants tether active extracellular signal-regulated MAPK1 and MAPK2 at promyelocytic leukemia protein nuclear bodies and act to regulate smooth muscle cell proliferation. J Biol Chem 285: 1311–1320.
22. Gough LL, Fan J, Chu S, Winnick S, Beck KA (2003) Golgi localization of Syne-1. Mol Biol Cell 14: 2410–2424.
23. Gough LL, Beck KA (2004) The spectrin family member Syne-1 functions in retrograde transport from Golgi to ER. Biochim Biophys Acta 1693: 29–36.
24. Kobayashi Y, Katanosaka Y, Iwata Y, Matsuoka M, Shigekawa M, et al. (2006) Identification and characterization of GSRP-56, a novel Golgi-localized spectrin repeat-containing protein. Exp Cell Res 312: 3152–3164.
25. Dou Y, Milne TA, Tackett AJ, Smith ER, Fukuda A, et al. (2005) Physical association and coordinate function of the H3 K4 methyltransferase MLL1 and the H4 K16 acetyltransferase MOF. Cell 121: 873–885.
26. Marme A, Zimmermann HP, Moldenhauer G, Schorpp-Kistner M, Muller C, et al. (2008) Loss of Drop1 expression already at early tumor stages in a wide range of human carcinomas. Int J Cancer 123: 2048–2056.
27. Nedivi E, Fieldust S, Theill LE, Hevron D (1996) A set of genes expressed in response to light in the adult cerebral cortex and regulated during development. Proc Natl Acad Sci U S A 93: 2048–2053.
28. Cottrell JR, Borok E, Horvath TL, Nedivi E (2004) CPG2: a brain- and synapse-specific protein that regulates the endocytosis of glutamate receptors. Neuron 44: 677–690.
29. Simpson JG, Roberts RG (2008) Patterns of evolutionary conservation in the nesprin genes highlight probable functionally important protein domains and isoforms. Biochem Soc Trans 36: 1359–1367.
30. Luke Y, Zaim H, Karakesisoglou I, Jaeger VM, Sellin L, et al. (2008) Nesprin-2 Giant (NUANCE) maintains nuclear envelope architecture and composition in skin. J Cell Sci 121: 1887–1898.
31. Kandert S, Luke Y, Kleinhenz T, Neumann S, Lu W, et al. (2007) Nesprin-2 giant safeguards nuclear envelope architecture in LMNA S143F progeria cells. Hum Mol Genet 16: 2944–2959.
32. Xin D, Hu L, Kong X (2008) Alternative promoters influence alternative splicing at the genomic level. PLoS One 3: e2377.
33. Pecci A, Viegas LR, Baranao JL, Beato M (2001) Promoter choice influences alternative splicing and determines the balance of isoforms expressed from the mouse bcl-X gene. J Biol Chem 276: 21062–21069.
34. Shmelkov SV, Jun L, St Clair R, McGarrigle D, Derderian CA, et al. (2004) Alternative promoters regulate transcription of the gene that encodes stem cell surface protein AC133. Blood 103: 2055–2061.
35. Zaika AI, Slade N, Erster SH, Sansome C, Joseph TW, et al. (2002) DeltaNp73, a dominant-negative inhibitor of wild-type p53 and TAp73, is up-regulated in human tumors. J Exp Med 196: 765–780.
36. Quelle DE, Zindy F, Ashmun RA, Sherr CJ (1995) Alternative reading frames of the INK4a tumor suppressor gene encode two unrelated proteins capable of inducing cell cycle arrest. Cell 83: 993–1000.
37. Vagner S, Waysbort A, Marenda M, Gensac MC, Amalric F, et al. (1995) Alternative translation initiation of the Moloney murine leukemia virus mRNA controlled by internal ribosome entry involving the p57/PTB splicing factor. J Biol Chem 270: 20376–20383.
38. Melefors O, Hentze MW (1993) Iron regulatory factor–the conductor of cellular iron regulation. Blood Rev 7: 251–258.
39. Eldad N, Yosefzon Y, Arava Y (2008) Identification and characterization of extensive intra-molecular associations between 3′-UTRs and their ORFs. Nucleic Acids Res 36: 6728–6738.
40. Aronov S, Aranda G, Behar L, Ginzburg I (2001) Axonal tau mRNA localization coincides with tau protein in living neuronal cells and depends on axonal targeting signal. J Neurosci 21: 6577–6587.
41. Tanguay RL, Gallie DR (1996) Translational efficiency is regulated by the length of the 3′ untranslated region. Mol Cell Biol 16: 146–156.
42. Loya A, Pnueli L, Yosefzon Y, Wexler Y, Ziv-Ukelson M, et al. (2008) The 3′-UTR mediates the cellular localization of an mRNA encoding a short plasma membrane protein. RNA 14: 1352–1365.
43. Mathonnet G, Fabian MR, Svitkin YV, Parsyan A, Huck L, et al. (2007) MicroRNA inhibition of translation initiation in vitro by targeting the cap-binding complex eIF4F. Science 317: 1764–1767.
44. Fabian MR, Andrew White K (2007) Extracting viral RNAs from plant protoplasts. Curr Protoc Microbiol Chapter 16: Unit 16E 11.
45. Dahiya A, Gavin MR, Luo RX, Dean DC (2000) Role of the LXCXE binding site in Rb function. Mol Cell Biol 20: 6799–6805.
46. Utsumi T, Sato M, Nakano K, Takemura D, Iwata H, et al. (2001) Amino acid residue penultimate to the amino-terminal gly residue strongly affects two cotranslational protein modifications, N-myristoylation and N-acetylation. J Biol Chem 276: 10505–10513.
47. Koutelou E, Sato S, Tomomori-Sato C, Florens L, Swanson SK, et al. (2008) Neuralized-like 1 (Neurl1) targeted to the plasma membrane by N-myristoylation regulates the Notch ligand Jagged1. J Biol Chem 283: 3846–3853.
48. Dawe HR, Adams M, Wheway G, Szymanska K, Logan CV, et al. (2009) Nesprin-2 interacts with meckelin and mediates ciliogenesis via remodelling of the actin cytoskeleton. J Cell Sci 122: 2716–2726.
49. Padmakumar VC, Abraham S, Braune S, Noegel AA, Tunggal B, et al. (2004) Enaptin, a giant actin-binding protein, is an element of the nuclear membrane and the actin cytoskeleton. Exp Cell Res 295: 330–339.
50. Nikolova-Krstevski V, Leimena C, Xiao XH, Kesteven S, Tan JC, et al. (2011) Nesprin-1 and actin contribute to nuclear and cytoskeletal defects in lamin A/C-deficient cardiomyopathy. J Mol Cell Cardiol 50: 479–486.
51. Attali R, Warwar N, Israel A, Gurt I, McNally E, et al. (2009) Mutation of SYNE-1, encoding an essential component of the nuclear lamina, is responsible for autosomal recessive arthrogryposis. Hum Mol Genet 18: 3462–3469.

Appendix II: Nesprin-1 variant accession numbers

Nucleotide

Display Settings: GenBank

Homo sapiens clone p56CHNesp1a nesprin-1 (SYNE1) mRNA, complete cds, alternatively spliced

GenBank: JQ740783.1

FASTA Graphics

Go to:

```
LOCUS       JQ740783               2720 bp    mRNA    linear   PRI 16-JUL-2012
DEFINITION  Homo sapiens clone p56CHNesp1a nesprin-1 (SYNE1) mRNA, complete
            cds, alternatively spliced.
ACCESSION   JQ740783
VERSION     JQ740783.1  GI:394999649
KEYWORDS    .
SOURCE      Homo sapiens (human)
  ORGANISM  Homo sapiens
            Eukaryota; Metazoa; Chordata; Craniata; Vertebrata; Euteleostomi;
            Mammalia; Eutheria; Euarchontoglires; Primates; Haplorrhini;
            Catarrhini; Hominidae; Homo.
REFERENCE   1  (bases 1 to 2720)
  AUTHORS   Rajgor,D., Mellad,J.A., Autore,F., Zhang,Q. and Shanahan,C.M.
  TITLE     Multiple novel nesprin-1 and nesprin-2 variants act as versatile
            tissue-specific intracellular scaffolds
  JOURNAL   PLoS ONE 7 (7), E40098 (2012)
   PUBMED   22768332
  REMARK    Publication Status: Online-Only
REFERENCE   2  (bases 1 to 2720)
  AUTHORS   Rajgor,D., Mellad,J.A. and Shanahan,C.M.
  TITLE     Direct Submission
  JOURNAL   Submitted (02-MAR-2012) Cardiovascular Division, King's College
            London, 125 Coldharbour Lane, James Black Centre, London SE5 9NU,
            UK
COMMENT     ##Assembly-Data-START##
            Assembly Method       :: Chromas v. 2.33
            Sequencing Technology :: Sanger dideoxy sequencing
            ##Assembly-Data-END##
FEATURES             Location/Qualifiers
     source          1..2720
                     /organism="Homo sapiens"
                     /mol_type="mRNA"
                     /db_xref="taxon:9606"
                     /clone="p56CHNesp1a"
     gene            1..2720
                     /gene="SYNE1"
     5'UTR           1..602
                     /gene="SYNE1"
     CDS             603..2087
                     /gene="SYNE1"
                     /note="transcribed off the same promoter as the nesprin-1
                     giant but terminates with a stop; alternatively spliced"
                     /codon_start=1
                     /product="nesprin-1"
                     /protein_id="AFN44378.1"
                     /db_xref="GI:394999650"
                     /translation="MATSRGASRCPRDIANVMQRLQDEQEIVQKRTFTKWINSHLAKR
                     KPPMVVDDLFEDMKDGVKLLALLEVLSGQKLPCEQGRRMKRIHAVANIGTALKFLEGR
                     KSMHRGSPIKLVNINSTDIADGRPSIVLGLMWTIILYFQIEELTSNLPQLQSLSSSAS
                     SVDSIVSSETPSPPSKRKVTTKIQGNAKKALLKWVQYTAGKQTGIEVKDFGKSWRSGV
                     AFHSVIHAIRPELVDLETVKGRSNRENLEDAFTIAETELGIPRLLDPEDVDVDKPDEK
                     SIMTYVAQFLKHYPDIHNASTDGQEDDEILPGFPSFANSVQNFKREDRVIFKEMKVWI
                     EQFERDLTRAQMVESNLQDKYQSFKHFRVQYEMKRKQIEHLIQPLHRDGKLSLDQALV
                     KQSWDRVTSRLFDWHIQLDKSLPAPLGTIGAWLYRAEVALREEITVQQVHEETANTIQ
                     RKLEQHKKIEAIRKELPPAPTATSTHLRNCICARIHALHFCYYG"
     3'UTR           2088..2720
                     /gene="SYNE1"
     polyA_signal    2686..2720
                     /gene="SYNE1"
ORIGIN
        1 cccgggcagt ggaaaccgtg ggcaaaagtt agctggcagg acagcgcagc tcctccaggc
       61 agcggaggca gcgcgtcccg gctctcaggg acatttcctt cccacctcga ccccgcggag
```

```
      121 gtggtcccgg tataaaggct cgctgagcgg gtgggtcaca gcacagcttt gcagctgcgg
      181 agaaacgccc aaggccgtgc atctccagga gggcggctgg gctcccgcag tcctgcagac
      241 cgcgcccgat cccggcgaca gggcgggcgg acagccgcgc atccccgggg tcccgccgag
      301 cctgggcgca gagagccggg aggaagcgtt cgctcgcttc gccttgctgc tgggaaactg
      361 aacgaggccg agagagaagg ttcttgagtt catgtaagag gacagtctta aaacggaaga
      421 agaaaaagaa gcagttcagt ctttgggaga gctgcctcct tgttgagtgc tgcaaaggcc
      481 tggaattcat ttatgacaga atagatctag aaaagtccaa gcatgttttc tagagtggtg
      541 tagccctgtg ctgcctccag tgaagagtct cttggtgttg gcttcgtgct tccggaggga
      601 ccatggcaac ctccagaggg gcctcccggt gtcctcggga tatcgccaat gtgatgcaga
      661 ggctgcaaga tgagcaagag atagtacaaa aacgaacttt cacaaaatgg atcaactctc
      721 atctggccaa gcggaaacct ccaatggtgg tggacgatct ttttgaagac atgaaagatg
      781 gtgttaaact gcttgccctt ctggaggtcc tgtctgggca gaaactgcct tgtgaacaag
      841 gacgccggat gaagcgaatc catgctgtgg ctaacattgg cacggcactc aagttcctcg
      901 aaggaagaaa gtccatgcac agaggatcac cgattaaatt agtcaacatt aactccaccg
      961 atatagctga tggccgaccc tcaatagttc ttggattgat gtggaccatt attctatatt
     1021 tccagattga agagttgacc agcaacctgc cccagctcca gtctttgtcc agcagcgcat
     1081 cctccgtgga cagcatagtt agctctgaga ctcccagccc accaagtaaa cggaaggtga
     1141 ccaccaagat ccaaggaaat gctaagaagg ctttattaaa gtgggttcag tacacagctg
     1201 gcaagcagac tggaatagaa gtaaaagatt ttgggaagag ttggagaagc ggggttgcct
     1261 ttcattcagt tattcatgcc attcgaccgg aattggtgga cttggagaca gtgaaaggca
     1321 gatccaaccg agaaaatttg gaggatgctt tcactatcgc cgaaacagaa ctggggatcc
     1381 caagactgct agatcctgaa gacgttgatg tggataaacc agatgagaaa tctattatga
     1441 cctatgtagc ccagtttctg aaacattatc ctgacatcca caatgcaagc actgatgggc
     1501 aagaggatga tgaaatactt ccaggtttcc catcttttgc aaattctgta caaaatttta
     1561 agagagaaga cagagtaatt tttaaggaaa tgaaagtttg gatagaacaa tttgagagag
     1621 atttgacaag agcacagatg gtggaatcaa atttacagga taaatatcag tcatttaagc
     1681 acttcagagt tcaatatgaa atgaagagga aacagattga acatttaata caaccattac
     1741 acagagacgg taaattgtca cttgaccaag cattggtaaa acaatcttgg gatagagtga
     1801 cctccaggct ctttgactgg catatacagc ttgataaatc tcttcctgca cctctgggca
     1861 ccataggtgc ctggctgtac agagcggagg tggccctgag agaggaaata accgttcaac
     1921 aggtccacga ggaaacagca aacacgatac aacggaaact tgagcaacat aagaaaatag
     1981 aagcaatcag aaaagaattg ccaccagctc ccacggccac atcaacccac ctacgcaatt
     2041 gcatctgtgc ccgaatacac gctcttcact tctgttacta tgggtgaacc atctgtgctc
     2101 tgggccgagg ccaacctctc tatgtgtaca ttagatccca ccctctctcc aaaaggtaat
     2161 tcctgtcctt cctcccttct ctatttttt ctctttcttt ctttgttgga gtttactcat
     2221 ccacatacaa atatgctgcc attaactcat ctttaaaagt ctttttctta gccccacttc
     2281 ccctcccagc tactgtccaa ttttcttcct tccttttaca gcaaagctct ttgagagaat
     2341 tggctctttc ttctttctaa attctcttct ctcattcttt ctaaaatcca ttccaatcaa
     2401 gcttttatct tgccatctac catgtgaagt ttaccaggct ttgcctcatt cctcatccaa
     2461 tggccagttc tcagtcttct tacatcacct gtcacaaaca tttcacatag ttgtcccttt
     2521 acccttgaaa gactttcttt aaggcatggt ggctcatact tataatccca gcatgttgag
     2581 aagccaaggc aggaggagca catgagtcca gaagtttgag accaacctgg ccaacaaagc
     2641 gagactctgt ctctacaaaa aataaaaata aaaaattagg catagtggaa aaaaaaaaaa
     2701 aaaaaaaaaa aaaaaaaaaa
//
```

Nucleotide

Display Settings: GenBank

Homo sapiens clone p50Nesp1c nesprin-1 (SYNE1) mRNA, complete cds, alternatively spliced

GenBank: JQ740784.1

FASTA Graphics

Go to:

```
LOCUS       JQ740784               1672 bp    mRNA    linear   PRI 16-JUL-2012
DEFINITION  Homo sapiens clone p50Nesp1c nesprin-1 (SYNE1) mRNA, complete cds,
            alternatively spliced.
ACCESSION   JQ740784
VERSION     JQ740784.1  GI:394999651
KEYWORDS    .
SOURCE      Homo sapiens (human)
  ORGANISM  Homo sapiens
            Eukaryota; Metazoa; Chordata; Craniata; Vertebrata; Euteleostomi;
            Mammalia; Eutheria; Euarchontoglires; Primates; Haplorrhini;
            Catarrhini; Hominidae; Homo.
REFERENCE   1  (bases 1 to 1672)
  AUTHORS   Rajgor,D., Mellad,J.A., Autore,F., Zhang,Q. and Shanahan,C.M.
  TITLE     Multiple novel nesprin-1 and nesprin-2 variants act as versatile
            tissue-specific intracellular scaffolds
  JOURNAL   PLoS ONE 7 (7), E40098 (2012)
   PUBMED   22768332
  REMARK    Publication Status: Online-Only
REFERENCE   2  (bases 1 to 1672)
  AUTHORS   Rajgor,D., Mellad,J.A. and Shanahan,C.M.
  TITLE     Direct Submission
  JOURNAL   Submitted (02-MAR-2012) Cardiovascular Division, King's College
            London, 125 Coldharbour Lane, James Black Centre, London SE5 9NU,
            UK
COMMENT     ##Assembly-Data-START##
            Assembly Method       :: Chromas v. 2.33
            Sequencing Technology :: Sanger dideoxy sequencing
            ##Assembly-Data-END##
FEATURES             Location/Qualifiers
     source          1..1672
                     /organism="Homo sapiens"
                     /mol_type="mRNA"
                     /db_xref="taxon:9606"
                     /clone="p50Nesp1c"
     gene            1..1672
                     /gene="SYNE1"
     5'UTR           1..78
                     /gene="SYNE1"
                     /note="N1-5'E83 UTR utilised by this nesprin-1 variant is
                     generated through alternative initiation of the nesprin-1
                     giant; first coding exon is exon 83 of the nesprin-1
                     giant"
     CDS             79..1389
                     /gene="SYNE1"
                     /note="alternatively spliced"
                     /codon_start=1
                     /product="nesprin-1"
                     /protein_id="AFN44379.1"
                     /db_xref="GI:394999652"
                     /translation="MQEKVKTNGKLVKQELKDREMVETQINSVKCWVQETKEYLGNPT
                     IEIDAQLEELQILLTEATNHRQNIEKMAEEQKEKYLGLYTILPSELSLQLAEVALDLK
                     IRDQIQDKIKEVEQSKATSQELSRQIQKLAKDLTTILTKLKAKTDNVVQAKTDQKVLG
                     EELDGCNSKLMELDAAVQKPLEQNGQLGKPLAKKIGKLTELHQQTIRQAENRLSKLNQ
                     AASHLEEYNEMLELILKWIEKAKVLAHGTIAMNSASQLREQYILHQTLLEESKEIDSE
                     LEAMTEKLQYLTSVYCTEKMSQQVAELGRETEELRQMIKIRLQNLQDAAKDMKKFEAE
                     LKKLQAALEQAQATLTSPEVGRLSLKEQLSHRQHLLSEMESLKPKVQAVQLCQSALRI
                     PEDVVASLPLCHAALRLQEEASRLQHTAIQQCNIMQAGAGYPHQ"
     3'UTR           1390..1672
                     /gene="SYNE1"
                     /note="terminates with the N1-3'E90 UTR where the last
                     coding exon is exon 90 plus an additional peptide sequence
                     generated through the exon extension of exon 90"
     polyA_signal    1630..1672
```

```
                     /gene="SYNE1"
ORIGIN
        1 tattggataa aatgttgcca agtattaggg ggttcctttc acttcacttc tgttttatcc
       61 ctgtaatgtt tctgaagcat gcaggagaaa gtgaagacta atggaaagtt ggtgaagcaa
      121 gagctgaagg accgagaaat ggtggagact cagatcaatt ctgtgaaatg ttgggttcag
      181 gaaacgaaag aatatttagg gaatccaaca atagaaatag atgctcaact tgaagaactt
      241 cagattctcc taacagaagc cacaaatcac cgacagaaca ttgaaaaaat ggcagaagaa
      301 cagaaggaga agtacttagg tctttatacc atattacctt ctgaactctc ccttcagttg
      361 gctgaagtgg cgttagatct aaagatccga gatcagatcc aagacaaaat aaaagaagtt
      421 gagcagagca aggccacgag ccaggaactc agccggcaaa ttcagaagtt agctaaagac
      481 ctcacaacta ttctaactaa gctgaaagcg aagacagata atgtagttca agctaaaact
      541 gaccaaaagg tgctgggaga ggaattagat ggctgtaatt caaagttaat ggaattagat
      601 gcagcagtac agaaattctt ggaacagaat ggccaactgg gtaagccact ggccaagaag
      661 ataggaaaac tgactgaact tcaccagcag accattagac aagctgagaa tcggctctcc
      721 aagctcaatc aggcagcatc acatttagaa gaatacaatg aaatgcttga attaattttg
      781 aagtggattg aaaaagctaa agtcttggct catggaacta ttgcatggaa ttctgcaagc
      841 cagcttcggg aacaatatat tttgcatcag accctgctag aagaatccaa agaaattgac
      901 agtgagctgg aagcaatgac tgagaaatta cagtacctca ctagcgtgta ctgtacagaa
      961 aaaatgtctc agcaagtggc agaactggga cgggagactg aggagttgcg acagatgatc
     1021 aaaattcgtt tgcagaacct ccaagatgca gctaaggata tgaaaaaatt tgaagcagag
     1081 ttgaaaaagt tacaagctgc cttggagcaa gcccaggcaa cactgacttc tccagaagtt
     1141 ggacgtctca gtctcaagga gcagctctct catcggcagc atttgttgtc tgagatggag
     1201 tcactgaagc cgaaggtgca agcagtgcag ctctgccaga gtgccctccg gatccccgag
     1261 gatgtggttg ccagcttacc tctctgtcat gctgctctgc ggctgcagga agaggccagc
     1321 cggctgcagc acaccgccat ccagcagtgt aacatcatgc aggcaggtgc agggtaccca
     1381 caccagtaga gcaattgctg atgaatcatg ggcttctttt cttagcattg tgtgggctca
     1441 gccatcaaaa cacatccagg gtgttgaatc tgacaggctg ttgtggtttt ataaaataag
     1501 gagattaaaa tgctgtcatt tggatcaccc acaaaagcct ggggaatgct atataaaaaa
     1561 tatccttggt gaaaattatc ttttagtgat atttttaaat aaataacttg taaagattaa
     1621 ttttctatga aaaaaaaaaa aaaaaaaaaa aaaaaaaaaa aaaaaaaaaa aa
//
```

Nucleotide

Display Settings: GenBank

Homo sapiens clone p41Nesp1a nesprin-1 (SYNE1) mRNA, complete cds, alternatively spliced

GenBank: JQ740786.1

FASTA Graphics

Go to:

```
LOCUS       JQ740786               1583 bp    mRNA    linear   PRI 16-JUL-2012
DEFINITION  Homo sapiens clone p41Nesp1a nesprin-1 (SYNE1) mRNA, complete cds,
            alternatively spliced.
ACCESSION   JQ740786
VERSION     JQ740786.1  GI:394999655
KEYWORDS    .
SOURCE      Homo sapiens (human)
  ORGANISM  Homo sapiens
            Eukaryota; Metazoa; Chordata; Craniata; Vertebrata; Euteleostomi;
            Mammalia; Eutheria; Euarchontoglires; Primates; Haplorrhini;
            Catarrhini; Hominidae; Homo.
REFERENCE   1  (bases 1 to 1583)
  AUTHORS   Rajgor,D., Mellad,J.A., Autore,F., Zhang,Q. and Shanahan,C.M.
  TITLE     Multiple novel nesprin-1 and nesprin-2 variants act as versatile
            tissue-specific intracellular scaffolds
  JOURNAL   PLoS ONE 7 (7), E40098 (2012)
   PUBMED   22768332
  REMARK    Publication Status: Online-Only
REFERENCE   2  (bases 1 to 1583)
  AUTHORS   Rajgor,D., Mellad,J.A. and Shanahan,C.M.
  TITLE     Direct Submission
  JOURNAL   Submitted (02-MAR-2012) Cardiovascular Division, King's College
            London, 125 Coldharbour Lane, James Black Centre, London SE5 9NU,
            UK
COMMENT     ##Assembly-Data-START##
            Assembly Method       :: Chromas v. 2.33
            Sequencing Technology :: Sanger dideoxy sequencing
            ##Assembly-Data-END##
FEATURES             Location/Qualifiers
     source          1..1583
                     /organism="Homo sapiens"
                     /mol_type="mRNA"
                     /db_xref="taxon:9606"
                     /clone="p41Nespla"
     gene            1..1583
                     /gene="SYNE1"
     5'UTR           1..199
                     /gene="SYNE1"
     CDS             200..1300
                     /gene="SYNE1"
                     /note="alternatively spliced"
                     /codon_start=1
                     /product="nesprin-1"
                     /protein_id="AFN44181.1"
                     /db_xref="GI:394999656"
                     /translation="MAEEQKEKYLGLYTILPSELSLQLAEVALDLKIRDQIQDKIKEV
                     EQSKATSQELSRQIQKLAKDLTTILTKLKAKTDNVVQAKTDQKVLGEELDGCNSKLME
                     LDAAVQKFLEQNGQLGKPLAKKIGKLTELHQQTIRQAENRLSKLNQAASHLEEYNEML
                     ELILKWIEKAKVLAHGTIAWNSASQLREQYILHQTLLEESKEIDSELEAMTEKLQYLT
                     SVYCTEKMSQQVAELGRETEELRQNIKIRLQNLQDAAKDMKKFEAELKKLQAALEQAQ
                     ATLTSPEVGRLSLKEQLSHRQHLLSEMESLKPKVQAVQLCQSALRIPEDVVASLPLCH
                     AALRLQEEASRLQHTAIQQCNIMQAGAGYPHQ"
     3'UTR           1301..1583
                     /gene="SYNE1"
                     /note="terminates with the N1-3'E90 UTR"
     polyA_signal    1539..1583
                     /gene="SYNE1"
ORIGIN
        1 catactttat attcagagac aaaagaacaa tgttgtatta agatattttt ctaattccac
       61 acttaattat atgttgatga aaaatataca gccttgccta taacagtccc cttagaaggt
      121 tcccagaaat ttcttatttt gatcttttct tcagattctc ctaacagaag ccacaaatca
      181 ccgacagaac attgaaaaaa tggcagaaga acagaaggag aagtacttag gtctttatac
      241 catattacct tctgaactct ccttcagtt ggctgaagtg gcgttagatc taaagatccg
```

```
      301 agatcagatc caagacaaaa taaaagaagt tgagcagagc aaggccacga gccaggaact
      361 cagccggcaa attcagaagt tagctaaaga cctcacaact attctaacta agctgaaagc
      421 gaagacagat aatgtagttc aagctaaaac tgaccaaaag gtgctgggag aggaattaga
      481 tggctgtaat tcaaagttaa tggaattaga tgcagcagta cagaaattct tggaacagaa
      541 tggccaactg ggtaagccac tggccaagaa gataggaaaa ctgactgaac ttcaccagca
      601 gaccattaga caagctgaga atcggctctc caagctcaat caggcagcat cacatttaga
      661 agaatacaat gaaatgcttg aattaatttt gaagtggatt gaaaaagcta aagtcttggc
      721 tcatggaact attgcatgga attctgcaag ccagcttcgg gaacaatata ttttgcatca
      781 gaccctgcta gaagaatcca aagaaattga cagtgagctg gaagcaatga ctgagaaatt
      841 acagtacctc actagcgtgt actgtacaga aaaaatgtct cagcaagtgg cagaactggg
      901 acgggagact gaggagttgc gacagatgat caaaattcgt ttgcagaacc tccaagatgc
      961 agctaaggat atgaaaaaat ttgaagcaga gttgaaaaag ttacaagctg ccttggagca
     1021 agcccaggca acactgactt ctccagaagt tggacgtctc agtctcaagg agcagctctc
     1081 tcatcggcag catttgttgt ctgagatgga gtcactgaag ccgaaggtgc aagcagtgca
     1141 gctctgccag agtgccctcc ggatccccga ggatgtggtt gccagcttac ctctctgtca
     1201 tgctgctctg cggctgcagg aagaggccag ccggctgcag cacaccgcca tccagcagtg
     1261 taacatcatg caggcaggtg cagggtaccc acaccagtag agcaattgct gatgaatcat
     1321 gggcttcttt tcttagcatt gtgtgggctc agccatcaaa acacatccag ggtgttgaat
     1381 ctgacaggct gttgtggttt tataaaataa ggagattaaa atgctgtcat ttggatcacc
     1441 cacaaaagcc tggggaatgc tatataaaaa atatccttgg tgaaaattat cttttagtga
     1501 tatttttaaa taaataactt gtaaagatta attttctatg aaaaaaaaaa aaaaaaaaaa
     1561 aaaaaaaaaa aaaaaaaaaa aaa
//
```

Nucleotide

Display Settings: GenBank

Homo sapiens clone p31Nesp1d nesprin-1 (SYNE1) mRNA, complete cds, alternatively spliced

GenBank: JQ740785.1

FASTA Graphics

Go to:

```
LOCUS       JQ740785               1275 bp    mRNA    linear   PRI 16-JUL-2012
DEFINITION  Homo sapiens clone p31Nesp1d nesprin-1 (SYNE1) mRNA, complete cds,
            alternatively spliced.
ACCESSION   JQ740785
VERSION     JQ740785.1  GI:394999653
KEYWORDS    .
SOURCE      Homo sapiens (human)
  ORGANISM  Homo sapiens
            Eukaryota; Metazoa; Chordata; Craniata; Vertebrata; Euteleostomi;
            Mammalia; Eutheria; Euarchontoglires; Primates; Haplorrhini;
            Catarrhini; Hominidae; Homo.
REFERENCE   1  (bases 1 to 1275)
  AUTHORS   Rajgor,D., Mellad,J.A., Autore,F., Zhang,Q. and Shanahan,C.M.
  TITLE     Multiple novel nesprin-1 and nesprin-2 variants act as versatile
            tissue-specific intracellular scaffolds
  JOURNAL   PLoS ONE 7 (7), E40098 (2012)
   PUBMED   22768332
  REMARK    Publication Status: Online-Only
REFERENCE   2  (bases 1 to 1275)
  AUTHORS   Rajgor,D., Mellad,J.A. and Shanahan,C.M.
  TITLE     Direct Submission
  JOURNAL   Submitted (02-MAR-2012) Cardiovascular Division, King's College
            London, 125 Coldharbour Lane, James Black Centre, London SE5 9NU,
            UK
COMMENT     ##Assembly-Data-START##
            Assembly Method       :: chromas v. 2.33
            Sequencing Technology :: Sanger dideoxy sequencing
            ##Assembly-Data-END##
FEATURES             Location/Qualifiers
     source          1..1275
                     /organism="Homo sapiens"
                     /mol_type="mRNA"
                     /db_xref="taxon:9606"
                     /clone="p31Nesp1d"
     gene            1..1275
                     /gene="SYNE1"
     5'UTR           1..78
                     /gene="SYNE1"
                     /note="N1-5'E83 utilised in this transcript is generated
                     through alternative initiation of the nesprin-1 gene;
                     first coding exon is exon 83 of the nesprin-1 gene"
     CDS             79..1221
                     /gene="SYNE1"
                     /note="alternatively spliced"
                     /codon_start=1
                     /product="nesprin-1"
                     /protein_id="AFN44180.1"
                     /db_xref="GI:394999654"
                     /translation="MQEKVKTNGKLVKQELKDREMVETQINSVKCWVQETKEYLGNPT
                     IEIDAQLEELQILLTEATNHRQNIEKMAEEQKEKYLGLYTILPSELSLQLAEVALDLK
                     IRDQTLEDLLGRMTWQVHGLFIFLRQSLALSPRLECSETISAYCNLLGLSSSRASASQ
                     VAGIPGMHHHTRLIFCIFSKKRQGFAMLASLVSNSWPQVSCLPQPPKVLGLQIQDKIK
                     EVEQSKATSQELSRQIQKLAKDLTYILTKLKAKTDNVVQAKTDQKVLGEELDGCNSKL
                     MELDAAVQKFLEQNGQLGKPLAKKIGKLTELHQQTIRQAENRLSKLNQAASHLEEYNE
                     MLELILKWIEKAKVLAHGTIAWNSASQLREQYILHQVTLGKIIFKK"
     3'UTR           1222..>1275
                     /gene="SYNE1"
                     /note="corresponds to the N1-3'E87 where the last coding
                     exon is exon 87 with an additional peptide seqeunce absent
                     from the giant nesprin-1 variant"
ORIGIN
        1 tattggataa aatgttgcca agtattaggg ggttcctttc acttcacttc tgttttatcc
       61 ctgtaatgtt tctgaagcat gcaggagaaa gtgaagacta atggaaagtt ggtgaagcaa
```

```
      121 gagctgaagg accgagaaat ggtggagact cagatcaatt ctgtgaaatg ttgggttcag
      181 gaaacgaaag aatatttagg gaatccaaca atagaaatag atgctcaact tgaagaactt
      241 cagattctcc taacagaagc cacaaatcac cgacagaaca ttgaaaaaat ggcagaagaa
      301 cagaaggaga agtacttagg tctttatacc atattacctt ctgaactctc ccttcagttg
      361 gctgaagtgg cgttagatct aaagatccga gatcagacat tggaagatct actgggaagg
      421 atgacttggc aagttcatgg tctttttata tttttgagac agagtctcgc tctgtccccc
      481 aggctggagt gcagtgaaac aatctcagct tactgcaacc tcctgggttt aagcagttct
      541 cgtgcctcag cctcccaagt agctgggatt ccaggcatgc accaccatac ccggctaatt
      601 ttttgtattt ttagtaaaaa gagacaaggt tttgccatgt tggccagcct ggtctcaaac
      661 tcctggcctc aagtgagctg cctgcctcag cctcccaaag tgctgggatt acagatccaa
      721 gacaaaataa aagaagttga gcagagcaag gccacgagcc aggaactcag ccggcaaatt
      781 cagaagttag ctaaagacct cacaactatt ctaactaagc tgaaagcgaa gacagataat
      841 gtagttcaag ctaaaactga ccaaaaggtg ctgggagagg aattagatgg ctgtaattca
      901 aagttaatgg aattagatgc agcagtacag aaattcttgg aacagaatgg ccaactgggt
      961 aagccactgg ccaagaagat aggaaaactg actgaacttc accagcagac cattagacaa
     1021 gctgagaatc ggctctccaa gctcaatcag gcagcatcac atttagaaga atacaatgaa
     1081 atgcttgaat taattttgaa gtggattgaa aaagctaaag tcttggctca tggaactatt
     1141 gcatggaatt ctgcaagcca gcttcgggaa caatatattt tgcatcaggt aaccttagga
     1201 aaaataatct ttaaaaagta accaagggca atttgattta actgggtaga ctgacacaac
     1261 acttagaggg ctgtg
//
```

Nucleotide

Display Settings: GenBank

Homo sapiens clone p23Nesp1d nesprin-1 (SYNE1) mRNA, complete cds, alternatively spliced

GenBank: JQ754364.1

FASTA Graphics

Go to:

```
LOCUS       JQ754364                868 bp    mRNA    linear   PRI 16-JUL-2012
DEFINITION  Homo sapiens clone p23Nesp1d nesprin-1 (SYNE1) mRNA, complete cds,
            alternatively spliced.
ACCESSION   JQ754364
VERSION     JQ754364.1  GI:394999657
KEYWORDS    .
SOURCE      Homo sapiens (human)
  ORGANISM  Homo sapiens
            Eukaryota; Metazoa; Chordata; Craniata; Vertebrata; Euteleostomi;
            Mammalia; Eutheria; Euarchontoglires; Primates; Haplorrhini;
            Catarrhini; Hominidae; Homo.
REFERENCE   1  (bases 1 to 868)
  AUTHORS   Rajgor,D., Mellad,J.A., Autore,F., Zhang,Q. and Shanahan,C.M.
  TITLE     Multiple novel nesprin-1 and nesprin-2 variants act as versatile
            tissue-specific intracellular scaffolds
  JOURNAL   PLoS ONE 7 (7), E40098 (2012)
   PUBMED   22768332
  REMARK    Publication Status: Online-Only
REFERENCE   2  (bases 1 to 868)
  AUTHORS   Rajgor,D., Mellad,J.A. and Shanahan,C.M.
  TITLE     Direct Submission
  JOURNAL   Submitted (07-MAR-2012) Cardiovascular Division, King's College
            London, 125 Coldharbour Lane, James Black Centre, London SE5 9NU,
            UK
COMMENT     ##Assembly-Data-START##
            Assembly Method       :: Chromas v. 2.33
            Sequencing Technology :: Sanger dideoxy sequencing
            ##Assembly-Data-END##
FEATURES             Location/Qualifiers
     source          1..868
                     /organism="Homo sapiens"
                     /mol_type="mRNA"
                     /db_xref="taxon:9606"
                     /clone="p23Nesp1d"
     gene            1..868
                     /gene="SYNE1"
     5'UTR           1..199
                     /gene="SYNE1"
     CDS             200..814
                     /gene="SYNE1"
                     /note="alternatively spliced"
                     /codon_start=1
                     /product="nesprin-1"
                     /protein_id="AFN44382.1"
                     /db_xref="GI:394999658"
                     /translation="MAEEQKEKYLGLYTILPSELSLQLAEVALDLKIRDQIQDKIKEV
                     EQSKATSQELSRQIQKLAKDLTTILTKLKAKTDNVVQAKTDQKVLGEELDGCNSKLME
                     LDAAVQKFLEQNGQLGKPLAKKIGKLTELHQQTIRQAENRLSKLNQAASHLEEYNEML
                     ELILKWIEKAKVLAHGTIAWNSASQLREQYILHQVTLGKIIFKK"
     3'UTR           815..868
                     /gene="SYNE1"
ORIGIN
        1 catactttat attcagagac aaaagaacaa tgttgtatta agatattttt ctaattccac
       61 acttaattat atgttgatga aaaatataca gccttgccta taacagtccc cttagaaggt
      121 tcccagaaat ttcttatttt gatcttttct tcagattctc ctaacagaag ccacaaatca
      181 ccgacagaac attgaaaaaa tggcagaaga acagaaggag aagtacttag gtctttatac
      241 catattacct tctgaactct cccttcagtt ggctgaagtg gcgttagatc taaagatccg
      301 agatcagatc caagacaaaa taaaagaagt tgagcagagc aaggccacga gccaggaact
      361 cagcggcaa attcagaagt tagctaaaga cctcacaact attctaacta agctgaaagc
      421 gaagacagat aatgtagttc aagctaaaac tgaccaaaag gtgctgggag aggaattaga
      481 tggctgtaat tcaaagttaa tggaattaga tgcagcagta cagaaattct tggaacagaa
      541 tggccaactg ggtaagccac tggccaagaa gataggaaaa ctgactgaac ttcaccagca
      601 gaccattaga caagctgaga atcggctctc caagctcaat caggcagcat cacatttaga
```

```
      661 agaatacaat gaaatgcttg aattaatttt gaagtggatt gaaaaagcta aagtcttggc
      721 tcatggaact attgcatgga attctgcaag ccagcttcgg gaacaatata ttttgcatca
      781 ggtaacctta ggaaaaataa tctttaaaaa gtaaccaagg gcaatttgat ttaactgggt
      841 agactgacac aacacttaga gggctgtg
//
```

Nucleotide

Display Settings: GenBank

Homo sapiens clone p12Nesp1a nesprin-1 (SYNE1) mRNA, complete cds, alternatively spliced

GenBank: JQ754365.1

FASTA Graphics

Go to:

```
LOCUS       JQ754365                524 bp    mRNA    linear   PRI 16-JUL-2012
DEFINITION  Homo sapiens clone p12Nespla nesprin-1 (SYNE1) mRNA, complete cds,
            alternatively spliced.
ACCESSION   JQ754365
VERSION     JQ754365.1  GI:394999659
KEYWORDS    .
SOURCE      Homo sapiens (human)
  ORGANISM  Homo sapiens
            Eukaryota; Metazoa; Chordata; Craniata; Vertebrata; Euteleostomi;
            Mammalia; Eutheria; Euarchontoglires; Primates; Haplorrhini;
            Catarrhini; Hominidae; Homo.
REFERENCE   1  (bases 1 to 524)
  AUTHORS   Rajgor,D., Mellad,J.A., Autore,F., Zhang,Q. and Shanahan,C.M.
  TITLE     Multiple novel nesprin-1 and nesprin-2 variants act as versatile
            tissue-specific intracellular scaffolds
  JOURNAL   PLoS ONE 7 (7), E40098 (2012)
   PUBMED   22768332
  REMARK    Publication Status: Online-Only
REFERENCE   2  (bases 1 to 524)
  AUTHORS   Rajgor,D., Mellad,J.A. and Shanahan,C.M.
  TITLE     Direct Submission
  JOURNAL   Submitted (07-MAR-2012) Cardiovascular Division, King's College
            London, 125 Coldharbour Lane, James Black Centre, London SE5 9NU,
            UK
COMMENT     ##Assembly-Data-START##
            Assembly Method       :: Chromas v. 2.33
            Sequencing Technology :: Sanger dideoxy sequencing
            ##Assembly-Data-END##
FEATURES             Location/Qualifiers
     source          1..524
                     /organism="Homo sapiens"
                     /mol_type="mRNA"
                     /db_xref="taxon:9606"
                     /clone="p12Nespla"
     gene            1..524
                     /gene="SYNE1"
     5'UTR           1..155
                     /gene="SYNE1"
                     /note="corresponds to the Nesprin-1beta1 5'UTR"
     CDS             156..470
                     /gene="SYNE1"
                     /note="alternatively spliced"
                     /codon_start=1
                     /product="nesprin-1"
                     /protein_id="AFN44383.1"
                     /db_xref="GI:394999660"
                     /translation="MELDAAVQKFLEQNGQLGKPLAKKIGKLTELHQQTIRQAENRLS
                     KLNQAASHLEEYNEMLELILKWIEKAKVLAHGTIAWNSASQLREQYILHQVTLGKIIF
                     KK"
     3'UTR           471..524
                     /gene="SYNE1"
ORIGIN
        1 atagtagaat tattcattat aatatttggc tttgacaaaa atcagtctga tctcgggaaa
       61 cctggagaaa tttatttttct gtactctaat gttctttcat tttggtgacc atcaaggtgc
      121 tgggagagga attagatggc tgtaattcaa agttaatgga attagatgca gcagtacaga
      181 aattcttgga acagaatggc caactgggta agccactggc caagaagata ggaaaactga
      241 ctgaacttca ccagcagacc attagacaag ctgagaatcg gctctccaag ctcaatcagg
      301 cagcatcaca tttagaagaa tacaatgaaa tgcttgaatt aattttgaag tggattgaaa
      361 aagctaaagt cttggctcat ggaactattg catggaattc tgcaagccag cttcgggaac
      421 aatatatttt gcatcaggta accttaggaa aaataatctt taaaaagtaa ccaagggcaa
      481 tttgatttaa ctgggtagac tgacacaaca cttagagggc tgtg
//
```